

CONSTRUCTING PREDICTABLE SUPRAMOLECULAR ARCHITECTURES USING
BUILDING BLOCKS DERIVED FROM VERSATILE AND 'GREEN' SYNTHETIC
ROUTES

by

ABHIJEET SHEKHAR SINHA

B.Sc., University of Delhi, 2005
M.Sc., University of Delhi, 2007

AN ABSTRACT OF A DISSERTATION

submitted in partial fulfillment of the requirements for the degree

DOCTOR OF PHILOSOPHY

Department of Chemistry
College of Arts and Sciences

KANSAS STATE UNIVERSITY
Manhattan, Kansas

2013

Abstract

A series of four bifunctional ligands based on β -diketonate moieties bearing methyl, chloro, bromo and iodo substituents and their corresponding Cu(II) complexes were synthesized and crystallographically characterized in order to explore the possibility of using relatively weak halogen...halogen contacts for the directed assembly of predictable architectures in coordination chemistry. The four ligands have characteristic O–H...O intramolecular hydrogen bonds, and the structures of the halogenated ligands contain extended 1-D architectures based on C=O...X halogen bonds, which can be explained on the basis of electrostatic considerations. The corresponding Cu(II) complexes show a constant coordination chemistry for all the ligands, wherein the metal ion sits in a slightly distorted square-planar pocket, without any coordinated or uncoordinated solvent molecules. Furthermore, the absence of halogen-bonds in the coordination complexes is due to the depleted charge on the potential halogen-bond acceptors. As a result, the halogen-bonds are unable to compete with the inherent close packing in the crystal lattice, and thus display a head to head close-packed motif for methyl, chloro, and bromo, substituted Cu(II) complexes. The enhanced polarizability of the iodine atom, produces a more electropositive surface which means that this structure cannot accommodate a linear head-to-head arrangement due to electrostatic repulsion, and thus a unique close-packed structure very different from the three iso-structural complexes is observed for the iodo substituted Cu(II) complex.¹

Oximes offer great opportunities in supramolecular chemistry (hydrogen-bond donors), as well as in coordination chemistry (strong coordinating ligands). Hence, we established a versatile and robust mechanochemical route to aldehyde/ketone–oxime conversions for a broad range of aldehydes² and ketones³ *via* a simple mortar–pestle grinding method. The relative reactivity of aldehydes *vs.* ketones under these conditions was also explored, along with an examination of the possible connection between reactivity and electronic substituent effects.

The growing interest in the oxime (RR'C=N–OH) functionality, and a lack of the systematic examinations of the structural chemistry of such compounds, prompted us to carry out analysis of intermolecular oxime...oxime interactions, and identify the hydrogen-bond patterns for four major categories of oximes (R' = –H, –CH₃, –NH₂, –CN), based on all available structural data in the CSD, complemented by three new relevant crystal structures.⁴ It was found

that the oximes could be divided into four groups depending on which type of predominant oxime...oxime interactions they present in the solid-state: (i) O–H...N dimers ($R_2^2(6)$), (ii) O–H...N catemers (C(3)), (iii) O–H...O catemers (C(2)), and (iv) oximes in which the R' group accepts a hydrogen bond from the oxime moiety catemers (C(6)).

In order to explore and establish a hierarchy between hydrogen (HB) and halogen (XB) bonds in supramolecular architectures, we designed and synthesized two ditopic HB/XB donors, and screened them with a series of 20 HB acceptors. IR was used as a preliminary and reliable tool to gather information on the presence/absence of HB/XB in the different cases. We were able to get the solved single-crystal data for three of the 40 reactions. In two out of two cases with symmetric ditopic acceptors, both HB and XB were present leading to 1-D infinite chains, which suggests that in a system of “equal opportunities”, both these interactions can be tolerant of each other. In the only case with asymmetric ditopic acceptor, the HB donor binds to the best acceptor, whereas XB donor binds to the second best acceptor. This selectivity can be rationalized on the basis of electrostatic considerations, where the HB donor was shown to have a higher molecular electrostatic potential than the XB donor.

Finally, we designed and synthesized a versatile and dynamic metallomacrocycle based on the 2,2'-bipyridyl backbone capable of controlling the metal-metal distance within the macrocycle cavity. The macrocycle was synthesized by high-dilution method and characterized by several spectroscopic techniques (IR, NMR, Mass, UV-Visible). Also, the macrocycle:Cu(II) stoichiometric ratio was determined by Job's continuous variation method using UV-Visible spectroscopy, and was found to be 1:2, respectively.

1 Aakeröy, C. B.; Sinha, A. S.; Chopade, P. D.; Desper, J. *Dalton Trans.* **2011**, 40, 12160.

2 Aakeröy, C. B.; Sinha, A. S.; Epa, K. N.; Spartz, C. L.; Desper, J. *Chem. Commun.* **2012**, 48, 11289.

3 Aakeröy, C. B.; Sinha, A. S. *RSC Adv.* **2013**, 3, 8168.

4 Aakeröy, C. B.; Sinha, A. S.; Epa, K. N.; Chopade, P. D.; Smith, M. M.; Desper, J. *Cryst. Growth Des.* **2013**, 13, 2687.

CONSTRUCTING PREDICATBLE SUPRAMOLECULAR ARCHITECTURES USING
BUILDING BLOCKS DERIVED FROM VERSATILE AND 'GREEN' SYNTHETIC
ROUTES

by

ABHIJEET SHEKHAR SINHA

B.Sc., University of Delhi, 2005
M.Sc., University of Delhi, 2007

A DISSERTATION

submitted in partial fulfillment of the requirements for the degree

DOCTOR OF PHILOSOPHY

Department of Chemistry
College of Arts and Sciences

KANSAS STATE UNIVERSITY
Manhattan, Kansas

2013

Approved by:

Major Professor
Dr. Christer B. Aakeröy

Abstract

A series of four bifunctional ligands based on β -diketonate moieties bearing methyl, chloro, bromo and iodo substituents and their corresponding Cu(II) complexes were synthesized and crystallographically characterized in order to explore the possibility of using relatively weak halogen...halogen contacts for the directed assembly of predictable architectures in coordination chemistry. The four ligands have characteristic O–H...O intramolecular hydrogen bonds, and the structures of the halogenated ligands contain extended 1-D architectures based on C=O...X halogen bonds, which can be explained on the basis of electrostatic considerations. The corresponding Cu(II) complexes show a constant coordination chemistry for all the ligands, wherein the metal ion sits in a slightly distorted square-planar pocket, without any coordinated or uncoordinated solvent molecules. Furthermore, the absence of halogen-bonds in the coordination complexes is due to the depleted charge on the potential halogen-bond acceptors. As a result, the halogen-bonds are unable to compete with the inherent close packing in the crystal lattice, and thus display a head to head close-packed motif for methyl, chloro, and bromo, substituted Cu(II) complexes. The enhanced polarizability of the iodine atom, produces a more electropositive surface which means that this structure cannot accommodate a linear head-to-head arrangement due to electrostatic repulsion, and thus a unique close-packed structure very different from the three iso-structural complexes is observed for the iodo substituted Cu(II) complex.¹

Oximes offer great opportunities in supramolecular chemistry (hydrogen-bond donors), as well as in coordination chemistry (strong coordinating ligands). Hence, we established a versatile and robust mechanochemical route to aldehyde/ketone–oxime conversions for a broad range of aldehydes² and ketones³ *via* a simple mortar–pestle grinding method. The relative reactivity of aldehydes *vs.* ketones under these conditions was also explored, along with an examination of the possible connection between reactivity and electronic substituent effects.

The growing interest in the oxime (RR'C=N–OH) functionality, and a lack of the systematic examinations of the structural chemistry of such compounds, prompted us to carry out analysis of intermolecular oxime...oxime interactions, and identify the hydrogen-bond patterns for four major categories of oximes (R' = –H, –CH₃, –NH₂, –CN), based on all available structural data in the CSD, complemented by three new relevant crystal structures.⁴ It was found

that the oximes could be divided into four groups depending on which type of predominant oxime...oxime interactions they present in the solid-state: (i) O–H...N dimers ($R_2^2(6)$), (ii) O–H...N catemers (C(3)), (iii) O–H...O catemers (C(2)), and (iv) oximes in which the R' group accepts a hydrogen bond from the oxime moiety catemers (C(6)).

In order to explore and establish a hierarchy between hydrogen (HB) and halogen (XB) bonds in supramolecular architectures, we designed and synthesized two ditopic HB/XB donors, and screened them with a series of 20 HB acceptors. IR was used as a preliminary and reliable tool to gather information on the presence/absence of HB/XB in the different cases. We were able to get the solved single-crystal data for three of the 40 reactions. In two out of two cases with symmetric ditopic acceptors, both HB and XB were present leading to 1-D infinite chains, which suggests that in a system of “equal opportunities”, both these interactions can be tolerant of each other. In the only case with asymmetric ditopic acceptor, the HB donor binds to the best acceptor, whereas XB donor binds to the second best acceptor. This selectivity can be rationalized on the basis of electrostatic considerations, where the HB donor was shown to have a higher molecular electrostatic potential than the XB donor.

Finally, we designed and synthesized a versatile and dynamic metallomacrocycle based on the 2,2'-bipyridyl backbone capable of controlling the metal-metal distance within the macrocycle cavity. The macrocycle was synthesized by high-dilution method and characterized by several spectroscopic techniques (IR, NMR, Mass, UV-Visible). Also, the macrocycle:Cu(II) stoichiometric ratio was determined by Job's continuous variation method using UV-Visible spectroscopy, and was found to be 1:2, respectively.

1 Aakeröy, C. B.; Sinha, A. S.; Chopade, P. D.; Desper, J. *Dalton Trans.* **2011**, 40, 12160.

2 Aakeröy, C. B.; Sinha, A. S.; Epa, K. N.; Spartz, C. L.; Desper, J. *Chem. Commun.* **2012**, 48, 11289.

3 Aakeröy, C. B.; Sinha, A. S. *RSC Adv.* **2013**, 3, 8168.

4 Aakeröy, C. B.; Sinha, A. S.; Epa, K. N.; Chopade, P. D.; Smith, M. M.; Desper, J. *Cryst. Growth Des.* **2013**, 13, 2687.

Table of Contents

List of Figures	xv
List of Tables	xxi
Acknowledgements.....	xxii
Dedication.....	xxiii
Preface.....	xxiv
Chapter 1 - Introduction.....	1
1.1 Supramolecular chemistry	1
1.2 Tools for communication between molecules	2
1.2.1 Covalent synthesis	2
1.2.2 Supramolecular synthesis.....	2
1.2.2.1 Coordinate bonds	3
1.2.2.1.1 0-D assemblies constructed from coordinate bonds	3
1.2.2.1.2 1-D assemblies constructed from coordinate bonds	4
1.2.2.1.3 2-D/3-D assemblies constructed from coordinate bonds.....	4
1.2.2.2 Hydrogen-bonds.....	5
1.2.2.2.1 Homomeric 0-D assemblies constructed from hydrogen-bonds.....	5
1.2.2.2.2 Homomeric 1-D assemblies constructed from hydrogen-bonds.....	6
1.2.2.2.3 Homomeric 2-D assemblies constructed from hydrogen-bonds.....	7
1.2.2.2.4 Homomeric 3-D assemblies constructed from hydrogen-bonds.....	8
1.2.2.3 Halogen-bonds	9
1.2.2.3.1 Halogen-bonds through N/O...X (X = Br or I).....	9
1.2.2.3.2 Halogen...halogen interactions	10
1.3 Crystal engineering	11
1.3.1 Supramolecular synthons	11
1.3.2 Graph set notation	12
1.3.3 Etter's rules for hydrogen-bonds	13
1.3.4 Crystal structure prediction.....	14
1.3.5 Multi-component crystals – Co-crystals	15

1.3.5.1 Co-crystals based on hydrogen-bonds	16
1.3.5.2 Co-crystals based on halogen-bonds.....	18
1.3.5.3 Applications of co-crystals	19
1.4 Goals	20
1.4.1 Investigating the importance of weak halogen···halogen bonds in predictably arranging coordination complexes in the solid-state.....	21
1.4.2 Establishing the versatility and robustness of a ‘green’ synthetic route to aldehyde/ketone-oxime conversions	21
1.4.3 Identifying the different ‘supramolecular synthons’ of the oxime motif.....	21
1.4.4 Establishing a hierarchical assembly approach through hydrogen and halogen bonding	22
1.4.5 Design and synthesis of a versatile metallomacrocycle.....	22
Chapter 2 - Halogen bonding or close packing? Examining the structural landscape in a series of Cu(II)-acac complexes.....	28
2.1 Introduction.....	28
2.2 Experimental.....	32
2.2.1 Synthesis	32
2.2.1.1 Synthesis of 3-(4-tolyl)-2,4-pentanedione, 3	33
2.2.1.2 Synthesis of 3-(4-chlorophenyl)-2,4-pentanedione, 4	34
2.2.1.3 Synthesis of 3-(4-bromophenyl)-2,4-pentanedione, 5	34
2.2.2 Synthesis of coordination complexes.....	35
2.2.2.1 Synthesis of {bis[3-(4-tolyl)-2,4-pentanedionato] copper(II)}, 3a	35
2.2.2.2 Synthesis of {bis[3-(4-chlorophenyl)-2,4-pentanedionato] copper(II)}, 4a	35
2.2.2.3 Synthesis of {bis[3-(4-bromophenyl)-2,4-pentanedionato] copper(II)}, 5a	35
2.2.2.4 Synthesis of {bis[3-(4-iodophenyl)-2,4-pentanedionato] copper(II)}, 2a	36
2.2.3 Molecular electrostatic potential charge calculations	36
2.3 Results.....	36
2.3.1 Structural characterization of the ligands	37
2.3.1.1 Crystal structure of 3	37
2.3.1.2 Crystal structure of 4 , 5 and 2	38
2.3.2 Structural characterization of the coordination complexes.....	39

2.3.2.1 Crystal structure of 3a , 4a and 5a	39
2.3.2.2 Crystal structure of 2a	39
2.4 Discussion.....	40
2.4.1 Characterization by ¹ H NMR spectroscopy.....	40
2.4.2 Characterization by IR spectroscopy.....	41
2.4.3 Comparison of the crystal structures of the ligands.....	42
2.4.3.1 Close packing in 3	42
2.4.3.2 Isostructural halogen-bonded architecture in 4 , 5 and 2	43
2.4.3.2.1 Iso-structurality.....	43
2.4.3.2.2 Halogen-bonds.....	43
2.4.4 Controlling the Cu(II) coordination geometry.....	44
2.4.5 Comparison of the crystal structures of the coordination complexes.....	45
2.4.5.1 Close-packed architecture in 3a , 4a and 5a	45
2.4.5.1.1 Structural equivalence in 3a and 4a	45
2.4.5.1.2 Crystal structure of 5a	45
2.4.5.1.3 Head-to-head motif in 3a , 4a and 5a	46
2.4.5.2 Crystal structure of 2a	46
2.4.6 Halogen-bond vs close packing.....	47
2.4.7 Halogen-bond vs hydrogen-bond.....	47
2.5 Conclusions.....	48
Chapter 3 - A versatile and green mechanochemical route for aldehyde/ketone-oxime conversions.....	52
3.1 Introduction.....	52
3.1.1 Green chemistry.....	52
3.1.2 Mechanochemistry.....	52
3.1.3 Oximes.....	53
3.2 Experimental.....	56
3.2.1 Synthesis.....	56
3.2.1.1 Synthesis of 4-((trimethylsilyl)ethynyl)benzaldehyde, 6	56
3.2.1.2 Synthesis of 4-ethynylbenzaldehyde, 7	57
3.2.1.3 Synthesis of 4-(bromoethynyl)benzaldehyde, 8	58

3.2.2 General synthesis of oximes	58
3.2.2.1 Aldoximes	59
3.2.2.1.1 Pentafluorobenzaldehyde oxime, 9	59
3.2.2.1.2 4-Bromo-2,3,5,6-tetrafluorobenzaldehyde oxime, 10	59
3.2.2.1.3 4-Iodo-2,3,5,6-tetrafluorobenzaldehyde oxime, 11	59
3.2.2.1.4 4-(Bromoethynyl)benzaldehyde oxime, 12	59
3.2.2.1.5 4-Iodobenzaldehyde oxime, 13	60
3.2.2.1.6 3-Iodobenzaldehyde oxime, 14	60
3.2.2.1.7 4-Cyanobenzaldehyde oxime, 15	60
3.2.2.1.8 3,5-Dimethoxybenzaldehyde oxime, 16	60
3.2.2.1.9 4-Carboxybenzaldehyde oxime, 17	61
3.2.2.1.10 3-Hydroxybenzaldehyde oxime, 18	61
3.2.2.1.11 2-Hydroxybenzaldehyde oxime, 19	61
3.2.2.1.12 5-Bromo-2-hydroxybenzaldehyde oxime, 20	61
3.2.2.1.13 5-Iodo-2-hydroxybenzaldehyde oxime, 21	62
3.2.2.1.14 4-Pyridinecarboxaldehyde oxime, 22	62
3.2.2.1.15 Dodecyl aldehyde oxime, 23	62
3.2.2.2 Ketoximes	62
3.2.2.2.1 4'-Chloroacetophenone oxime, 24	62
3.2.2.2.2 4'-Bromoacetophenone oxime, 25	63
3.2.2.2.3 3'-Bromoacetophenone oxime, 26	63
3.2.2.2.4 4'-Iodoacetophenone oxime, 27	63
3.2.2.2.5 4'-Cyanoacetophenone oxime, 28	63
3.2.2.2.6 4'-Methylacetophenone oxime, 29	64
3.2.2.2.7 3'-Methylacetophenone oxime, 30	64
3.2.2.2.8 3'-Hydroxyacetophenone oxime, 31	64
3.2.2.2.9 2'-Hydroxyacetophenone oxime, 32	64
3.2.2.2.10 4'-Aminoacetophenone oxime, 33	65
3.2.2.2.11 3'-Aminoacetophenone oxime, 34	65
3.2.2.2.12 (E)-1-(pyridin-4-yl)ethanone oxime, 35	65
3.2.2.2.13 (E)-1-(pyridin-3-yl)ethanone oxime, 36	65

3.2.2.2.14 (E)-1-(pyridin-2-yl)ethanone oxime, 37	66
3.2.2.2.15 (1E,1'E)-1-(6-((E)-1-(hydroxyimino)ethyl)pyridin-2-yl)ethanone oxime, 38	66
3.2.2.2.16 (1E,1'E)-1-(4-((E)-1-(hydroxyimino)ethyl)phenyl)ethanone oxime, 39	66
3.2.2.2.17 (1E,1'E)-1-(3-((E)-1-(hydroxyimino)ethyl)phenyl)ethanone oxime, 40	66
3.2.2.2.18 (E)-pentan-2-one oxime, 41	67
3.2.2.2.19 (E)-5-hydroxypentan-2-one oxime, 42	67
3.2.2.2.20 (2E,4E)-pentane-2,4-dione dioxime, 43	67
3.3 Results and discussion	67
3.3.1 Characterization of oximes	67
3.3.1.1 Infra-red spectroscopy	67
3.3.1.2 ¹ H NMR spectroscopy	68
3.3.2 Versatile synthetic method for aldehyde/ketone-oxime conversions	69
3.3.3 Relative reactivity of aldehyde-oxime versus ketone-oxime conversions.....	72
3.4 Conclusions.....	74
Chapter 4 - Structural chemistry of oximes	77
4.1 Introduction.....	77
4.1.1 Oximes	77
4.1.1.1 Applications of oximes	78
4.1.1.2 Hydrogen-bonding in oximes	79
4.2 Experimental.....	81
4.2.1 Synthesis and single-crystal growth.....	81
4.2.2 CSD search.....	82
4.2.3 Molecular electrostatic potential calculations.....	82
4.3 Results.....	83
4.3.1 Aldoximes (R' = H).....	83
4.3.1.1 Crystal structure of 13	83
4.3.1.2 CSD data	84
4.3.2 Ketoximes (R' = CH ₃)	85
4.3.2.1 Crystal structure of 27	85
4.3.2.2 Crystal structure of 28	85

4.3.2.3 CSD data	86
4.3.3 Amidoximes (R' = NH ₂).....	87
4.3.3.1 CSD data	87
4.3.4 Cyano-oximes (R' = CN)	88
4.4 Discussion.....	88
4.4.1 Bond lengths and bond angles in dimers and catemers	89
4.4.2 Explanation of trends	89
4.4.2.1 Aldoximes (R' = H) and amidoximes (R' = NH ₂).....	90
4.4.2.2 Ketoximes (R' = CH ₃).....	90
4.4.2.3 C(2) catemers (via O-H···O interactions) in aldoximes and ketoximes	91
4.4.2.4 Cyano-oximes (R' = CN)	91
4.5 Conclusions.....	92
Chapter 5 - Hydrogen-bond and halogen-bond donors in supramolecular assembly – complementary or competitive?	96
5.1 Introduction.....	96
5.1.1 Existing studies	96
5.1.1 Rationale for design	98
5.2 Experimental.....	101
5.2.1 Synthesis	101
5.2.1.1 Synthesis of 4-(iodoethynyl)benzaldehyde, 44	102
5.2.1.2 Synthesis of 4-(iodoethynyl)benzaldehyde oxime, 45	102
5.2.2 Synthesis of co-crystals.....	103
5.2.2.1 Synthesis of 4-(bromoethynyl)benzaldehyde oxime:4,4'-bipyridine, 12F	103
5.2.2.2 Synthesis of 4-(bromoethynyl)benzaldehyde oxime:1,2-bis(4-pyridyl)ethylene, 12K	103
5.2.2.3 Synthesis of 4-(iodoethynyl)benzaldehyde oxime:4,4'-bipyridine-N-monoxide, 45N	103
5.2.3 Molecular electrostatic potential calculations.....	103
5.3 Results.....	104
5.3.1 Structural characterization of the co-crystals.....	105
5.3.1.1 Crystal structure of 12F	105

5.3.1.2 Crystal structure of 12K	106
5.3.1.3 Crystal structure of 45N	107
5.4 Discussion.....	107
5.4.1 Characterization of the co-crystals by infra-red spectroscopy (IR)	107
5.4.2 Trends and explanations.....	113
5.4.2.1 Co-crystals with symmetric ditopic acceptors	114
5.4.2.2 Co-crystals with asymmetric ditopic acceptors	114
5.4.2.3 Br vs I.....	115
5.4.3 Comparison with activated perfluorinated systems	116
5.5 Conclusions.....	117
Chapter 6 - Versatile 2,2'-bipyridine-copper(II) based metallo-macrocycles.....	120
6.1 Introduction.....	120
6.1.1 Macrocyclic compounds	120
6.1.1.1 Anion binding in macrocycles	121
6.1.2 Rationale for the design of the metallo-macrocycle	123
6.1.2.1 Molecular modeling of the macrocycle	123
6.1.2.2 Goals	124
6.2 Experimental.....	124
6.2.1 Synthesis	124
6.2.1.1 Synthesis of 6,6'-dimethyl-2,2'-bipyridine, 46	125
6.2.1.2 Synthesis of 2,2'-bipyridine-6,6'-dicarboxylic acid, 47	126
6.2.1.3 Synthesis of di(prop-2-yn-1-yl)[2,2'-bipyridine]-6,6'-dicarboxylate, 48	126
6.2.1.4 Synthesis of bis(di(prop-2-yn-1-yl)[2,2'-bipyridine]-6,6'-dicarboxylate), 49	127
6.2.2 UV-visible spectroscopy titrations.....	128
6.2.3 Molecular modeling.....	130
6.3 Results and discussion	131
6.3.1 Characterization of 49	131
6.3.1.1 Infra-red spectroscopy	131
6.3.1.2 ¹ H NMR spectroscopy	131
6.3.1.3 Mass spectroscopy	132
6.3.1.4 UV-visible spectroscopy.....	133

6.3.2 Coordination of 49 with copper(II) ions and determination of stoichiometry	135
6.3.3 Future work	137
6.3.3.1 Modularity in the macrocyclic system	137
6.3.3.2 Modifying the solubility	138
6.4 Conclusions.....	138
Chapter 7 - Summary	140
Appendix A - ^1H and ^{13}C NMR data.....	142

List of Figures

Figure 1.1 Molecular recognition of a substrate by an enzyme.	1
Figure 1.2 Sheehan's total synthesis of penicillin V.....	2
Figure 1.3 A zero-dimensional Ag(I) metallacycle.	3
Figure 1.4 A one-dimensional luminescent Eu(III) coordination polymer.....	4
Figure 1.5 A highly porous three-dimensional metal-organic framework.	5
Figure 1.6 Self-complementary hydrogen-bonded dimer in carboxylic acids (a), amides (b), and aldoximes (c).....	5
Figure 1.7 Homomeric zero-dimensional dimers in benzoic acid (a), acetophenone oxime (b) and 2-aminopyridine (c).	6
Figure 1.8 Homomeric 1-D motifs formed in phenols (a), amides (b), oximes (c), aminopyrimidines (d), ureas (e), dioximes (f), dicarboxylic acids (g) and imidazoles (h).....	7
Figure 1.9 Homomeric 2-D architecture constructed from self-complementary hybrid ureidoimidazole moieties.	8
Figure 1.10 Homomeric hydrogen-bonded 3-D diamondoid networks found in polyhedral organosilanols.	8
Figure 1.11 (a) Conventional halogen-bond; (b) Type-I halogen-halogen contacts; (c) Type-II halogen-halogen contacts.....	9
Figure 1.12 Infinite 1-D chains seen in the single-crystal structure of 4-iodopyridine (a) and 4-iodo/bromobenzonitrile (b).	10
Figure 1.13 1-D chains seen in the single-crystal structure of 4-iodoacetophenone.	10
Figure 1.14 Homomeric bifurcated halogen-halogen interactions in halogenated aryls (X = Cl, Br, I).....	11
Figure 1.15 Examples of supramolecular synthons; (a) carboxylic acid dimer, (b) amide dimer, and (c) carboxylic acid-pyridine dimer.	12
Figure 1.16 Examples of different graph set notations.	13
Figure 1.17 Single-crystal structure of a 1:1 co-crystal of 4-bromophenylcyanooxime and 1-[(3-cyanophenyl)-methyl]-5,6-dimethylbenzimidazole.....	14
Figure 1.18 Recrystallization (homomeric) vs co-crystallization (heteromeric).....	15

Figure 1.19 A 0-D hydrogen-bonded co-crystal of benzoic acid:2-aminopyrimidine (2:1).....	17
Figure 1.20 An infinite 1-D chain in the hydrogen-bonded co-crystal of 4,4'-biphenol:4,4'- bipyridine.	17
Figure 1.21 Two-dimensional tapes formed in the hydrogen-bonded co-crystal of piperazine-2,5- dione:fumaric acid.	18
Figure 1.22 Two-dimensional halogen-bonded motifs formed in the 1:1 co-crystal of 1,1'- (butane-1,4-diyl)bis(3-pyridin-3-ylurea):2,3,5,6-tetrafluoro-1,4-di-iodobenzene.	19
Figure 1.23 Molecular structure of meloxicam.....	20
Figure 1.24 Design and synthesis of predictable and reliable supramolecular architectures.	20
Figure 2.1 (a) Hydrogen-bonded dimer in carboxylic acids; (b) Pyridine-acid O-H...N interactions; Carboxylic acids (c) and pyridines (d) coordinating with metals.	28
Figure 2.2 (a) Conventional halogen-bond; (b) Type I halogen-halogen contacts; (c) Type II halogen-halogen contacts.....	29
Figure 2.3 A three-component modular strategy for the assembly of halogen-bonded coordination complexes	30
Figure 2.4 Synthesis of halogen-bonded infinite 1D supramolecular ribbons.....	30
Figure 2.5 Tetra-coordinated copper(II)-acac center.	31
Figure 2.6 Possible halogen-bond acceptors in the free ligands.....	32
Figure 2.7 Close packing in the crystal structure of 3	37
Figure 2.8 Section of the crystal structure of 4 (a), 5 (b) and 2 (c) displaying the intramolecular hydrogen-bond and the intermolecular halogen-bond.	38
Figure 2.9 Head to head close-packed arrangement in the crystal structure of 3a (a), 4a (b) and 5a (c).	39
Figure 2.10 Infinite zig-zag pattern in the crystal structure of 2a	40
Figure 2.11 Two tautomeric forms of acetyl acetonates.....	40
Figure 2.12 ¹ H NMR spectrum of 4	41
Figure 2.13 IR spectrum of 5 before (left) and after (right) complexation with copper(II) ion. ..	42
Figure 2.14 Anti-parallel close packing arrangement in the crystal structure of 3 (a), and 3-(4- cyanophenyl)-2,4-pentanedione (b).	42
Figure 2.15 Halogen-bond acceptors and donor in 4 , 5 and 2	44
Figure 2.16 Head-to-head close-packed arrangement in 3a (a) and 4a (b).	45

Figure 2.17 Head-to-head close-packed arrangement in 5a	46
Figure 2.18 Zig-zag close-packed architecture in 2a	47
Figure 2.19 Hydrogen-bonded dimers and halogen-bonded chains in 4-iodobenzoic acid.	48
Figure 3.1 Twelve principles of green chemistry.	52
Figure 3.2 Mechanochemical synthesis of metal-organic frameworks.	53
Figure 3.3 Different types of oximes.	53
Figure 3.4 Synthesis of nitriles (a) and amines (b) from oximes.	54
Figure 3.5 (a) Coordination of oximes with metals; (b) Oximes as hydrogen-bond donors; (c) Self-complementary hydrogen-bonded dimers in oximes.	54
Figure 3.6 Synthesis of oximes by ball-milling at elevated temperatures (a), and by using nanostructured pyrophosphates as catalysts (b).	55
Figure 3.7 One-pot mechanochemical conversion of aldehydes and ketones to oximes.	56
Figure 3.8 Monitoring ketone-oxime conversions by IR spectroscopy.	68
Figure 3.9 ¹ H NMR spectrum of 16	68
Figure 3.10 ¹ H NMR spectrum of 37	69
Figure 3.11 ¹ H NMR spectrum of the ground mixture of 12	70
Figure 3.12 ¹ H NMR spectrum of 14 before (a) and after (b) an aqueous wash.	71
Figure 3.13 ¹ H NMR spectrum of ground mixture of 33	72
Figure 3.14 Relative reactivity of aldehyde-oxime <i>versus</i> ketone-oxime conversions.	73
Figure 3.15 Relative reactivity of aldehyde <i>vs</i> ketone group when present on the same backbone.	73
Figure 3.16 Effect of substituents on the ketone-oxime conversions.	73
Figure 4.1 (a) Hydrogen-bonded $R_2^2(8)$ dimer in carboxylic acids; (b) Hydrogen-bonded infinite C(4) $R_4^2(8)$ ribbons in amides.	77
Figure 4.2 Single-crystal structure of isophthalaldehyde dioxime highlighting the oxime-oxime dimer.	78
Figure 4.3 Different types of oximes.	78
Figure 4.4 Number of reported single crystals for oximes (R' = -H, -CH ₃ , -NH ₂ , -CN), 1988- 2012.	79

Figure 4.5 (a) Hydrogen-bond donor/acceptors in oximes; (b) Hydrogen-bonded dimers; (c) Catemer formation via –O–H···N hydrogen-bonded chains; (d) Catemer formation via –O–H···O hydrogen-bonded chains.....	80
Figure 4.6 (a) Hydrogen-bonded chains via O–H···N≡C interactions in cyano-oximes; (b) Hydrogen-bonded chains via O–H···NH ₂ interactions in amidoximes.....	80
Figure 4.7 Four major categories of oximes examined in this chapter.....	81
Figure 4.8 Defined parameters in the CSD during the search for data on oximes.....	82
Figure 4.9 Section of the crystal structure of 13 displaying the hydrogen bonded R ₂ ² (6) dimer and an I···O halogen bond.....	83
Figure 4.10 HO···N bond distance (Å) vs O–H···N bond angle (°) for dimers and catemers of aldoximes.....	84
Figure 4.11 Section of the crystal structure of 27 displaying the hydrogen bonded R ₂ ² (6) dimer and an I···O halogen bond.....	85
Figure 4.12 Dimer formation (R ₂ ² (6)) in the crystal structure of 28	86
Figure 4.13 HO···N bond distance (Å) vs O–H···N bond angle (°) for dimers and catemers of ketoximes.....	87
Figure 4.14 HO···N bond distance (Å) vs O–H···N bond angle (°) for dimers and catemers of amidoximes.....	88
Figure 4.15 Molecular electrostatic potentials (MEPs) for aldoximes and amidoximes.....	90
Figure 4.16 Molecular electrostatic potentials (MEPs) for ketoximes.....	91
Figure 4.17 Molecular electrostatic potentials (MEPs) for cyano-oximes.....	91
Figure 4.18 Calculated hydrogen-bond parameters α_i , β_j and interaction-site pairing energies, for dimers, and O–H···N≡C catemer for cyano-oximes (a); and for 28 (b).....	92
Figure 5.1 Orthogonal self-assembly of an open organic framework by combining hydrogen and halogen bonds.....	97
Figure 5.2 Competing hydrogen-bond and halogen-bond donors in crystal engineering.....	98
Figure 5.3 Design of the ligand.....	99
Figure 5.4 Hydrogen-bond (HB) and halogen-bond (XB) donors.....	99
Figure 5.5 Monotopic HB/XB acceptors.....	100
Figure 5.6 Symmetric ditopic HB/XB acceptors.....	100

Figure 5.7 Asymmetric ditopic HB/XB acceptors.....	101
Figure 5.8 Section of the crystal structure of 12F displaying the infinite 1-D chains formed by a combination of hydrogen-bonds and halogen-bonds.....	106
Figure 5.9 Section of the crystal structure of 12K displaying the infinite 1-D chains formed by a combination of hydrogen-bonds and halogen-bonds.....	106
Figure 5.10 Section of the crystal structure of 45N displaying the infinite 1-D chains formed by a combination of hydrogen-bonds and halogen-bonds.....	107
Figure 5.11 Postulated outcomes for co-crystallization with symmetric ditopic acceptors.	114
Figure 5.12 Postulated outcomes for co-crystallization with asymmetric ditopic acceptors.....	115
Figure 5.13 Section of the crystal structure of the co-crystal of 2,3,5,6-tetrafluoro-4-bromobenzaldehyde oxime:1,2-bis(4-pyridyl)ethylene.....	116
Figure 5.14 Section of the crystal structure of the co-crystal of of 2,3,5,6-tetrafluoro-4-iodobenzaldehyde oxime:4,4'-bipyridine-N-monoxide.	117
Figure 6.1 A calixsalen macrocycle as a selective fluorescent sensor for zinc(II) ions.	120
Figure 6.2 Macrocycles with switchable 2,2'-bipyridine based metal binding sites.....	121
Figure 6.3 Encapsulation of halide ions by diammonium katapinands.	122
Figure 6.4 A dinuclear Cu(II) complex capable of binding chloride ions.	122
Figure 6.5 Design of a versatile and modular macrocycle capable of guest capture.....	123
Figure 6.6 Force-field geometry optimization of the macrocycle (left), and the metallo-macrocycle (right).....	123
Figure 6.7 Dynamic macrocycle based on the 2,2'-bipyridyl backbone.	124
Figure 6.8 High dilution synthesis of 49	128
Figure 6.9 IR spectra illustrating the conversion of the alkyne pre-cursor (48) to the macrocycle (49).....	131
Figure 6.10 ¹ H NMR spectra illustrating the conversion of the alkyne pre-cursor (48) to the macrocycle (49).....	132
Figure 6.11 ESI-MS spectrum of 49 (Inset - isotopic pattern).	133
Figure 6.12 UV-visible spectrum of 49	133
Figure 6.13 Calculated molecular orbitals (HOMO and LUMO) for 49	134
Figure 6.14 Determination of 49 : Cu ²⁺ stoichiometry by continuous variation method using UV-visible spectroscopy (a); new absorption band (b).	135

Figure 6.15 Job's plot for determining the macrocycle : metal stoichiometry at $\lambda_{\text{max}} = 330.0$ nm
(a), and at $\lambda_{\text{max}} = 338.0$ nm (b)..... 137

Figure 6.16 Easily modifiable arms for tuning the selectivity and the pocket size. 138

Figure 6.17 Improving the solubility by functionalizing the macrocycle with solubilizing groups.
..... 138

List of Tables

Table 2.1 IR stretches for the C=O bonds in the acac ligands and C=C stretch for the corresponding coordination complexes.	37
Table 2.2 Hydrogen-bond geometries for 3 , 4 , 5 and 2	37
Table 2.3 Halogen-bond geometric parameters for 4 , 5 and 2	38
Table 2.4 Unit cell parameters of 4 , 5 and 2	43
Table 2.5 Molecular electrostatic potentials (MEPs) for 4 , 5 and 2	44
Table 2.6 Number of structures with head-to-head motifs	46
Table 4.1 Single-crystal growth details and melting points of 13 , 27 and 28	81
Table 4.2 Key geometric parameters in the crystal structures of 27 and 28	85
Table 4.3 Primary motifs in crystal structures of oximes.	89
Table 5.1 Significant FT-IR bands (A-J).....	104
Table 5.2 Significant IR bands (K-T).....	105
Table 5.3 FT-IR band shifts (A-J).....	109
Table 5.4 FT-IR band shifts (K-T).....	110
Table 5.5 Determining the nature of bonding in the co-crystals on the basis of FT-IR shifts (A-T).....	111
Table 5.6 Molecular electrostatic potentials (MEPs) for 12 and 45	112
Table 5.7 Molecular electrostatic potentials for the HB/XB acceptors, A-T	113
Table 6.1 UV-visible data for the Job's plot at $\lambda_{\max} = 330$ nm.	129
Table 6.2 UV-visible data for the Job's plot at $\lambda_{\max} = 338$ nm.	130

Acknowledgements

I would like to first thank my advisor Professor Christer Aakeröy, as without his help and motivation, this thesis, and my research would not have been possible. He has always motivated me to think beyond the interpretation of data alone, and thus made me a better and confident scientist. Thanks to his encouragement, I want to pursue a career in teaching, and I really hope that one day, I can be as good an advisor as him.

I would also like to thank my Ph. D. advisory committee Professor Eric Maatta, Professor Paul Smith, Professor Jennifer Anthony, and Professor Liang-Wu Cai for their valuable time and input.

Thanks to Dr. John Desper, for collecting all the data sets and solving the crystal structures in this thesis. Many thanks to Dr. Leila Maurmann for helping out with NMR studies.

Thanks to Mr. Jim Hodgson, Mr. Ron Jackson, Mr. Tobe Eggers, Ms. Mary Dooley, and Ms. Kimberly Ross, as they made my research and life at KSU easier.

To members of the Aakeröy group, past and present, who I attended conferences with and had good times, both inside and outside of the lab. It was a joy to work with you all.

To all my friends who have always stood by me and made life really enjoyable, Pratik, Shanish, Evan, and Kanishka.

I would like to thank Kanika for being very helpful, and for always being there whenever I needed her. Thanks for being patient with me for the past six months.

Finally, I would like to thank my family for being supportive of all my decisions throughout my life, and for their unconditional love and support.

Dedication

I dedicate this dissertation to my grandfather (gone, but never forgotten), my caring and supportive father, my amazing mother (for her endless love and support), and my awesome brother (for always being there for me).

Preface

Research carried out at Kansas State University for this dissertation led to the following publications in scientific journals:

- 1) C. B. Aakeröy, A. S. Sinha, P. D. Chopade and J. Desper, “Halogen bonding or close packing? Examining the structural landscape in a series of Cu(II)-acac complexes”, *Dalton Trans.* **2011**, *40*, 12160-12168.
- 2) C. B. Aakeröy, A. S. Sinha, K. N. Epa, C. L. Spartz and J. Desper, “A versatile and green mechanochemical route for aldehyde–oxime conversions”, *Chem. Commun.* **2012**, *48*, 11289-11291.
- 3) C. B. Aakeröy and A. S. Sinha, “Synthesis of ketoximes *via* a solvent-assisted and robust mechanochemical pathway”, *RSC Adv.* **2013**, *3*, 8168-8171.
- 4) C. B. Aakeröy, A. S. Sinha, K. N. Epa, P. D. Chopade, M. M. Smith and J. Desper, “Structural chemistry of oximes”, *Cryst. Growth Des.* **2013**, *13*, 2687-2695.

Chapter 1 - Introduction

1.1 Supramolecular chemistry

The seminal work by H. E. Fischer in 1894, wherein he described the enzyme-substrate interactions, as being analogous to that of a ‘lock and key’,¹ sowed the seed for the concepts of ‘molecular recognition’² and ‘supramolecular chemistry’.³ Molecular recognition, as the name suggests, refers to the specific interactions between two or more molecules, akin to that of a lock having a specific key (Figure 1.1). These interactions are usually non-covalent in nature to allow for reversibility and dynamism in the system (required in biological processes).

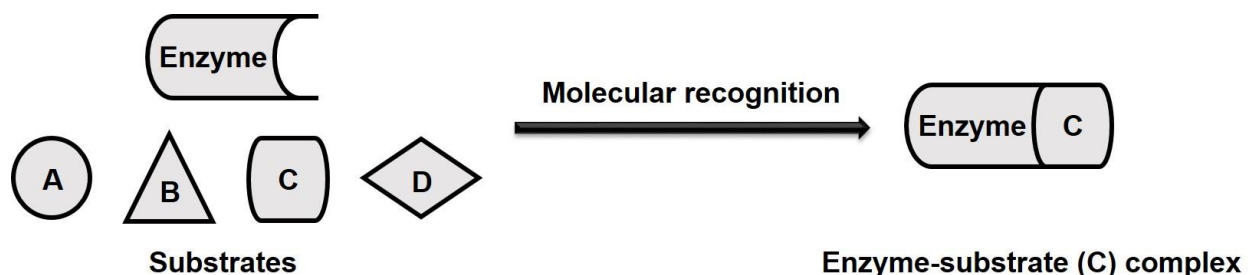


Figure 1.1 Molecular recognition of a substrate by an enzyme.

Fischer’s work was followed by a period of intense research on the design and synthesis of molecular systems that mimicked biological processes. Finally, in 1969, the term ‘supramolecular chemistry’ was put forth by Jean-Marie Lehn as part of his study on inclusion compounds.^{2,4} He defined it as ‘the chemistry of the inter-molecular bond’, which encompasses the self-assembly of two or more molecules into different and distinct architectures *via* non-covalent forces of interaction.

An important aspect of supramolecular chemistry is communication and change, which leads to the predictable assembly of solid-state architectures from smaller molecular building blocks, as opposed to random and serendipitous assembly. An ideal supramolecular process is dynamic in nature, wherein the molecular building blocks are so designed, that they can express specific and directional intermolecular interactions, so as to achieve controlled and directed assembly of the molecules, which in turn leads to a better understanding of the macroscopic properties of materials.⁵ Thus, it is not only important to fully understand the nature of these tools of communication between the molecules required for supramolecular assembly, but also to have a handle on these forces of interaction.

1.2 Tools for communication between molecules

1.2.1 Covalent synthesis

Covalent synthesis, as we know it today, is a powerful and an ever-growing field in chemistry, as synthetic chemists have been working for over a century to come up with novel reactions in order to synthesize more and more complicated compounds (Figure 1.2).⁶ Organic transformations can be defined in a simplistic way as – ‘the conversion of A to B, using C as the reagent’. These transformations involve the breaking and making of covalent bonds, which makes it possible to carry out multi-step reactions, and to isolate intermediates and products. Systematic studies of organic reactions over the years has enabled organic chemists to better understand molecular structure, reactivity, and reaction pathways.⁶

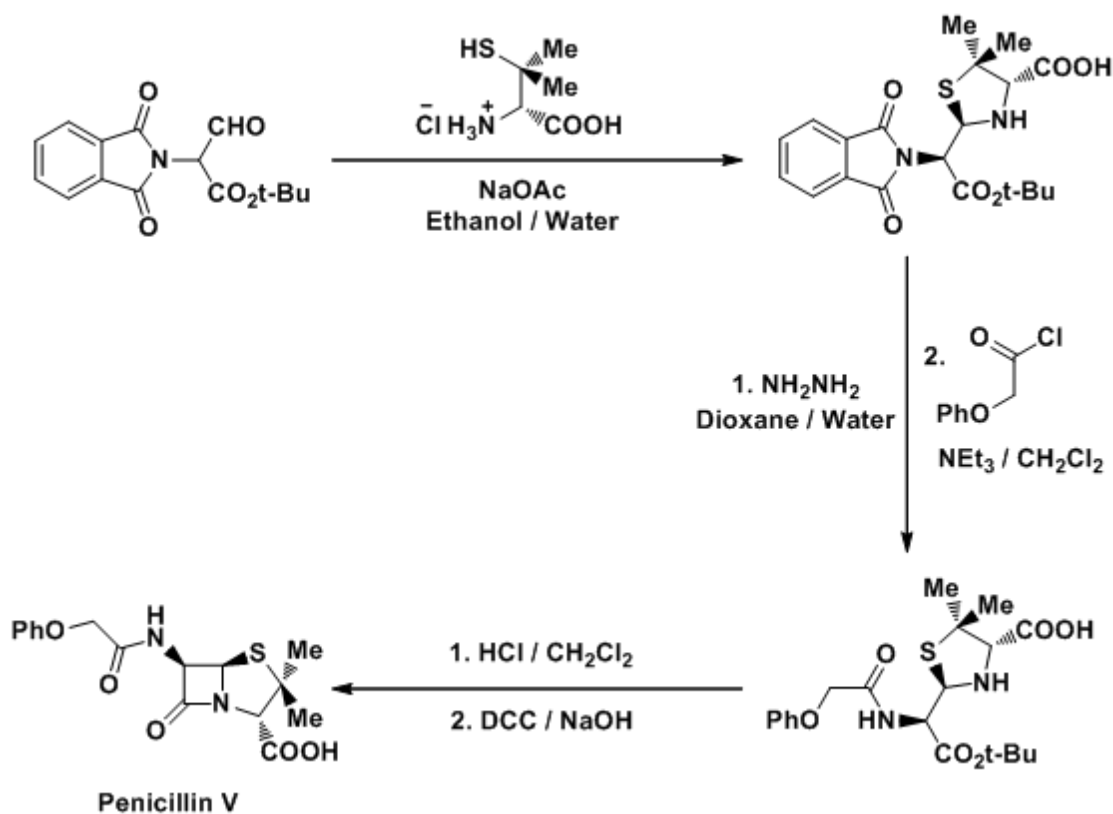


Figure 1.2 Sheehan's total synthesis of penicillin V.⁷

1.2.2 Supramolecular synthesis

Supramolecular synthesis is an area of research, which is still largely unexplored, when compared to covalent synthesis.⁸ This can be attributed to the use of reversible intermolecular interactions such as hydrogen-bonds, halogen-bonds, and π - π interactions, which normally

restricts solution-phase experiments to single-step (one-pot) process. Thus, it is important to understand these weaker forces of interaction, and to establish reliable synthetic routes towards the assembly of complicated supramolecular architectures.

1.2.2.1 Coordinate bonds

The ground breaking work by Alfred Werner in 1893, wherein he proposed the octahedral configuration of transition metal complexes,⁹ led to an increased interest in the field of coordination chemistry, where the synthesis, characterization and properties of coordination complexes attract tremendous attention. A key element is controlling the metal-ligand interactions in a coordination architecture, in a bid to assemble networks of precise topology and pre-determined connectivity.^{10,11} These varied architectures are ubiquitous in the field of catalysis,¹² host-guest chemistry,¹³ sensors¹⁴ and drug delivery.¹⁵ Different metal ion sizes and coordination preferences, coupled with the varying coordination modes of coordinating ligands can lead to the formation of zero- to three-dimensional architectures, thus providing considerable flexibility and versatility in metal-ligand chemistry.¹¹

1.2.2.1.1 0-D assemblies constructed from coordinate bonds

An example of a zero-dimensional coordination complex is the silver(I) metallacycle synthesized by Fromm *et al.* (Figure 1.3).¹⁶

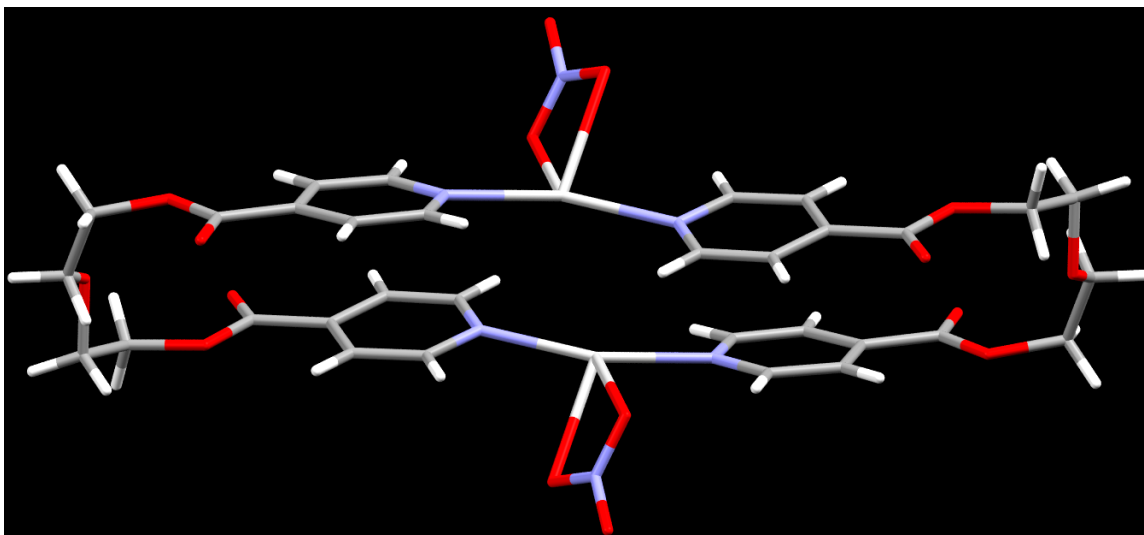


Figure 1.3 A zero-dimensional Ag(I) metallacycle.¹⁶

The bidentate pyridyl based flexible ligand (L) adopts a U-shape conformation and coordinates to two Ag(I) metal ions, thus forming a $[\text{Ag}_2\text{L}_2]^{2+}$ metallacycle, where the nitrate

counterion is coordinated to two silver cations in a μ^2 -fashion, providing a distorted T-shape coordination motif for the metal atom.¹⁶ Another recent example showcase a tridentate ligand (1-(4-(1H-pyrazol-1-yl)phenyl)butane-1,3-dione) coordinated to two Zn(II) ions as a two-connected linker, thus giving rise to discrete binuclear [2 + 2] metallomacrocycles.¹⁷

1.2.2.1.2 1-D assemblies constructed from coordinate bonds

One-dimensional coordination polymers/complexes having useful properties such as magnetism¹⁸ and photoluminescence¹⁹ are well known. Ye *et al.* synthesized a 1-D polymer $\{[\text{Eu}(\text{OAc})_2(\text{H}_2\text{O})(\text{OBPT})] \cdot 3\text{H}_2\text{O}\}_n$ (OBPT = 4,6-bis(2-pyridyl)-1,3,5-triazin-2-ol), where the coordination geometry around each Eu^{3+} metal ion can be described as a distorted tricapped trigonal prism with six oxygen atoms (four oxygen atoms from two acetate ions, one oxygen atom from the water molecule, and one oxygen atom from the ligand) and three nitrogen atoms (from the ligand) (Figure 1.4).²⁰ This polymer shows selective luminescence enhancement for sensing small organic molecules.

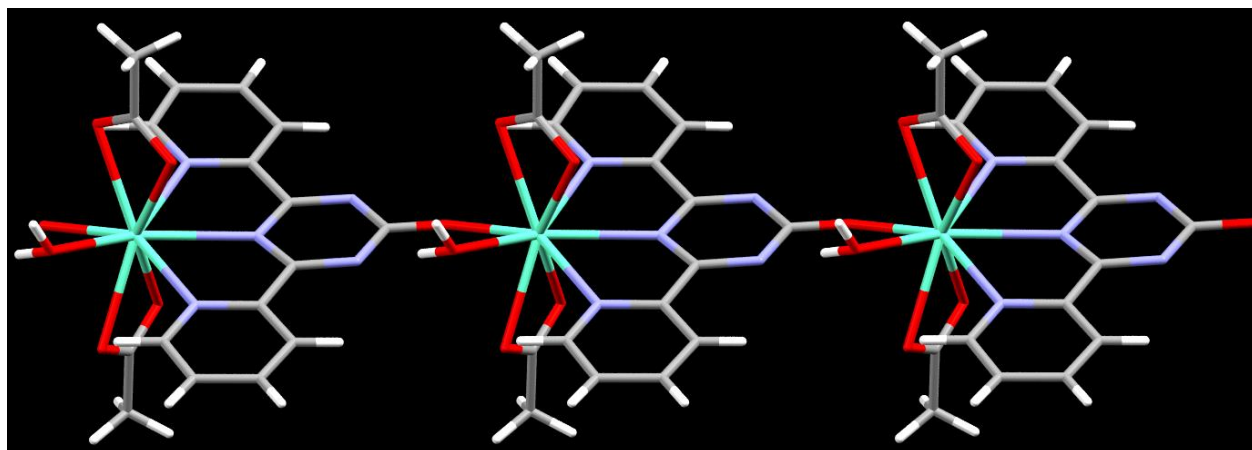


Figure 1.4 A one-dimensional luminescent Eu(III) coordination polymer.²⁰

1.2.2.1.3 2-D/3-D assemblies constructed from coordinate bonds

Metal-organic frameworks (MOFs) are the most extensively researched higher order coordination complexes,²¹ and is arguably one of the most prolific fields in current inorganic chemistry.²² There is increased research in controlling the topology of the metal-ligand bonds (primary synthetic vector) in MOFs as the resulting architectures are of significant interest, and can give rise to porous frameworks that can be used in catalysis,¹² gas-sorption,²³ chemical separations,²⁴ sensors¹⁴ and drug delivery.¹⁵ Hupp *et al.* have synthesized MOFs that have the

highest Brunauer-Emmett-Teller (BET) surface areas of any reported porous materials to date (Figure 1.5).²⁵

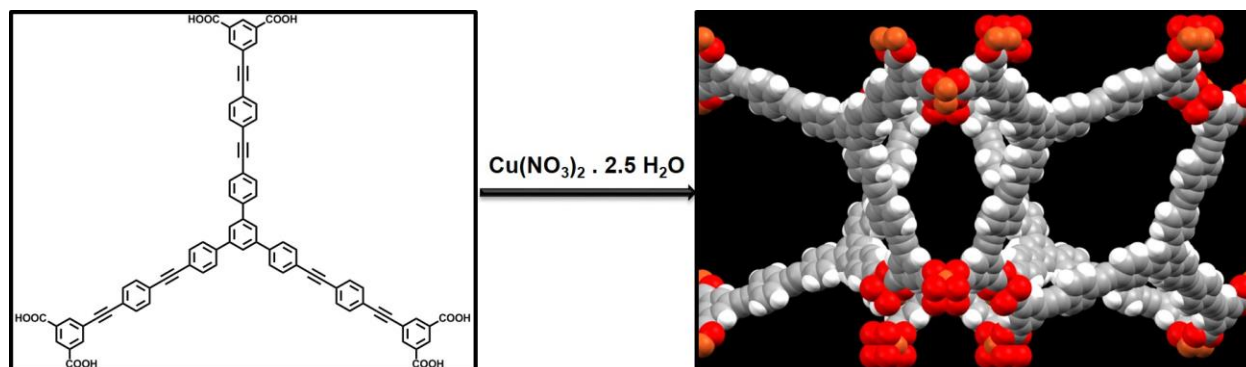


Figure 1.5 A highly porous three-dimensional metal-organic framework.²⁵

1.2.2.2 Hydrogen-bonds

Hydrogen-bonds represent one of the most studied intermolecular interactions in supramolecular synthesis, due to the strength and directionality of such interactions, when compared to many other intermolecular interactions.²⁶ Hydrogen-bond complementarity (geometry, and number of hydrogen-bond donors and acceptors) can offer reliable tools for constructing supramolecular architectures,²⁷ and many self-complementary homomeric interactions are well documented, of which the carboxylic acid,²⁸ amide^{29,30} and oxime³¹ dimers are most notable examples (Figure 1.6).

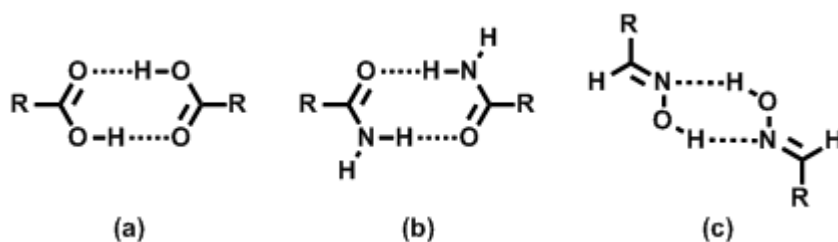


Figure 1.6 Self-complementary hydrogen-bonded dimer in carboxylic acids (a), amides (b), and aldoximes (c).

1.2.2.2.1 Homomeric 0-D assemblies constructed from hydrogen-bonds

Self-complementary hydrogen-bonding groups such as carboxylic acids, aldoximes, ketoximes, pyrazoles and amino-pyridines are all capable of forming homomeric zero-dimensional dimers (Figure 1.7).^{32,33,34}

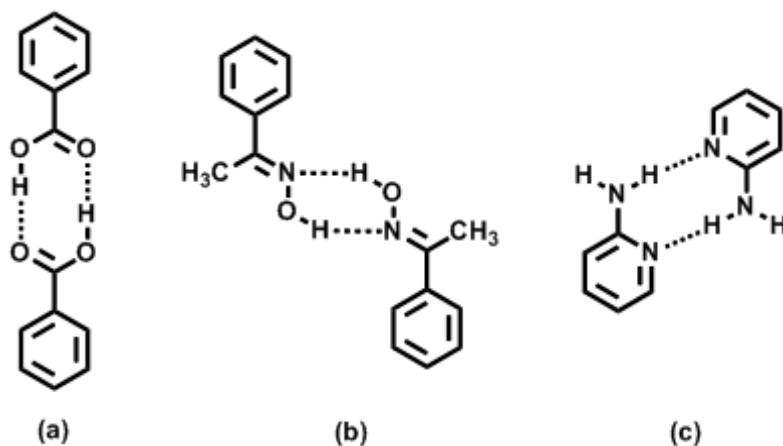


Figure 1.7 Homomeric zero-dimensional dimers in benzoic acid (a), acetophenone oxime (b) and 2-aminopyridine (c).

Intermolecular O-H \cdots O, O-H \cdots N and N-H \cdots N interactions are responsible for the hydrogen-bonded dimers formed in benzoic acid,³² acetophenone oxime³³ and 2-aminopyridine,³⁴ respectively. These interactions are robust and are consistently expressed in the solid-state in the absence of any competing strong hydrogen-bond donors or acceptors.

1.2.2.2.2 Homomeric 1-D assemblies constructed from hydrogen-bonds

Self-complementary interactions in phenols,³⁵ imidazoles,³⁶ amides,^{29,30} dioximes,³¹ dicarboxylic acids,³⁷ amino-pyrimidines³⁸ and ureas³⁹ can lead to homomeric 1-D chains in the solid-state (Figure 1.8). Phenols and imidazoles can form homomeric 1-D catemers via O-H \cdots O and N-H \cdots N intermolecular interactions, respectively. Two separate motifs in amides combine to form the catemeric chains, wherein the *syn*-proton forms a dimer via self-complementary N-H \cdots O hydrogen-bonds, and the *anti*-proton is involved in N-H \cdots O hydrogen-bonds with the bifurcated carbonyl oxygen atom. Oximes are capable of forming homomeric hydrogen-bonded dimers, as well as 1-D catemers in the solid-state via O-H \cdots N interactions, and there are a few examples in literature of oximes that exist in the catemeric state,⁴⁰ whereas most of the dioximes form 1-D chains via two distinct self-complementary dimers.

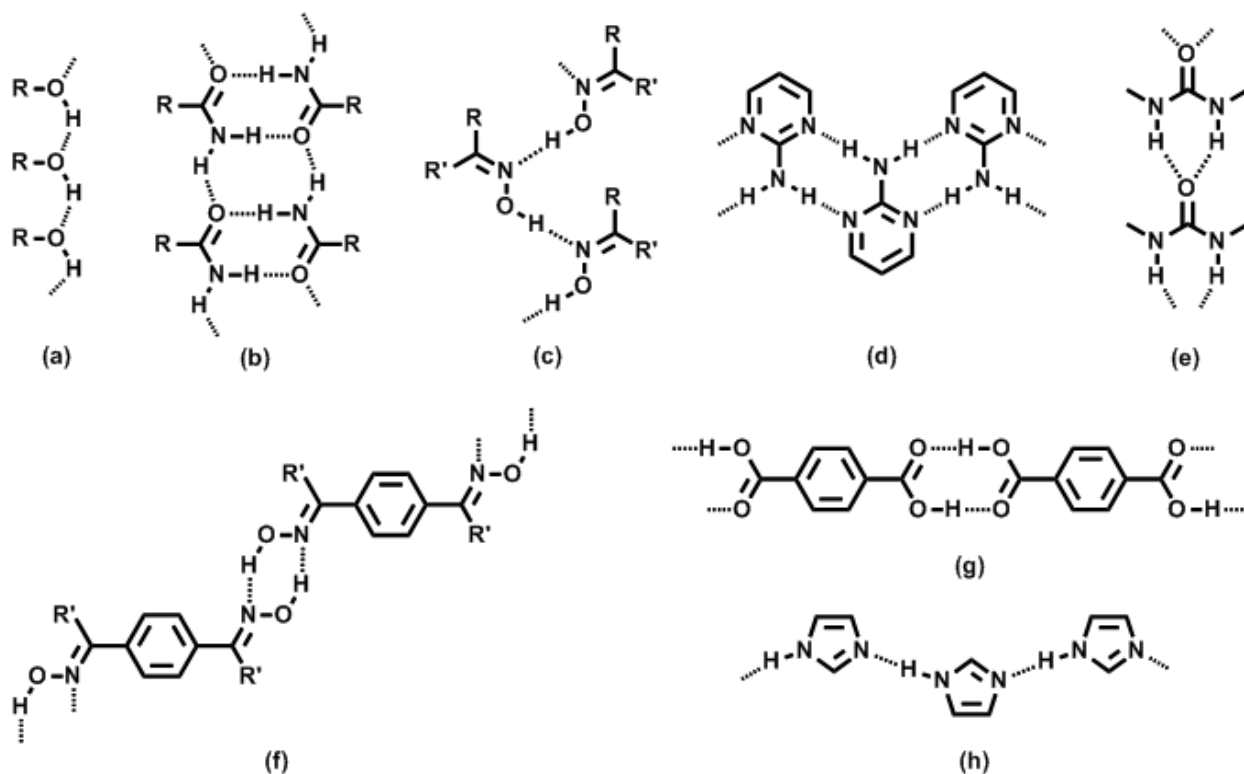


Figure 1.8 Homomeric 1-D motifs formed in phenols (a), amides (b), oximes (c), amino-pyrimidines (d), ureas (e), dioximes (f), dicarboxylic acids (g) and imidazoles (h).

Dicarboxylic acids (aliphatic or aromatic) and amino-pyrimidines form two distinct self-complementary hydrogen-bonded dimers via O-H \cdots O and N-H \cdots N interactions, respectively, which extends these architectures into homomeric one-dimensional chains. Ureas can form 1-D chains via bifurcated N-H \cdots O hydrogen-bonds between the amide N-H moiety and the carbonyl oxygen atom³⁹

1.2.2.2.3 Homomeric 2-D assemblies constructed from hydrogen-bonds

A combination of two or more identical or different hydrogen-bonding motifs can in principle lead to the assembly of two-dimensional supramolecular architectures. A common example of homomeric 2-D architecture assembled via identical hydrogen-bonding motifs is benzene-1,3,5-tricarboxylic acid, wherein self-complementary O-H \cdots O hydrogen-bonds lead to the formation of hexagonal networks.⁴¹ A combination of self-complementary hydrogen-bonding moieties such as urea and imidazole gives rise to a homomeric 2-D hydrogen-bonded architecture by the independent combination of urea-urea (bifurcated N-H \cdots O hydrogen-bonds

between amide N-H moiety and the carbonyl oxygen atom) and imidazole-imidazole (N-H \cdots N interactions) moieties (Figure 1.9).³⁶

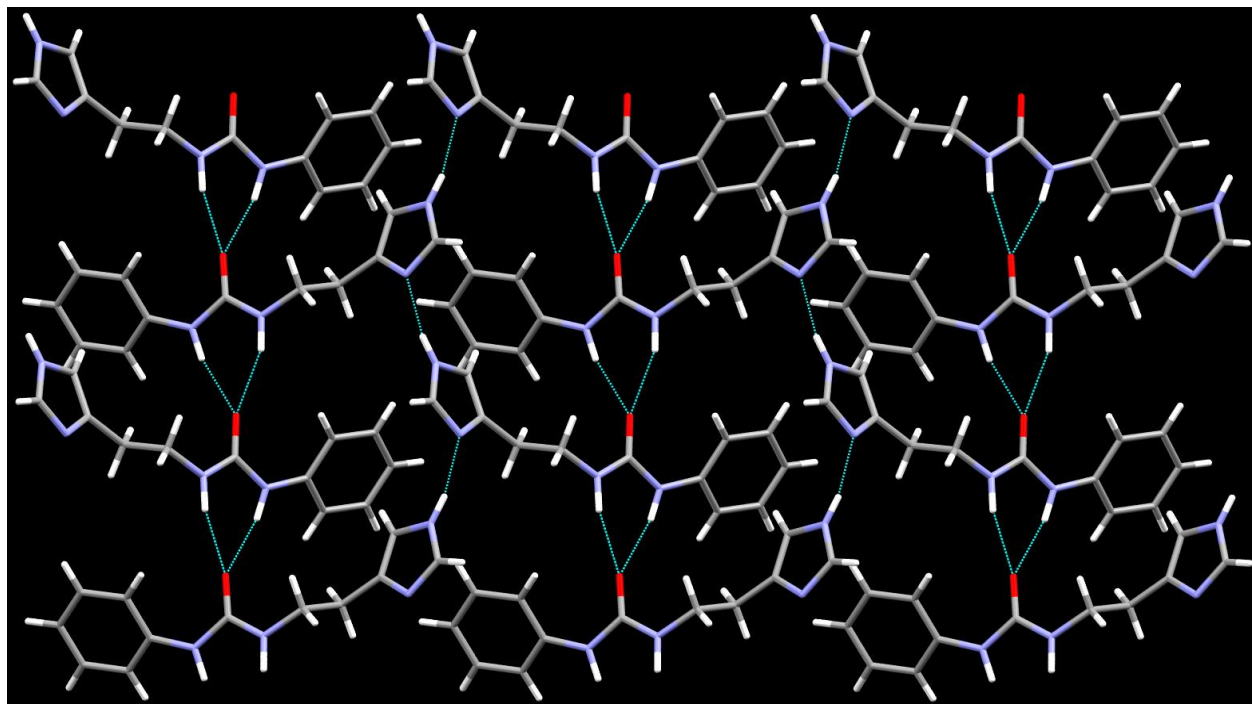


Figure 1.9 Homomeric 2-D architecture constructed from self-complementary hybrid ureido-imidazole moieties.³⁶

1.2.2.2.4 Homomeric 3-D assemblies constructed from hydrogen-bonds

Polyhedral organosilanols, such as tetrakis[4-(diisopropylhydroxysilyl)phenyl]methane⁴² and carboxylic acids, such as adamantane-1,3,5,7-tetracarboxylic acid⁴³ form 3-D diamondoid networks through self-complementary O-H \cdots O hydrogen-bonds (Figure 1.10). A hydrogen-bonded 3-D structure is even observed in the case of crystalline glycerol.⁴⁴

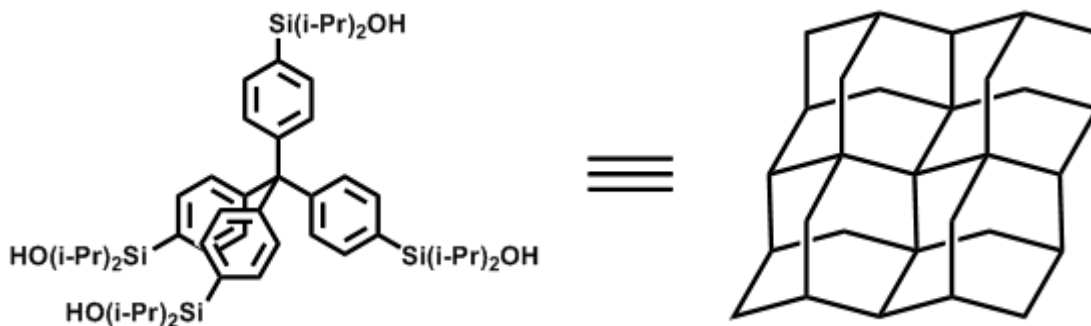


Figure 1.10 Homomeric hydrogen-bonded 3-D diamondoid networks found in polyhedral organosilanols.

1.2.2.3 Halogen-bonds

The halogen-bond (XB) is a non-covalent interaction, which has been used for the assembly of predictable and directional supramolecular architectures.⁴⁵ It is electrostatic in nature⁴⁶ and is comparable in strength to hydrogen-bonds.⁴⁶ There are three types of halogen contacts (Figure 1.11);⁴⁷ (i) a conventional halogen-bond takes place between electronegative atoms such as nitrogen or oxygen atom, and the electron-deficient tip of a halogen atom, (ii) type-I halogen-halogen contacts which are due to van der Waals interactions between two halogen atoms (characteristic C-X...X angle = 120°, X = Br, I), and (iii) type-II halogen-halogen contacts between the electron-rich and electron-deficient regions on a halogen atom (characteristic C-X...X angle = 90°, X = Br, I).



Figure 1.11 (a) Conventional halogen-bond; (b) Type-I halogen-halogen contacts; (c) Type-II halogen-halogen contacts.

1.2.2.3.1 Halogen-bonds through N/O...X (X = Br or I)

Pyridines and nitriles can act as halogen-bond acceptors, as can be seen from the single-crystal structures of 4-iodopyridine,⁴⁸ 4-iodobenzonitrile⁴⁹ and 4-bromobenzonitrile,⁴⁹ wherein the structure-directing force of interaction is the N...X halogen-bond between the pyridine/nitrile nitrogen atom and the halogen atom (X = Br, I), which gives rise to infinite 1-D chains (Figure 1.12).

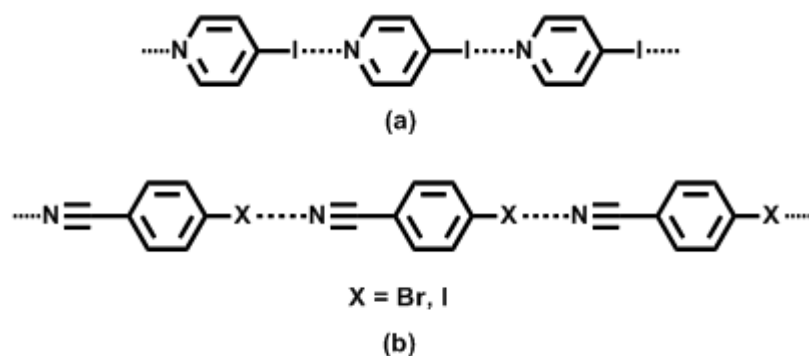


Figure 1.12 Infinite 1-D chains seen in the single-crystal structure of 4-iodopyridine (a) and 4-iodo/bromobenzonitrile (b).

Fluorination of the aromatic rings results in shorter $\text{N}\cdots\text{X}$ ($\text{X} = \text{Br, I}$) bond distances, as in the case of 4-iodo-2,3,5,6-tetrafluorobenzonitrile⁵⁰ and 4-bromo-2,3,5,6-tetrafluorobenzonitrile.⁵⁰ This is expected, as the electron-withdrawing effect of the fluorine atoms on the phenyl ring increases the positive charge on the tip of the halogen atoms, thus strengthening the electrostatic interaction between the nitrogen atom and the halogen atom.

Carbonyl oxygen atoms can also act as effective halogen-bond acceptors, as seen in 4-iodoacetophenone⁵¹ and 4-bromoacetophenone,⁵¹ wherein the directional $\text{C}=\text{O}\cdots\text{X}$ ($\text{X} = \text{Br, I}$) halogen-bonds give rise to 1-D chains in the solid-state (Figure 1.13).

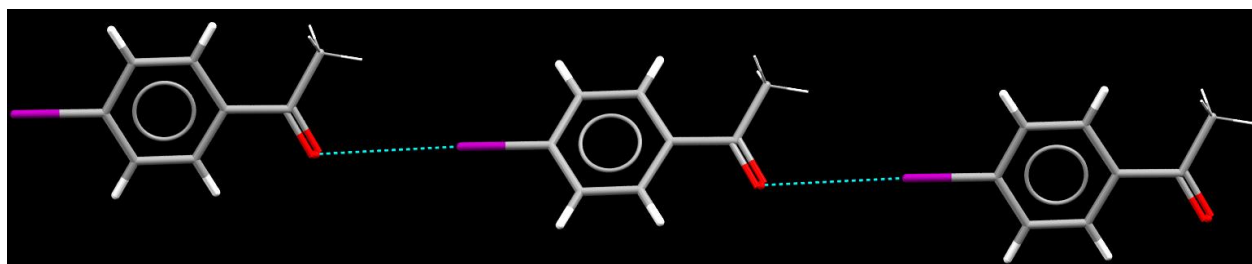


Figure 1.13 1-D chains seen in the single-crystal structure of 4-iodoacetophenone.⁵¹

1.2.2.3.2 Halogen \cdots halogen interactions

Halogenated aryls ($\text{X} = \text{Cl, Br, I}$) are known to form structure-directing bifurcated halogen \cdots halogen interactions in the solid-state (Figure 1.14),⁵² and these interactions have been used for the assembly of supramolecular architectures.⁴⁵

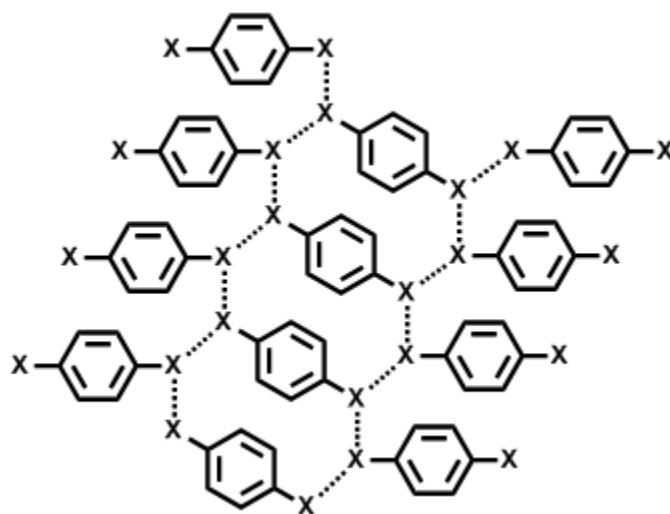


Figure 1.14 Homomeric bifurcated halogen \cdots halogen interactions in halogenated aryls (X = Cl, Br, I).

1.3 Crystal engineering

‘Crystal engineering’ is the design and synthesis of *predictable* and *controllable* solid-state architectures with desired properties, based on the knowledge of different intermolecular interactions. This term was first used by Schmidt in 1971 as part of his study on the photodimerization reactions in crystalline cinnamic acids.⁵³ The meaning of this term has broadened since then to include solid-state supramolecular chemistry, and a more modern definition has been provided by Desiraju, who defined it as “*the understanding of intermolecular interactions in the context of crystal packing and the utilization of such understanding in the design of new solids with desired physical and chemical properties*”.⁵⁴ Thus, it is important to control the arrangement of the molecules in the solid-state, as this would enable us to control many of the bulk-properties of the materials.⁵⁵

1.3.1 Supramolecular synthons

A molecular recognition event usually involves an interaction between complementary forces, such as hydrogen-bonding motifs or a metal and a ligand. Desiraju coined the term ‘supramolecular synthon’ as an analogy to the retrosynthetic approach to organic synthesis, and defined it as “*structural units within supermolecules that can be formed and/or assembled by known or conceivable synthetic operations involving intermolecular interactions*”.²⁹ Common synthons include the carboxylic acid and amide homomeric dimers, and the carboxylic acid-

pyridine heteromeric dimer (Figure 1.15). Supramolecular synthons are an integral part of crystal engineering, and it is important to identify the limits and conditions under which these synthons can be used to reliably assemble supramolecular architectures with specific topologies.

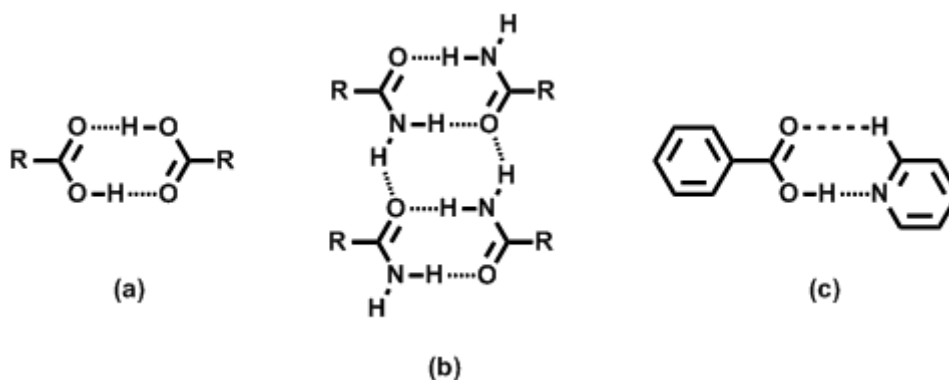


Figure 1.15 Examples of supramolecular synthons; (a) carboxylic acid dimer, (b) amide dimer, and (c) carboxylic acid-pyridine dimer.

1.3.2 Graph set notation

Graph set notation can be used to describe the hydrogen-bonded motifs, and was first introduced in 1990 by Etter *et al.* to differentiate between the different motifs on the basis of number of donors and acceptors present in the crystal structure.^{56,57} It is written as:

$$\mathbf{G}_d^a(\mathbf{n})$$

where **G** denotes the observed pattern, **n** is the degree or the total number of atoms in the motif, **a** is the number of acceptors, and **d** is the number of donors. **G** can denote one of the four possible patterns; (i) **S** (self) for intramolecular hydrogen-bonds, (ii) **C** (chain) for infinite chains, (iii) **R** (ring) for intermolecular rings, and (iv) **D** (discrete) for finite structures. The terms **a** and **d** are omitted when **a** = **d** = 1, and also **n** is omitted in the case of **D** when there is only one hydrogen-bond. Some examples of different graph set notations are given in Figure 1.16.

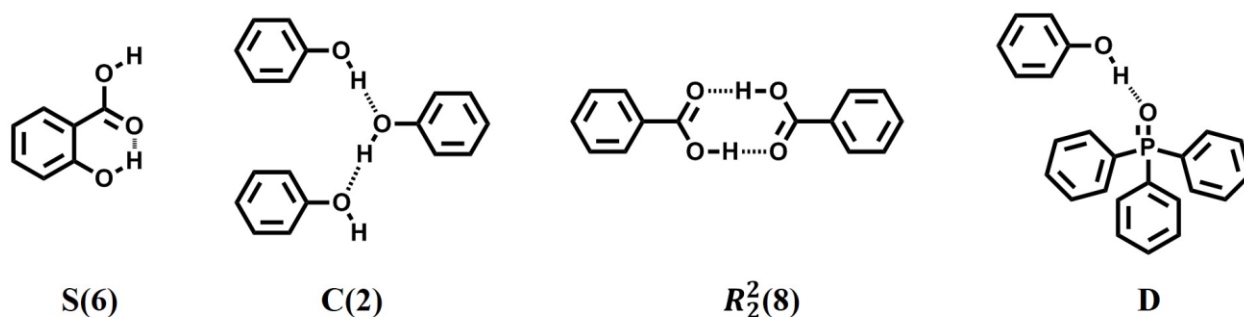


Figure 1.16 Examples of different graph set notations.

1.3.3 Etter's rules for hydrogen-bonds

A systematic examination of the single-crystal structures of hydrogen-bonded organic compounds, led Etter *et al.* to establish three guidelines pertaining to these architectures:^{56,58}

1. All good hydrogen-bond donors and acceptors in a system are involved in hydrogen-bonding.⁵⁹
2. Six-membered ring intramolecular hydrogen-bonds form in preference to intermolecular hydrogen-bonds.
3. The best hydrogen-bond donor and the best hydrogen-bond acceptor remaining after intramolecular hydrogen-bond formation will form intermolecular hydrogen-bonds with each other.

In general, the hydrogen-bond donor capabilities of a proton increase with the increasing acidity of the proton. Also, the intramolecular hydrogen-bond is preferred over the intermolecular hydrogen-bond, because it has been shown by competition studies that intramolecular hydrogen-bonds are more difficult to break than intermolecular hydrogen-bonds involving the same set of donors and acceptors. The third rule is illustrated by an examination of the crystal structure of the co-crystal of 4-bromophenylcyanooxime and 1-[(3-cyanophenyl)-methyl]-5,6-dimethylbenzimidazole (1:1) (Figure 1.17),⁶⁰ in which the best donor (oxime O-H proton) binds to the best acceptor (benzimidazole nitrogen atom).

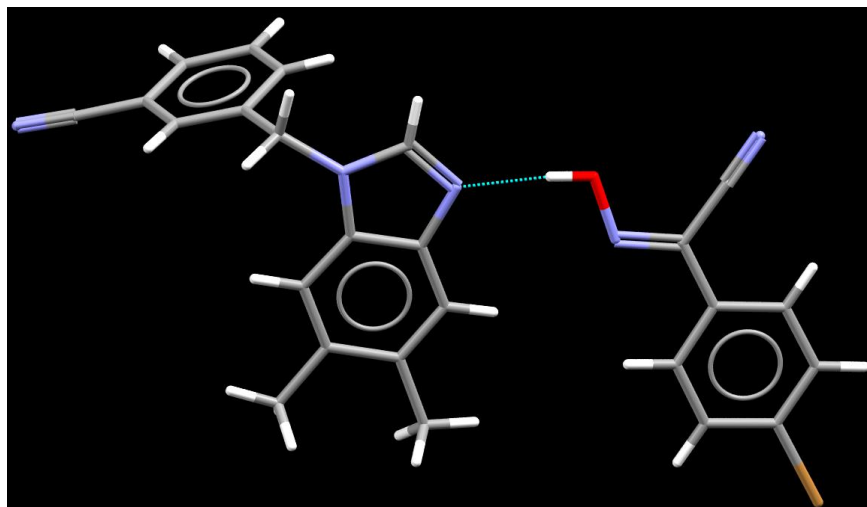


Figure 1.17 Single-crystal structure of a 1:1 co-crystal of 4-bromophenylcyanooxime and 1-[(3-cyanophenyl)-methyl]-5,6-dimethylbenzimidazole.⁶⁰

1.3.4 Crystal structure prediction

It is important to know the crystal structure of single and multi-component crystals for the purpose of understanding the role played by different intermolecular interactions in the solid-state. Consequently, there has been much research into crystal structure prediction (CSP) in the past few decades, and the goal is the development of a reliable computational method for predicting how a molecule will crystallize in the solid-state, with only the chemical diagram and the crystallization conditions known.⁶¹ The main methodology used in CSP is global lattice energy minimization, wherein structure searching methods are used to generate the different possible ways of packing a molecule into a crystal, which are then ranked on the basis of their calculated energies.⁶² These structures and their corresponding energies are used to map out the crystal energy landscape for a given system, and the structures corresponding to the lowest energy values on the crystal energy landscape are assumed to be the ones that are most likely going to be observed experimentally. The results of such calculations have demonstrated that a large number of different crystal structures are possible for most molecules, and that these structures are usually so close in energy that relative crystal energies need to be accurate to a fraction of a kJ mol^{-1} for making a confident ranking.⁶²

The reliability of CSP has been evaluated by blind tests conducted periodically by the Cambridge Crystallographic Data Centre (CCDC). The tests were started in 1999 (CSP1999)⁶³ and showed only occasional success in 2001 (CSP2001)⁶⁴ and 2004 (CSP2004),⁶⁵ until there was

a significant level of success in predicting the crystal structures with small organic molecules in 2007⁶⁶ (CSP2007). The latest blind test conducted by CCDC in 2010 (CSP2010)⁶¹ showed mixed results, and few participating groups were able to predict the crystal structure of the three small molecules included in the test. Also, the crystal structure prediction of salts and solvates posed a serious challenge to all the participating groups,⁶¹ with the highlight being the successful prediction of the crystal structure of a model pharmaceutical compound.⁶²

It has been demonstrated by these blind tests that methodologies such as dispersion-corrected density functional theory (DFT-D) can be reliably used to predict the crystal structures involving small rigid organic molecules, but significant progress needs to be made in order to successfully predict the crystal structures of more complex systems.⁶¹ Hence, single-crystal X-ray crystallography remains the most reliable and robust method till date for determining the crystal structures of compounds, thus allowing for a detailed study of the intermolecular interactions present in the solid-state.

1.3.5 Multi-component crystals – Co-crystals

Recrystallization (coming together of like molecules in the crystal lattice - homomeric product) has been a reliable method of purification for centuries, and the inherent selfish nature of molecules is responsible for this phenomenon.⁶⁷ On the other hand, co-crystallization can be defined as bringing together two or more different molecular species in a crystalline lattice without the breaking or making of covalent bonds (heteromeric product) (Figure 1.18).⁶⁸ In general, recrystallization is greatly favored over co-crystallization, hence it is important to come up with reliable and robust synthetic routes towards the directed assembly of molecular co-crystals.

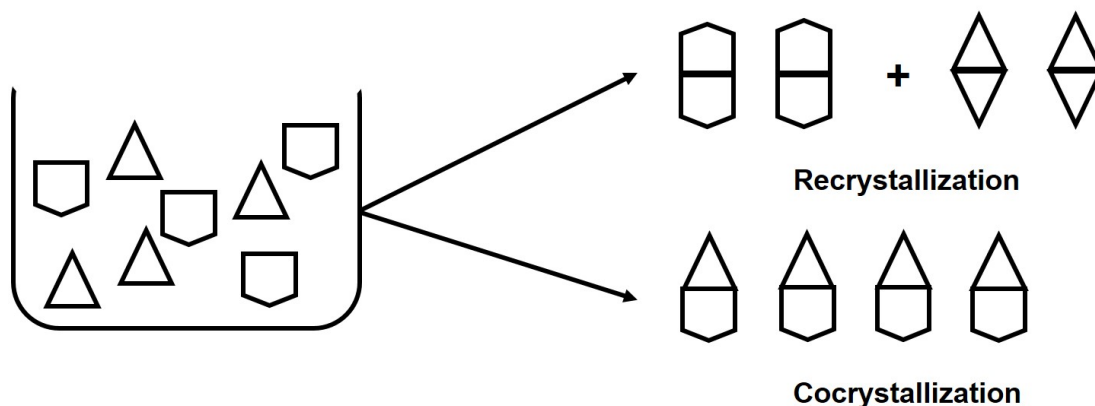


Figure 1.18 Recrystallization (homomeric) vs co-crystallization (heteromeric).

The definition of the term ‘co-crystal’ has been debated for long,⁶⁹ but for all practical purposes, the three salient features are as follows:

1. A structurally homogeneous crystalline compound constructed from discrete *neutral* molecular species is considered as a co-crystal,⁶⁸ whereas charged species are considered salts.
2. The reactants must be solids under ambient conditions. All cases where there is accidental inclusion of molecules or solvents in the crystal lattice (not intended initially), such as solvates and hydrates have been excluded.
3. The stoichiometric amounts of all the neutral building blocks must be definite.

Solution-based methods are usually employed in the synthesis of co-crystals, wherein the building blocks are dissolved in a suitable solvent (moderate to good solubility of the building blocks), and the solvent is evaporated under ambient conditions. More recently, solid-state grinding⁷⁰ and melting⁷¹ have also been utilized in the synthesis of co-crystals.

A better understanding of the intermolecular forces of interaction that are responsible for two or more molecules binding to one another in a crystalline lattice, and exerting a supramolecular control (fine-tuning electrostatics) on these forces of interaction is the way to a directed and predictable assembly of supramolecular architectures (binary/ternary co-crystals) from smaller building blocks.

1.3.5.1 Co-crystals based on hydrogen-bonds

Assembly of molecular co-crystals based on hydrogen-bonds can in principle lead to 0-D, 1-D, 2-D, and 3-D supramolecular architectures, depending upon the building blocks and the intermolecular interactions present in the crystal lattice.

Some examples of 0-D hydrogen-bonded binary co-crystals include heteromeric: carboxylic acid:carboxylic acid dimers (1:1),⁷² carboxylic acid:amide dimers (1:1),⁷³ carboxylic acid:pyridine dimers (1:1),⁷⁴ and carboxylic acid:2-aminopyrimidine trimers (2:1),⁷⁵ (Figure 1.19).

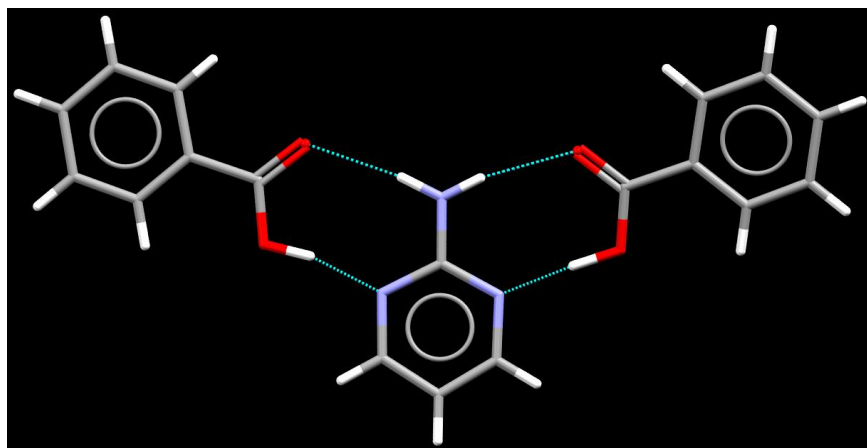


Figure 1.19 A 0-D hydrogen-bonded co-crystal of benzoic acid:2-aminopyrimidine (2:1).⁷⁵

Common examples of hydrogen-bonded co-crystals containing infinite 1-D motifs are bipyridine:dihydroxybenzene (Figure 1.20),⁷⁶ 2-aminopyrimidine:dicarboxylic acids,⁷⁷ diols:diamines,^{35b} and 2-aminopyrimidine:dicarboxylic acids.⁷⁸

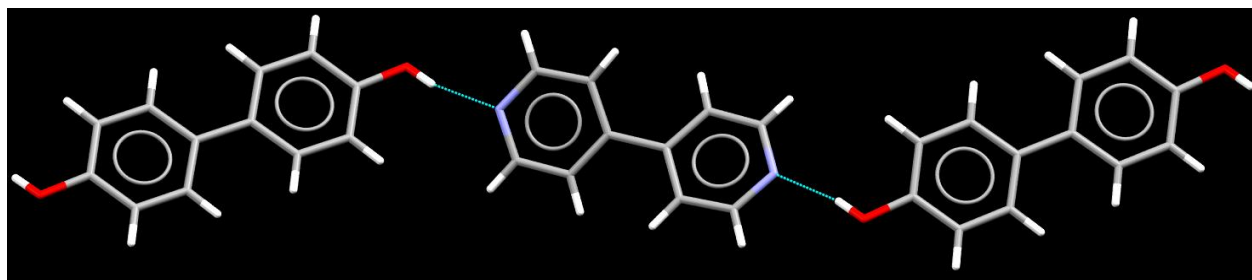


Figure 1.20 An infinite 1-D chain in the hydrogen-bonded co-crystal of 4,4'-biphenol:4,4'-bipyridine.⁷⁶

Common examples of 2-D architectures in hydrogen-bonded co-crystals include: piperazine:carboxylic acid (Figure 1.21),⁷⁹ trithiocyanuric acid:bipyridine,⁸⁰ triazine:uracil,⁸¹ and isonicotinamide:dicarboxylic acid.⁸²

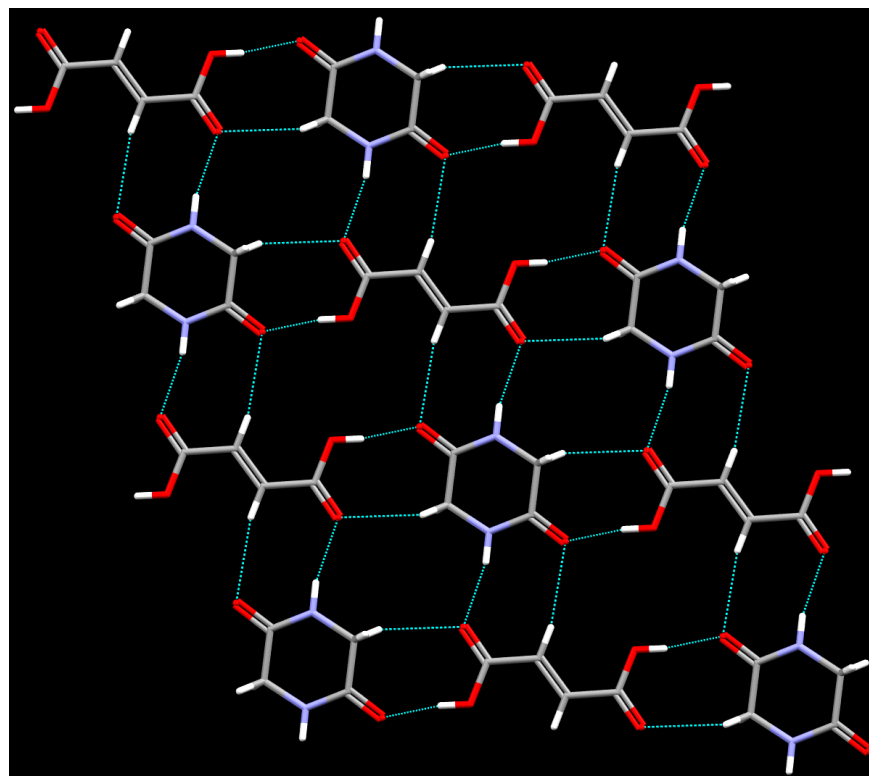


Figure 1.21 Two-dimensional tapes formed in the hydrogen-bonded co-crystal of piperazine-2,5-dione:fumaric acid.⁷⁹

1.3.5.2 Co-crystals based on halogen-bonds

As explained in Section 1.2.2.3, a halogen-bond is an electrostatic interaction between the electron-deficient tip of a halogen atom and electronegative atoms such as N/O/S.⁴⁷ Increased positive charge on the tip of the halogen atom ($I > Br > Cl$) results in stronger halogen-bonds.⁸³ Fluorinating the aliphatic/aromatic compounds has often been used as a tool to increase the halogen-bond donor strength of the halogen atoms, resulting in stronger halogen-bonds.⁵⁰

Much work has been done in the past ten years on the directed assembly of heteromeric molecular co-crystals based on halogen-bonds.⁴⁵ Some common halogen-bond donors include iodo/bromo-perfluoroalkyls, iodo/bromo-perfluoroaromatics, and iodo/bromoaromatic compounds, whereas common halogen-bond acceptors include (but are not limited to) pyridines, nitriles, carbonyls and thiols.^{45,47,84}

Steed *et al.* have synthesized a halogen-bonded supramolecular gel based on the 1:1 co-crystal of 1,1'-(butane-1,4-diyl)bis(3-pyridin-3-ylurea):2,3,5,6-tetrafluoro-1,4-di-iodobenzene (Figure 1.22).⁸⁵

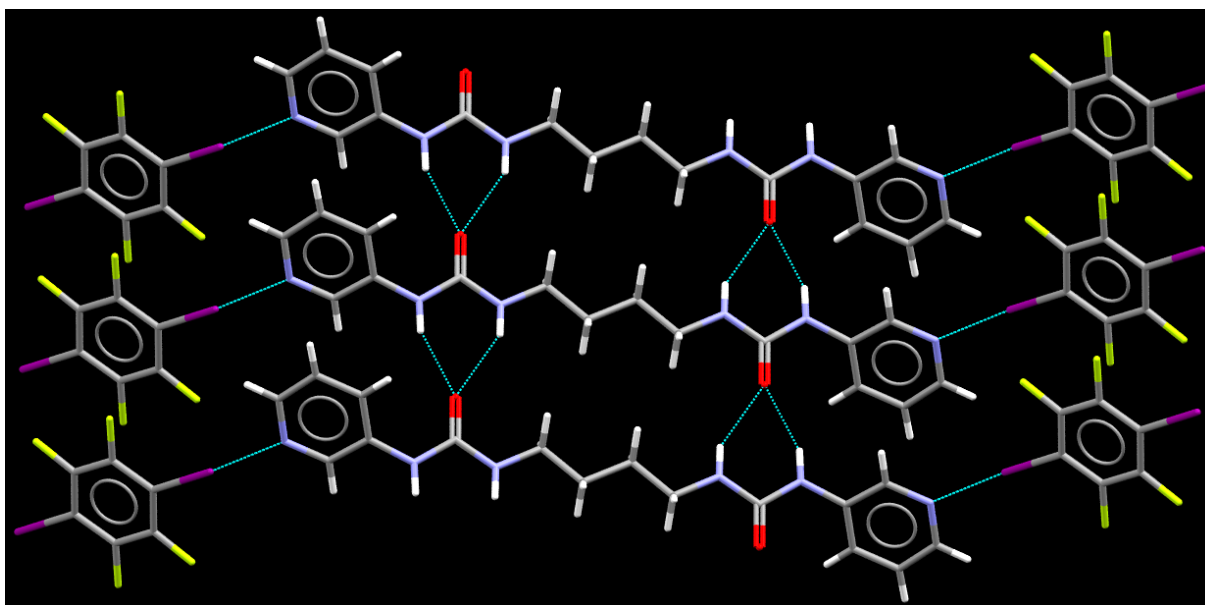


Figure 1.22 Two-dimensional halogen-bonded motifs formed in the 1:1 co-crystal of 1,1'-(butane-1,4-diyl)bis(3-pyridin-3-ylurea):2,3,5,6-tetrafluoro-1,4-di-iodobenzene.⁸⁵

1.3.5.3 Applications of co-crystals

A common and persistent problem in the pharmaceutical industry is the bio-availability of active pharmaceutical ingredient (API), due to poor physicochemical properties of the API.⁸⁶ Traditionally, this problem has been tackled by crystal form modifications, such as by forming salts, polymorphs and hydrates.⁸⁷ More recently, directed co-crystallization has been used as a technique for modifying the physicochemical properties of APIs.⁸⁸ The potential benefits of such a targeted assembly include: (i) all APIs (acidic, basic, non-ionizable) can potentially be used to form co-crystals, (ii) most of the co-formers included in API co-crystallization are non-toxic, and (iii) co-crystalline architectures are often reliable and controllable, as opposed to polymorphs and solvates, which are often serendipitous. Thus, a directed and controlled co-crystallization of APIs with inexpensive and non-toxic coformers is an attractive route to modifying the physicochemical properties, such as solubility and stability.

An example is meloxicam which has poor aqueous solubility, and is a non-steroidal anti-inflammatory drug. Meloxicam has sulfonyl groups which can act as potential hydrogen-bond acceptors (Figure 1.23), consequently Zaworotko *et al.* co-crystallized it with twelve carboxylic acids (hydrogen-bond donors), and observed that of the twelve co-crystals, nine showed greater maximum meloxicam concentration, when compared to the drug by itself.⁸⁹ In particular, two co-

crystalline forms of meloxicam showed remarkable improvement in the aqueous solubility of the drug, and hypothetical therapeutic serum concentration was achieved.

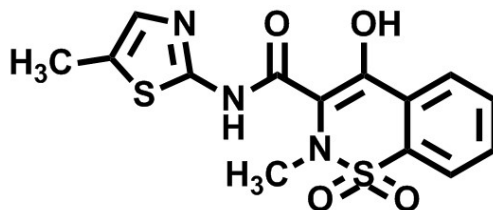


Figure 1.23 Molecular structure of meloxicam.

1.4 Goals

Supramolecular chemistry is analogous to change, and for change to take effect, one needs effective tools of communication. For advancing this change to a predictable and directed assembly of architectures with useful properties, one needs to gain a handle over the various tools of communication, which in turn will allow us to synthesize new supramolecular architectures with a high degree of specificity and reliability (Figure 1.24).

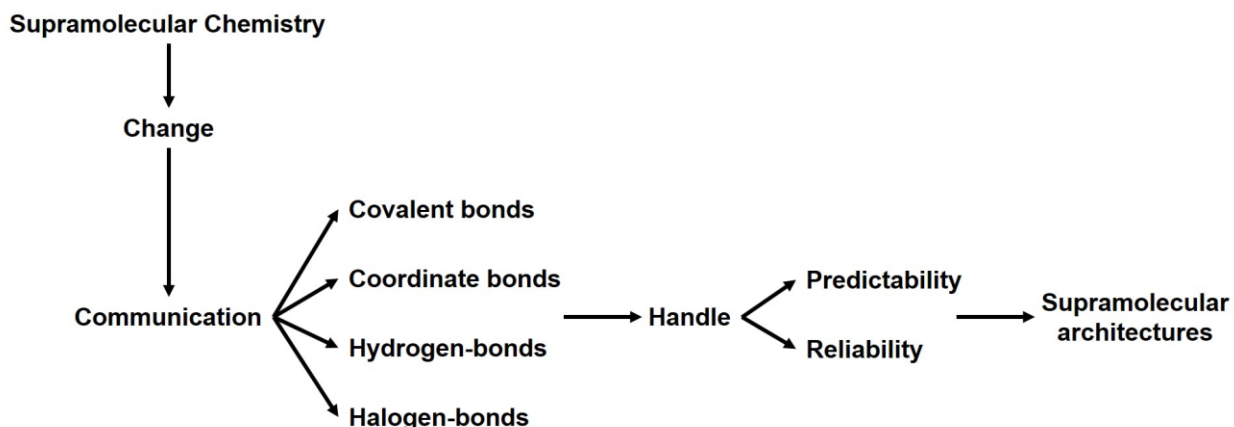


Figure 1.24 Design and synthesis of predictable and reliable supramolecular architectures.

The primary goals of this thesis are centered on predictably arranging molecular building-blocks into supermolecules through reliable and robust intermolecular interactions, wherein the building-blocks have been derived from versatile and 'green' synthetic routes. Consequently, the following chapters will be aimed mostly at mapping out the synthetic landscape surrounding these reactions and establishing a reliable hierarchy of the non-covalent interactions in the solid-state.

1.4.1 Investigating the importance of weak halogen···halogen bonds in predictably arranging coordination complexes in the solid-state

Directed assembly of copper(II) coordination complexes with bi-functional ligands containing a metal-coordinating moiety and a halogen-bond donor will be explored for establishing the relevance of weaker halogen···halogen interactions with comparison to close-packing in the solid-state (Chapter 2). We will use the acetylacetonate moiety as the metal-coordinating ligand, in order to assemble coordination complexes in the absence of any counterions and solvents, for the purpose of exclusively focusing on the weaker intermolecular interactions. The organic backbone will also be decorated with four different substituents (CH₃, Cl, Br, I) to test the balance between close-packing and halogen-bonding in the crystalline lattice.

1.4.2 Establishing the versatility and robustness of a ‘green’ synthetic route to aldehyde/ketone-oxime conversions

A solvent-assisted mechanochemical route to aldehyde/ketone-oxime conversions will be explored for the oxime functional group (ubiquitous in both research laboratories and in industries) (Chapter 3). The limits and limitations (if any) of this synthetic procedure will be examined by decorating the starting materials with a range of substituents, such as electron withdrawing, electron donating, structurally active functional groups, multi-functionalized, and aliphatic groups. The products will be characterized by infra-red spectroscopy and ¹H NMR spectroscopy, and the reliability of these characterization techniques for identifying oximes will also be established. Any electronic effects affecting this transformation will also be explored.

1.4.3 Identifying the different ‘supramolecular synthons’ of the oxime motif

The oxime moiety (RR'C=N-OH) has multiple hydrogen-bond acceptors and one donor, which gives rise to different self-complementary hydrogen-bonding motifs in the solid-state, such as dimers and catemers. The hierarchy and reliability of these homomeric oxime···oxime motifs for four major categories of oximes (R' = H, CH₃, NH₂, CN) will be established by examining the available single-crystal data in the Cambridge Structural Database (CSD), complemented by three new crystal structures (Chapter 4). The observed trends will be explained on the basis of molecular electrostatic potentials (MEPs), along with identifying and establishing the common supramolecular synthons for oxime···oxime interactions.

1.4.4 Establishing a hierarchical assembly approach through hydrogen and halogen bonding

A hierarchy must be established in order to rationally design any supramolecular architecture, in which multiple competing non-covalent interactions exist, such as hydrogen and halogen-bonds. We will employ a series of ethynylhalogenated/oxime ligands, capable of simultaneous and/or halogen/hydrogen-bonding, to form predictable supramolecular products through a combination of hydrogen and halogen-bonds (Chapter 5). We will compare the relative halogen-bond donor strength of the bromo and iodo substituents, along with exploring the relative competition between the ethynylhalogenated and oxime moieties.

1.4.5 Design and synthesis of a versatile metallomacrocycle

Metallomacrocycles capable of controlling the metal-metal distance find use in anion-binding, host-guest chemistry, etc. We will design and synthesize a dynamic and modular metallomacrocycle based on the 2,2'-bipyridyl backbone, capable of controlling the intramolecular metal-metal distance within the macrocycle cavity (Chapter 6). The macrocycle will be synthesized by high-dilution method and characterized by several spectroscopic techniques (IR, NMR, Mass, UV-Visible). Also, the macrocycle:Cu(II) stoichiometric ratio will be determined by Job's continuous variation method using UV-Visible spectroscopy.

References

- 1 Fischer, E. *Ber. Dt. Chem. Ges.* **1894**, *27*, 2985.
- 2 Lehn, J.-M. *Supramolecular Chemistry: Concepts and Perspectives* **1995**, VCH, Weinheim.
- 3 Desiraju, G. R. *Nature* **2001**, *412*, 397.
- 4 Lehn, J.-M. *Pure & Appl. Chem.* **1980**, *52*, 2441.
- 5 (a) Bolton, O.; Simke, L. R.; Pagoria, P. F.; Matzger, A. J. *Cryst. Growth Des.* **2012**, *12*, 4311. (b) Kim, S.; Li, Z.; Tseng, Y.-C.; Nar, H.; Spinelli, E.; Varsolona, R.; Reeves, J. T.; Lee, H.; Song, J. J.; Smoliga, J.; Yee, N.; Senanayake, C. *Org. Proc. Res. Dev.* **2013**, *17*, 540.
- 6 (a) Corey, E. J. *Chem. Soc. Rev.* **1988**, *17*, 111. (b) Nicolaou, K. C.; Sorenson, E. J. *Classics in total synthesis*, Wiley-VCH, Weinheim, 1996. (c) Corey, E. J. *Angew. Chem., Int. Ed.* **2009**, *48*, 2100.
- 7 Sheehan, J. C.; Henery-Logan, K. R. *J. Am. Chem. Soc.* **1959**, *81*, 3089.
- 8 (a) Moulton, B.; Zaworotko, M. J. *Chem. Rev.* **2001**, *101*, 1629. (b) Desiraju, G. R. *Acc. Chem. Res.* **2002**, *35*, 565.
- 9 Werner, A. Z. *Anorg. Allg. Chem.* **1893**, *3*, 267.
- 10 (a) Bailar, J. C., Jr. *Coord. Chem. Rev.* **1980**, *31*, 53. (b) Bailar, J. C., Jr. *Coord. Chem. Rev.* **1990**, *100*, 1.
- 11 (a) Wiester, M. J.; Ulmann, P. A.; Mirkin, C. A. *Angew. Chem., Int. Ed.* **2011**, *50*, 114. (b) Garcia, J.; Allen, M. J. *Eur. J. Inorg. Chem.* **2012**, *29*, 4550. (c) Reedijk, J. *Chem. Soc. Rev.* **2013**, *42*, 1776.
- 12 (a) Lee, J.; Farha, O. K.; Roberts, J.; Scheidt, K. A.; Nguyen, S. T.; Hupp, J. T. *Chem. Soc. Rev.* **2009**, *38*, 1450. (b) Ma, L.; Abney, C.; Lin, W. *Chem. Soc. Rev.* **2009**, *38*, 1248.
- 13 (a) Carra, J. R.; Walton, K. S. *Langmuir* **2008**, *24*, 8620. (b) Allendorf, M. D.; Bauer, C. A.; Bhakta, R. K.; Houk, R. J. T. *Chem. Soc. Rev.* **2009**, *38*, 1330.
- 14 (a) Liu, Z.; He, W.; Guo, Z. *Chem. Soc. Rev.* **2013**, *42*, 1568. (b) Wenger, O. S. *Chem. Rev.* **2013**, *113*, 3686.
- 15 (a) Horcajada, P.; Serre, C.; Maurin, G.; Ramsahye, N. A.; Balas, F.; Vallet-Regi, M.; Sebban, M.; Taulelle F.; Fèrey, G. *J. Am. Chem. Soc.* **2008**, *130*, 677. (b) Taylor-Pashow, K. M. L.; Rocca, J. D.; Huxford, R. C.; Lin, W. *Chem. Commun.* **2010**, *46*, 5832. (c) Huxford, R. C.; Rocca, J. D.; Lin, W. *Curr. Opin. Chem. Biol.* **2010**, *14*, 262.
- 16 Sague, J. L.; Meuwly, M.; Fromm, K. M. *CrystEngComm* **2008**, *10*, 1542.
- 17 Yang, P.; Wu, J.-J.; Zhou, H.-Y.; Ye, B.-H. *Cryst. Growth Des.* **2012**, *12*, 99.
- 18 (a) Guo, Y.; Shi, T.; Si, Z.; Duan, Q.; Shi, L. *Inorg. Chem. Commun.* **2013**, *34*, 15. (b) Tian, J.; Li, B.; Zhang, X.; Li, X.; Li, X.; Zhang, J. *Dalton Trans.* **2013**, *42*, 8504. (c) Amo-Ochoa, P.; Delgado, E.; Gomez-Garcia, C. J.; Hernandez, D.; Hernandez, E.; Martin, A.; Zamora, F. *Inorg. Chem.* **2013**, *52*, 5943.
- 19 (a) Bharti, A.; Bharati, P.; Bharty, M. K.; Dani, R. K.; Singh, S.; Singh, N. K. *Polyhedron* **2013**, *54*, 131. (b) Liu, B.; Wang, R.; Jin, G.; Meng, X. J. *Coord. Chem.* **2013**, *66*, 1784.
- 20 Wu, J.-J.; Ye, Y.-X.; Qiu, Y.-Y.; Qiao, Z.-P.; Cao, M.-L.; Ye, B.-H. *Inorg. Chem.* **2013**, *52*, 6450.
- 21 (a) Evans, O. R.; Xiong, R.-G.; Wang, Z.; Wong, G. K.; Lin, W. *Angew. Chem., Int. Ed.* **1999**, *38*, 536. (b) O'Keeffe, M.; Peskov, M. A.; Ramsden S. J.; Yaghi, O. M. *Acc. Chem. Res.* **2008**, *41*, 1782.

-
- 22 (a) Batten, S. R.; Robson, R. *Angew. Chem., Int. Ed.* **1998**, *37*, 1460. (b) Blake, A. J.; Champness, N. R.; Hubberstey, P.; Li, W.-S.; Withersby, M. A.; Schröder, M. *Coord. Chem. Rev.* **1999**, *183*, 117. (c) Wang, Z.; Cohen, S. M. *Chem. Soc. Rev.* **2009**, *38*, 1315. (d) Cohen, S. M. *Chem. Sci.* **2010**, *1*, 32.
- 23 (a) Parkes, M. V.; Staiger, C. L.; Perry, J. J., IV; Allendorf, M. D.; Greathouse, J. A. *Phys. Chem. Chem. Phys.* **2013**, *15*, 9093. (b) Weston, M. H.; Delaquil, A. A.; Sarjeant, A. A.; Farha, O. K.; Hupp, J. T.; Nguyen, S. T. *Cryst. Growth Des.* **2013**, DOI:10.1021/cg400342m.
- 24 (a) Duerinck, T.; Bueno-Perez, R.; Vermoortele, F.; De Vos, D. E.; Calero, S.; Baron, G. V.; Denayer, J. F. M. *J. Phys. Chem. C* **2013**, *117*, 12567. (b) Herm, Z. R.; Wiers, B. M.; Mason, J. A.; van Baten, J. M.; Hudson, M. R.; Zajdel, P.; Brown, C. M.; Masciocchi, N.; Krishna, R.; Long, J. R. *Science* **2013**, *340*, 960.
- 25 Farha, O. K.; Eryazici, I.; Jeong, N. C.; Hauser, B. G.; Wilmer, C. E.; Sarjeant, A. A.; Snurr, R. Q.; Nguyen, S. T.; Yazaydin, A. O.; Hupp, J. T. *J. Am. Chem. Soc.* **2012**, *134*, 15016.
- 26 (a) Seto, C. T.; Whitesides, G. M. *J. Am. Chem. Soc.* **1991**, *113*, 712. (b) Aakeröy, C. B.; Seddon, K. R. *Chem. Soc. Rev.* **1993**, *22*, 397. (c) Tiekink, E. R. T.; Vittal, J.; Zaworotko, M. *Organic Crystal Engineering: Frontiers in Crystal Engineering*, 1st ed.; Wiley, John & Sons, Inc.: Chichester, U.K., 2010.
- 27 (a) Lehn, J.-M. *Science* **2002**, *295*, 2400. (b) Wittenberg, J. B.; Isaacs, L. Complementarity and Preorganization. In *Supramolecular Chemistry: From Molecules to Nanomaterials*, 2012; Vol. 1; pp 25-43.
- 28 (a) Hamilton, W. C.; Ibers, J. A. *Hydrogen Bonding in Solids*; W. A. Benjamin: New York, 1968. (b) Herbstein, F. H. In *Comprehensive Supramolecular Chemistry*; MacNicol, D. D.; Toda, F.; Bishop, R., Ed.; Pergamon Press: New York, 1996; Vol. 6; pp 61-83.
- 29 Desiraju, G. R. *Angew. Chem., Int. Ed. Engl.* **1995**, *34*, 2311.
- 30 Mareque Rivas, J. C.; Brammer, L. *New J. Chem.* **1998**, *22*, 1315.
- 31 (a) Bertalosi, V.; Gilli, G.; Veronese, A. *Acta. Crystallogr., Sect. B.* **1982**, *B38*, 502. (b) Bruton, E. A.; Brammer, L.; Pigge, F. C.; Aakeröy, C. B.; Leinen, D. S. *New J. Chem.* **2003**, *27*, 1084.
- 32 Cai, W.; Katrusiak, A. *CrystEngComm* **2012**, *14*, 4420.
- 33 Herbstein, F. H.; Marsh, R. E. *Acta. Crystallogr., Sect. B.: Struct. Sci.* **1998**, *54*, 677.
- 34 Chao, M.; Schempp, E.; Rosenstein, R. D. *Acta. Crystallogr., Sect. B.: Struct. Crystallogr. Cryst. Chem.* **1975**, *31*, 2922.
- 35 (a) Bordwell, F. G.; McCallum, R. J.; Olmstead, W. N. *J. Org. Chem.* **1984**, *49*, 1424. (b) Ermer, O.; Eling, A. *J. Chem. Soc., Perkin Trans. 2* **1994**, 925.
- 36 Legrand, Y.-M.; Michau, M.; van der Lee, A.; Barboiu, M. *CrystEngComm* **2008**, *10*, 490.
- 37 Bailey, M.; Brown, C. J. *Acta. Crystallogr.* **1967**, *22*, 387.
- 38 Aakeröy, C. B.; Desper, J.; Elisabeth, E.; Helfrich, B. A.; Levin, B.; Urbina, J. F. *Z. Kristallogr.* **2005**, *220*, 325.
- 39 Kurth, T. L.; Lewis, F. D. *J. Am. Chem. Soc.* **2003**, *125*, 13760.
- 40 Low, J. N.; Santos, L. M. N. B. F.; Lima, C. F. R. A. C.; Brandao, P.; Gomes, L. R. *Eur. J. Chem.* **2010**, *1*, 61.
- 41 Duchamp, D. J.; Marsh, R. E. *Acta. Crystallogr., Sect. B.* **1969**, *25*, 5.
- 42 Kawakami, Y.; Sakuma, Y.; Wakuda, T.; Nakai, T.; Shirasaka, M.; Kabe, Y. *Organometallics* **2010**, *29*, 3281.

-
- 43 Ermer, O. *J. Am. Chem. Soc.* **1988**, *110*, 3747.
- 44 Kusukawa, T.; Niwa, G.; Sasaki, T.; Oosawa, R.; Himeno, W.; Kato, M. *Bull. Chem. Soc. Jpn.* **2013**, *86*, 351.
- 45 (a) Metrangolo, P.; Resnati, G. *Cryst. Growth Des.* **2012**, *12*, 5835. (b) Troff, R. W.; Mäkelä, T.; Topic', F.; Valkonen, A.; Raatikainen, K.; Rissanen, K. *Eur. J. Org. Chem.* **2013**, 1617.
- 46 (a) Corradi, E.; Meille, S. V.; Messina, M. T.; Metrangolo, P.; Resnati, G. *Angew. Chem., Int. Ed.* **2000**, *39*, 178. (b) Aakeröy, C. B.; Schultheiss, N.; Desper, J.; Moore, C. *CrystEngComm* **2007**, *9*, 421. (c) Friščić, T.; Meštrović, E.; Šamec, D. S.; Kaitner, B.; Fábíán, L. *Chem. Eur. J.* **2009**, *15*, 12644. (d) Lapadula, G.; Judaš, N.; Friščić, T.; Jones, W. *Chem. Eur. J.* **2010**, *16*, 7400. (e) Aakeröy, C. B.; Chopade, P. D.; Ganser, C.; Desper, J. *Chem. Commun.* **2011**, *47*, 4688.
- 47 (a) Pedireddi, V. R.; Reddy, D. S.; Goud, G. S.; Craig, D. C.; Rae, A. D.; Desiraju, G. R. *J. Chem. Soc. Perkin Trans. II* **1994**, *11*, 2353. (b) Metrangolo, P.; Resnati, G. *Chem. Eur. J.* **2001**, *7*, 2511. (c) Metrangolo, P.; Resnati, G. ed. *Halogen Bonding: Fundamentals and Applications, Structure and Bonding*, Springer, Berlin, 2007. (d) Brammer, L.; Espallargas, G. M.; Libri, S. *CrystEngComm* **2008**, *10*, 1712.
- 48 Ahrens, B.; Jones, P. G. *Acta Crystallogr., Sect. C.: Cryst. Struct. Commun.* **1999**, *55*, 1308.
- 49 Desiraju, G. R.; Harlow, R. L. *J. Am. Chem. Soc.* **1989**, *111*, 6757.
- 50 Bond, A. D.; Griffiths, J.; Rawson, J. M.; Hulliger, J. *Chem. Commun.* **2001**, 2488.
- 51 Britton, D.; Brennessel, W. W. *Acta Crystallogr., Sect. C.: Cryst. Struct. Commun.* **2004**, *60*, o552.
- 52 (a) Maiga, A.; Haget, Y.; Cuevas-Diarte, M. A. *J. Appl. Crystallogr.* **1984**, *17*, 210. (b) Estop, E.; Alvarez-Ilerena, A.; Belaaraj, A.; Solans, X.; Labrador, M. *Acta Cryst. C.* **1997**, *53*, 1932.
- 53 Schmidt, G. M. J. *Pure Appl. Chem.* **1971**, *27*, 647.
- 54 Desiraju, G. R. *Crystal Engineering: The design of Organic Solids*, Elsevier, Amsterdam, 1989.
- 55 (a) Aakeröy, C. B.; Scott, B. M. T.; Smith, M. M.; Urbina, J. F.; Desper, J. *Inorg. Chem.* **2009**, *48*, 4052. (b) Garzon-Tovar, L.; Duarte-Ruiz, A.; Wurst, K. *Inorg. Chem. Commun.* **2013**, *32*, 64. (c) Mes, T.; Cantekin, S.; Balkenende, D. W. R.; Frissen, M. M. M.; Gillissen, M. A. J.; De Waal, B. F. M.; Voets, I. K.; Meijer, E. W.; Palmans, A. R. A. *Chem. Eur. J.* **2013**, *19*, 8642.
- 56 Etter, M. C. *Acc. Chem. Res.* **1990**, *23*, 120.
- 57 Bernstein, J.; Davis, R. E.; Shimoni, L.; Chang, N.-L. *Angew. Chem., Int. Ed. Engl.* **1995**, *34*, 1555.
- 58 (a) Etter, M. C.; Frankenbach, G. M. *Chem. Mater.* **1989**, *1*, 10. (b) Etter, M. C. *J. Phys. Chem.* **1991**, *95*, 4601.
- 59 Donohue, J. *J. Phys. Chem.* **1952**, *56*, 502.
- 60 Aakeröy, C. B.; Salmon, D. J.; Smith, M. M.; Desper, J. *CrystEngComm* **2009**, *11*, 439.
- 61 Bardwell, D. A.; Adjiman, C. S.; Arnautova, Y. A.; Bartashevich, E.; Boerrigter, S. X. M.; Braun, D. E.; Cruz-Cabeza, A. J.; Day, G. N.; Della Valle, R. G.; Desiraju, G. R.; van Eijck, B. P.; Facelli, J. C.; Ferraro, M. B.; Grillo, D.; Habgood, M.; Hofmann, D. W. M.; Hofmann, F.; Jovan Jose, K. V.; Karamertzanis, P. G.; Kazantsev, A. V.; Kendrick, J.; Kuleshova, L. N.; Leusen, F. J. J.; Maleev, A. V.; Misquitta, A. J.; Mohamed, S.; Needs, R. J.; Neumann, M. A.; Nikylov, D.; Orendt, A. M.; Pal, R.; Pantelides, C. C.; Pickard, C. J.; Price, L. S.; Price, S. L.;

-
- Scheraga, H. A.; van de Streek, J.; Thakur, T. S.; Tiwari, S.; Venuti, E.; Zhitkov, I. K. *Acta Crystallogr., Sect. B.* **2011**, *B67*, 535.
- 62 Kazantsev, A. V.; Karamertzanis, P. G.; Adjiman, C. S.; Pantelides, C. C.; Price, S. L.; Galek, P. T. A.; Day, G. M.; Cruz-Cabeza, A. J. *Int. J. Pharm.* **2011**, *418*, 168.
- 63 Lommerse, J. P. M.; Motherwell, W. D. S.; Ammon, H. L.; Dunitz, J. D.; Gavezzotti, A.; Hofmann, D. W. M.; Leusen, F. J. J.; Mooij, W. T. M.; Price, S. L.; Schweizer, B.; Schmidt, M. U.; van Eijck, B. P.; Verwer, P.; Williams, D. E. *Acta Crystallogr. Sect. B.* **2000**, *B56*, 697.
- 64 Motherwell, W. D. S.; Ammon, H. L.; Dunitz, J. D.; Dzyabchenko, A.; Erk, P.; Gavezzotti, A.; Hofmann, D. W. M.; Leusen, F. J. J.; Lommerse, J. P. M.; Mooij, W. T. M.; Price, S. L.; Scheraga, H.; Schweizer, B.; Schmidt, M. U.; van Eijck, B. P.; Verwer, P.; Williams, D. E. *Acta Crystallogr. Sect. B.* **2002**, *B58*, 647.
- 65 Day, G. M.; Motherwell, W. D. S.; Ammon, H. L.; Boerrigter, S. X. M.; Della Valle, R. G.; Venuti, E.; Dzyabchenko, A.; Dunitz, J. D.; Schweizer, B.; van Eijck, B. P.; Erk, P.; Facelli, J. C.; Bazterra, V. E.; Ferraro, M. B.; Hofmann, D. W. M.; Leusen, F. J. J.; Liang, C.; Pantelides, C. C.; Karamertzanis, P. G.; Price, S. L.; Lewis, T. C.; Nowell, H.; Torrisi, A.; Scheraga, H. A.; Arnautova, Y. A.; Schmidt, M. U.; Verwer, P. *Acta Crystallogr. Sect. B.* **2005**, *B61*, 511.
- 66 Day, G. M.; Cooper, T. G.; Cruz-Cabeza, A. J.; Hejczyk, K. E.; Ammon, H. L.; Boerrigter, S. X. M.; Tan, J. S.; Della Valle, R. G.; Venuti, E.; Jose, J.; Gadre, S. R.; Desiraju, G. R.; Thakur, T. S.; van Eijck, B. P.; Facelli, J. C.; Bazterra, V. E.; Ferraro, M. B.; Hofmann, D. W. M.; Neumann, M. A.; Leusen, F. J. J.; Kendrick, J.; Price, S. L.; Misquitta, A. J.; Karamertzanis, P. G.; Welch, G. W. A.; Scheraga, H. A.; Arnautova, Y. A.; Schmidt, M. U.; van de Streek, J.; Wolf, A. K.; Schweizer, B. *Acta Crystallogr. Sect. B.* **2009**, *B65*, 107.
- 67 Dunitz, J. D. in *Perspectives in Supramolecular Chemistry: The Crystal as a Supramolecular Entity*, ed. Desiraju, G. R., Wiley, Amsterdam, 1995.
- 68 Aakeröy, C. B.; Salmon, D. J. *CrystEngComm* **2005**, *7*, 439.
- 69 (a) Desiraju, G. R. *CrystEngComm* **2003**, *5*, 466. (b) Dunitz, J. D. *CrystEngComm* **2003**, *5*, 506.
- 70 Zhang, G.-C.; Lin, H.-L.; Lin, S.-Y. *J. Pharm. Biomed. Anal.* **2012**, *66*, 162.
- 71 Liu, X.; Lu, M.; Guo, Z.; Huang, L.; Feng, X.; Wu, C. *Pharm. Res.* **2012**, *29*, 806.
- 72 Sarma, J. A. R. P.; Desiraju, G. R. *J. Chem. Soc., Perkin Trans. 2* **1985**, 1905.
- 73 Aakeröy, C. B.; Desper, J.; Helfrich, B. A. *CrystEngComm* **2004**, *6*, 19.
- 74 Sugiyama, T.; Meng, J.; Matsuura, T. *J. Mol. Struct.* **2002**, *611*, 53.
- 75 Skovsgaard, S.; Bond, A. D. *CrystEngComm* **2009**, *11*, 444.
- 76 Glidewell, C.; Ferguson, G.; Gregson, R. M.; Lough, A. J. *Acta, Crystallogr., Sect. C.: Cryst. Struct. Commun.* **1999**, *55*, 2133.
- 77 Garcia-Tellado, F.; Geib, S. J.; Goswami, S.; Hamilton, A. D. *J. Am. Chem. Soc.* **1991**, *113*, 9265.
- 78 Etter, M. C.; Adsmond, D. A. *J. Chem. Soc., Chem. Commun.* **1990**, 589.
- 79 Luo, T.-J. M.; Palmore, G. T. R. *Cryst. Growth Des.* **2002**, *2*, 337.
- 80 Pedireddi, V. R.; Chatterjee, S.; Ranganathan, A.; Rao, C. N. R. *J. Am. Chem. Soc.* **1997**, *119*, 10867.

-
- 81 Beijer, F. H.; Sijbesma, R. P.; Vekemans, J. A. J. M.; Meijer, E. W.; Kooijman, H.; Spek, A. L. *J. Org. Chem.* **1996**, *61*, 6371.
- 82 Vishweshwar, P.; Nangia, A.; Lynch, V. M. *Cryst. Growth Des.* **2003**, *3*, 783.
- 83 (a) Clark, T.; Hennemann, M.; Murray, J. S.; Politzer, P. *J. Mol. Model.* **2007**, *13*, 291. (b) Politzer, P.; Murray, J. S.; Clark, T. *Phys. Chem. Chem. Phys.* **2013**, *15*, 11178.
- 84 (a) Fourmigué, M.; Batail, P. *Chem. Rev.* **2004**, *104*, 5379. (b) Rissanen, K. *CrystEngComm* **2008**, *10*, 1107. (c) Cavallo, G.; Metrangolo, P.; Pilati, T.; Resnati, G.; Sansotera, M.; Terraneo, G. *Chem. Soc. Rev.* **2010**, *39*, 3772.
- 85 Meazza, L.; Foster, J. A.; Fucke, K.; Metrangolo, P.; Resnati, G.; Steed, J. W. *Nature Chem.* **2013**, *5*, 42.
- 86 Kola, I.; Landis, J. *Nature Reviews Drug Discovery* **2004**, *3*, 711.
- 87 Rodriguez-Spong, B.; Price, C. P.; Jayasankar, A.; Matzger, A. J.; Rodriguez-Hernedo, N. *Adv. Drug. Deliv. Rev.* **2004**, *56*, 241.
- 88 (a) Walsh, R. D. B.; Bradner, M. W.; Fleischman, S.; Morales, L. A.; Moulton, B.; Rodriguez-Hernedo, N.; Zaworotko, M. J. *Chem. Commun.* **2003**, 186. (b) Aakeröy, C. B.; Forbes, S.; Desper, J. *J. Am. Chem. Soc.* **2009**, *131*, 17048.
- 89 Weyna, D. R.; Cheney, M. L.; Shan, N.; Hanna, M.; Zaworotko, M. J.; Sava, V.; Song, S.; Sanchez-Ramos, J. R. *Mol. Pharm.* **2012**, *9*, 2094.

Chapter 2 - Halogen bonding or close packing? Examining the structural landscape in a series of Cu(II)-acac complexes

2.1 Introduction

Interest in synthesis, characterization and properties of coordination complexes over the years has led to a recent spike in research on arranging these complexes into networks of precise topology and predictable connectivity.¹ Any such research benefits the area of metal-organic frameworks (MOFs), which is arguably one of the most important fields in coordination chemistry today,² and have been used in catalysis,³ host-guest chemistry⁴ and drug delivery.⁵ An important factor in advancing the area of MOFs, is the manipulation of metal-coordinating building blocks into predictable and distinct architectures using a range of bonds of differing strengths and properties. Coordinate covalent bonds have been extensively used for this purpose,⁶ whereas more recently other weaker forces of interactions such as hydrogen bonds have also been used to impart structure-directing properties for the assembly of MOFs.⁷ However, the use of hydrogen bonds for organizing coordination complexes carries potential problems, due to the metal-coordinating ability of common hydrogen-bond donors/acceptors such as carboxylic acids and pyridines (Figure 2.1), which might hinder the predictable assembly of metal-coordinated architectures.

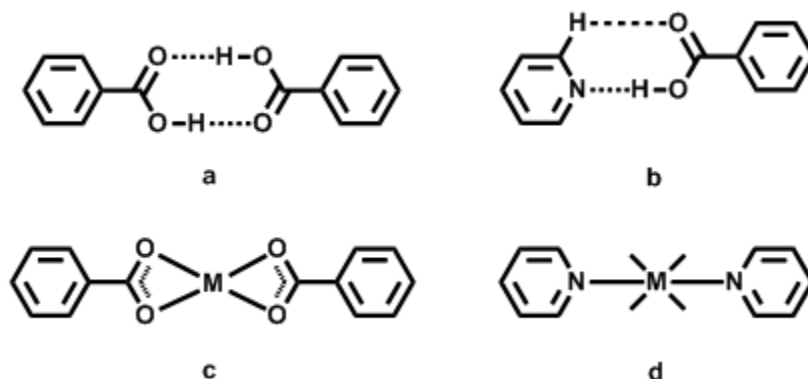


Figure 2.1 (a) Hydrogen-bonded dimer in carboxylic acids; (b) Pyridine-acid O-H...N interactions; Carboxylic acids (c) and pyridines (d) coordinating with metals.

Halogen bonding (XB) is electrostatic in nature and can be classified into three types;⁸ (i) the conventional halogen-bond which takes place primarily between electronegative atoms such

as nitrogen and oxygen (XB acceptor) atoms, and an electron deficient p-orbital of polarizable halogen atoms (XB donor), (ii) type I halogen-halogen bond due to the van der Waals interactions between two halogen atoms, and (iii) type II halogen-halogen bond based on the weaker interactions between the electropositive end of halogen atoms and their respective electronegative ends (Figure 2.2).

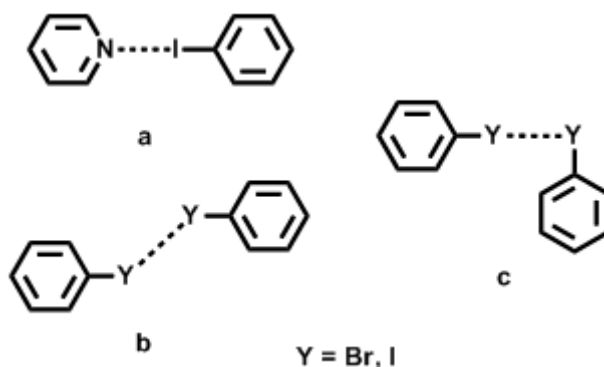


Figure 2.2 (a) Conventional halogen-bond; (b) Type I halogen-halogen contacts; (c) Type II halogen-halogen contacts.⁸

The use of halogen bonds for the assembly of metal-coordinated architectures is a feasible alternative, since they comparable strengths to other structure-directing non-covalent interactions,⁹ and they are less likely to interfere with the metal-ligand interactions which are the building blocks of these architectures. A few studies have focused on halogen-bonded supramolecular self-assembly of coordination compounds. A systematic investigation by Brammer *et. al.* on halogen-bonding in neutral metal-organic complexes showed the presence of directional C-X \cdots Cl-M halogen-bonds for X = Cl, Br, I,¹⁰ whereas Goldberg *et. al.* utilized halogen-bonds to synthesize chiral porphyrins functionalized with iodophenyl and pyridyl groups, in which the assembly was directed by weak C-I \cdots N(pyridine) and C-I \cdots π halogen-bonds.¹¹ Jones *et. al.* showcased a three component modular strategy for the assembly of coordination complexes linked by halogen bonds to O, S and π acceptors (Figure 2.3).¹² The resulting wheel-and-axle shaped coordination assemblies were held together by O \cdots I/S \cdots I halogen-bonds between the morpholine/thiomorpholine moiety and the iodine atom of 1,4-diiodotetrafluorobenzene (tfib), as well as short C \cdots I contacts between the phenyl rings of dibenzoylmethanate moiety and the iodine atom of tfib. These assemblies also contain additional tfib molecules as guests, and thus resemble a halogen-bonded analogy of metal-based inclusion compounds.

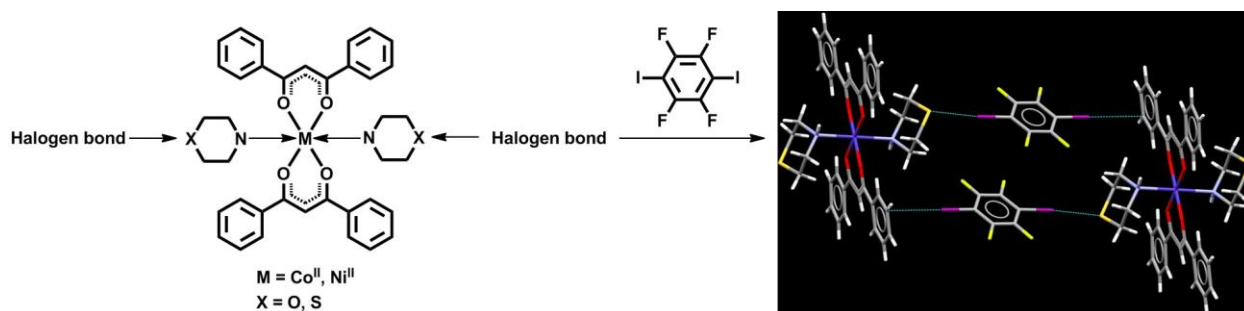


Figure 2.3 A three-component modular strategy for the assembly of halogen-bonded coordination complexes.¹²

More recently, Resnati *et al.* synthesized and characterized one-dimensional (1D) hybrid organic-organometallic supramolecular ribbons by co-crystallizing *trans*-[Pt(PCy₃)₂(C≡C-4-py)₂] with tfib and *trans*-1,2-bis-(2,3,5,6-tetrafluoro-4-iodophenyl)-ethylene (Figure 2.4).¹³ N⋯I interactions are largely responsible for the formation of these 1D infinite chains with alternating XB donors and acceptors, where the conjugated metal- π -perfluorinated repeating unit Pt-C≡C-py⋯IC₆F₄I is spread along the supramolecular organometallic copolymer.

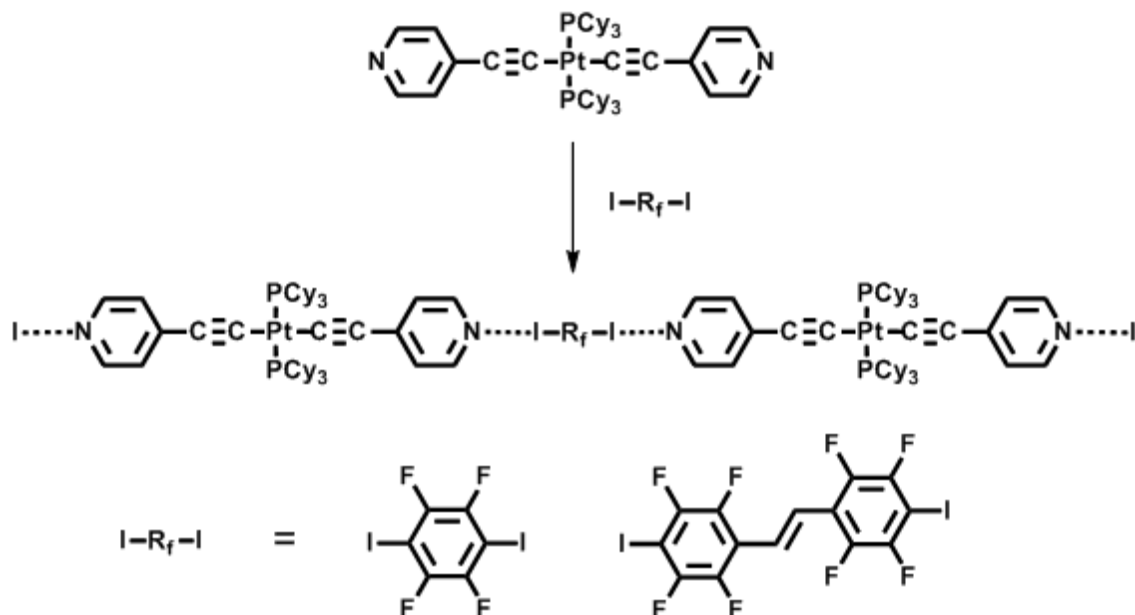


Figure 2.4 Synthesis of halogen-bonded infinite 1D supramolecular ribbons.¹³

Despite the recent interest and extensive research on the predictable assembly of coordination complexes using halogen-bonds as a supramolecular tool, very little is known about the possibility of using the non-interfering, but weaker halogen-halogen interactions as a synthetic tool for the directed assembly of metal-coordinated architectures. Such a synthetic strategy has a possible downside because the weaker halogen-halogen contacts might not be

strong enough to overcome non-directional close-packing forces, and thus will not be able to express themselves in the crystal energy landscape.

The study of weaker forces between coordination complexes demands the absence of solvent molecules and disruptive coordinated/non-coordinated counter-anions, as these molecules can mask the effect of the weaker forces of interaction. Thus, it is important to design and synthesize coordination complexes with pre-determined chemical composition, as this will allow us to systematically explore the effects of the weaker forces of interaction in the crystal lattice. For this purpose, we chose 3-phenyl-2,4-pentanedione as the coordinating ligand, since the acetyl acetonate (acac) moiety is known for forming neutral coordination complexes with various metal ions.^{14,15,16} The preferred metal ion was copper(II) as Cu(II)-acac complexes are known to preferentially form four-coordinated coordination complexes, that do not require the presence of any interfering solvent molecules or counter-ions in the crystal lattice.¹⁵ Whereas, other metal ions such as Ni(II) and Zn(II) exist in the 4 + 2 coordination environment upon complexation with acac moieties, in which two acac moieties are accompanied by two axial solvent molecules.¹⁶ Thus, the combination of the singly charged acac moiety with the copper(II) metal ion should lead to the desired neutral and solvent-free complexes.

For the purpose of investigating the effects of different substituents on the structural outcome of the appropriate Cu(II)-acac bearing core, we decorated the ligands with a series of substituents with varying polarizability and halogen-bond capability (Cl, Br, I). The series also included 3-(4-tolyl)-2,4-pentanedione as the methyl group is non-polarizable, but it is of similar size as the chlorine atom. The resulting four ligands and their corresponding Cu(II) complexes (Figure 2.5), allow for a systematic study of the role played by weaker interactions when competing with non-directional close packing forces.

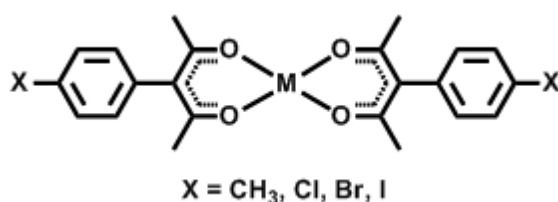


Figure 2.5 Tetra-coordinated copper(II)-acac center.

First, it can be assumed that the methyl and chloro substituted ligands and their corresponding complexes would be iso-structural due to their similar sizes, whereas the bromo and iodo substituted ligands could potentially offer structure-directing halogen bonds. In the case

of any halogen-bonding taking place in the free ligands, there are three available potential acceptor sites; (i) the *exo* lone pair on the keto oxygen atom, (ii) the lone pair on the hydroxyl oxygen atom, and (iii) an electronegative region on all the halogen atoms (Figure 2.6). If this interaction is indeed electrostatic in nature, then the best acceptor can be identified by calculating the molecular electrostatic potential (MEPs) for all the ligands.

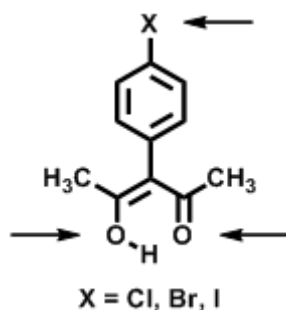


Figure 2.6 Possible halogen-bond acceptors in the free ligands.

Herein, we have outlined strategy for investigating the role of the weaker halogen-halogen interactions as a structure-directing tool in coordination architectures, when competing with non-directional close packing forces. We are particularly interested in:

- Attempting to control the coordination geometry around the metal center to facilitate the exclusion of any counter-ions or solvent molecules for the purpose of studying the role of weaker halogen-halogen interactions.
- Investigating the halogen-bonding capabilities of the halogen atoms (Cl, Br, I) in the free ligands and in their corresponding copper(II) complexes.
- Comparing of the halogen-bond accepting capabilities of the acac species in the free ligand as well as in the coordinated complexes.
- Categorizing the balance between the various intermolecular forces as outlined above.

The reliability of the overall assembly process has been examined by synthesizing and characterizing a series of four ligands with varying substituents and their corresponding copper(II) complexes.

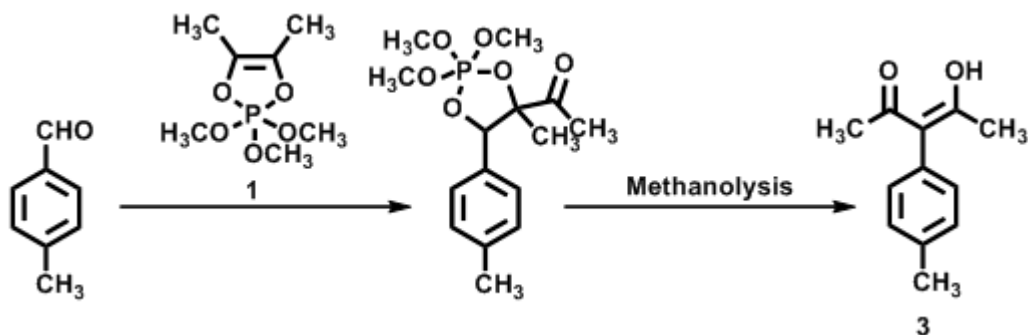
2.2 Experimental

2.2.1 Synthesis

All chemicals, unless otherwise noted were purchased from Aldrich and used without further purification. The synthesis of biacetyl-trimethylphosphite adduct¹⁷ (**1**) and 3-(4-

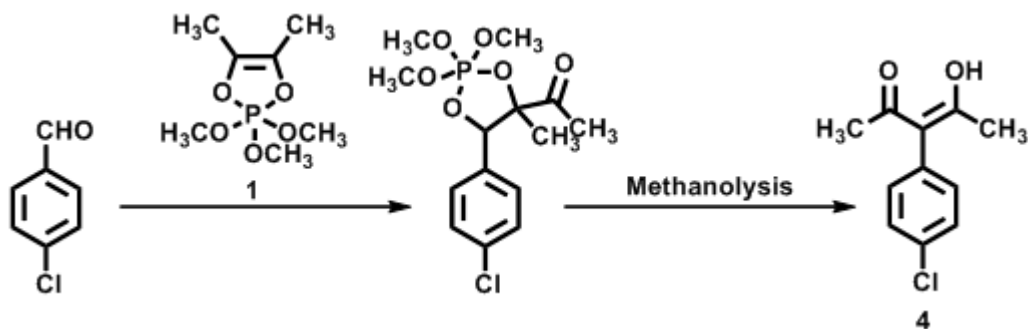
iodophenyl)-2,4-pentanedione¹⁸ (**2**) was carried out according to previously reported procedures. Melting points were determined on a Fisher-Johns melting point apparatus and are uncorrected. ¹H and ¹³C NMR spectra were recorded on a Varian Unity plus 400 MHz spectrometer in CDCl₃. Infrared spectroscopy (IR) was done on a Nicolet 380 FT-IR.

2.2.1.1 Synthesis of 3-(4-tolyl)-2,4-pentanedione, **3**



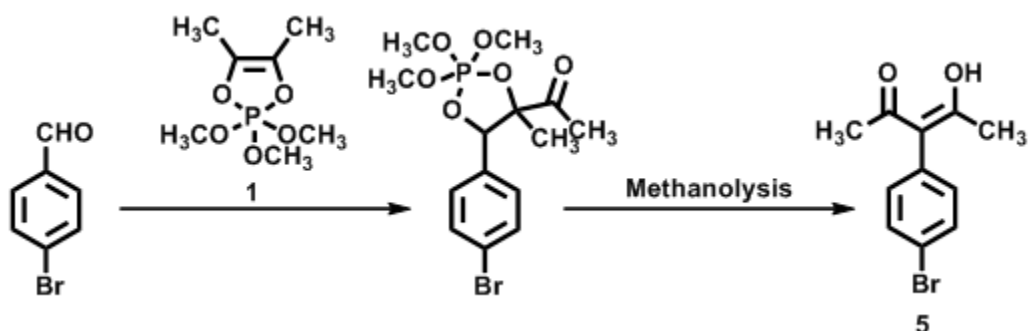
4-Methylbenzaldehyde (0.5 g, 4.16 mmol) was placed in a 100 mL round bottom flask under a N₂ atmosphere. **1** (1.14 g, 5.41 mmol) was added to the flask with continuous stirring. The resulting slurry was stirred for 24 h at room temperature under a N₂ atmosphere. After this, 50 mL of methanol was added and the clear solution was heated under reflux for 4 h under a N₂ atmosphere. Upon cooling the solution was concentrated via rotary evaporation to produce a yellow oil. The residue was dissolved in 50 mL methanol and cooled to -78°C to yield a white crystalline solid, which was further washed with cold methanol. Colorless plate shaped crystals of **3** suitable for single-crystal X-ray diffraction were grown using slow evaporation from methanol at 0°C. Yield: 0.59 g (74%); mp 70-72°C (lit.,¹⁹ 75-76°C); ¹H NMR (δ_H; CDCl₃, 400MHz): 1.88 (s, 6 H), 2.38 (s, 3 H), 7.05 (d, *J*=7.78 Hz, 2 H), 7.19 (d, *J*=8.32 Hz, 2 H), 16.65 (s, 1 H); ¹³C NMR (δ_C; CDCl₃, 400MHz): 191.04, 137.11, 133.79, 130.86, 129.47, 114.96, 24.14, 21.17; IR (neat, ν/cm⁻¹): 3025, 2918, 1594 (br), 1514, 1402 (br), 1328 (br), 813.

2.2.1.2 Synthesis of 3-(4-chlorophenyl)-2,4-pentanedione, 4



4-Chlorobenzaldehyde (0.5 g, 3.56 mmol) was placed in a 100 mL round bottom flask under a N₂ atmosphere. **1** (0.97 g, 4.63 mmol) was added to the flask with continuous stirring. The resulting slurry was stirred for 24 h at room temperature under a N₂ atmosphere. After this, 50 mL of methanol was added and the clear solution was heated under reflux for 4 h under a N₂ atmosphere. Upon cooling the solution was concentrated via rotary evaporation to produce a yellow oil. The residue was dissolved in 50 mL methanol and cooled to -78°C to yield a white crystalline solid, which was further washed with cold methanol. Colorless plate shaped crystals of **4** suitable for single-crystal X-ray diffraction were grown using slow evaporation from methanol at 0°C. Yield: 0.56 g (75%); mp 80-82°C (lit., 80-82°C)¹⁸; ¹H NMR (δ_H; CDCl₃, 400MHz): 16.67 (s, 1 H), 7.37 (d, *J*=8.6 Hz, 2 H), 7.11 (d, *J*=8.6 Hz, 2 H), 1.89 (s, 6 H); ¹³C NMR (δ_C; CDCl₃, 400MHz): 190.82, 135.38, 133.61, 132.45, 129.08, 114.06, 24.12; IR (neat, ν/cm⁻¹): 1568 (br), 1490, 1410 (br), 1329 (br), 1091, 994, 823.

2.2.1.3 Synthesis of 3-(4-bromophenyl)-2,4-pentanedione, 5



4-Bromobenzaldehyde (0.5 g, 2.70 mmol) was placed in a 100 mL round bottom flask under a N₂ atmosphere. **1** (0.74 g, 3.51 mmol) was added to the flask with continuous stirring. The resulting slurry was stirred for 24 h at room temperature under a N₂ atmosphere. After this,

50 mL of methanol was added and the clear solution was heated under reflux for 4 h under a N₂ atmosphere. Upon cooling the solution was concentrated via rotary evaporation to produce a colorless oil. The residue was dissolved in 50 mL methanol and cooled to -78°C to yield a white crystalline solid, which was further washed with cold methanol. Clear prismatic crystals of **5** suitable for single-crystal X-ray diffraction were grown using slow evaporation from methanol at 0°C. Yield: 0.57 g (82%); mp 102-103°C (lit., 102-103°C)¹⁸; ¹H NMR (δ_H; CDCl₃, 400MHz): 16.68 (s, 1 H), 7.52 (d, *J*=8.1 Hz, 2 H), 7.06 (d, *J*=8.1 Hz, 2 H), 1.89 (s, 6 H); ¹³C NMR (δ_C; CDCl₃, 400MHz): 190.76, 135.86, 132.80, 132.06, 121.75, 114.08, 24.15; IR (neat, ν/cm⁻¹): 1577 (br), 1484, 1406 (br), 1326 (br), 1069, 994, 820.

2.2.2 Synthesis of coordination complexes

2.2.2.1 Synthesis of {bis[3-(4-tolyl)-2,4-pentanedionato] copper(II)}, **3a**

Ligand **3** (0.15 g, 0.79 mmol) was dissolved in 10.0 mL of acetonitrile and 1.6 mL of triethylamine was added to the mixture in a screw cap vial. To this solution was added copper(II) tetrafluoroborate hydrate (0.21 g, 0.79 mmol) in 10.0 mL of acetonitrile. The resulting slurry was mixed well and kept for slow evaporation at room temperature. Dark green crystals of **3a** suitable for single-crystal X-ray diffraction were harvested from the vial after two days. Yield: 0.11 g (65%); mp 235°C (decomp.); IR (ν/cm⁻¹): 1562 (C=C stretch), 1417, 1365, 1334, 1316, 1007, 918, 820.

2.2.2.2 Synthesis of {bis[3-(4-chlorophenyl)-2,4-pentanedionato] copper(II)}, **4a**

Ligand **4** (0.15 g, 0.71 mmol) was dissolved in 10.0 mL of acetonitrile and 1.6 mL of triethylamine was added to the mixture in a screw cap vial. To this solution was added copper(II) perchlorate (0.26 g, 0.71 mmol) in 10.0 mL acetonitrile. The resulting slurry was mixed well and kept for slow evaporation at room temperature. Dark green crystals of **4a** suitable for single-crystal X-ray diffraction were harvested from the vial after two days. Yield: 0.12 g (69%); mp 260°C (decomp.); IR (ν/cm⁻¹): 1566 (C=C stretch), 1414, 1368, 1320, 1008, 917, 825.

2.2.2.3 Synthesis of {bis[3-(4-bromophenyl)-2,4-pentanedionato] copper(II)}, **5a**

Ligand **5** (0.15 g, 0.59 mmol) was dissolved in 10.0 mL of acetonitrile and 1.6 mL of triethylamine was added to the mixture in a screw cap vial. To this solution was added copper(II) tetrafluoroborate hydrate (0.15 g, 0.59 mmol) in 10.0 mL of acetonitrile. The resulting slurry was

mixed well and kept for slow evaporation at room temperature. Dark green crystals of **5a** suitable for single-crystal X-ray diffraction were harvested from the vial after two days. Yield: 0.13 g (76%); mp 280°C (decomp.); IR (ν/cm^{-1}): 1563 (C=C stretch), 1416, 1368, 1318, 1005, 979, 917, 822.

2.2.2.4 Synthesis of {bis[3-(4-iodophenyl)-2,4-pentanedionato] copper(II)}, **2a**

Ligand **2** (0.15 g, 0.5 mmol) was dissolved in 10.0 mL of acetonitrile and 1.6 mL of triethylamine was added to the mixture in a screw cap vial. To this solution was added copper(II) nitrate trihydrate (0.12 g, 0.5 mmol) in 10.0 mL of acetonitrile. The resulting slurry was mixed well and kept for slow evaporation at room temperature. Dark green crystals of **2a** suitable for single-crystal X-ray diffraction were harvested from the vial after two days. Yield: 0.10 g (59%); mp 275°C (decomp.); IR (ν/cm^{-1}): 1571 (C=C stretch), 1420, 1371, 1338, 1313, 1004, 974, 920, 819.

2.2.3 Molecular electrostatic potential charge calculations

Charge calculations were performed on ligands **2**, **4** and **5** using Spartan'04 (Wavefunction, Inc. Irvine, CA). All three molecules were geometry optimized using PM3, with the maxima and minima in the electrostatic potential surface (0.002 e au⁻¹ iso-surface) determined using a positive point charge in the vacuum as a probe.

2.3 Results

We have structurally characterized three ligands, *i.e.* **3**, **4** and **5**, as well as four coordination complexes, *i.e.* **3a**, **4a**, **5a** and **2a**, using single-crystal X-ray diffraction. The single-crystal structure of **2** has been previously reported.¹⁸ Table 2.1 lists the IR stretches for the C=O bond of the acac moiety in the ligands **3**, **4**, **5** and **2**, and the C=C stretch of the acac moiety in the corresponding coordination complexes, *i.e.* **3a**, **4a**, **5a** and **2a**. Detailed hydrogen-bond geometries for the ligands **3**, **4**, **5** and **2** are listed in Table 2.2.

Table 2.1 IR stretches for the C=O bonds in the acac ligands and C=C stretch for the corresponding coordination complexes.

Ligand	C=O stretch (cm ⁻¹)	Coordination complex	C=C stretch (cm ⁻¹)
3	1594 (br)	3a	1562
4	1568 (br)	4a	1566
5	1577 (br)	5a	1563
2	1574 (br)	2a	1571

Table 2.2 Hydrogen-bond geometries for **3**, **4**, **5** and **2**

Ligand	D-H...A	$d(\text{D-H})/\text{\AA}$	$d(\text{H...A})/\text{\AA}$	$d(\text{D...A})/\text{\AA}$	$\text{Angle}(\text{D-H...A})/^\circ$
3ⁱ	O(12)-H(12)...O(14)	1.19(2)	1.33(2)	2.452(2)	153(2)
4ⁱⁱ	O(12)-H(12)...O(14)	0.97(2)	1.53(2)	2.447(2)	157(2)
5ⁱⁱ	O(12)-H(12)...O(14)	0.78(3)	1.76(3)	2.451(2)	147(3)
2^{ii, 18}	O(12)-H(12)...O(14)	0.91(3)	1.60(3)	2.459(2)	156(3)

Symmetry code: (i) $x, -y+1/2, z$; (ii) #1 $x-1/2, y, -z+1/2$; #2 $x+1/2, y, -z+1/2$; #3 $x, -y+1/2, z$

2.3.1 Structural characterization of the ligands

2.3.1.1 Crystal structure of **3**

The crystal structure determination of **3** shows that it exists as the keto-enol tautomer and displays the expected intramolecular O-H...O hydrogen bond (Table 2.2). There is no evidence of any structure-directing intermolecular interactions, because the methyl group does not take part in any form of electrostatic interactions. Hence the structure is close-packed, wherein neighboring rows of molecules are arranged in an anti-parallel fashion (Figure 2.7).

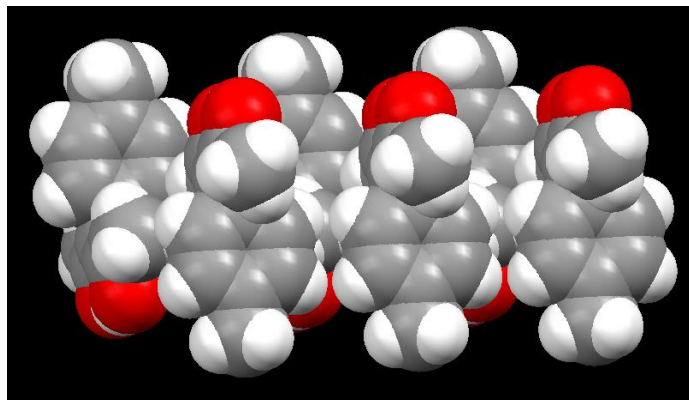


Figure 2.7 Close packing in the crystal structure of **3**.

2.3.1.2 Crystal structure of 4, 5 and 2

The crystal structure analysis of **4**, **5** and **2**¹⁸ revealed two interesting features. First, there is an expected intramolecular hydrogen-bond between the *endo* lone pair of the keto oxygen atom and the hydroxyl group on the acac moiety (Table 2.2). Second, they all display an intermolecular halogen-bond between the halogen atoms (chlorine/bromine/iodine) and the *exo* lone pair of the keto oxygen atom of an adjacent molecule, which extends the individual molecules into an infinite 1D chain (Figure 2.8). An average C=O...X bond angle of 120° and O...X bond length of 3.2 Å indicates that this is an electrostatically driven interaction (Table 2.3). The increased polarizability of iodine when compared to chlorine/bromine results in a shorter C=O...I contact in **2**.

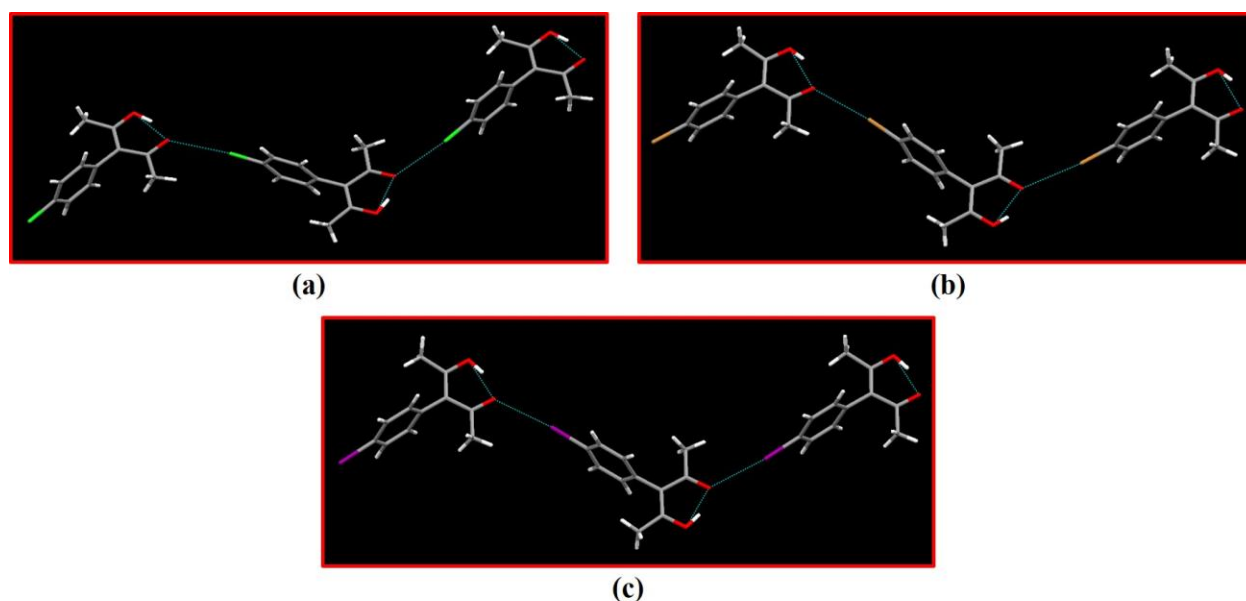


Figure 2.8 Section of the crystal structure of **4** (a), **5** (b) and **2**¹⁸ (c) displaying the intramolecular hydrogen-bond and the intermolecular halogen-bond.

Table 2.3 Halogen-bond geometric parameters for **4**, **5** and **2**

Ligand	C=O...X	$d(\text{O}\cdots\text{X})/\text{\AA}$	$\text{Angle}(\text{C}=\text{O}\cdots\text{X})/^\circ$
4	C(14)-O(14)...Cl(1)	3.223(1)	119.58(9)
5	C(14)-O(14)...Br(1)	3.216(1)	120.5(1)
2 ¹⁸	C(14)-O(14)...I(1)	3.267(1)	122.4(1)

X = Cl/Br/I; Symmetry code: $x+1/2, y, -z+1/2$

2.3.2 Structural characterization of the coordination complexes

2.3.2.1 Crystal structure of 3a, 4a and 5a

The crystal structure determination of **3a**, **4a** and **5a**, shows that the tetra-coordinated copper ion is chelated by two acetyl-acetonate groups, and sits in a distorted square planar geometry (Figure 2.9). The substituents (methyl/chloro/bromo) on adjacent molecules are observed to be in a head to head arrangement, and there are no striking structure-directing intermolecular interactions present in the crystal structures, thus giving rise to a close-packed architecture for **3a**, **4a** and **5a**.

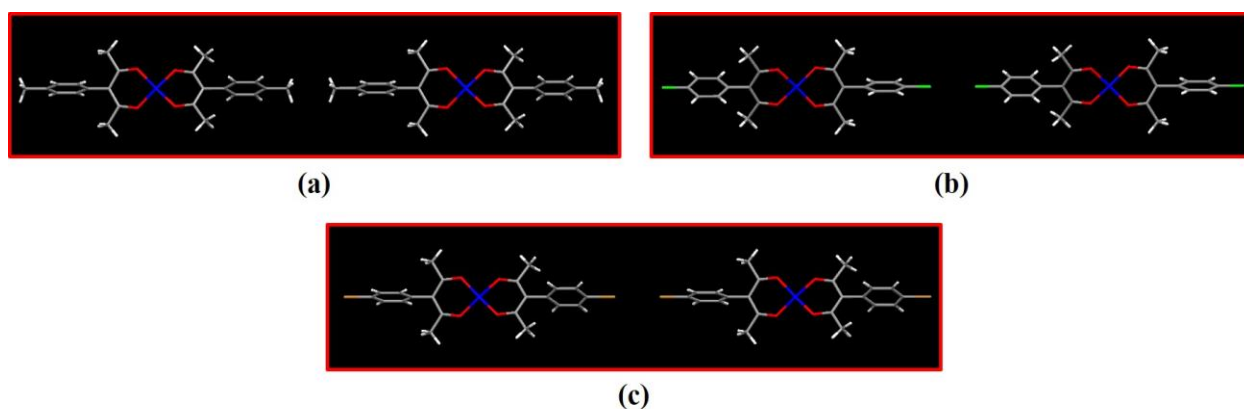


Figure 2.9 Head to head close-packed arrangement in the crystal structure of **3a** (a), **4a** (b) and **5a** (c).

2.3.2.2 Crystal structure of 2a

The crystal structure analysis of **2a**, shows a different arrangement when compared to the packing in **3a**, **4a** and **5a**. Even though the copper ion is still bis-chelated in a distorted square-planar pocket, there is an absence of short I...I contacts in the lattice. Consequently, the iodine atoms on adjacent molecules are not aligned in a head to head fashion, and instead the molecules appear to be forming an infinite zig-zag pattern (Figure 2.10). This kind of packing can be attributed to non-directional close-packing.

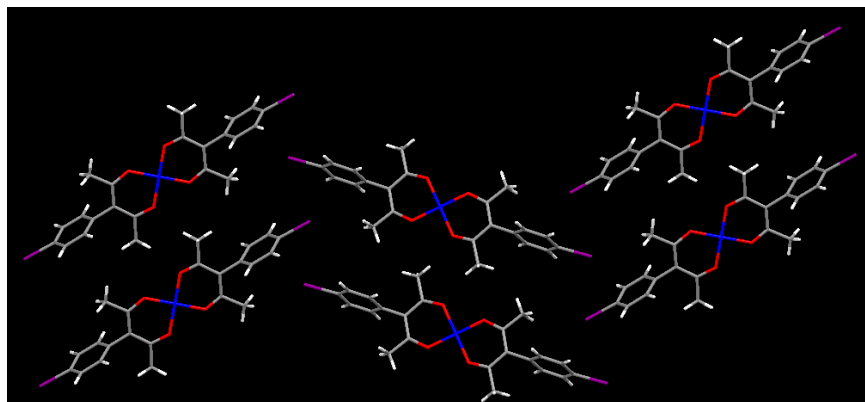


Figure 2.10 Infinite zig-zag pattern in the crystal structure of **2a**.

2.4 Discussion

2.4.1 Characterization by ^1H NMR spectroscopy

The acetyl acetonate moiety can exist in two tautomeric forms, *i.e.* the keto-enol or the diketo form, both of which are clearly distinguishable by ^1H NMR spectroscopy (Figure 2.11). A peak at about 16.0 ppm in the ^1H NMR spectrum is characteristic of the highly deshielded (due to intramolecular hydrogen bonding) hydroxyl hydrogen atom of the keto-enol tautomer, whereas the upfield shifted (absence of intramolecular hydrogen-bonds) methenyl hydrogen atom of the diketo tautomer shows up around 4.0 ppm.

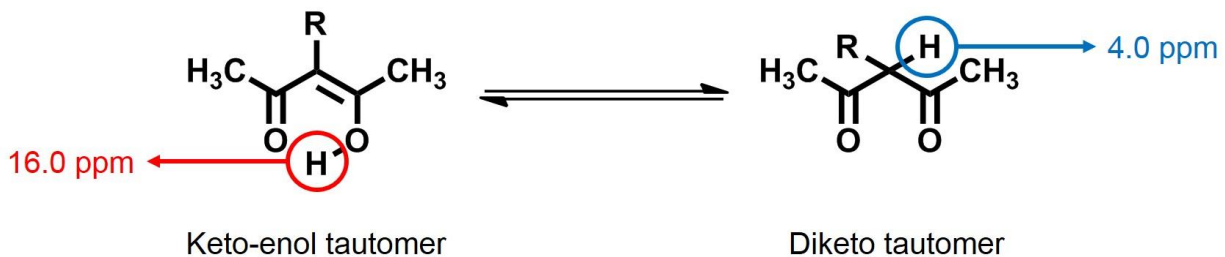


Figure 2.11 Two tautomeric forms of acetyl acetonates.

In the case of **3**, **4**, **5** and **2**, an examination of the ^1H NMR spectra reveals a distinct peak at about 16.0 ppm, which shows that all the ligands exist as the keto-enol tautomer (Figure 2.12).

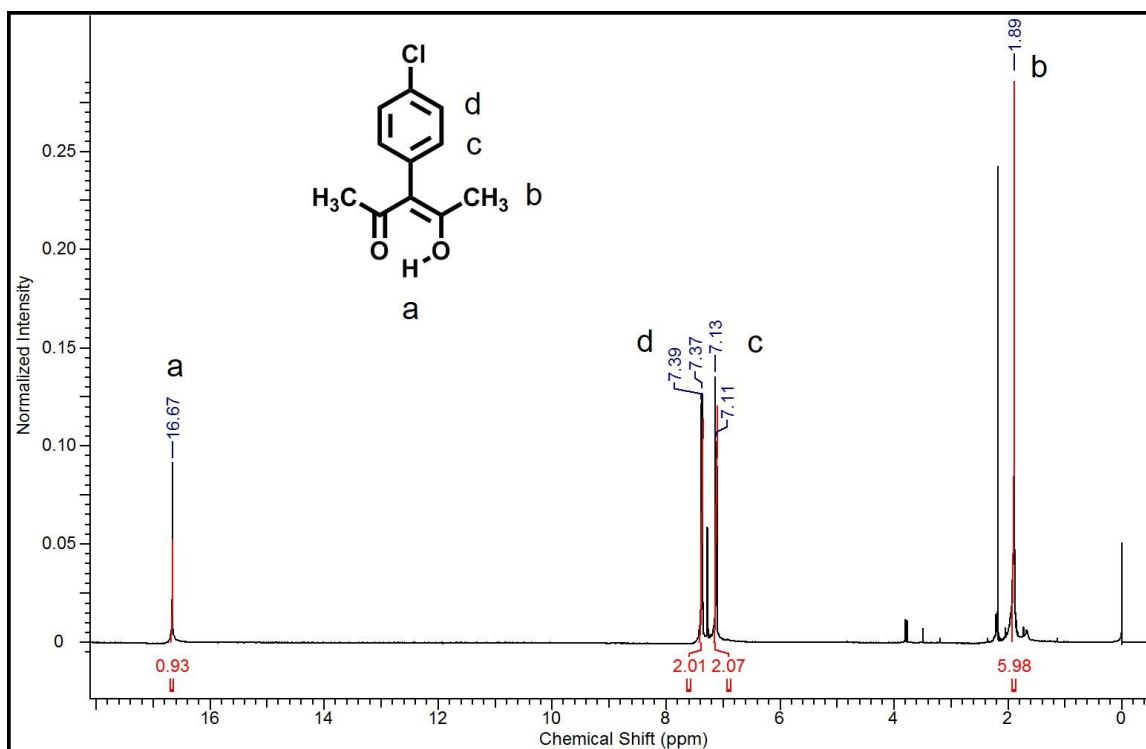


Figure 2.12 ^1H NMR spectrum of **4**.

2.4.2 Characterization by IR spectroscopy

IR is an effective tool for the characterization of the acac ligands and their corresponding copper complexes. A salient feature in the IR spectra of the ligands is the intense broad continuum observed in the $1650\text{--}1150\text{ cm}^{-1}$ region, which can be attributed to the ligand in the keto-enol form (Figure 2.13). This is consistent with what has been observed in literature for 3-substituted β -diketonate derivatives.²⁰ There is a dramatic change in the IR spectrum upon complexation with copper(II), as the broad continuum is replaced by a well-defined region, with significant shifts being observed for the C=O and the C=C stretches. In accordance with existing literature data on the IR stretches of metal-acac complexes,²¹ we can assign the peak at 1565 cm^{-1} to the C=C stretch of the complexed ligand.

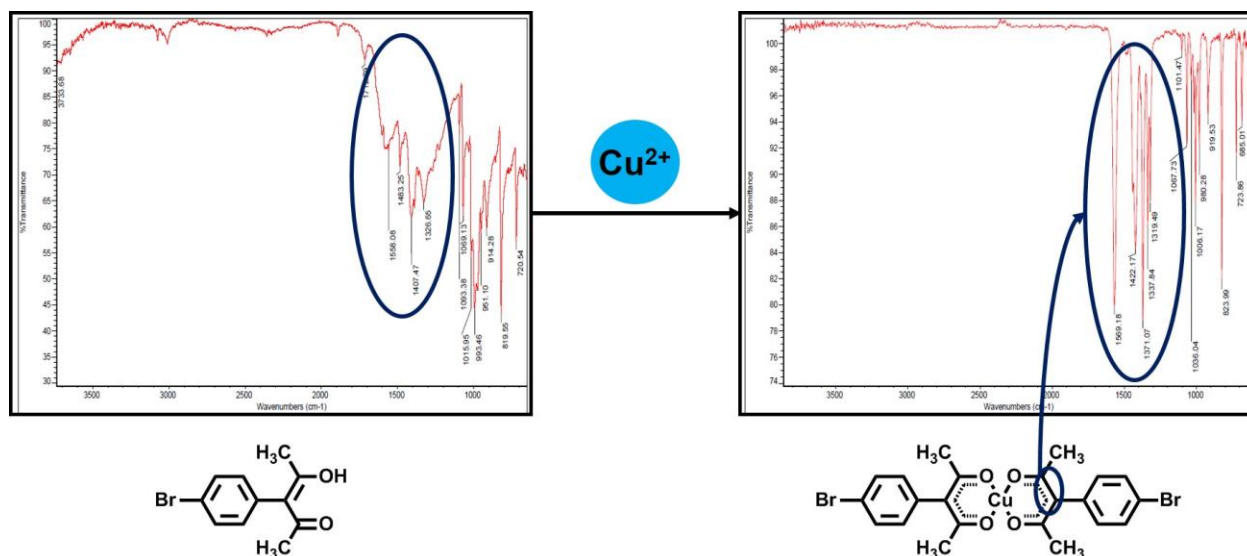


Figure 2.13 IR spectrum of **5** before (left) and after (right) complexation with copper(II) ion.

2.4.3 Comparison of the crystal structures of the ligands

2.4.3.1 Close packing in **3**

The crystal structure of **3** is different from the other ligands as the methyl group is a spectator substituent, and thus there is an absence of point-to-point electrostatic stabilization in the lattice. This observation can be rationalized on the basis of dipole moments, wherein the molecules on adjacent rows are arranged in an anti-parallel manner to maximize dipole-dipole attraction. A similar anti-parallel arrangement is also seen in the case of 3-(4-cyanophenyl)-2,4-pentanedione,¹⁵ where one molecule is sandwiched between two molecules to facilitate the dipole-dipole attraction (Figure 2.14).

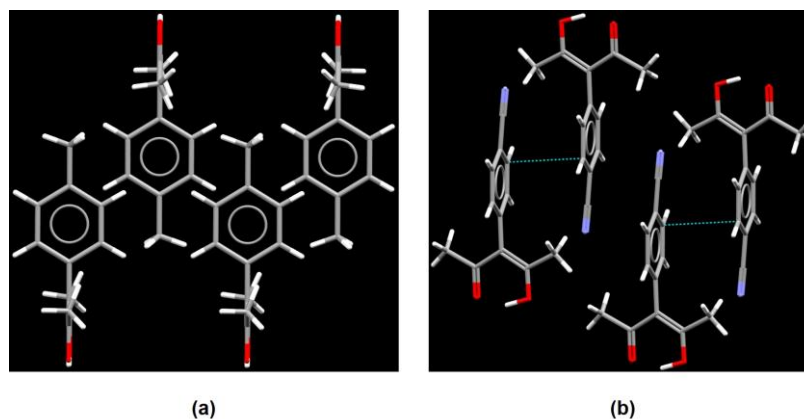


Figure 2.14 Anti-parallel close packing arrangement in the crystal structure of **3** (a), and 3-(4-cyanophenyl)-2,4-pentanedione (b).¹⁵

2.4.3.2 Isostructural halogen-bonded architecture in 4, 5 and 2

2.4.3.2.1 Iso-structurality

There are two common features between the isostructural ligands **4**, **5** and **2**¹⁸ (Table 2.4). First, they all exhibit the expected (for β -diketonate derivatives) intramolecular hydrogen-bond between the keto oxygen atom and the hydroxyl proton, and the corresponding geometric parameters (Table 2.2) are consistent with reported distances for C=O and C-OH bond lengths at 1.27 Å and 1.32 Å, respectively. Second, there is an intermolecular halogen-bond between the *exo* lone pair of the keto oxygen atom and the respective halogen atoms of the ligands, which extends the molecules into an infinite 1D chain. Iso-structurality in chloro, bromo and iodo bearing compounds has already been attributed to the structural equivalence of these substituents.²²

Table 2.4 Unit cell parameters of **4**, **5** and **2**.

Ligand	4	5	2
Crystal system	Orthorhombic	Orthorhombic	Orthorhombic
Space group, Z	<i>Pnma</i> , 4	<i>Pnma</i> , 4	<i>Pnma</i> , 4
<i>a</i> , Å	20.2258(14)	20.4766(18)	21.0708(12)
<i>b</i> , Å	6.7622(5)	6.8070(6)	6.9034(4)
<i>c</i> , Å	7.3688(5)	7.3506(6)	7.3624(4)
α , (°)	90.00	90.00	90.00
β , (°)	90.00	90.00	90.00
γ , (°)	90.00	90.00	90.00
<i>V</i> , Å ³	1007.84(12)	1024.56(15)	1070.94(10)

2.4.3.2.2 Halogen-bonds

There are three potential halogen-bond acceptors (keto oxygen atom, hydroxyl oxygen atom, and the electronegative regions of each halogen atom) in **4**, **5** and **2**¹⁸ (Figure 2.15), but still the halogen-bond donors (electropositive tip of each halogen atom) consistently halogen-bond with the keto oxygen atom. Halogen bonds, like hydrogen bonds, are primarily electrostatic in nature,⁸ and this observation can be explained on the basis of semi-empirical PM3 electrostatic potential charge calculations (Table 2.5).

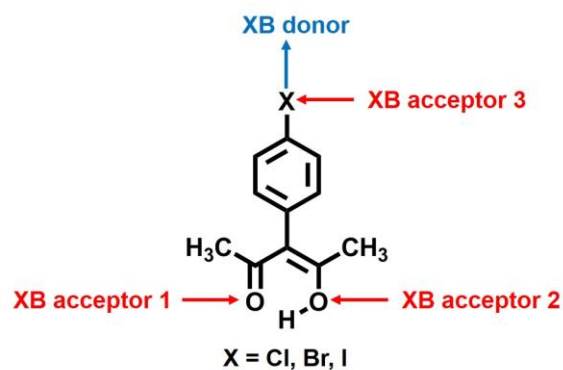


Figure 2.15 Halogen-bond acceptors and donor in **4**, **5** and **2**.

Table 2.5 Molecular electrostatic potentials (MEPs) for **4**, **5** and **2**.

Ligand	C=O (MEP in kJ mol ⁻¹)	O-H (MEP in kJ mol ⁻¹)	X (MEP in kJ mol ⁻¹)
4	-245	-178	+44 (Cl)
5	-251	-177	+88 (Br)
2	-253	-178	+115 (I)

The highest negative surface potential value for the *exo* lone pair on the keto oxygen atom makes it the most electronegative atom in **4**, **5** and **2**, and thus it is expected that the halogen bonding should occur between the keto oxygen atom and the respective halogen atoms, which is observed for all the ligands. Also, iodine is the most polarizable atom when compared to bromine and chlorine, and thus the magnitude of charge decreases in the order I > Br > Cl. This would affect the intermolecular halogen-bond strength, and should be reflected in the observed O...X bond distance (Table 2.3). Despite the fact that iodine has a larger van der Waals radius, the O...I intermolecular distance is comparable to O...Br and O...Cl bond distances. This observation, coupled with the approach of the halogen atom along the direction of the lone pair on the oxygen atom, underscores the electrostatic nature of these interactions.

2.4.4 Controlling the Cu(II) coordination geometry

The observed coordination geometry of the copper(II) ion in all the complexes, *i.e.* **3a**, **4a**, **5a** and **2a** is identical, as they all contain a four-coordinate Cu(II) that sits in a slightly distorted square planar pocket. The absence of any counter-ions or solvents in the crystal lattice facilitates the study of the weaker non-covalent forces of interaction, and hence justifies the

choice of the acac moiety as the coordinating ligand and Cu(II) as the metal atom for our study. Four-coordinate acetyl acetonate based copper(II) complexes are well known, as revealed by a CSD (Cambridge Structural Database) search on the Cu(II)-acac moiety. Of the 20 hits, 8 had copper(II) atom sitting in a slightly distorted square planar pocket, whereas the remaining 12 existed in a square planar geometry.

2.4.5 Comparison of the crystal structures of the coordination complexes

2.4.5.1 Close-packed architecture in 3a, 4a and 5a

2.4.5.1.1 Structural equivalence in 3a and 4a

The copper(II) ion in the isostructural crystal structures of **3a** and **4a** sits in a distorted square planar pocket and is four-coordinate. The methyl and chloro substituents sit in a face-to-face arrangement, and the overall structure is close-packed (Figure 2.16). The observed similarity in the crystal structures of **3a** and **4a** is due to the structural equivalence of the methyl and chloro substituents (respective volumes 23.5 Å³ and 19.9 Å³), which is well known, and has been used to construct isostructural solids in crystal engineering.²²

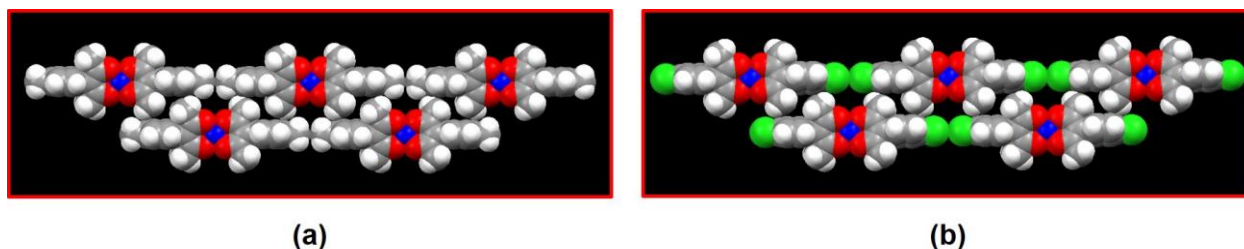


Figure 2.16 Head-to-head close-packed arrangement in **3a** (a) and **4a** (b).

2.4.5.1.2 Crystal structure of 5a

The crystal structure of **5a** has a greater probability of displaying stabilizing halogen bonds, because the bromine atom has a higher polarizability than the chlorine atom. Despite this, no such interactions are observed. The four-coordinate copper ion sits in the distorted square planar pocket, and the overall assembly is isostructural to **3a** and **4a** (Figure 2.17). The decreased electronegativity of the acac oxygen atoms (no longer a competitive XB acceptor) upon complexing with the electron-withdrawing metal center is responsible for the lack of stabilizing O··Br halogen-bonds in **5a**, which was observed in the free ligand **5**. Furthermore, a potential

Br \cdots Br attraction is not strong enough to overcome the favored head-to-head close-packed arrangement in **5a**.

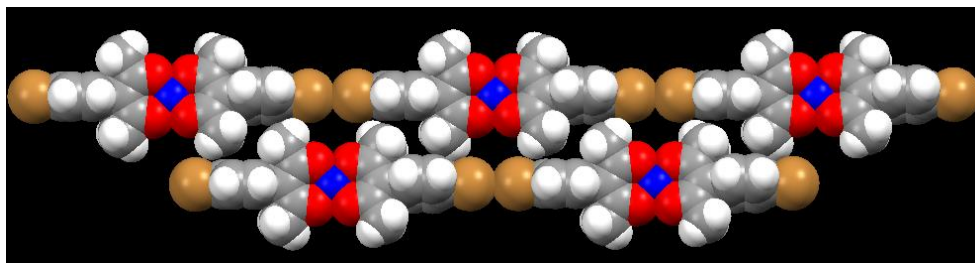


Figure 2.17 Head-to-head close-packed arrangement in **5a**.

2.4.5.1.3 Head-to-head motif in **3a**, **4a** and **5a**

The close-packed coordination complexes **3a**, **4a** and **5a**, display a common motif in which the substituents (CH₃, Cl and Br, respectively) sit in a head-to-head fashion. This kind of close-packing of such substituents is not uncommon, as revealed by a CSD search for non-solvated, single-component organic/organometallic compounds that display a similar motif in their crystal structures (Table 2.6).

Table 2.6 Number of structures with head-to-head motifs

Substituent	Number of structures with head-to-head motifs
CH ₃	3784
Cl	128
Br	49

2.4.5.2 Crystal structure of **2a**

The crystal structure of **2a** is remarkably different from the other members of this series (**3a**, **4a** and **5a**). The highly polarizable iodine atom is the strongest halogen-bond donor in this series, but despite this, there are no structure-stabilizing halogen-bonds present in the crystal lattice, which can be explained by looking at the available halogen-bond acceptors in the complexed ligand. Due to the electron-withdrawing effect of the metal ion on the acac oxygen atoms, they are no longer an attractive alternative for halogen bonding, and thus no stabilizing O \cdots I interactions are found (as seen in the free ligand). Weaker I \cdots I interactions are also absent in the crystal lattice, as they cannot compete with the non-directional close-packing forces. But, we no longer see a head-to-head close packing arrangement in **2a**, as seen in **3a**, **4a** and **5a**, because the increased positive charge on the tip of iodine makes this arrangement highly unfavorable due

to electrostatic repulsion between the iodine atoms on adjacent molecules. Consequently, the structure of **2a** is still close-packed, but displays a zig-zag pattern, so as to minimize the electrostatic repulsions in the lattice (Figure 2.18).

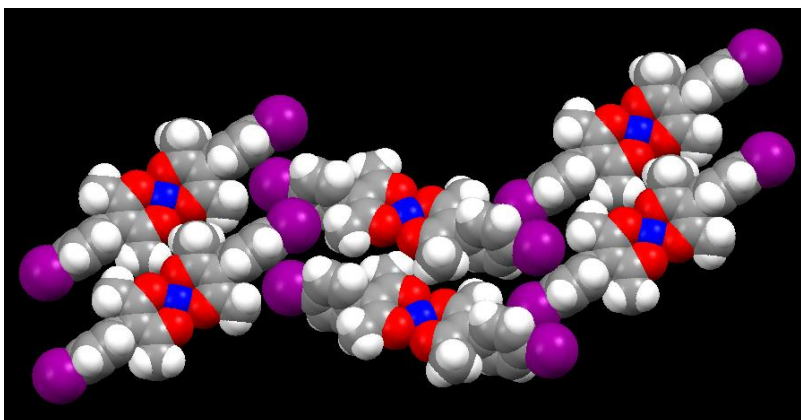


Figure 2.18 Zig-zag close-packed architecture in **2a**.

2.4.6 Halogen-bond vs close packing

Despite the fact that the same halogen-bond donors (Cl, Br, I) are present in both the free ligands and the copper(II)-complexes, any form of structure-stabilizing halogen-bonds in **3a**, **4a** and **5a** are clearly absent, due to the lack of a suitable halogen-bond acceptor in the metal-complexes (due to the electron-withdrawing nature of the metal atom). This means that the structure-directing halogen-bonds are no longer able to rise above the close-packing ‘noise’ in the crystal lattice, and thus all the copper(II)-complexes of our series are dominated by non-directional close packing forces.

2.4.7 Halogen-bond vs hydrogen-bond

It would be interesting to observe the behavior of halogen-bonds when compared to hydrogen-bonds, since they are known to be similar in strength. For this purpose, an examination of the crystal structure of 4-iodobenzoic acid²³ is in order, as the hydrogen-bonded acid-acid dimer resembles a four-coordinate copper(II)-acac moiety, but is weaker in strength to the coordinate-covalent bonds in the metal-complex, and thus allows for a fair comparison of the actual structure-directing capabilities of the halogen-bond (Figure 2.19).

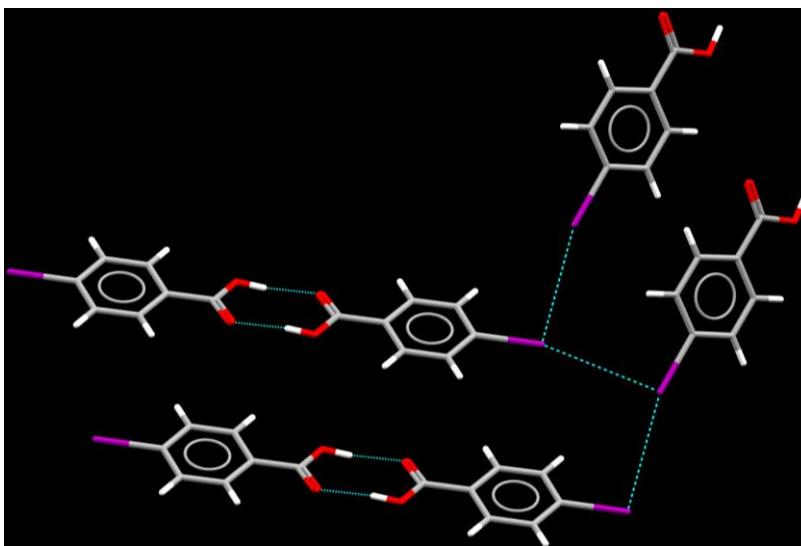


Figure 2.19 Hydrogen-bonded dimers and halogen-bonded chains in 4-iodobenzoic acid.²³

There are two interesting features in the crystal structure of 4-iodobenzoic acid. First, as expected the carboxyl group is forming a dimer *via* two identical $C=O\cdots H-O$ hydrogen-bonds. Second, the iodine atom forms a bifurcated halogen-bond with two iodine atoms on adjacent molecules, by simultaneously acting as a halogen-bond donor (*via* the electropositive tip) and a halogen-bond acceptor (*via* the electronegative region on the halogen atom). This shows that in a more evenly contested system, halogen-bonds are more likely to play significant structure-directing roles.

2.5 Conclusions

We have synthesized a series of acetyl acetonate (acac) based ligands (with four different substituents, *i.e.* CH_3 , Cl, Br and I) and their corresponding Cu(II) complexes, with an aim to constructing a system with a predictable chemical composition and a controllable coordination geometry, that will in turn allow us to examine the fine balance between weak intermolecular interactions in the solid-state.¹⁸ The resulting non-solvated four-coordinate Cu(II)-acac complexes offer a platform for studying the direct connections between covalent modifications and the resulting structural consequences. The chloro/bromo/iodo substituted free ligands display structure-directing intermolecular interactions *via* $C=O\cdots X$ halogen-bonds, and the halogen-bond donor picks out the best halogen-bond acceptor in each case (based on MEPs). This observation coupled with the geometric parameters for the $C=O\cdots X$ interactions underscores the electrostatic nature of these interactions. Though the halogen-bond donors remain the same in the Cu(II)-acac

complexes, any form of structure-directing halogen-bonds are clearly absent due to a lack of suitable acceptors (electron-withdrawing effect of the metal atom on the acac moiety), and the inability of the weaker X \cdots X interactions to express themselves in the crystal lattice. In such a scenario, all the metal-complexes are governed by non-directional close packing forces.

References

- 1 O'Keeffe, M.; Peskov, M. A.; Ramsden, S. J.; Yaghi, O. M. *Acc. Chem. Res.* **2008**, *41*, 1782.
- 2 (a) Batten, S. R.; Robson, R. *Angew. Chem., Int. Ed.* **1998**, *37*, 1460. (b) Wang, Z.; Cohen, S. M. *Chem. Soc. Rev.* **2009**, *38*, 1315. (c) Cohen, S. M. *Chem. Sci.* **2010**, *1*, 32.
- 3 (a) Ma, L.; Abney, C.; Lin, W. *Chem. Soc. Rev.* **2009**, *38*, 1248. (b) Lee, J.; Farah, O. K.; Roberts, J.; Scheidt, K. A.; Nguyen, S. T.; Hupp, J. T. *Chem. Soc. Rev.* **2009**, *38*, 1450.
- 4 (a) Carra, J. R.; Walton, K. S. *Langmuir* **2008**, *24*, 8620. (b) Allendorf, M. D.; Bauer, C. A.; Bhakta, R. K.; Houk, R. J. T. *Chem. Soc. Rev.* **2009**, *38*, 1330.
- 5 (a) Horchjada, P.; Serry, C.; Vallet-Regi, M.; Sebban, M.; Taulelle, F.; Ferey, G. *Angew. Chem., Int. Ed.* **2006**, *118*, 6120. (b) Rieder, W. J.; Taylor, K. M. L.; Lin, W. *J. Am. Chem. Soc.* **2007**, *129*, 9852. (c) Huxford, R. C.; Rocca, J. D.; Lin, W. *Curr. Opin. Chem. Biol.* **2010**, *14*, 262.
- 6 Czaja, A. U.; Trukhan, N.; Muller, U. *Chem. Soc. Rev.* **2009**, *38*, 1284.
- 7 (a) Aakeröy, C. B.; Desper, J.; Waldes-Martinez, J. *CrystEngComm* **2004**, *6*, 413. (b) Brammer, L. *Chem. Soc. Rev.* **2004**, *33*, 476. (c) Aakeröy, C. B.; Desper, J.; Smith, M. M.; Urbina, J. F. *Dalton Trans.* **2005**, 2462. (d) Wuest, J. D. *Chem. Commun.* **2005**, 5830. (e) Baudron, S. A.; Salazar-Mendoza, D.; Hosseini, M. W. *CrystEngComm* **2009**, *11*, 1245. (f) Duong, A.; Metivaud, V.; Maris, T.; Wuest, J. D. *Cryst. Growth Des.* **2011**, *11*, 2026.
- 8 (a) Pedireddy, V. R.; Reddy, D. S.; Gaud, G. S.; Craig, D. C.; David Rae, A.; Desiraju, G. R. *J. Chem. Soc. Perkin Trans. II* **1994**, *11*, 2353. (b) Metrangolo, P.; Resnati, G. ed. *Halogen Bonding: Fundamentals and Applications, Structure and Bonding*, Springer, Berlin, 2007.
- 9 (a) Corradi, E.; Meilli, S. V.; Messina, M. T.; Metrangolo, P.; Resnati, G. *Angew. Chem., Int. Ed.* **2000**, *39*, 178. (b) Aakeröy, C. B.; Schultheiss, N.; Desper, J.; Moore, C. *CrystEngComm* **2007**, *9*, 421. (c) Aakeröy, C. B.; Schultheiss, N.; Rajbanshi, A.; Desper, J.; Moore, C. *Cryst. Growth Des.* **2009**, *9*, 432.
- 10 Espallargas, G. M.; Zordan, F.; Marin, L. A.; Adams, H.; Shankland, K.; van de Streek, J.; Brammer, L. *Chem. Eur. J.* **2009**, *15*, 7554.
- 11 Muniappan, S.; Lipstman, S.; Goldberg, I. *Chem. Commun.* **2008**, 1777.
- 12 Lapadula, G.; Judaš, N.; Frišćić, T.; Jones, W. *Chem. Eur. J.* **2010**, *16*, 7400.
- 13 Sgarbossa, P.; Bertani, R.; Di Noto, V.; Piga, M.; Giffin, G. A.; Terraneo, G.; Pilati, T.; Metrangolo, P.; Resnati, G. *Crts. Growth Des.* **2012**, *12*, 297.
- 14 (a) Dohring, A.; Goddard, R.; Jolly, P. W.; Kruger, C.; Polyakov, V. R. *Inorg. Chem.* **1997**, *36*, 177. (b) Vreshch, V. D.; Lysenko, A. B.; Chernega, A. N.; Howard, J. A. K.; Krautscheid, H.; Sieler, J.; Domasvitch K. V. *Dalton Trans.* **2004**, 2899. (c) Pariya, C.; Sparrow, C. R.; Back, C.-K.; Sandi, G.; Fronczek, F. R.; Maverick, A. W. *Angew. Chem., Int. Ed.* **2007**, *119*, 6421.
- 15 Chen, B.; Fronczek, F. R.; Maverick, A. W. *Acta. Crystallogr., Sect. C: Cryst. Struct. Commun.* **2004**, *60*, m147.
- 16 Polyakov, V. R.; Czerwinski, M. *Inorg. Chem.* **2001**, *40*, 4798.
- 17 Ramirez, F.; Patwardhan, A. V.; Ramanathan, N.; Desai, N. B.; Greco, C. V.; Heller, S. R. *J. Am. Chem. Soc.* **1965**, *87*, 543.

-
- 18 Aakeröy, C. B.; Sinha, A. S.; Chopade, P. D.; Desper, J. *Dalton Trans.* **2011**, *40*, 12160.
- 19 Pinhey, J. T.; Rowe, B. A. *Aust. J. Chem.* **1979**, *32*, 1561.
- 20 Emsley, J.; Ma, L. Y. Y.; Bates, P. A.; Motevalli, M.; Hursthouse, M. B. *J. Chem. Soc. Perkin Trans. II* **1989**, 527.
- 21 (a) Nakamoto, K.; Morimoto, Y.; Mertell, A. E. *J. Phys. Chem.* **1962**, *66*, 346. (b) Socrates, G. *Infrared and Raman characteristic group frequencies: tables and charts*, John Wiley & Sons, 2004.
- 22 (a) Cinčić, D.; Friščić, T.; Jones, W. *New J. Chem.* **2008**, *32*, 1776. (b) Cinčić, D.; Friščić, T.; Jones, W. *Chem. Eur. J.* **2008**, *14*, 747. (c) Jones, P. G.; Vancea, F. *CrystEngComm* **2003**, *5*, 303.
- 23 Nygren, C. L.; Wilson, C. C.; Turner, J. F. C. *J. Phys. Chem. A* **2005**, *109*, 2586.

Chapter 3 - A versatile and green mechanochemical route for aldehyde/ketone-oxime conversions

3.1 Introduction

3.1.1 Green chemistry

‘Green chemistry’ is an area of research that has received considerable attention in recent years.¹ As the name suggests, it is chemistry by a greener route or by environmentally less stressful means, and can be achieved by utilizing non-toxic components, reducing waste production or improving efficiency. For any chemical process to be green in nature, it is to adhere to most of the “twelve principles” of green chemistry (Figure 3.1).²



Figure 3.1 Twelve principles of green chemistry.²

3.1.2 Mechanochemistry

Traditionally, most chemical syntheses are both expensive and environmentally pollutive, as they involve excessive use of organic solvents, long reaction times, high temperatures, and

cumbersome methods of product separation and purification. Thus, there is a need for better and greener alternatives. A solid-state based mechanochemical process,³ which is usually carried out in the absence of, or with minimal use of, solvents, may be a feasible alternative, as it adheres to most of the principles of green chemistry. Typically, these simple processes involve ball-milling⁴ or grinding,⁵ and represent attractive options in covalent synthesis and supramolecular chemistry, as is showcased by their ubiquitous influence in many industries, such as pharmaceutical, chemical and metallurgical industries. Frišćić *et. al.* have not only demonstrated the synthesis of several metal-organic frameworks by mechanochemical means,⁶ but also real-time monitoring of the reaction profiles,⁶ the formation of intermediates, and interconversion of framework topologies (Figure 3.2).⁶

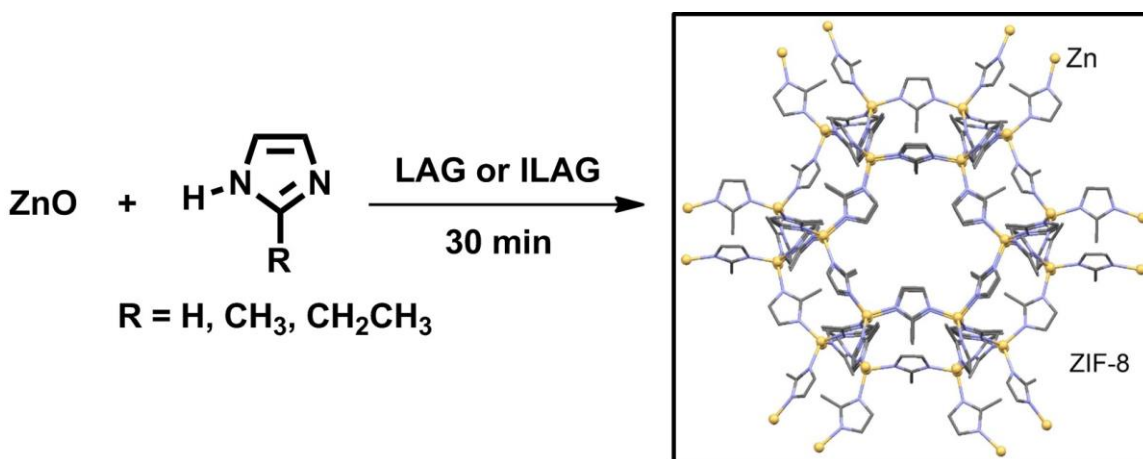


Figure 3.2 Mechanochemical synthesis of metal-organic frameworks.⁶

3.1.3 Oximes

Oximes form an important class of organic compounds having the general formula $\text{RR}'\text{C}=\text{N}-\text{OH}$ (Figure 3.3).

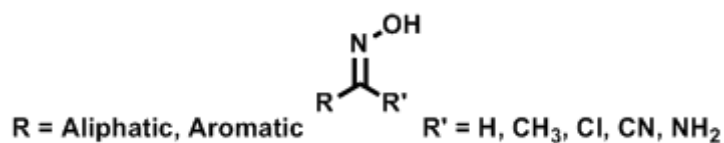


Figure 3.3 Different types of oximes.

Aldoximes ($\text{R}' = \text{H}$) and ketoximes ($\text{R}' = \text{CH}_3$) are the two most common types of oximes, that find use in synthetic organic chemistry, where they are employed for the protection, purification⁷ and characterization of aldehydes and ketones.⁸ They also are important precursors to functional groups such as nitriles,⁹ amines,¹⁰ nitro compounds¹¹ and amides (Figure 3.4).¹²

They are also used in the pharmaceutical industry as organic medicinal agents for the treatment of organophosphate poisoning,¹³ and in the paints/lacquers industry as anti-skinning agents.¹⁴

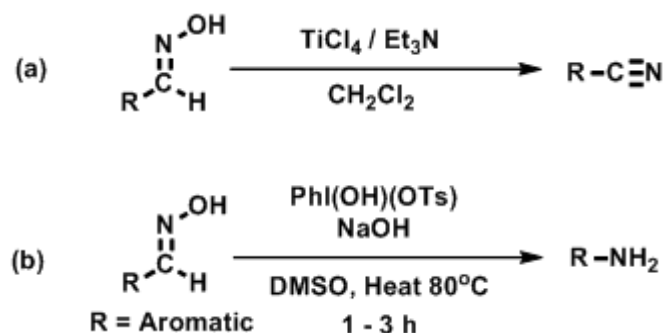


Figure 3.4 Synthesis of nitriles (a) and amines (b) from oximes.

Furthermore, upon deprotonation they can act as strongly coordinating ligands in metal-coordination chemistry,¹⁵ whereas in supramolecular chemistry they have been known to offer structure-directing capabilities by virtue of being strong hydrogen-bond donors as well as being self-complementary synthons (Figure 3.5).¹⁶

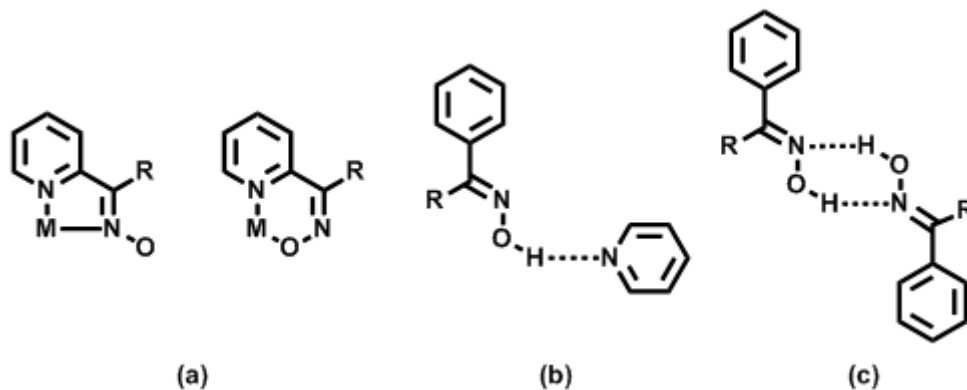


Figure 3.5 (a) Coordination of oximes with metals; (b) Oximes as hydrogen-bond donors; (c) Self-complementary hydrogen-bonded dimers in oximes.

The traditional synthesis of aldoximes and ketoximes involves refluxing an aqueous/alcoholic solution of the corresponding aldehyde or ketone with hydroxylamine hydrochloride and base, followed by solvent-extraction to obtain the pure product.⁸ The excessive use of organic solvents, long reaction times, high temperatures, and extensive work-up procedures, make this solution-based synthetic method environmentally stressful and expensive. Thus, there is a need for better and cheaper alternatives, of which a greener mechanochemical path may be a feasible option.

Some advances have been made in the synthesis of aldoximes/ketoximes from the corresponding aldehydes/ketones; for example in the presence of catalysts ($\text{BF}_3 \cdot \text{OEt}_2$,¹⁷ basic Al_2O_3 ,¹⁸ CaO)¹⁹ in conjunction with microwave irradiation, or by ball-milling at elevated temperatures (Figure 3.6).²⁰ Also, nanostructured pyrophosphates have been used as catalysts under solvent-free conditions at high temperatures to achieve high yielding aldehyde/ketone-oxime conversions.²¹ Finally, a study of several carbonyl-oxime conversions *via* a simple grinding method has been reported,²² but a more systematic investigation into the versatility of a greener and facile solvent-assisted mechanochemical route to aldehyde/ketone-oxime conversions has not yet been presented.

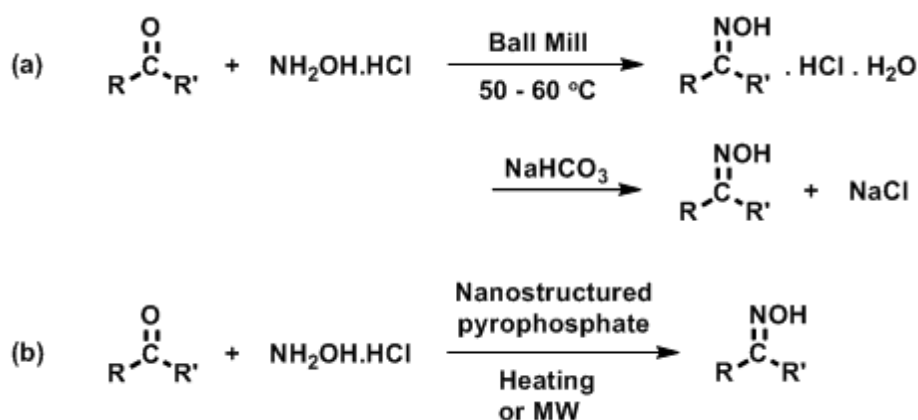


Figure 3.6 Synthesis of oximes by ball-milling at elevated temperatures (a), and by using nanostructured pyrophosphates as catalysts (b).

Herein, we have synthesized 15 aldoximes and 20 ketoximes decorated with a range of substituents, *via* solvent-assisted mechanochemical grinding of the corresponding aldehydes and ketones with hydroxylamine hydrochloride and sodium hydroxide (Figure 3.7). The products have been isolated by a simple aqueous washing procedure to remove of any inorganic salts. The minimal use of solvents, short reaction times (5 - 10 minutes), ambient conditions, and simple work-up procedures, make this synthetic strategy a greener route to aldehyde/ketone-oximes.



Figure 3.7 One-pot mechanochemical conversion of aldehydes and ketones to oximes.

In this chapter, we are particularly interested in:

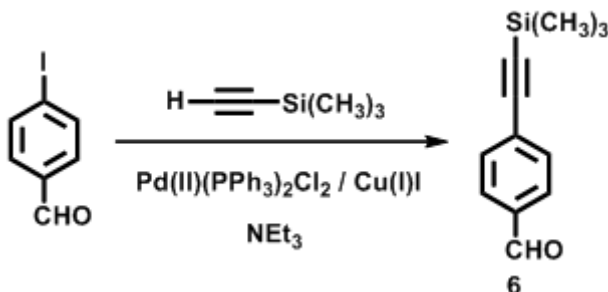
- Establishing the versatility and robustness of this mechanochemical route by determining the limits and limitations (if any) of this synthetic strategy.
- Examining the relative reactivity of aldehyde-oxime *versus* ketone-oxime conversions.
- Investigating the possible electronic effects involved in such transformations.

3.2 Experimental

3.2.1 Synthesis

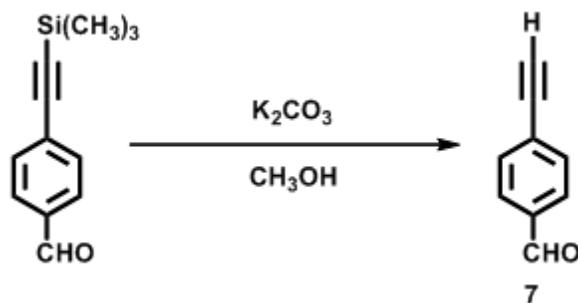
All the chemicals were purchased from Aldrich and used without further purification, unless otherwise noted. The synthesis of 4-iodobenzaldehyde was carried out according to the published procedure.²³ Melting points were determined on a Fisher-Johns melting point apparatus and are uncorrected. ¹H and ¹³C NMR spectra were recorded on a Varian Unity plus 400 MHz spectrometer in CDCl₃ or d₆-DMSO. Infrared spectroscopy (IR) was done on a Nicolet 380 FT-IR.

3.2.1.1 Synthesis of 4-((trimethylsilyl)ethynyl)benzaldehyde, **6**



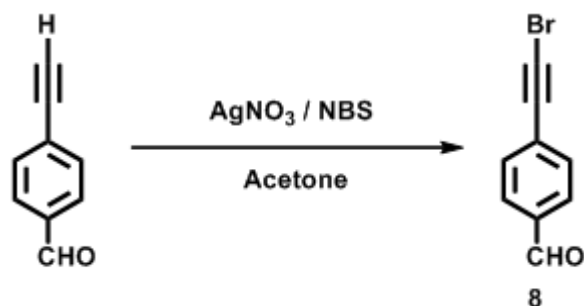
A mixture of 4-iodobenzaldehyde (9.0 g, 38.79 mmol), copper(I) iodide (0.178 g, 0.93 mmol), and *bis*(triphenylphosphine)palladium(II) dichloride (0.327 g, 0.47 mmol) were added to a round bottom flask. 120 mL of triethylamine was also added and the resulting mixture was degassed on a Schlenk line. Trimethylsilylacetylene (6.6 mL, 46.55 mmol) was then added to the mixture, and it was stirred overnight at room temperature under a dinitrogen atmosphere. The reaction was monitored by TLC, and upon completion the solvent was removed under vacuum. The brown residue was then dissolved in chloroform (80 mL), washed with water (3 x 80 mL), and then washed with saturated aqueous sodium chloride (1 x 50 mL). The organic layer was separated and dried over magnesium sulfate. The solvent was removed on a rotary evaporator and the residue chromatographed on silica with hexane/ethyl acetate (9 : 1) mixture as the eluent. The product was isolated as a dark yellow solid. Yield: 6.53 g (83%); mp 61-63°C (lit., 66°C)²⁴; ¹H NMR (δH; CDCl₃, 400MHz): 0.28 (s, 9 H), 7.61 (d, *J*=8.20 Hz, 2 H), 7.83 (d, *J*=8.20 Hz, 2 H), 10.01 (s, 1 H).

3.2.1.2 Synthesis of 4-ethynylbenzaldehyde, 7



A mixture of **6** (4.0 g, 19.77 mmol) and potassium carbonate (4.1g, 29.66 mmol) were stirred in methanol (60 mL) at room temperature for 2 hours. The solvent was then removed under vacuum, and the residue was dissolved in ethyl acetate (50 mL), and washed with water (4 x 50 mL). The organic layer was separated and dried over magnesium sulfate. The solvent was removed on a rotary evaporator and the product was isolated as a yellow solid. Yield: 2.51 g (97%); mp 84-86°C (lit., 87°C)²⁵; ¹H NMR (δH; CDCl₃, 400MHz): 3.30 (s, 1 H), 7.66 (d, *J*=8.20 Hz, 2 H), 7.86 (d, *J*=8.20 Hz, 2 H), 10.03 (s, 1 H).

3.2.1.3 Synthesis of 4-(bromoethynyl)benzaldehyde, **8**



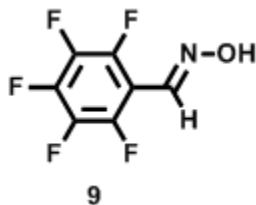
To a stirred solution of **7** (1.6 g, 12.29 mmol) in acetone (300 mL) was added 0.21 g of silver(I) nitrate (1.23 mmol). The mixture was stirred for 30 minutes, then N-bromosuccinimide (5.47 g, 30.74 mmol) was added. The mixture was protected from light and stirred for 3 days. Upon completion of the reaction, acetone was evaporated under vacuum and the solid mixture was chromatographed over a short pad of silica gel with hexane as the eluent and the product was isolated as a yellow solid. Yield: 2.26 g (88%); mp 96-98°C; ¹H NMR (δH; CDCl₃, 400MHz):²⁶ 7.60 (d, *J*=8.06 Hz, 2 H), 7.84 (d, *J*=8.06 Hz, 2 H), 10.01 (s, 1 H).

3.2.2 General synthesis of oximes

In a mortar, 1.0 mmole of aldehyde/ketone and 1.2 mmoles (per aldehyde/ketone present) of hydroxylamine hydrochloride is ground together with a pestle. Then, 1.2 mmoles (per aldehyde/ketone present) of crushed sodium hydroxide is added and the mixture is ground further with the addition of 0.1-0.2 mL methanol, for 2 minutes at room temperature. The reaction mixture is left for 5 minutes, after which it is ground for another 2 minutes with 0.1-0.2 mL methanol. At this stage the reaction is examined by TLC. Upon completion of the reaction, a ¹H NMR spectrum of the crude mixture is taken in d₆-DMSO to confirm the formation of oxime. The crude mixture is washed with water to get rid of any inorganic salts and it is air dried, after which the melting point is taken to establish purity of product.

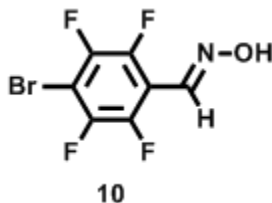
3.2.2.1 Aldoximes

3.2.2.1.1 Pentafluorobenzaldehyde oxime, 9



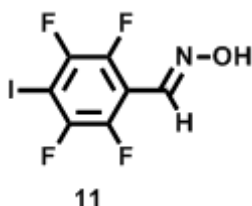
Yield: 78%; mp 128-132°C (lit., 133°C)²⁷; ¹H NMR (δH; DMSO-d₆, 400MHz): 8.14 (s, 1 H), 12.27 (br. s., 1 H).

3.2.2.1.2 4-Bromo-2,3,5,6-tetrafluorobenzaldehyde oxime, 10



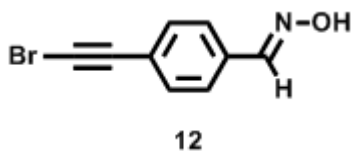
Yield: 80%; mp 138-140°C dec (lit., 138°C dec)²⁷; ¹H NMR (δH; DMSO-d₆, 400MHz): 8.16 (s, 1 H), 12.33 (s, 1 H).

3.2.2.1.3 4-Iodo-2,3,5,6-tetrafluorobenzaldehyde oxime, 11



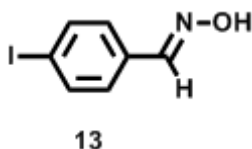
Yield: 87%; mp 165-169°C (lit., 165-169°C)²⁸; ¹H NMR (δH; DMSO-d₆, 400MHz): 8.15 (s, 1 H), 12.26 (s, 1 H).

3.2.2.1.4 4-(Bromoethynyl)benzaldehyde oxime, 12



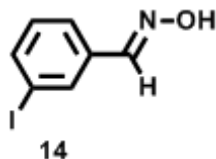
Yield: 85%; mp 119-121°C (lit., 119-121°C)²⁸; ¹H NMR (δH; DMSO-d₆, 400MHz): 7.49 (d, *J*=7.50 Hz, 2 H), 7.59 (d, *J*=7.79 Hz, 2 H), 8.15 (s, 1 H), 11.41 (br. s., 1 H); ¹³C NMR (δC; DMSO-d₆, 400MHz): 54.20, 79.55, 122.40, 126.52, 132.13, 133.58, 147.47.

3.2.2.1.5 4-Iodobenzaldehyde oxime, 13



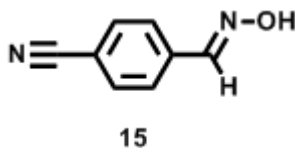
Yield: 61%; mp 101-103°C (lit., 101-103°C)²⁸; ¹H NMR (δH; DMSO-d₆, 400MHz): 7.38 (d, *J*=8.33 Hz, 2 H), 7.76 (d, *J*=8.06 Hz, 2 H), 8.10 (s, 1 H), 11.34 (s, 1 H).

3.2.2.1.6 3-Iodobenzaldehyde oxime, 14



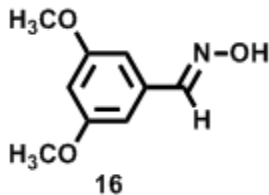
Yield: 59%; mp 66-68°C (lit., 66-68°C)²⁸; ¹H NMR (δH; DMSO-d₆, 400MHz): 7.20 (t, *J*=7.79 Hz, 1 H), 7.61 (d, *J*=7.79 Hz, 1 H), 7.73 (d, *J*=7.79 Hz, 1 H), 7.94 (s, 1 H), 8.10 (s, 1 H), 11.41 (br. s., 1 H).

3.2.2.1.7 4-Cyanobenzaldehyde oxime, 15



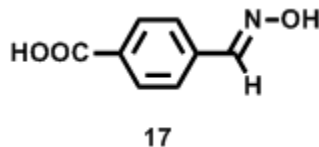
Yield: 76%; mp 175-177°C (lit., 174°C)²⁹; ¹H NMR (δH; DMSO-d₆, 400MHz): 7.74 - 7.80 (m, 2 H), 7.83 - 7.88 (m, 2 H), 8.23 (s, 1 H), 11.73 (br. s., 1 H).

3.2.2.1.8 3,5-Dimethoxybenzaldehyde oxime, 16



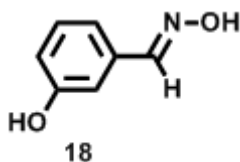
Yield: 89%; mp 112-114°C (lit., 117°C)³⁰; ¹H NMR (δH; DMSO-d₆, 400MHz): 3.34 (s, 6 H), 6.50 (br. s., 1 H), 6.75 (d, *J*=1.61 Hz, 2 H), 8.05 (s, 1 H), 11.24 (br. s., 1 H).

3.2.2.1.9 4-Carboxybenzaldehyde oxime, 17



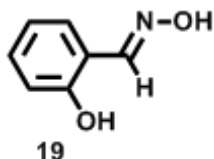
Yield: 67%; mp 212-216°C (lit., 218°C)³¹; ¹H NMR (δH; DMSO-d₆, 400MHz): 7.70 (d, *J*=8.59 Hz, 2 H), 7.95 (d, *J*=8.20 Hz, 2 H), 8.21 (s, 1 H), 11.53 (s, 1 H), 13.04 (br. s., 1 H).

3.2.2.1.10 3-Hydroxybenzaldehyde oxime, 18



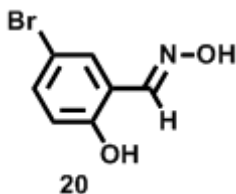
Yield: 62%; mp 83-90°C (lit., 87-88°C)³²; ¹H NMR (δH; DMSO-d₆, 400MHz): 6.67 - 6.76 (m, 1 H), 6.85 (d, *J*=7.42 Hz, 1 H), 6.95 (br. s., 1 H), 7.10 (t, *J*=7.81 Hz, 1 H), 7.98 (s, 1 H).

3.2.2.1.11 2-Hydroxybenzaldehyde oxime, 19



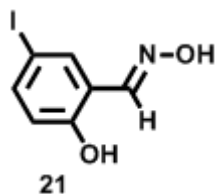
Yield: 71%; mp 110-116°C (lit., 117°C)³³; ¹H NMR (δH; DMSO-d₆, 400MHz): 6.79 - 6.92 (m, 2 H), 7.17 - 7.26 (m, 1 H), 7.47 (d, *J*=7.52 Hz, 1 H), 8.32 (s, 1 H), 10.12 (br. s., 1 H), 11.25 (br. s., 1 H).

3.2.2.1.12 5-Bromo-2-hydroxybenzaldehyde oxime, 20



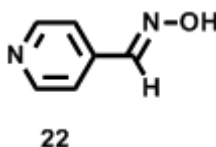
Yield: 83%; mp 112-114°C (lit., 112-114°C)²⁸; ¹H NMR (δH; DMSO-d₆, 400MHz): 6.87 (d, *J*=8.60 Hz, 1 H), 7.32 (dd, *J*=8.73, 2.28 Hz, 1 H), 7.61 (d, *J*=2.42 Hz, 1 H), 8.26 (s, 1 H), 11.21 (br. s., 2 H).

3.2.2.1.13 5-Iodo-2-hydroxybenzaldehyde oxime, 21



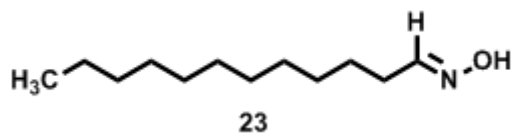
Yield: 76%; mp 124-126°C (lit., 124-126°C)²⁸; ¹H NMR (δH; DMSO-d₆, 400MHz): 6.74 (d, *J*=8.60 Hz, 1 H), 7.45 (d, *J*=8.60 Hz, 1 H), 7.77 (s, 1 H), 8.23 (s, 1 H), 11.14 (br. s., 2 H).

3.2.2.1.14 4-Pyridinecarboxaldehyde oxime, 22



Yield: 83%; mp 130-132°C (lit., 132°C)³⁴; ¹H NMR (δH; DMSO-d₆, 400MHz): 7.54 (d, *J*=1.00 Hz, 2 H), 8.18 (s, 1 H), 8.59 (d, *J*=1.00 Hz, 2 H), 11.83 (br. s., 1 H).

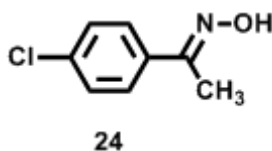
3.2.2.1.15 Dodecyl aldehyde oxime, 23



Yield: 77%; mp 70-72°C (lit., 72°C)³⁵; ¹H NMR (δH; DMSO-d₆, 400MHz): 0.85 (t, *J*=6.72 Hz, 3 H), 1.24 (br. s., 16 H), 1.34 - 1.43 (m, 2 H), 2.21 (td, *J*=7.32, 5.51 Hz, 2 H), 6.62 (t, *J*=5.37 Hz, 1 H), 10.69 (s, 1 H).

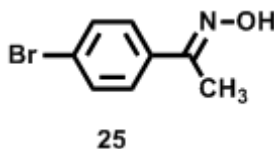
3.2.2.2 Ketoximes

3.2.2.2.1 4'-Chloroacetophenone oxime, 24



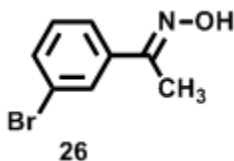
Yield: 88%; mp 90-93°C (lit., 97-99°C)³⁶; ¹H NMR (δH; DMSO-d₆, 400MHz): 2.14 (s, 3 H), 7.44 (d, *J*=8.87 Hz, 2 H), 7.66 (d, *J*=8.60 Hz, 2 H), 11.31 (br. s., 1 H).

3.2.2.2.2 4'-Bromoacetophenone oxime, 25



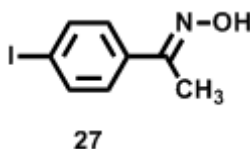
Yield: 84%; mp 126-129°C (lit., 128-130°C)³⁶; ¹H NMR (δH; DMSO-d₆, 400MHz): 2.14 (s, 3 H), 7.59 (d, *J*=1.88 Hz, 4 H), 11.32 (s, 1 H).

3.2.2.2.3 3'-Bromoacetophenone oxime, 26



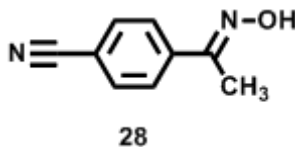
Yield: 91%; mp 93-96°C (lit., 92-93°C)³⁷; ¹H NMR (δH; DMSO-d₆, 400MHz): 2.14 (s, 3 H), 7.35 (t, *J*=7.93 Hz, 1 H), 7.56 (dt, *J*=7.93, 0.87 Hz, 1 H), 7.65 (dd, *J*=7.79, 0.81 Hz, 1 H), 7.80 (t, *J*=1.61 Hz, 1 H), 11.39 (s, 1 H).

3.2.2.2.4 4'-Iodoacetophenone oxime, 27



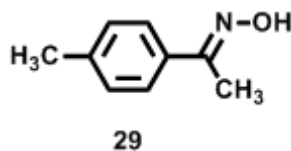
Yield: 78%; mp 156-160°C (lit., 156-158°C)³⁸; ¹H NMR (δH; DMSO-d₆, 400MHz): 2.11 (s, 3 H), 7.43 (d, *J*=8.60 Hz, 2 H), 7.74 (d, *J*=8.60 Hz, 2 H), 11.29 (s, 1 H).

3.2.2.2.5 4'-Cyanoacetophenone oxime, 28



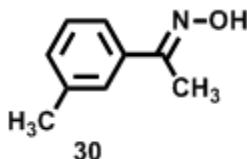
Yield: 72%; mp 150-153°C (lit., 150-153°C)³⁹; ¹H NMR (δH; DMSO-d₆, 400MHz): 2.17 (s, 3 H), 7.69 - 7.91 (m, 4 H), 11.67 (br. s., 1 H).

3.2.2.2.6 4'-Methylacetophenone oxime, 29



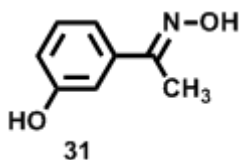
Yield: 71%; mp 81-83°C (lit., 84-86°C)³⁶; ¹H NMR (δH; DMSO-d₆, 400MHz): 2.03 (s, 3 H), 2.26 (s, 3 H), 7.07 (d, *J*=7.52 Hz, 2 H), 7.50 (d, *J*=7.52 Hz, 2 H).

3.2.2.2.7 3'-Methylacetophenone oxime, 30



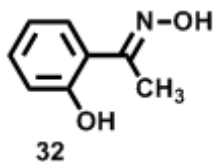
Yield: 68%; mp 50-53°C (lit., 51-52°C)³⁷; ¹H NMR (δH; DMSO-d₆, 400MHz): 2.14 (s, 3 H), 2.32 (s, 3 H), 7.12 - 7.20 (m, 1 H), 7.26 (t, *J*=7.66 Hz, 1 H), 7.38 - 7.50 (m, 2 H), 11.14 (s, 1 H).

3.2.2.2.8 3'-Hydroxyacetophenone oxime, 31



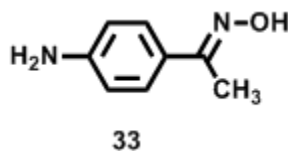
Yield: 76%; mp 148-152°C (lit., 148-149°C)⁴⁰; ¹H NMR (δH; DMSO-d₆, 400MHz): 2.08 (s, 3 H), 6.73 - 6.79 (m, 1 H), 6.98 - 7.03 (m, 1 H), 7.07 (t, *J*=1.75 Hz, 1 H), 7.10 - 7.16 (m, 1 H), 10.53 (br. s., 2 H).

3.2.2.2.9 2'-Hydroxyacetophenone oxime, 32



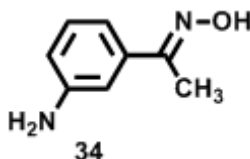
Yield: 57%; mp 206-208°C (lit., 209-210°C)⁴⁰; ¹H NMR (δH; DMSO-d₆, 400MHz): 2.25 (s, 3 H), 6.83 - 6.99 (m, 2 H), 7.19 - 7.34 (m, 1 H), 7.47 (d, *J*=7.42 Hz, 1 H), 11.55 (br. s., 2 H).

3.2.2.2.10 4'-Aminoacetophenone oxime, 33



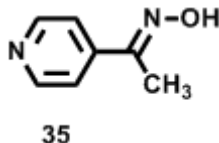
Yield: 70%; mp 128-132°C (lit., 132-133°C)⁴¹; ¹H NMR (δH; DMSO-d₆, 400MHz): 2.04 (s, 3 H), 5.27 (s, 2 H), 6.53 (d, *J*=8.60 Hz, 2 H), 7.33 (d, *J*=8.60 Hz, 2 H), 10.60 (s, 1 H).

3.2.2.2.11 3'-Aminoacetophenone oxime, 34



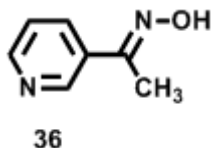
Yield: 68%; mp 134-136°C (lit., 135-137°C)⁴²; ¹H NMR (δH; DMSO-d₆, 400MHz): 2.07 (s, 3 H), 5.09 (s, 2 H), 6.55 (dd, *J*=8.06, 1.34 Hz, 1 H), 6.77 (d, *J*=7.79 Hz, 1 H), 6.87 (s, 1 H), 7.00 (t, *J*=7.79 Hz, 1 H), 10.96 (s, 1 H).

3.2.2.2.12 (E)-1-(pyridin-4-yl)ethanone oxime, 35



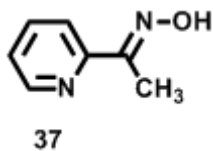
Yield: 65%; mp 162-165°C (lit., 160°C)⁴³; ¹H NMR (δH; DMSO-d₆, 400MHz): 2.15 (s, 3 H), 7.55 - 7.65 (m, 2 H), 8.51 - 8.60 (m, 2 H), 11.70 (br. s., 1 H).

3.2.2.2.13 (E)-1-(pyridin-3-yl)ethanone oxime, 36



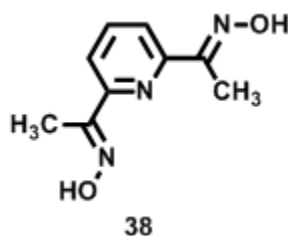
Yield: 56%; mp 114-116°C (lit., 118°C)⁴³; ¹H NMR (δH; DMSO-d₆, 400MHz): 2.18 (s, 3 H), 7.41 (dd, *J*=8.06, 4.84 Hz, 1 H), 8.01 (d, *J*=8.06 Hz, 1 H), 8.55 (d, *J*=4.57 Hz, 1 H), 8.84 (d, *J*=2.15 Hz, 1 H), 11.46 (br. s., 1 H).

3.2.2.2.14 (E)-1-(pyridin-2-yl)ethanone oxime, 37



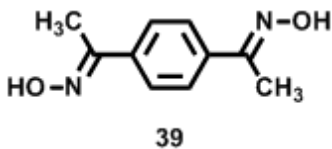
Yield: 67%; mp 120-122°C (lit., 119-121°C)³⁶; ¹H NMR (δH; DMSO-d₆, 400MHz): 2.21 (s, 3 H), 7.34 - 7.38 (m, 1 H), 7.73 - 7.81 (m, 1 H), 7.81 - 7.88 (m, 1 H), 8.52 - 8.62 (m, 1 H), 11.48 (s, 1 H).

3.2.2.2.15 (1E,1'E)-1-(6-((E)-1-(hydroxyimino)ethyl)pyridin-2-yl)ethanone oxime, 38



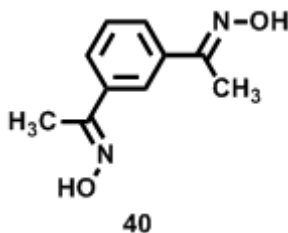
Yield: 89%; mp 235°C dec (lit., 236-238°C)⁴⁴; ¹H NMR (δH; DMSO-d₆, 400MHz): 2.25 (s, 6 H), 7.73 - 7.86 (m, 3 H), 11.51 (br. s., 2 H).

3.2.2.2.16 (1E,1'E)-1-(4-((E)-1-(hydroxyimino)ethyl)phenyl)ethanone oxime, 39



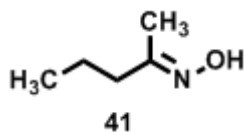
Yield: 93%; mp 247°C dec (lit., 248-250°C)⁴⁵; ¹H NMR (δH; DMSO-d₆, 400MHz): 2.15 (s, 6 H), 7.63 - 7.69 (m, 4 H), 11.25 (s, 2 H).

3.2.2.2.17 (1E,1'E)-1-(3-((E)-1-(hydroxyimino)ethyl)phenyl)ethanone oxime, 40



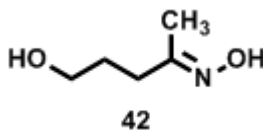
Yield: 78%; mp 209-211°C (lit., 206-208°C)⁴⁶; ¹H NMR (δH; DMSO-d₆, 400MHz): 2.17 (s, 6 H), 7.40 (t, *J*=7.66 Hz, 1 H), 7.63 (d, *J*=7.79 Hz, 2 H), 7.92 (s, 1 H), 11.24 (s, 2 H).

3.2.2.2.18 (*E*)-pentan-2-one oxime, 41



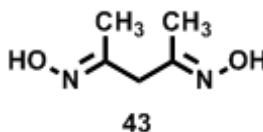
Yield: 53%; Oil; $^1\text{H NMR}$ (δH ; DMSO- d_6 , 400MHz): 0.79 - 0.92 (m, 3 H), 1.38 - 1.51 (m, 2 H), 1.65 - 1.78 (m, 3 H), 1.99 - 2.12 (m, 2 H), 10.21 (s, 1 H).

3.2.2.2.19 (*E*)-5-hydroxypentan-2-one oxime, 42



Yield: 59%; mp 58-62°C (lit., 61-62°C)⁴⁷; $^1\text{H NMR}$ (δH ; DMSO- d_6 , 400MHz): 1.52 - 1.62 (m, 2 H), 1.70 - 1.74 (m, 3 H), 2.08 - 2.15 (m, 2 H), 3.39 (dt, $J=6.45, 3.22$ Hz, 2 H), 4.42 (br. s., 1 H), 10.18 (s, 1 H).

3.2.2.2.20 (*2E,4E*)-pentane-2,4-dione dioxime, 43



Yield: 64%; mp 127-129°C (lit., 128-134°C)⁴⁸; $^1\text{H NMR}$ (δH ; DMSO- d_6 , 400MHz): 1.69 (s, 6 H), 2.93 (s, 2 H), 10.50 (s, 2 H).

3.3 Results and discussion

3.3.1 Characterization of oximes

3.3.1.1 Infra-red spectroscopy

IR spectroscopy is an effective qualitative technique for the preliminary characterization of the ground mixtures of all oximes. A salient feature in the IR spectra is the disappearance of the carbonyl stretch of the aldehydes and ketones (around 1700 cm^{-1}), upon conversion to the corresponding oximes, along with the appearance of the -OH stretch of the oxime (around 3100 - 3300 cm^{-1}) (Figure 3.8). This observation is unambiguous and distinctive for all the aldehyde/ketone - oxime conversions.

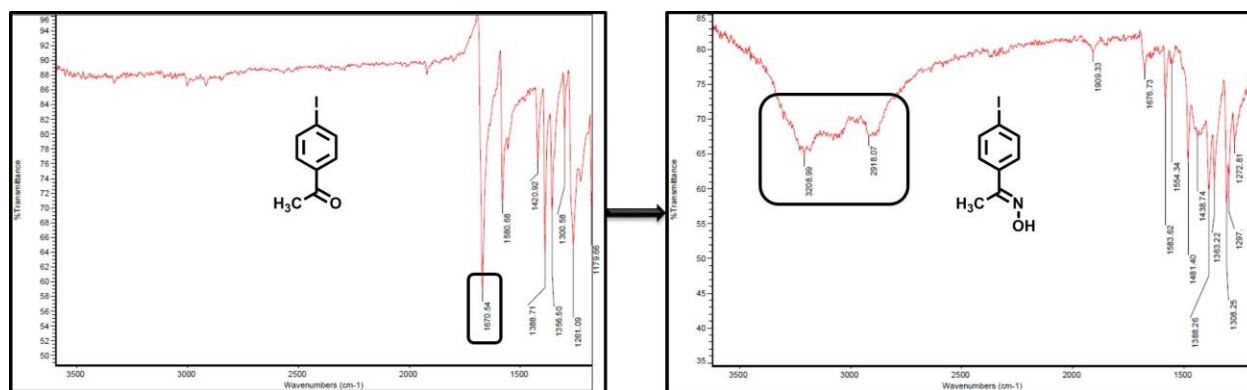


Figure 3.8 Monitoring ketone-oxime conversions by IR spectroscopy.

3.3.1.2 ^1H NMR spectroscopy

^1H NMR spectroscopy has been used to characterize the products in all ground mixtures. A distinctive feature in the ^1H NMR spectrum of aldehydes is the peak for the $-\text{CH}$ proton at 10.0 ppm, which shifts upfield by about 2.0 ppm, upon conversion to the corresponding aldoxime, and is accompanied by the appearance of the oxime $-\text{OH}$ peak at about 11.0 ppm (Figure 3.9).

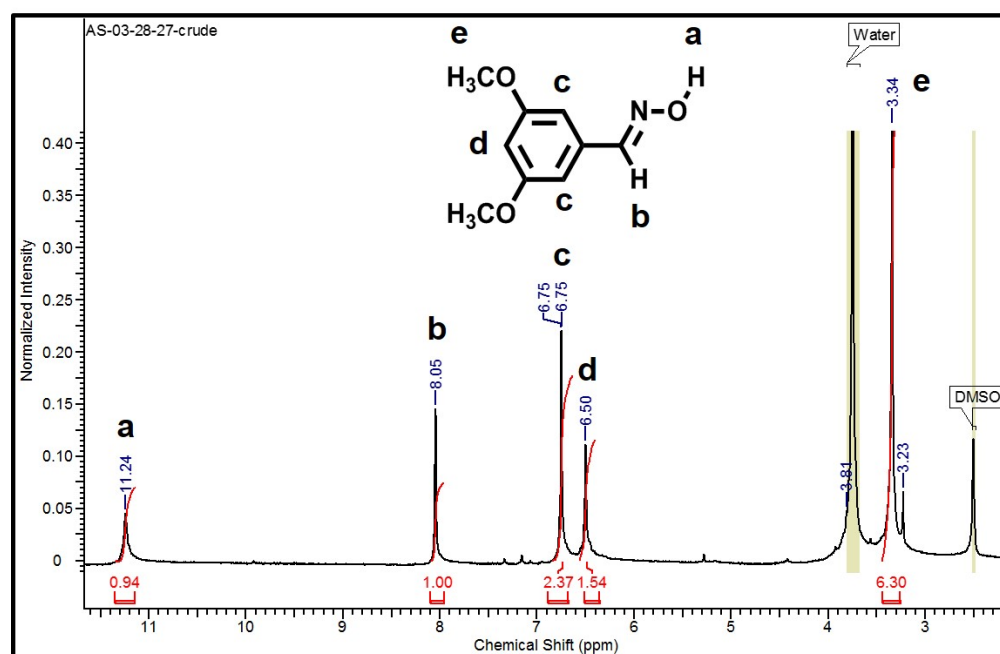


Figure 3.9 ^1H NMR spectrum of 16.

In the case of ketone-oxime synthesis, the products are characterized by monitoring the $-\text{CH}_3$ protons, which shift upfield by 0.3-0.5 ppm upon successful conversion of the ketone to the corresponding ketoxime, and are accompanied by the appearance of the oxime $-\text{OH}$ peak at about 11.0 ppm (Figure 3.10).

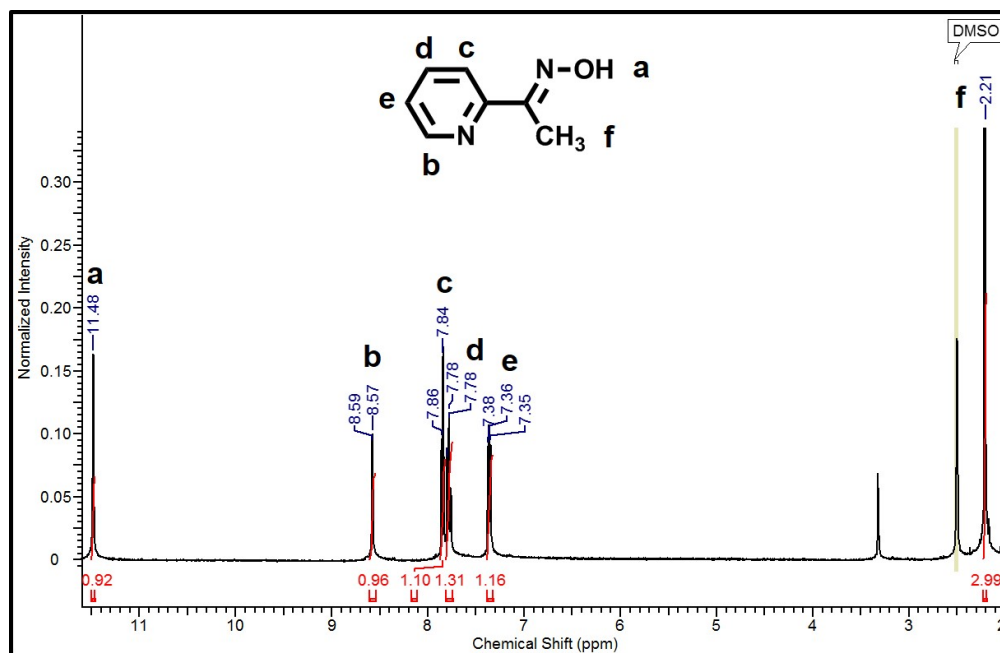


Figure 3.10 ^1H NMR spectrum of **37**.

3.3.2 Versatile synthetic method for aldehyde/ketone-oxime conversions

The chosen aldehydes and ketones were selected with an aim to determining the versatility and robustness of a solvent-assisted mechanochemical route for aldehyde/ketone-oxime conversions. Seven aldehydes (**9-15**) and five ketones (**24-28**) contained electron withdrawing substituents, one aldehyde (**16**) and two ketones (**29** and **30**) were decorated with an electron donating substituent, six aldehydes (**17-22**) and eight ketones (**31-38**) contained structurally active functional groups such as $-\text{COOH}$, $-\text{OH}$, $-\text{NH}_2$ and pyridyl group, two ketones were multi-functionalized (**39** and **40**), and finally one aliphatic aldehyde (**23**) and three aliphatic ketones (**41-43**) were included. The broad range of starting materials will help establish the versatility of this green and facile route to oxime synthesis.

Complete stoichiometric conversion of the aldehydes/ketones to the corresponding oximes was observed in 27 of 35 reactions (**9-12**, **15-16**, **18**, **20-31**, **34-41**), as a clean ^1H NMR spectrum for the products was obtained from the ground mixture itself (Figure 3.11). There was no evidence of unwanted side reactions taking place, and pure compounds (by melting point determination) were obtained by washing the crude ground mixture with water to remove any inorganic salts.

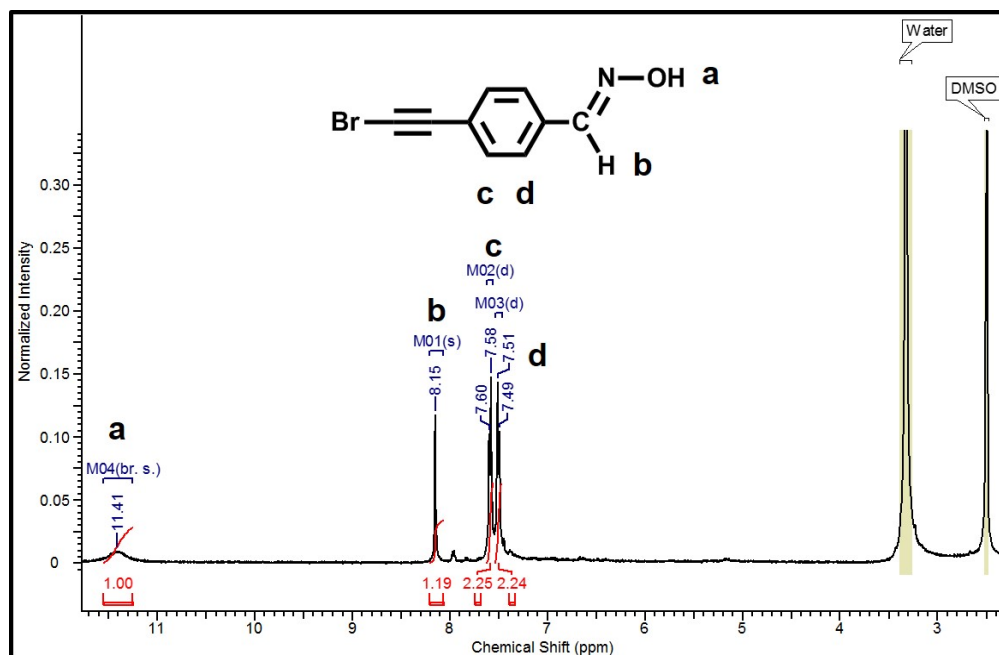
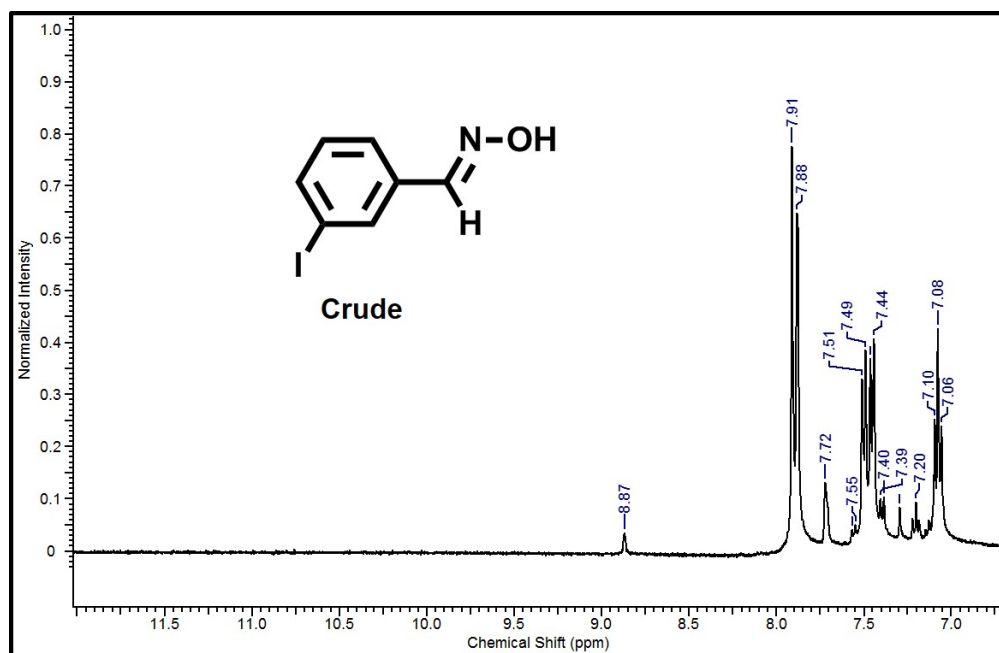
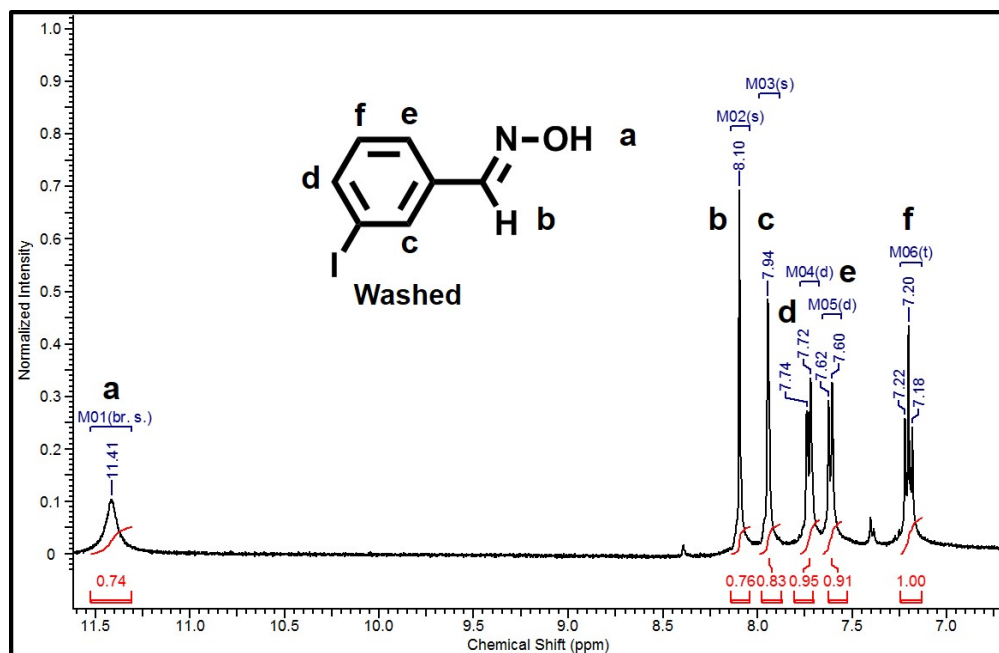


Figure 3.11 ^1H NMR spectrum of the ground mixture of **12**.

In eight cases (**13**, **14**, **17**, **19**, **32**, **33**, **42**, and **43**), an extra set of peaks was observed in the aromatic region of the ^1H NMR spectrum, which was attributed to a small amount of deprotonated oxime in the ground mixture (due to presence of excess base) (Figure 3.12). Upon washing the crude mixtures with water, the oximes become protonated again, and pure compounds (based on a clean ^1H NMR spectrum, and melting point determination) were obtained in each case.



(a)



(b)

Figure 3.12 ^1H NMR spectrum of **14** before (a) and after (b) an aqueous wash.

It is apparent that the presence of electron withdrawing (**9-15**, **24-28**), electron donating (**16**, **29-30**), or structurally active functionalities such as $-\text{COOH}$ (**17**), $-\text{OH}$ (**18-21**, **31-32**), and pyridyl group (**22**, **35-38**), does not adversely affect this mechanochemical route and successful

aldehyde/ketone-oxime conversions can be achieved in each case. Furthermore, multi-functional (**39-40**) and aliphatic (**23**, **41-43**) reactants can also be efficiently converted to the corresponding oximes under ambient conditions.

In the case of 4-aminoacetophenone (**33**), only a 70% conversion to the corresponding oxime could be obtained (Figure 3.13), even upon increasing the ratios of hydroxylamine hydrochloride and base, which can be attributed to the strongly electron donating effect of the -NH₂ group in the 4-position. Whereas, in the case of 3-aminoacetophenone (**34**), 100% conversion to the corresponding oxime is achieved, because the -NH₂ group in the 3-position in **34**, does not exert a similar electron donating effect as seen in **33**.

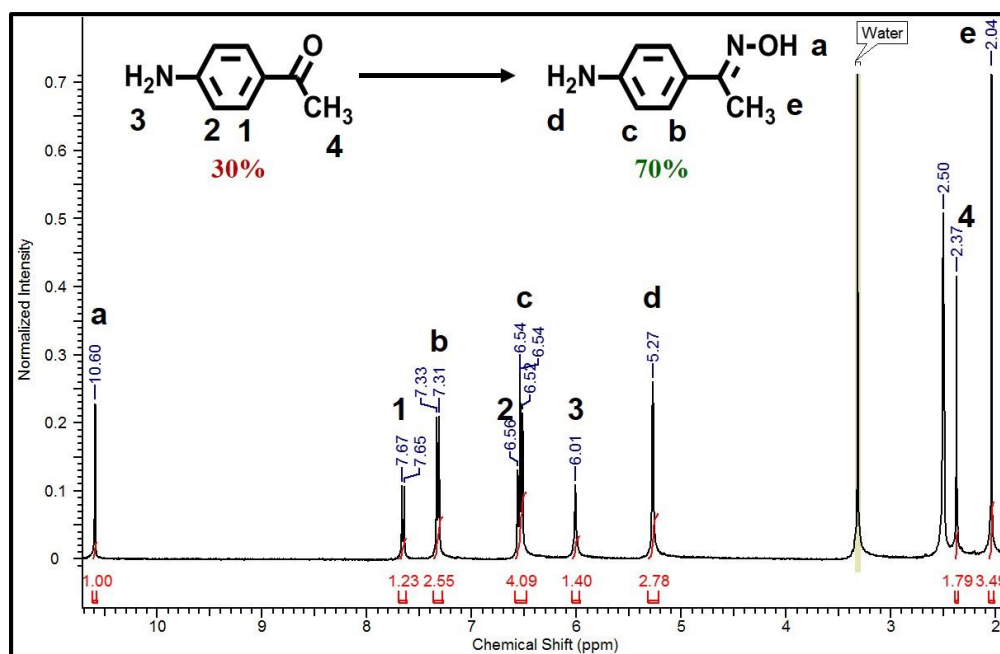


Figure 3.13 ¹H NMR spectrum of ground mixture of **33**.

3.3.3 Relative reactivity of aldehyde-oxime versus ketone-oxime conversions

In order to examine the relative reactivity of aldehyde-oxime *versus* ketone-oxime conversions (Figure 3.14), a 1 : 1 mmol ratio of benzaldehyde and acetophenone were ground together with 1 mmol of hydroxylamine and base. The obtained product ratio was 95% : 5% in favour of the aldehyde, which illustrates the greater reactivity of the aldehyde group when the two functional groups are located on different molecules. A similar product distribution (100% : 0%) has been observed in a previous study²⁰ involving competitive ball-milling of *ortho/para* nitrobenzaldehyde *vs.* *ortho/para* nitroacetophenone at room temperature.

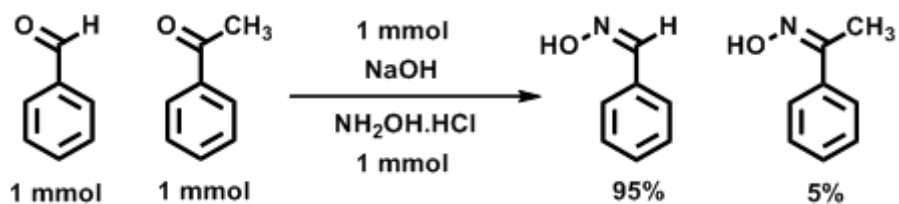


Figure 3.14 Relative reactivity of aldehyde-oxime *versus* ketone-oxime conversions.

There was a distinct change in the product ratio, when the two functional groups were located on the same backbone (Figure 3.15). Upon grinding 1 mmol of 4-acetylbenzaldehyde with 1 mmol of hydroxylamine and base, the obtained product distribution was 65% : 35% in favour of the aldehyde-oxime. This can be attributed to a possible electronic factor that comes into play, when the two functional groups are on the same backbone, as the electron withdrawing effect of the aldehyde group may enhance the reactivity of the ketone.

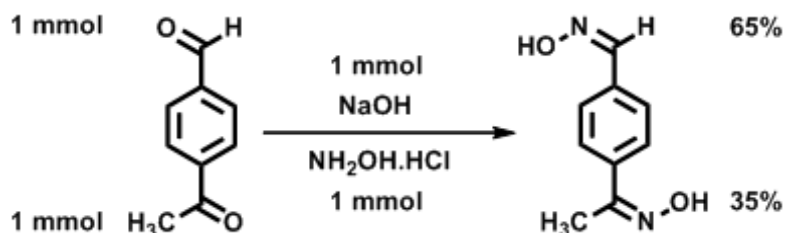


Figure 3.15 Relative reactivity of aldehyde *vs* ketone group when present on the same backbone.

A third experiment was designed to test this explanation, where 1 mmol each of 4-methylacetophenone (electron donating substituent) and 4-cyanoacetophenone (electron withdrawing substituent) were ground together in the presence of 1 mmol of hydroxylamine and base (Figure 3.16). It is observed that 80% of 4-cyanoacetophenone was converted to the corresponding oxime, as compared to only 20% conversion in case of 4-methylacetophenone, which further shows that the electron withdrawing effect of the nitrile group enhances the reactivity of the ketone group, and thus facilitates ketone-oxime conversions.

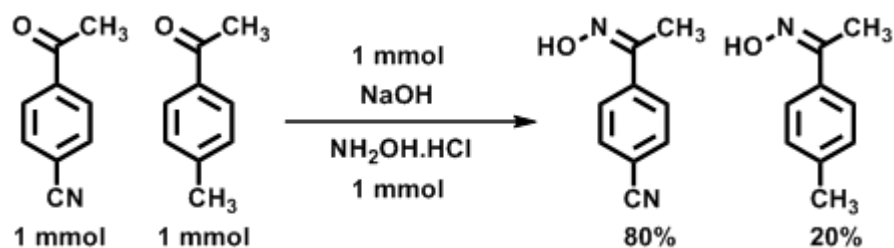


Figure 3.16 Effect of substituents on the ketone-oxime conversions.

3.4 Conclusions

A green and facile mechanochemical route to aldehyde/ketone-oxime conversions has been established by examining 15 aldehydes²⁸ and 20 ketones³⁹ that are decorated with different functional groups. It is clear that the presence of electron withdrawing (**9-15**, **24-28**), electron donating (**16**, **29-30**), structurally active (**17-22**, **31-38**), multi-functionalized (**39-40**), or aliphatic (**23**, **41-43**) substituents, does not adversely affect this robust synthetic route. Competitive experiments have shown that the aldehyde group has a greater reactivity in comparison to the ketone group, and also electron withdrawing substituents enhance, whereas electron donating substituents reduce the relative reactivity of a reactant. The simplicity of this ambient condition synthetic process, coupled with the ease of scalability make this route a better and greener alternative to existing methods of aldehyde/ketone-oxime conversions.

References

- 1 (a) Sheldon, R. A. *Chem. Soc. Rev.* **2012**, *41*, 1437. (b) Dunn, P. J. *Chem. Soc. Rev.* **2012**, *41*, 1452.
- 2 Anastas, P. T.; Warner, J. C. *Green Chemistry: Theory and Practice*, Oxford University Press: New York, 1998.
- 3 (a) Delori, A.; Friščić, T.; Jones, W. *CrystEngComm* **2012**, *14*, 2350. (b) Friščić, T. *Chem. Soc. Rev.* **2012**, *41*, 3493.
- 4 James, S. L.; Adams, C. J.; Bolm, C.; Braga, D.; Collier, P.; Friščić, T.; Grepioni, F.; Harris, K. D. M.; Hyett, G.; Jones, W.; Krebs, A.; Mack, J.; Maini, L.; Orpen, A. G.; Parkin, I. P.; Shearouse, W. C.; Steed, J. W.; Waddell, D. *Chem. Soc. Rev.* **2012**, *41*, 413.
- 5 Friščić, T. *J. Mater. Chem.* **2010**, *20*, 7599.
- 6 Friščić, T.; Halasz, I.; Beldon, P. J.; Belenguer, A. M.; Adams, F.; Kimber, S. A. J.; Honkimaki, V.; Dinnebier, R. E. *Nature Chem.* **2013**, *5*, 66.
- 7 Frutos, R. P.; Spero, D. M. *Tetrahedron Lett.* **1998**, *39*, 2475.
- 8 Sasatani, S.; Miyazak, T.; Maruoka, K.; Yamamoto, H. *Tetrahedron Lett.* **1983**, *24*, 4711; S. Negi, M. Matsukura, M. Mizuno and K. Miyake, *Synthesis*, 1996, 991.
- 9 (a) Anand, N.; Owston, N. A.; Parker, A. J.; Slatforda, P. A.; Williamsa, J. M. J. *Tetrahedron Lett.* **2007**, *48*, 7761. (b) Mendelsohn, B. A.; Lee, S.; Kim, S.; Teyssier, F.; Aulakh, V. S.; Ciufolini, M. A. *Org.Lett.* **2009**, *11*, 1539.
- 10 Li, H. Q.; Xiao, Z. P.; Luo, Y.; Yan, T.; Lv, P. C.; Zhu, H. L. *Eur. J. Med. Chem.* **2009**, *44*, 2246.
- 11 (a) Dave, P. R.; Forshar, F. *J. Org. Chem.* **1996**, *61*, 8897. (b) Olah, G. A.; Ramaiah, P.; Lee, C. S.; Suryaprakash, G. K. *SynLett.* **1992**, 337.
- 12 Chandrasekhar, S.; Gopalaiah, K. *Tetrahedron Lett.* **2001**, *42*, 8123.
- 13 <http://books.mcgraw-hill.com/EST10/site/supparticles/Oxime-480600.pdf>
- 14 http://ntp.niehs.nih.gov/ntp/htdocs/ST_rpts/tox051.pdf
- 15 (a) Konidaris, K. F.; Katsoulakou, E.; Kaplanis, M.; Bekiari, V.; Terzis, A.; Raptopoulou, C. P.; Manessi-Zoupa, E.; Perlepes, S. P. *Dalton Trans.* **2010**, *39*, 4492. (b) Chaudhuri, P.; Weyhermüller, T.; Wagner, R.; Khanra, S.; Biswas, B. Bothe, E.; Bill, E. *Inorg. Chem.* **2007**, *46*, 9003.
- 16 (a) Aakeröy, C. B.; Fasulo, M.; Schultheiss, N.; Desper, J.; Moore, C. *J. Am. Chem. Soc.* **2007**, *129*, 13772. (b) Low, J. N.; Santos, L. M. N. B. F.; Lima, C. F. R. A. C.; Brandão, P.; Gomes, L. R. *Eur. J. Chem.* **2010**, *1*, 61.
- 17 Sridhar, M.; Narsaiah, C.; Raveendra, J.; Reddy, G. K.; Reddy, M. K. K.; Ramanaiah, B. C. *Tetrahedron Lett.* **2011**, *52*, 4701.
- 18 Kad, G. L.; Bhandari, M.; Kaur, J.; Rathee, R.; Singh, J. *Green Chemistry* **2001**, *3*, 275.
- 19 Sharjhi, H.; Sarvari, M. H. *J. Chem. Res. (S)* **2000**, *1*, 24.
- 20 Mokhtari, J.; Naimi-Jamal, M. R.; Hamzeali, H.; Dekamin, M. G.; and Kaupp, G. *ChemSusChem* **2009**, *2*, 248.
- 21 Elmakssoudi, A.; Abdelouahdi, K.; Zahouily, M.; Clark, J.; Solhy, A. *Catalysis Communications* **2012**, *29*, 53.
- 22 Damljanović, I.; Vukićević, M.; and Vukićević, R. D. *Monatsh. Chem.* **2006**, *137*, 301.
- 23 Thamyongkit, P.; Muresan, A. Z.; Diers, J. R.; Holten, D.; Bocian, D. F.; Lindsey, J. S. *J. Org. Chem.* **2007**, *72*, 5207.

-
- 24 Thorand, S.; Krause, N. *J. Org. Chem.* **1998**, *63*, 8551.
- 25 Wautelet, P.; Le Moigne, J.; Videva, V.; Turek, P. *J. Org. Chem.* **2003**, *68*, 8025.
- 26 Osowska, K.; Lis, T.; Szafert, S. *Eur. J. Org. Chem.* **2008**, 4598.
- 27 Aakeröy, C. B.; Fasulo, M.; Schultheiss, N.; Desper, J.; Moore, C. *J. Am. Chem. Soc.* **2007**, *129*, 13772.
- 28 Aakeröy, C. B.; Sinha, A. S.; Epa, K. N.; Spartz, C. L.; Desper, J. *Chem. Commun.* **2012**, *48*, 11289.
- 29 Tavares, A.; Schneider, P. H.; Merlo, A. A. *Eur. J. Org. Chem.* **2009**, *6*, 889.
- 30 Ahmed, M.; Nencetti, S.; Mazzoni, M. R.; Porchia, F.; Antonelli, F.; Lapucci, A. *Med. Chem.* **2008**, *4*, 298.
- 31 Toyo Rayon Co. Ltd., Patent # *FR 1402475 (A)*, 1965.
- 32 J. Buckingham and F. MacDonald, *Dictionary of Organic Compounds, Sixth Edition*, Chapman and Hall Electronic Publishing, 1995.
- 33 Wiemann, J.; Glacet, Ch. *Bulletin de la Societe Chimique de France* **1950**, 176.
- 34 Ginsburg, S.; Wilson, I. B. *J. Am. Chem. Soc.* **1957**, *79*, 481.
- 35 Yukawa, Y.; Sakai, M.; Suzuki, S. *Bull. Chem. Soc. Jpn.* **1966**, *39*, 2266.
- 36 Prateptongkum, S.; Jovel, I.; Jackstell, R.; Vogl, N.; Weckbecker, C.; Beller, M. *Chem. Commun.* **2009**, *15*, 1990.
- 37 Neufeldt, S. R.; Sanford, M. S. *Org. Lett.* **2010**, *12*, 532.
- 38 Lyle, R. E.; Troscianiec, H. J. *J. Org. Chem.* **1955**, *20*, 1757.
- 39 Aakeröy, C. B.; Sinha, A. S. *RSC Adv.* **2013**, *3*, 8168.
- 40 Reddy, N. S.; Reddy, R. B.; Mukkanti, K. *Tetrahedron. Lett.* **2011**, *52*, 4888.
- 41 Witek, S.; Bielawski, J.; Bielawska, A. *Polish J. Chem.* **1981**, *55*, 2589.
- 42 Dong, W-K.; Zhang, S-T.; Sun, Y-X.; Liu, M.; Zhang, Y-J.; Gao, X-H. *Zeitschrift fuer Kristallographie-New Crystal Structures* **2012**, *227*, 99.
- 43 Ende, D. J. am; Ripin, D. H. B.; Weston, N. P. *Thermochimica Acta* **2004**, *419*, 83.
- 44 Glynn, C. W.; Turnbull, M. M. *Transition Metal Chemistry* **2002**, *27*, 822.
- 45 Baddeley, G.; Wrench, E. *J. Chem. Soc.* **1956**, 4943.
- 46 Bruton, E. A.; Brammer, L.; Pigge, F. C.; Aakeröy, C. B.; Leinen, D. S. *N. J. Chem.* **2003**, *27*, 1084.
- 47 Carmack, M.; Bullitt, O. H.; Handrick, G. R.; Kissinger, L. W.; Von, I. *J. Am. Chem. Soc.* **1946**, *68*, 1220.
- 48 Zaitsev, A. B.; Schmidt, E. Yu.; Mikhaleva, A. M.; Afonin, A. V.; Ushakov, I. A. *Chemistry of Heterocyclic Compounds* **2005**, *41*, 722.

Chapter 4 - Structural chemistry of oximes

4.1 Introduction

The predictable chemical reactivity that is associated with functional groups such as aldehydes, esters, and amines, etc. is one of the reasons for the unparalleled success of synthetic organic chemistry.¹ Likewise, detailed information about the structural preferences and patterns of behavior that can be expected from specific chemical functionalities^{2,3} is required for the targeted assembly of desired solid-state architectures⁴ or of multi-component crystals with pre-determined stoichiometry and metrics.⁵ Hence, for the advancement of crystal engineering to a higher level of complexity, the structural chemistry of key functional groups such as acids ($R_2^2(8)$ motif),^{6,7,8} amides ($C(4)R_4^2(8)$ motifs)^{7,9} and phenols ($C(2)$ chains)¹⁰ have been systematically examined and subsequently established to such an extent that confident predictions can be made as to how such entities are likely to self-assemble in the solid-state (Figure 4.1).²

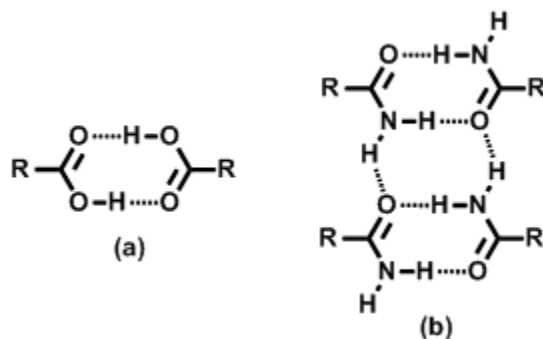


Figure 4.1 (a) Hydrogen-bonded $R_2^2(8)$ dimer in carboxylic acids; (b) Hydrogen-bonded infinite $C(4)R_4^2(8)$ ribbons in amides.

4.1.1 Oximes

Oximes are well-known,^{11,12} easily available¹² and ubiquitous in both research laboratories and in large-scale production,^{13,14} and studies pertaining to the structural aspects of some oximes have been presented. The patterns of hydrogen-bonding in crystalline oximes have been previously analyzed by Bertolasi *et al.*,¹⁵ which was followed by a systematic investigation of hydrogen-bonding in aromatic and aliphatic dioximes by Bruton *et al.*, wherein they observed

that the most common hydrogen-bonding motif responsible for propagating the network structures was the oxime...oxime $R_2^2(6)$ dimer (via O-H...N interactions) (Figure 4.2).¹⁶

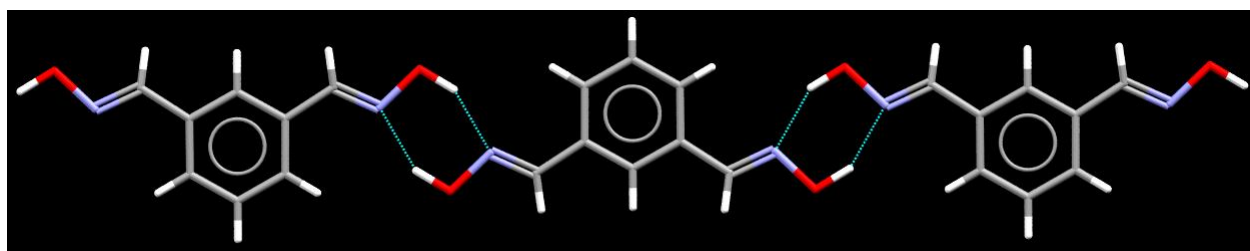


Figure 4.2 Single-crystal structure of isophthalaldehyde dioxime highlighting the oxime...oxime dimer.

Recently, Low *et. al.* examined the hydrogen-bonding patterns in aldoximes, ketoximes, and O-alkylated ketoximes, with and without competing acceptors (other acceptors than the oxime nitrogen atom).¹⁷ The different hydrogen-bonding motifs present, and the effect of competing acceptors on the assembly of these motifs for aldoximes and ketoximes were outlined in this study. However, a systematic and parallel investigation of the structural chemistry of the most common and important members of the oxime family, has not yet been done.

4.1.1.1 Applications of oximes

The general formula for oximes is $RR'C=N-OH$ (Figure 4.3), and due to their potential to act as both a weak acid ($pK_a \approx 11$) and a weak base ($pK_b \approx 12$), the oxime anions tend to be ambident in nature and thus, can be used for the synthesis of different compounds such as oxime ethers¹⁴ or nitrones.¹⁴ They have also been employed in the characterization, purification and protection of functionalities such as aldehydes and ketones.¹⁸ Moreover, their nature of being strong coordinating ligands upon deprotonation has been exploited in metal-coordination chemistry.¹⁹

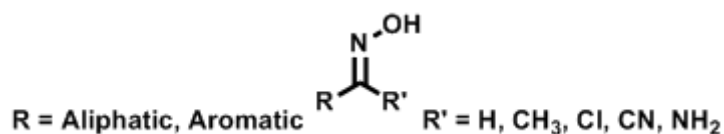


Figure 4.3 Different types of oximes.

An examination of the Cambridge Structural Database (CSD)^{20,21} for the literature on the structural chemistry of oxime-containing compounds reveals the popularity of this class of organic compounds; the four most common types of oximes ($R' = -H, -CH_3, -NH_2, -CN$) give a total of 2392 hits, of which 592 are organic substances. An elevated interest in the synthesis and

applications of oximes over the past few years shows the wide interest in this chemical functionality (Figure 4.4). Furthermore, as the previous cumbersome solution-based methods¹⁸ of synthesis of oximes are likely to be replaced with more versatile routes including green and robust mechanochemical pathways,^{22,23} the use and importance of oximes are likely to continue to grow.

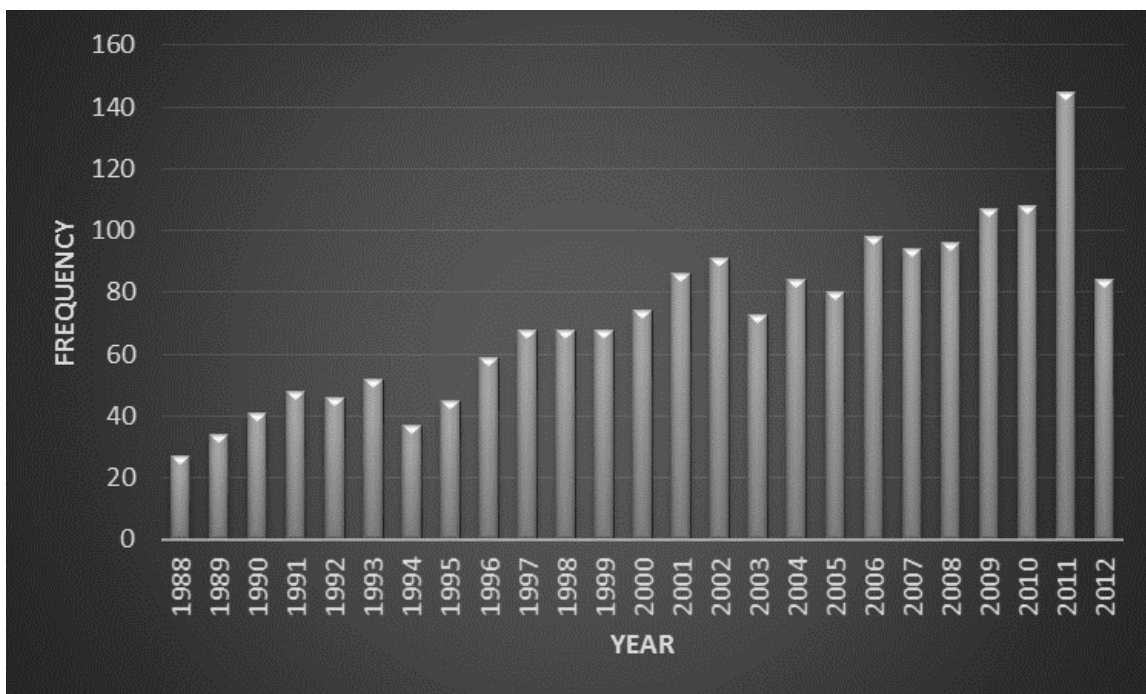


Figure 4.4 Number of reported single crystals for oximes ($R' = -H, -CH_3, -NH_2, -CN$), 1988-2012.

4.1.1.2 Hydrogen-bonding in oximes

Oximes can act as both hydrogen-bond donors (via the $-O-H$ moiety), and as hydrogen-bond acceptors (via the $-C=N$ and the $-OH$ moieties). Consequently, they can either form dimers *via* $O-H \cdots N$ intermolecular interactions, or oxime \cdots oxime catemers *via* intermolecular $O-H \cdots N=C$ and $O-H \cdots OH$ hydrogen-bonds in the solid-state (Figure 4.5).¹⁵

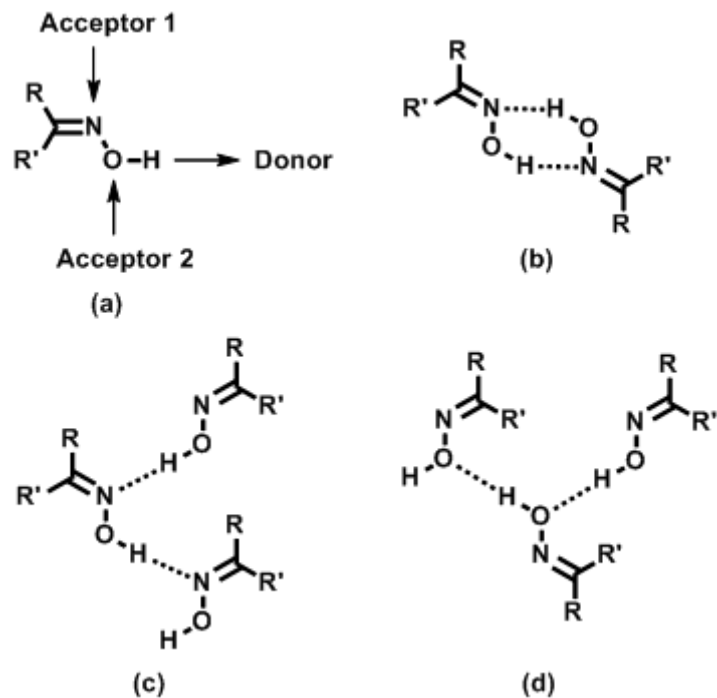


Figure 4.5 (a) Hydrogen-bond donor/acceptors in oximes; (b) Hydrogen-bonded dimers; (c) Catemer formation via $-O-H\cdots N$ hydrogen-bonded chains; (d) Catemer formation via $-O-H\cdots O$ hydrogen-bonded chains.

Moreover, the structural chemistry of oximes having substituents (R') such as $H_2N-/N\equiv C-$ moieties, may also be affected via $O-H\cdots NH_2$ and $O-H\cdots N\equiv C$ interactions in the solid-state (Figure 4.6).

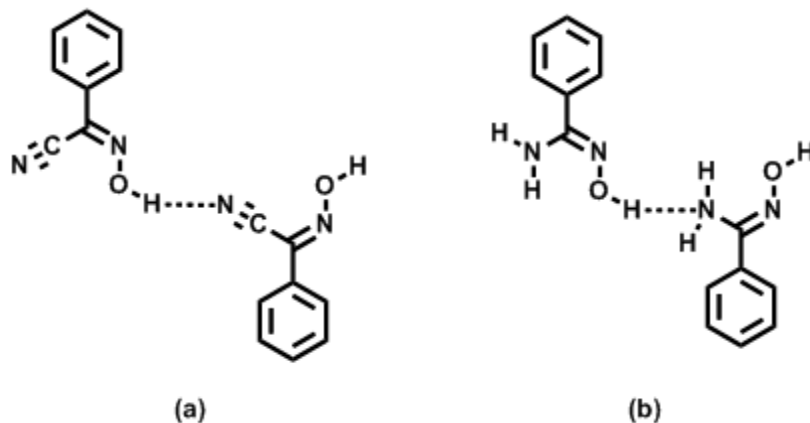


Figure 4.6 (a) Hydrogen-bonded chains via $O-H\cdots N\equiv C$ interactions in cyano-oximes; (b) Hydrogen-bonded chains via $O-H\cdots NH_2$ interactions in amidoximes.

Despite the increasing number of crystallographic studies of oximes, a detailed examination of their structural chemistry and behavioral patterns in solid-state has not yet been clearly established. In this chapter, we are particularly interested in:

- Classifying the different hydrogen-bonded homomeric intermolecular oxime...oxime interactions for the four major categories of oximes ($R' = -H, -CH_3, -NH_2, -CN$) (Figure 4.7), by analyzing the available solid-state data in the CSD, complemented by three new crystal structures.
- Establishing the patterns of behavior of the four major categories of oximes ($R' = -H, -CH_3, -NH_2, -CN$).
- Investigating the possible structural or electronic effects that govern the binding preferences of oximes as a function of R' group.

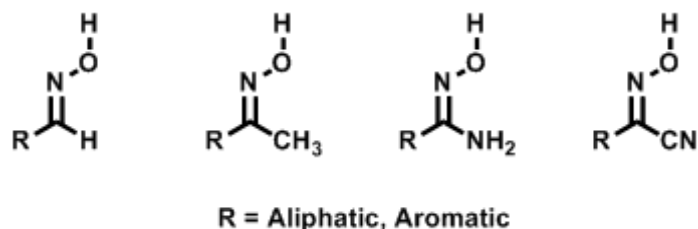


Figure 4.7 Four major categories of oximes examined in this chapter.

4.2 Experimental

4.2.1 Synthesis and single-crystal growth

All chemicals, unless otherwise noted, were purchased from Aldrich and used without further purification. The synthesis of 4-iodobenzaldehyde oxime (**13**), 4-iodoacetophenone oxime (**27**) and 4-cyanoacetophenone oxime (**28**) are described in Chapter 3. Melting points were determined on a Fisher-Johns melting point apparatus and are uncorrected. The single-crystal growth conditions and melting points of **13**, **27** and **28** are given in Table 4.1.

Table 4.1 Single-crystal growth details and melting points of **13**, **27** and **28**.

Compound	Solvent for crystal growth	Observed melting point (°C)	Literature melting point (°C)
4-Iodobenzaldehyde oxime (13)	Ethyl acetate	100 - 102	101 - 103 ²²
4-Iodoacetophenone oxime (27)	Ethyl acetate	150 - 153	150 - 153 ²³
4-Cyanoacetophenone oxime (28)	Ethyl acetate	156 - 160	156 - 158 ²⁴

4.2.2 CSD search

Oxime...oxime intermolecular interactions were mined from data in the CSD using four different searches (Figure 4.8). Search 1 in the CSD on the four major types of oximes ($R' = -H, -CH_3, -NH_2, -CN$), gives data that show oxime...oxime O-H...N hydrogen bonds, whereas search 2 gives all the O-H...N hydrogen-bonded dimers. The difference between the data sets of search 1 and 2 represents the catemers produced by O-H...N hydrogen-bonds. Search 3 finds O-H...O hydrogen-bonded catemers, whereas search 4 finds the O-H...NH₂ chains found in amidoximes. In order to focus on oxime...oxime interactions in the solid-state, all inorganic substances, salts and co-crystals have been excluded from the search, and N/O heterocycles, α -carbonyl substituted oximes and solvates have also been excluded, as they can act as hydrogen-bond acceptors and donors, and thus disrupt oxime...oxime interactions. In addition, as we are focusing on oxime...oxime intermolecular interactions, all 1,2-disubstituted bisoximes have been excluded, as they are more prone to intramolecular hydrogen-bonded motifs. The existing CSD data has been complemented by adding three new crystal structures.

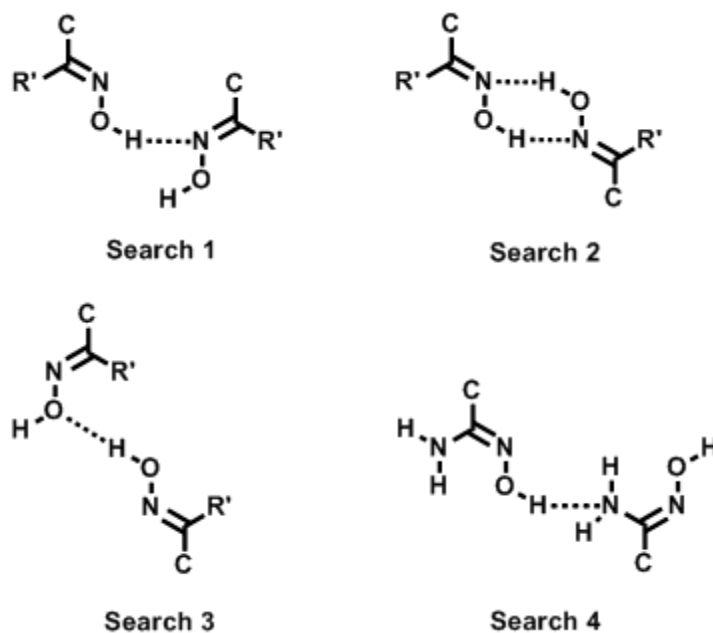


Figure 4.8 Defined parameters in the CSD during the search for data on oximes.

4.2.3 Molecular electrostatic potential calculations

Charge calculations were performed using Spartan'04 (Wavefunction, Inc. Irvine, CA). All molecules were geometry optimized using DFT B3LYP/6-31+G* *ab initio* calculations, with

the maxima and minima in the electrostatic potential surface (0.002 e au⁻¹ iso-surface) determined using a positive point charge in vacuum as a probe.

4.3 Results

The intermolecular interactions between two or more oximes in the solid-state depends upon the presence of different acceptors and donors in oximes, and can be classified into four major categories; (i) dimers based on –O–H···N hydrogen-bonds ($R_2^2(6)$ motif), (ii) catemers directed by –O–H···N interactions (C(3) chains), (iii) catemers governed by –O–H···O hydrogen-bonds (C(2) chains), and (iv) oximes in which the R' group plays a dominant role by accepting a hydrogen-bond from the oxime moiety (C(6) catemeric chains).

4.3.1 Aldoximes ($R' = H$)

4.3.1.1 Crystal structure of **13**

An examination of the single-crystal structure of **13** reveals that the hydrogen-bond donors (the –OH moieties) are involved in –O–H···N intermolecular interactions with oxime nitrogen atoms (the C=N moiety) of neighboring molecules (O17···N17 2.839(2) Å, O17–H17···N17 2.08(3) Å), thereby forming dimers (Figure 4.9). The interlinking of these dimers occurs *via* halogen bonds between an iodine atom of one molecule and the lone pair of an oxygen atom of an adjacent molecule, thus indicating that these are electrostatically driven interactions. The C–I···O bond angle is 154.74(5)° and the O···I bond distance is 3.4471(15) Å.

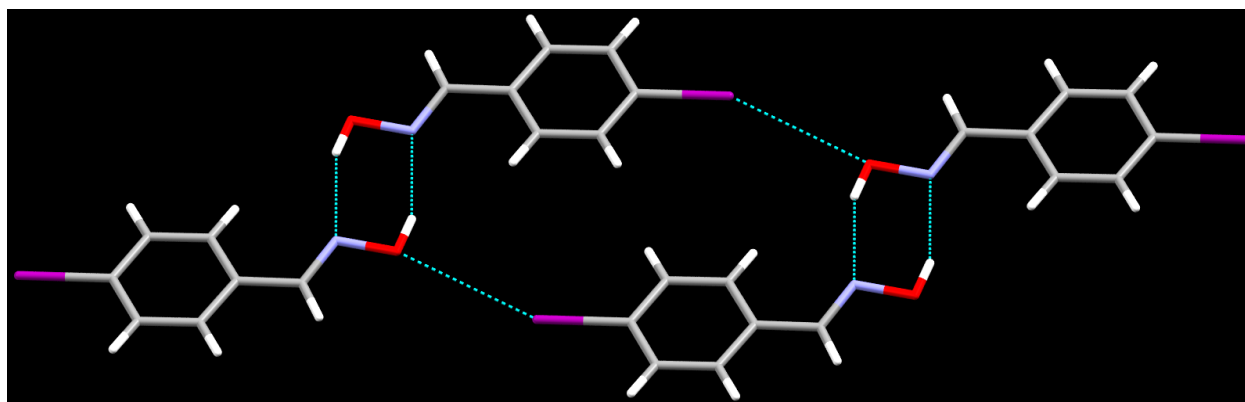


Figure 4.9 Section of the crystal structure of **13** displaying the hydrogen bonded $R_2^2(6)$ dimer and an I···O halogen bond.

4.3.1.2 CSD data

There are a total of 58 crystal structures of aldoximes in the CSD, 42 of which form hydrogen-bonded dimers via $\text{-O-H}\cdots\text{N}$ interactions (average $\text{HO}\cdots\text{N}$ bond distance and $\text{O-H}\cdots\text{N}$ bond angle is $2.82(4)$ Å and $150(7)$ °, respectively) (Figure 4.10). There are fourteen aldoximes in which catemer formation is directed by $\text{-O-H}\cdots\text{N}$ interactions (average $\text{HO}\cdots\text{N}$ bond distance and $\text{O-H}\cdots\text{N}$ bond angle is $2.79(4)$ Å and $171(5)$ °, respectively), whereas in two cases the primary interactions are $\text{-O-H}\cdots\text{O}$ hydrogen-bonds leading to catemers. Upon summarizing these observations, it shows that 72% aldoximes exist as dimers, 24% as catemers with $\text{-O-H}\cdots\text{N}$ interactions, and 4% display $\text{-O-H}\cdots\text{O}$ hydrogen-bonded catemers.

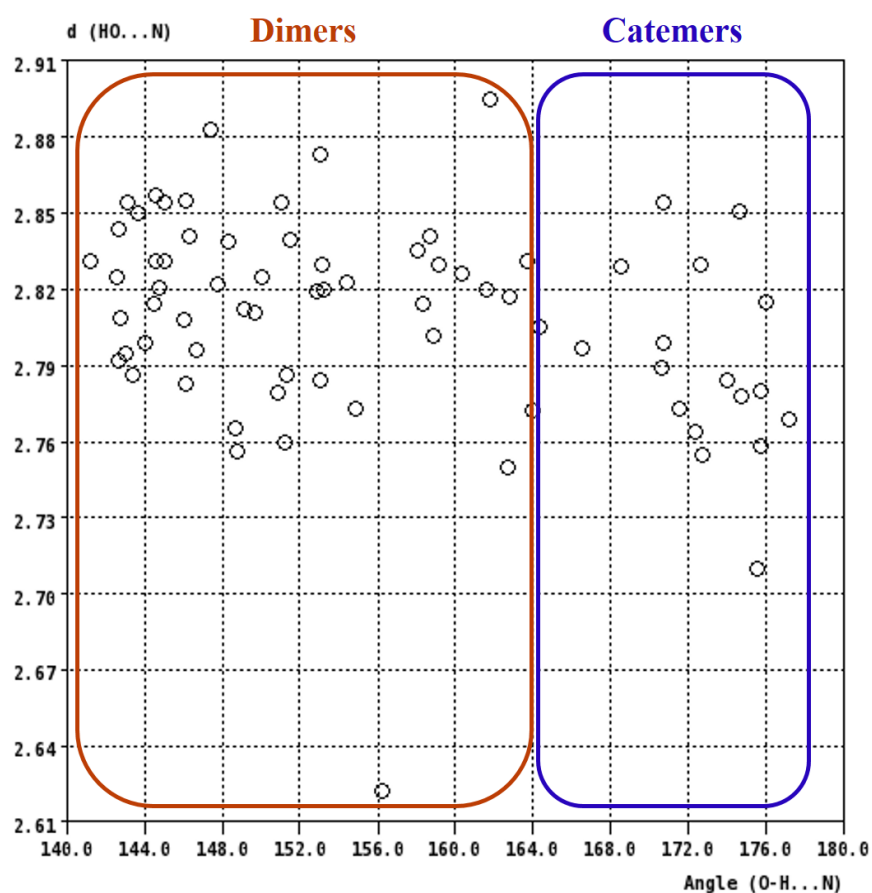


Figure 4.10 $\text{HO}\cdots\text{N}$ bond distance (Å) vs $\text{O-H}\cdots\text{N}$ bond angle (°) for dimers and catemers of aldoximes.

4.3.2 Ketoximes ($R' = CH_3$)

4.3.2.1 Crystal structure of 27

Upon examining the crystal structure of **27**, the key features were found to be identical to those displayed by **13**. The primary motif is the -O-H \cdots N hydrogen-bonded dimer with a HO \cdots N bond distance of 2.813(3) Å (O27 \cdots N17) (Table 4.2). The neighboring hydrogen-bonded dimers are interconnected by -C-I \cdots O halogen-bonds, where the I \cdots O bond distance is 3.1727(17) Å (Figure 4.11) (Table 4.2). The presence of a pseudo two-fold rotation axis relates the two asymmetric units in **27**.

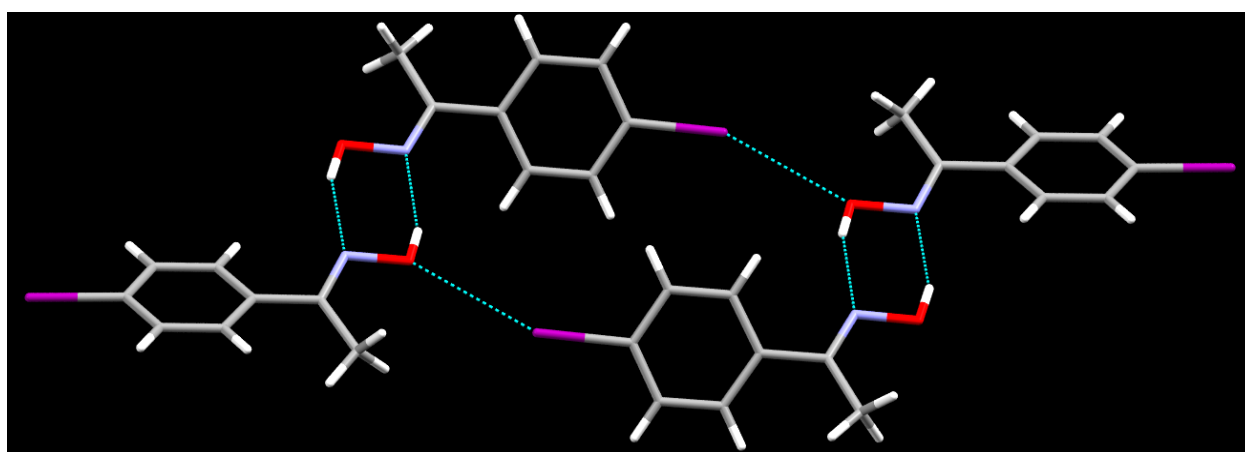


Figure 4.11 Section of the crystal structure of **27** displaying the hydrogen bonded $R_2^2(6)$ dimer and an I \cdots O halogen bond.

Table 4.2 Key geometric parameters in the crystal structures of **27** and **28**.

Ligand	$d(\text{OH}\cdots\text{N})/\text{\AA}$	$d(\text{HO}\cdots\text{N})/\text{\AA}$	Angle (O-H \cdots N)/ $^\circ$	$d(\text{I}\cdots\text{O})/\text{\AA}$	Angle (C-I \cdots O)/ $^\circ$
27	2.00(4)	2.813(3)	155(3)	3.1727(17)	154.37(7)
28	1.812(15)	2.7614(14)	160.5(15)	-	-

4.3.2.2 Crystal structure of 28

An examination of the crystal structure of **28** showed the hydrogen-bonded dimers constructed from -O-H \cdots N interactions between adjacent oxime molecules with an HO \cdots N bond distance of 2.7614(14) Å (Figure 4.12) (Table 4.2).

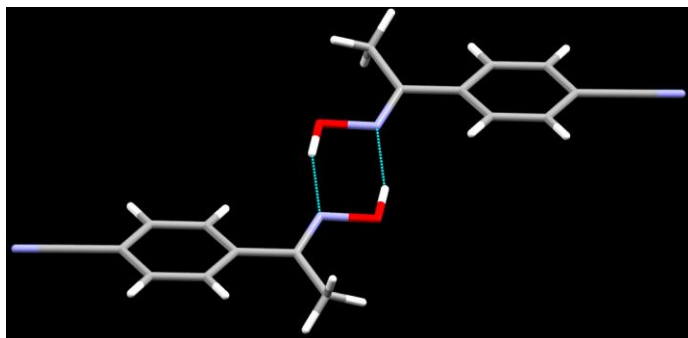


Figure 4.12 Dimer formation ($R_2^2(6)$) in the crystal structure of **28**.

4.3.2.3 CSD data

A search of the CSD generated 37 crystal structures of single-component ketoximes, 32 (87%) of which are dimers directed by $-O-H\cdots N$ hydrogen bonds (average $HO\cdots N$ bond distance and $O-H\cdots N$ bond angle is $2.81(3)$ Å and $154(9)$ °, respectively) (Figure 4.13). The remaining five (13%) ketoximes revealed catemeric chains directed by $-O-H\cdots N$ interactions (average $HO\cdots N$ bond distance and $O-H\cdots N$ bond angle is $2.81(6)$ Å and $172(5)$ °, respectively), whereas none of the ketoximes showed intermolecular $-O-H\cdots O$ hydrogen-bonds.

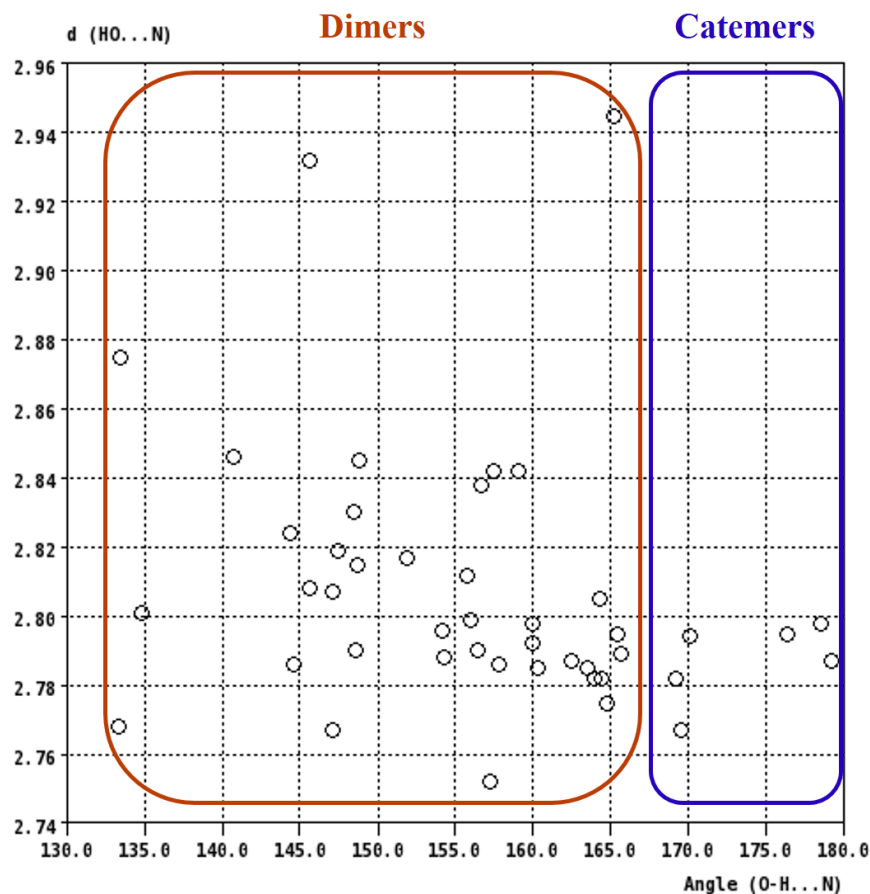


Figure 4.13 HO...N bond distance (Å) vs O-H...N bond angle (°) for dimers and catemers of ketoximes.

4.3.3 Amidoximes ($R' = NH_2$)

4.3.3.1 CSD data

A total of 21 crystal structures are known for amidoximes, fourteen (67%) of which are dimers directed by -O-H...N interactions between adjacent oxime molecules (average HO...N bond distance and O-H...N bond angle is 2.77(4) Å and 145(7)°, respectively) (Figure 4.14). Out of the remaining seven crystal structures, six (28%) form catemeric chains interconnected *via* -O-H...N hydrogen-bonds (average HO...N bond distance and O-H...N bond angle is 2.75(7) Å and 171(8)°, respectively), whereas one (5%) amidoxime forms catemers *via* -O-H...O interactions.

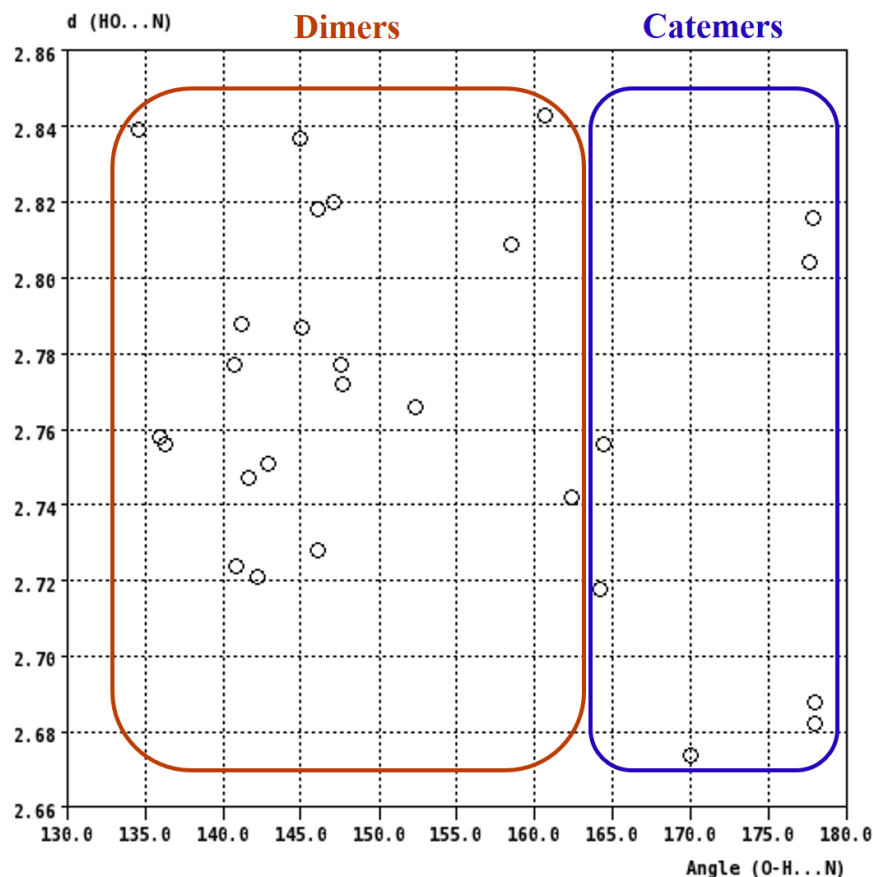


Figure 4.14 HO...N bond distance (Å) vs O-H...N bond angle (°) for dimers and catemers of amidoximes.

4.3.4 Cyano-oximes ($R' = CN$)

A CSD search for cyano-oximes by themselves generated nine crystal structures, all of which showed O-H...N≡C hydrogen-bonds between the oxime moiety and the nitrile nitrogen atom.

4.4 Discussion

An examination of the single-crystal data in the CSD for the four major categories of oximes, subsequently revealed that the oximes can be grouped into four categories based on the specific structure-directing interactions present in order to fully recognize the electronic or structural effects of the substituents (R') on the structures. A summary of the data is given in Table 4.3.

Table 4.3 Primary motifs in crystal structures of oximes.

Type of oxime	$\text{-O-H}\cdots\text{N}$ $\mathbf{R}_2^2(6)$ dimers	$\text{-O-H}\cdots\text{N}$ C(3) catemers	$\text{-O-H}\cdots\text{O}$ C(2) catemers	$\text{-O-H}\cdots\text{N}\equiv\text{C}$ C(6) catemers
Aldoximes ($\text{R}' = \text{H}$)	42 (72%)	14 (24%)	2 (4%)	-
Ketoximes ($\text{R}' = \text{CH}_3$)	32 (87%)	5 (13%)	0 (0%)	-
Amidoximes ($\text{R}' = \text{NH}_2$)	14 (67%)	6 (28%)	1 (5%)	-
Cyano-oximes ($\text{R}' = \text{CN}$)	0 (0%)	0 (0%)	0 (0%)	9 (100%)

4.4.1 Bond lengths and bond angles in dimers and catemers

The formation of dimers and $\text{O-H}\cdots\text{N}$ hydrogen-bonded catemers is only observed for three categories ($\text{R}' = \text{-H, -CH}_3, \text{-NH}_2$). All dimers and $\text{O-H}\cdots\text{N}$ hydrogen-bonded catemers behave in a similar manner in terms of $\text{O-H}\cdots\text{N}$ bond distances (\AA) and $\text{O-H}\cdots\text{N}$ bond angles ($^\circ$), regardless of the substituent present on these oximes. In the case of all dimers, the $\text{O-H}\cdots\text{N}$ bond angles (average value is 150°) show that these hydrogen-bonds lack linearity, and thus highlights the relatively strained $\mathbf{R}_2^2(6)$ motif which is formed in oxime dimers. On the other hand, the hydrogen bonds in the C(3) catemeric chains are closer to linear (average bond angle is 171°) and less constrained, as is expected with catemer formation.

4.4.2 Explanation of trends

For both dimers and catemers, the primary intermolecular interactions are very similar (two $\text{O-H}\cdots\text{N}$ interactions / two molecules) based on enthalpic considerations, but entropically catemer formation is favored over dimers.²⁵ The greater number of dimers in the case of oximes can however be explained on the basis of the three components of the “kinetic chelate effect”;^{25,26} (i) the increased effective concentration of the tethered oxime moiety in dimers when compared to the second hydrogen-bonding molecule in catemers, (ii) the ease with which the tethered moiety can rotate and hydrogen-bond to form dimers, in comparison to the required second effective collision in catemers, and (iii) the lower rate of dissociation in dimers because,

even if one hydrogen-bond breaks, a second one is still holding the moiety in place and consequently, they can quickly rejoin.

4.4.2.1 Aldoximes ($R' = H$) and amidoximes ($R' = NH_2$)

According to the above hypothesis, we would expect to predominantly see $R_2^2(6)$ dimers for each category of oximes via O-H \cdots N interactions between two oxime moieties. However, upon comparing the four types of oximes ($R' = -H, -CH_3, -NH_2, -CN$), it is observed that aldoximes (24%) and amidoximes (28%) show a larger number of C(3) catemeric chains. This behavior can be explained on the basis of molecular electrostatic potential charge calculations (MEPs) (Figure 4.15).

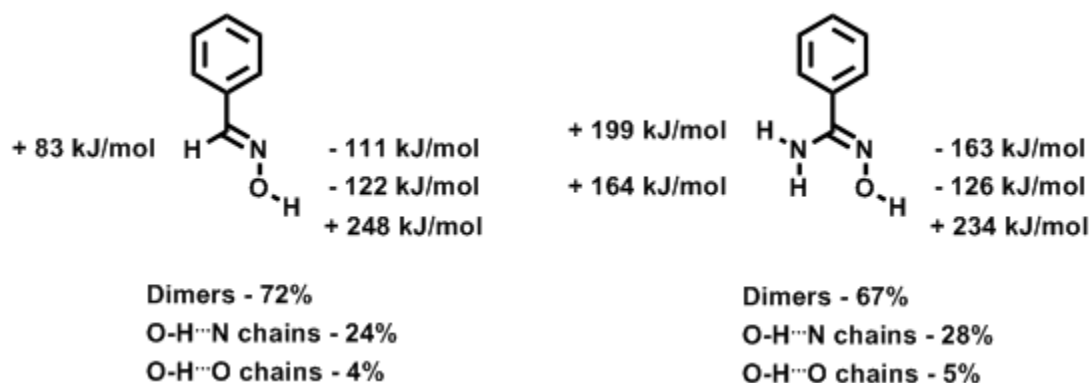


Figure 4.15 Molecular electrostatic potentials (MEPs) for aldoximes and amidoximes.

Both aldoximes and amidoximes possess an acidic proton ($R' = H, NH_2$) on the oxime moiety, which can potentially act as an alternative hydrogen-bond donor. Any such C-H \cdots N / N-H \cdots N interaction between the substituent and the oxime nitrogen atom will hinder the formation of dimers, and thus increase the propensity for the formation of C(3) catemers, as seen in aldoximes and amidoximes.

4.4.2.2 Ketoximes ($R' = CH_3$)

Ketoximes contain two hydrogen-bond acceptors, the oxime nitrogen atom (- 137 kJ/mol) and the oxime oxygen atom (- 117 kJ/mol) (Figure 4.16). Upon comparing the MEP values, it can be inferred that the oxime nitrogen atom is a better hydrogen-bond acceptor. The presence of only one hydrogen-bond donor, the -O-H moiety (+ 250 kJ/mol), coupled with the absence of any interfering substituents on the oxime moiety, directs the ketoximes preferentially towards the formation of $R_2^2(6)$ dimers (87%) in the solid-state.

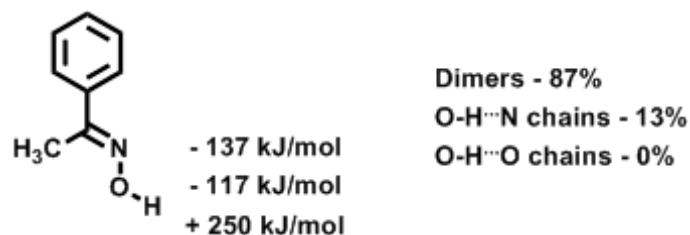


Figure 4.16 Molecular electrostatic potentials (MEPs) for ketoximes.

4.4.2.3 C(2) catemers (via O-H...O interactions) in aldoximes and ketoximes

Two aldoximes (4%) show C(2) catemeric chains in the solid-state via O-H...O interactions, whereas none of the ketoximes do so. For aldoximes, the electrostatic potential charges on the oxime nitrogen atom and oxygen atom are -111 and -122 kJ/mol respectively. Since, these values for the electrostatic potential charges are quite similar, the chances of catemer formation via the oxime oxygen atom increases in the case of aldoximes. On the other hand, the electrostatic potential charge on the oxime nitrogen atom (-137 kJ/mol) in ketoximes is significantly greater than the charge on the oxygen atom (-117 kJ/mol), which makes the nitrogen atom the far better acceptor, thus making it more unfavourable to form catemers directed by O-H...O hydrogen-bonds.

4.4.2.4 Cyano-oximes ($R' = CN$)

Cyano-oximes do not form any dimers or catemers in the solid-state, and this can again be rationalized using the MEPs (Figure 4.17). Cyano-oximes contain three potential hydrogen-bond acceptors, wherein the nitrile nitrogen atom bearing the highest charge (-166 kJ/mol) is the best acceptor. Moreover, there is only one hydrogen-bond donor, the $-O-H$ moiety ($+297$ kJ/mol), hence the primary electrostatic interaction is likely to be the hydrogen-bond between the $-O-H$ moiety and the nitrile nitrogen atom, which is the case for cyano-oximes (100%). This observation is consistent with earlier studies on nitriles based on pK_{HB} , wherein the nitrile moiety has been shown to be a competent hydrogen-bond acceptor.²⁷

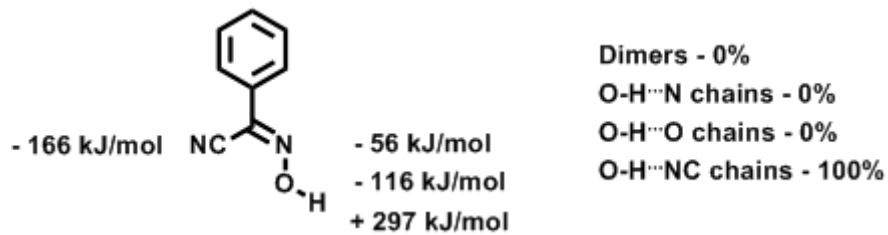


Figure 4.17 Molecular electrostatic potentials (MEPs) for cyano-oximes.

The behavior of cyano-oximes is also supported by calculating the interaction-site pairing energies (ΔE in kJ) using the hydrogen-bond donor parameters (α_i), and the hydrogen-bond acceptor parameters (β_j), utilized by Hunter and coworkers (Figure 4.18).²⁸

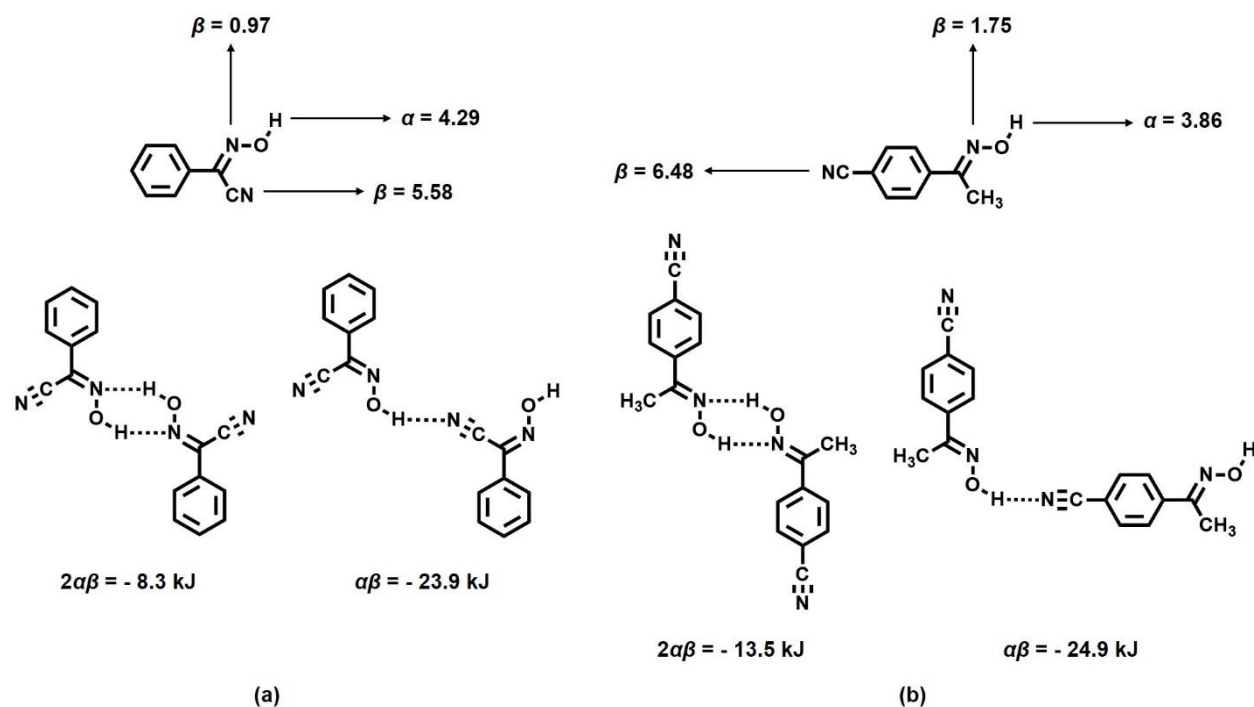


Figure 4.18 Calculated hydrogen-bond parameters α_i , β_j and interaction-site pairing energies, for dimers, and O-H \cdots N \equiv C catemer for cyano-oximes (a); and for **28** (b).

In the case of cyano-oximes, the pairing energies for dimer formation (*via* O-H \cdots N interactions), and for hydrogen-bonding through the nitrile moiety (Figure 4.18 a), show a net benefit of 15–16 kJ for the nitrile-based C(6) catemer, thus making it the more favorable interaction. However, the increased charge on the nitrogen atom of the oxime moiety in the case of **28**, leads to a net benefit of only 10–11 kJ in favor of hydrogen-bonding *via* the nitrile moiety over the formation of dimers (Figure 4.18 b). Despite this, in the case of **28**, the preferential formation of dimers in the solid-state via O-H \cdots N interactions between the oxime moieties, indicates that a net advantage of 11 kJ is not sufficient to break the kinetically favorable dimers, and consequently lead to other interactions in the solid-state for oximes.

4.5 Conclusions

The available solid-state data in the CSD on the four major categories of oximes (R' = -H, -CH₃, -NH₂, -CN), complemented by three new relevant crystal structures, has provided the

foundation for an examination of the structural chemistry and dominating intermolecular oxime...oxime hydrogen-bonding patterns present in the solid-state.²⁹ A higher number of C(3) catemers are observed in the case of aldoximes and amidoximes, which can be explained by the presence of an acidic proton on the R' group, which may hinder the formation of $R_2^2(6)$ dimers, thus yielding higher number of catemers. Ketoximes show the higher charge on the oxime nitrogen atom, and also have an inactive R' group, which clearly tilts the balance towards the formation of $R_2^2(6)$ dimers. Cyano-oximes have a strong hydrogen-bond acceptor in the form of the nitrile nitrogen atom, as shown by molecular electrostatic potential calculations and the interaction-site pairing energies, and thus only show O-H...N≡C based C(6) catemers in the crystal lattice. In summary, it is noted that intermolecular homomeric oxime...oxime interactions give rise to four distinct supramolecular synthons;^{9b} (i) $R_2^2(6)$ dimers, (ii) C(3) chains, (iii) C(2) chains, and (iv) C(6) chains.

References

- 1 (a) Corey, E. J. *Angew. Chem., Int. Ed.* **2009**, *48*, 2100-2117. (b) Corey, E. J. *Angew. Chem., Int. Ed.* **2002**, *41*, 1650.
- 2 Desiraju, G. R.; Vittal, J. J.; Ramanan, A. *Crystal Engineering: A Textbook*; World Scientific Publishing Company, Inc.: Hackensack, NJ, 2011.
- 3 Aakeröy, C. B.; Champness, N. R.; Janiak, C. *CrystEngComm* **2010**, *12*, 22.
- 4 Tiekink, E. R. T.; Vittal, J.; Zaworotko, M. *Organic Crystal Engineering: Frontiers in Crystal Engineering*, 1st ed.; Wiley, John & Sons, Inc.: Chichester, U.K., 2010.
- 5 Braga, D.; Grepioni, F. *Making Crystals by Design: Methods, Techniques and Applications*, 1st ed.; Wiley-VCH: Weinheim, Germany, 2006.
- 6 Herbststein, F. H., In *Comprehensive Supramolecular Chemistry*; MacNicol D. D.; Toda, F.; Bishop, R., Ed.; Pergamon Press: New York, 1996; Vol. 6; pp 61-83.
- 7 (a) Hadzi, D.; Detoni, S. Hydrogen bonding in carboxylic acids and derivatives. In *Acid Derivatives*, Vol. 1; Patai, S., Ed.; John Wiley & Sons, Ltd.: Chichester, U.K., 1979. (b) Hamilton, W. C.; Ibers, J. A. *Hydrogen Bonding in Solids*; W. A. Benjamin: New York, 1968.
- 8 For a description of graph set notation for classifying hydrogen-bonding patterns, see: (a) Bernstein, J.; Davis, R. E.; Shimoni, L.; Chang, N.-L. *Angew. Chem., Int. Ed. Engl.* **1995**, *34*, 1555. (b) Etter, M. C. *Acc. Chem. Res.* **1990**, *23*, 120.
- 9 (a) Mareque Rivas, J. C.; Brammer, L. *New. J. Chem.* **1998**, *22*, 1315. (b) Desiraju, G. R. *Angew. Chem., Int. Ed. Engl.* **1995**, *34*, 2311.
- 10 (a) Laurence, C.; Berthelot, M.; Graton, J. Hydrogen-Bonded Complexes of Phenols. In *Phenols*; Rappoport, Z., Ed.; John Wiley & Sons, Ltd.: Chichester, U.K., 2003. (b) Ermer, O.; Eling, A. *J. Chem. Soc., Perkin Trans. 2* **1994**, 925. (c) Bordwell, F. G.; McCallum, R. J.; Olmstead, W. N. *J. Org. Chem.* **1984**, *49*, 1424.
- 11 (a) Eyer, P. A.; Worek, F. Oximes. In *Chemical Warfare Agents: Toxicology and Treatment*, 2nd ed.; Marrs, T. C.; Maynard, R. L.; Sidell, F. R., Eds.; John Wiley & Sons, Ltd.: Chichester, U.K., 2007. (b) Marsman, A. W.; Leusink, E. D.; Zwikker, J. W.; Jenneskens, L. W.; Smeets, W. J. J.; Veldman, N.; Spek, A. L. *Chem. Mater.* **1999**, *11*, 1484.
- 12 Rappoport, Z.; Liebman, J. F. *The Chemistry of Hydroxylamines, Oximes and Hydroxamic Acids, Part 1*; Patai Series: The Chemistry of Functional Groups; John Wiley & Sons, Ltd.: Chichester, U.K., 2009.
- 13 (a) Aakeröy, C. B.; Salmon, D. J.; Smith, M. M.; Desper, J. *CrystEngComm* **2009**, *11*, 439. (b) Aakeröy, C. B.; Fasulo, M.; Schultheiss, N.; Desper, J.; Moore, C. *J. Am. Chem. Soc.* **2007**, *129*, 13772. (c) Scarso, A.; Pellizzaro, L.; De Lucchi, O.; Linden, A.; Fabris, F. *Angew. Chem., Int. Ed.* **2007**, *46*, 4972. (d) Mazik, M.; Bläser, D.; Boese, R. *Tetrahedron* **1999**, *55*, 7835. (e) Burka, L. T. NTP Technical Report on the Toxicity Studies of Methyl Ethyl Ketoxime, 1999. http://ntp.niehs.nih.gov/ntp/htdocs/ST_rpts/tox051.pdf.
- 14 McGraw-Hill. Oxime, 2007. <http://books.mcgraw-hill.com/EST10/site/supparticles/Oxime-480600.pdf>.
- 15 Bertalosi, V.; Gilli, G.; Veronese, A. *Acta. Crystallogr., Sect. B.* **1982**, *B38*, 502.

-
- 16 Bruton, E. A.; Brammer, L.; Pigge, F. C.; Aakeröy, C. B.; Leinen, D. S. *New J. Chem.* **2003**, *27*, 1084.
- 17 Low, J. N.; Santos, L. M. N. B. F.; Lima, C. F. R. A. C.; Brandão, P.; Gomes, L. R. *Eur. J. Chem.* **2010**, *1*, 61.
- 18 (a) Frutos, R. P.; Spero, D. M. *Tetrahedron Lett.* **1998**, *39*, 2475. (b) Negi, S.; Matsukura, M.; Mizuno, M.; Miyake, K. *Synthesis* **1996**, *8*, 991. (c) Sasatani, S.; Miyazak, T.; Maruoka, K.; Yamamoto, H. *Tetrahedron Lett.* **1983**, *24*, 4711.
- 19 (a) Konidaris, K. F.; Katsoulakou, E.; Kaplanis, M.; Bekiari, V.; Terzis, A.; Raptopoulou, C. P.; Manessi-Zoupa, E.; Perlepes, S. P. *Dalton Trans.* **2010**, *39*, 4492. (b) Chaudhuri, P.; Weyhermüller, T.; Wagner, R.; Khanra, S.; Biswas, B.; Bothe, E.; Bill, E. *Inorg. Chem.* **2007**, *46*, 9003.
- 20 Allen, F. H. *Acta. Crystallogr., Sect. B.* **2002**, *B58*, 380.
- 21 *CSD ConQuest 1.15*; Cambridge Crystallographic Data Centre: Cambridge, U.K., 2012.
- 22 Aakeröy, C. B.; Sinha, A. S.; Epa, K. N.; Spartz, C. L.; Desper, J. *Chem. Commun.* **2012**, *48*, 11289.
- 23 Aakeröy, C. B.; Sinha, A. S. *RSC Adv.* **2013**, DOI: 10.1039/C3RA40585K.
- 24 Lyle, R. E.; Troscianiec, H. J. *J. Org. Chem.* **1955**, *20*, 1757.
- 25 Carter, M. J.; Beattie, J. K. *Inorg. Chem.* **1970**, *9*, 1233.
- 26 Aakeröy, C. B.; Rajbanshi, A.; Desper, J. *Chem. Commun.* **2011**, *47*, 11411.
- 27 (a) Le Questel, J.-Y.; Berthelot, M.; Laurence, C. *J. Chem. Soc., Perkin Trans. 2* **1997**, 2711. (b) Berthelot, M.; Helbert, M.; Laurence, C.; Le Questel, J.-Y.; Anvia, F.; Taft, R. W. *J. Chem. Soc., Perkin Trans. 2* **1993**, 625.
- 28 (a) Musumeci, D.; Hunter, C. A.; Prohens, R.; Scuderi, S.; McCabe, J. F. *Chem. Sci.* **2011**, *2*, 883. (b) Hunter, C. A. *Angew. Chem., Int. Ed.* **2004**, *43*, 5310.
- 29 Aakeröy, C. B.; Sinha, A. S.; Epa, K. N.; Chopade, P. D.; Smith, M. M.; Desper, J. *Cryst. Growth Des.* **2013**, *13*, 2687.

Chapter 5 - Hydrogen-bond and halogen-bond donors in supramolecular assembly – complementary or competitive?

5.1 Introduction

Hydrogen-bonds (HB) is one of the most extensively studied intermolecular interactions in supramolecular synthesis, due to the strength and directionality of this force, when compared to other intermolecular interactions,¹ and it is a reliable tool for constructing supramolecular architectures.² Halogen-bonds (XB), on the other hand have been exploited to a much lesser extent for assembling supermolecules, even though they are similar in strength and directionality to the ubiquitous hydrogen-bonding.³ Hydrogen-bond strengths range from 4-60 kJ mol⁻¹,⁴ in comparison to halogen-bond strengths of 5-180 kJ mol⁻¹ (the higher number is for anionic halogen-bonding of the type I₂⋯I⁻).³ Halogen-bonds have been successfully used for the controlled self-assembly of several host-guest solids, with applications in ion-pair recognition,⁵ organic phosphorescent materials⁶ and chemical separation.⁷

5.1.1 Existing studies

Some recent efforts in crystal engineering have focused on designing and synthesizing supramolecular systems with a combination of hydrogen-bonds and halogen-bonds.⁸ Due to their analogous high strength, specificity and directionality, they can be used in conjunction with each other to assemble complicated architectures with a high degree of robustness and precision.⁹ In a recent study, Resnati *et al.* demonstrated the orthogonal self-assembly of an open organic framework with 2-D channels by combining hydrogen and halogen bonds, wherein the framework was able to host various guest molecules (Figure 5.1).¹⁰

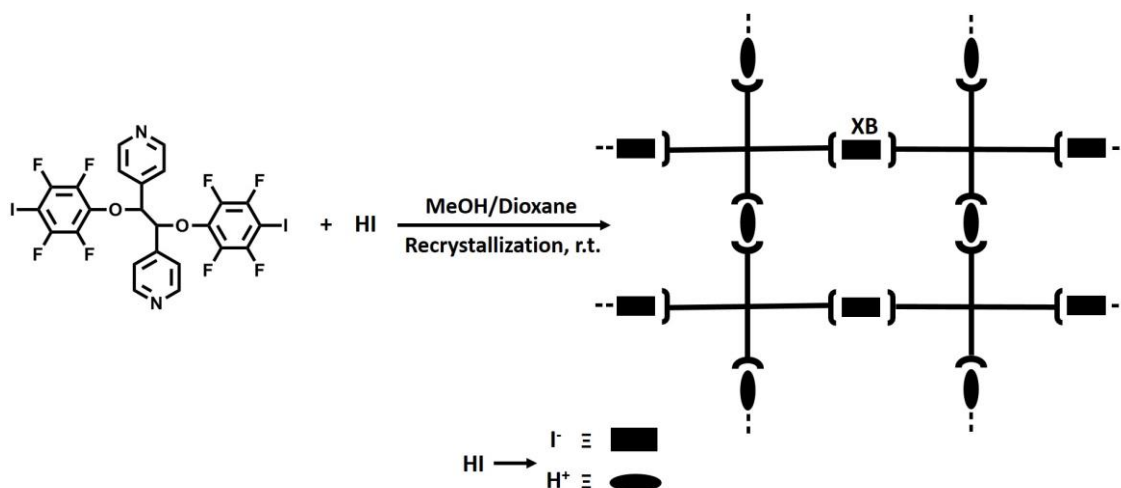


Figure 5.1 Orthogonal self-assembly of an open organic framework by combining hydrogen and halogen bonds.

Consequently, it is important to investigate the structure-directing balance between hydrogen-bonding and halogen-bonding, because any such study, will directly benefit crystal engineers looking to design complicated supramolecular architectures based on these intermolecular interactions. Some studies on the complementary/competing nature of hydrogen-bonds with halogen-bonds have been presented. For example, Aakeröy *et al.*¹¹ examined the competition between hydrogen-bond donors (acids, phenols and oximes) and halogen-bond donors (activated Br/I by fluorination) on the same organic backbone, by co-crystallizing them with two azo-pyridine based ditopic acceptors. They found that the orientation of the binding site in the acceptor greatly influenced the supramolecular assembly, wherein the hydrogen-bond was the driving force for the 3,3'-azopyridine acceptor, and for the 4,4'-azopyridine acceptor, the two forces of interaction equally contributed to the assembly process (Figure 5.2).

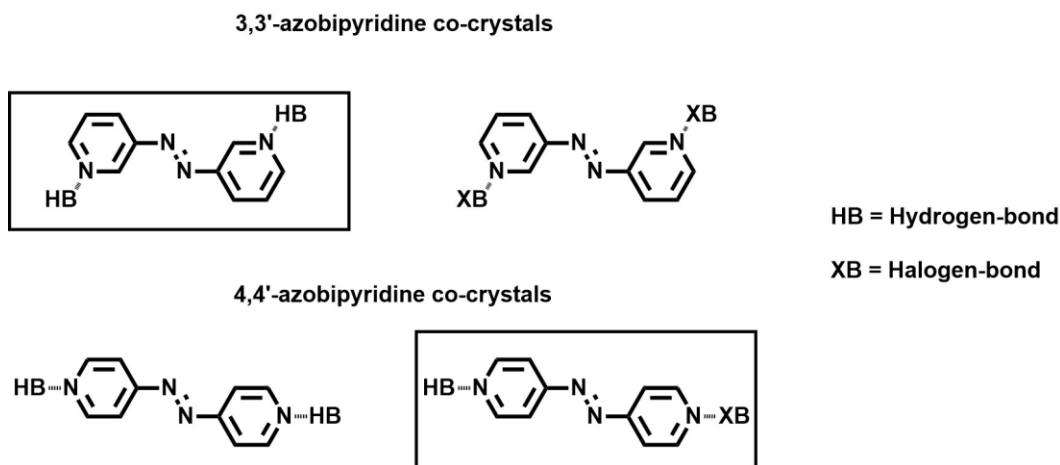


Figure 5.2 Competing hydrogen-bond and halogen-bond donors in crystal engineering.

In another study by Resnati *et al.* on the patterning behavior of azobenzene-containing materials assembled *via* hydrogen-bonds and halogen-bonds, showed that both hydrogen and halogen-bonds can be used for assembling supramolecular polymer-azobenzene complexes, but they concluded that the higher directionality of the halogen-bond promoted the patterning efficiency when compared to hydrogen-bonds.¹² Another notable single-pot competitive experiment by Resnati *et al.* involved co-crystallizing 1,2-bis(4-pyridyl)-ethane (symmetric acceptor) with 1,4-diiodotetrafluorobenzene (halogen-bond donor) and hydroquinone (hydrogen-bond donor), wherein selective halogen-bond co-crystal formation occurred, and the hydrogen-bond donor remained in solution.¹³ Complementary work has been done by Bruce *et al.*¹⁴ and Cho *et al.*¹⁵ on designing liquid crystals involving a combination of hydrogen and halogen-bonds affixed on the same backbone.

Despite these studies on the competition between hydrogen-bonds and halogen-bonds, there is still a need for systems which will allow us to explore the complementarity/competition between these interactions, in the absence of other structure-directing factors such as geometric bias and sterics.

5.1.1 Rationale for design

In order to investigate the competition between hydrogen and halogen-bonds, in the absence of other structure-directing factors, it is necessary to design a system in which the hydrogen-bond donors and the halogen-bond donors are on the same organic backbone and lack steric hindrance (Figure 5.3).

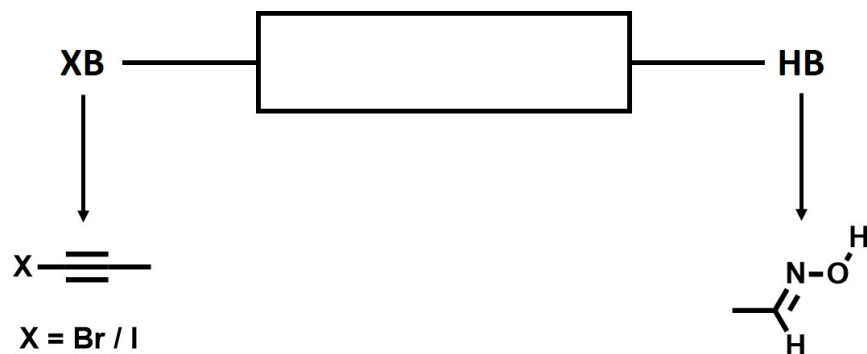


Figure 5.3 Design of the ligand.

Aldoxime was chosen as the hydrogen-bond donor (HB), keeping in mind the hydrogen-bonding capabilities of the oxime moiety¹⁶ (can act as a hydrogen-bond donor *via* the O-H moiety, and can also form self-complementary supramolecular synthons). Also, oximes are easy to synthesize by mechanochemical means,¹⁷ and are ubiquitous in both research laboratories¹⁸ and in industries.¹⁹ Although, the traditional activated halogen-bond donors (XB) include perfluorinated aromatic/aliphatic compounds,²⁰ a recent review by Rissanen *et al.*²¹ outlined alternative and effective halogen-bonding motifs. We chose ethynylhalogenated compounds as the halogen-bond donor, as they have been shown to act as effective halogen-bond donors,²² and have also been used to design functional materials such as conducting nano-wires²³ and insulation materials.²⁴

The suitable ligands containing the hydrogen/halogen-bond donors examined in this chapter are shown in Figure 5.4.

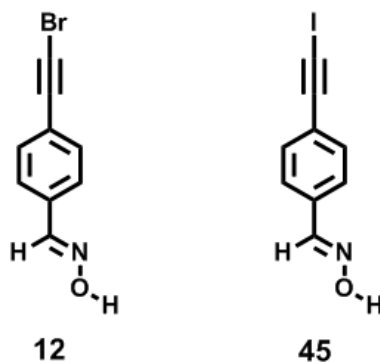


Figure 5.4 Hydrogen-bond (HB) and halogen-bond (XB) donors.

For the purpose of exploring the HB and XB donor capabilities of the donors in the presence of each other, we will co-crystallize them with a series of 20 different hydrogen-bond

acceptors belonging to three different categories; (i) monotopic acceptor (Figure 5.5), (ii) symmetric ditopic acceptors (Figure 5.6), and (iii) asymmetric ditopic acceptors (Figure 5.7).

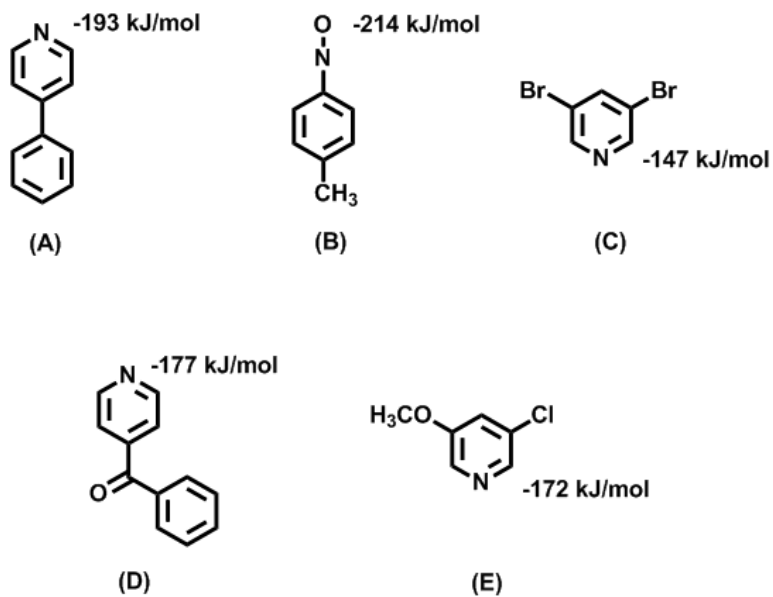


Figure 5.5 Monotopic HB/XB acceptors.

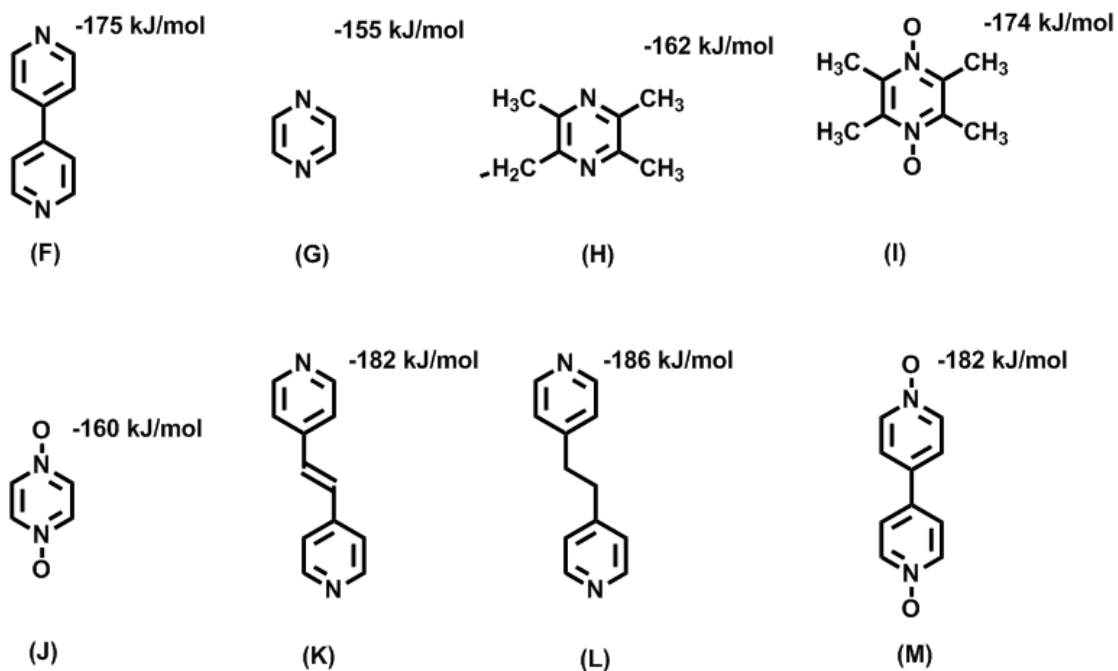


Figure 5.6 Symmetric ditopic HB/XB acceptors.

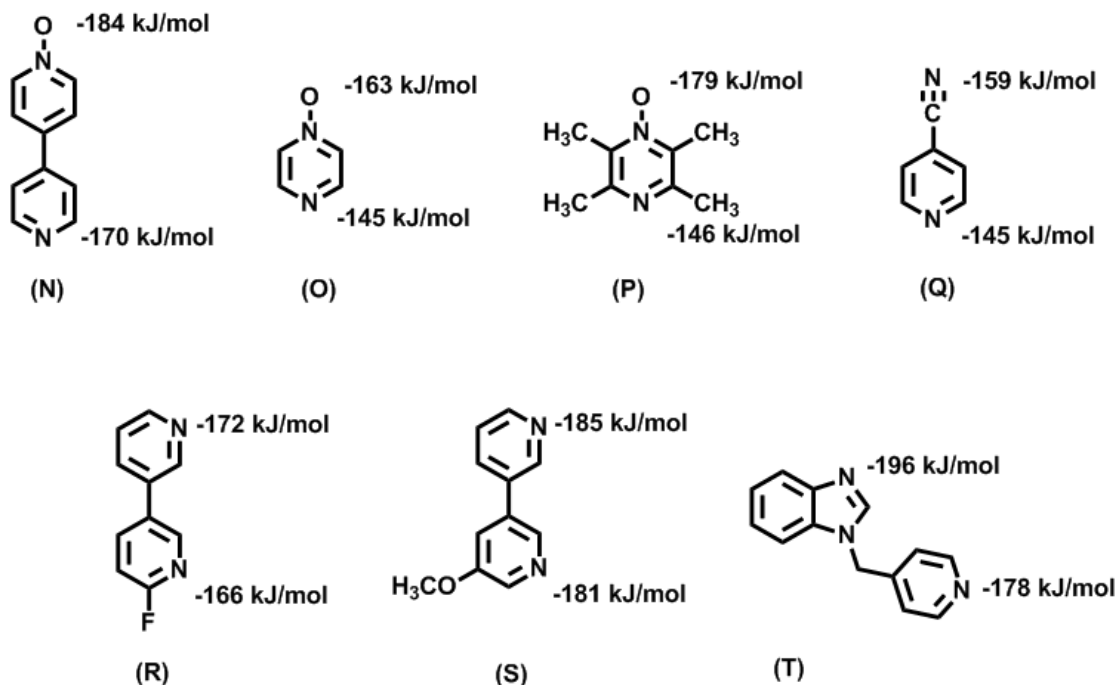


Figure 5.7 Asymmetric ditopic HB/XB acceptors.

The co-crystals will be analyzed by infra-red spectroscopy (IR) and by single-crystal X-ray diffraction, for the purpose of examining the competition and selectivity (if any) in the system between hydrogen-bonds and halogen-bonds. As both hydrogen and halogen-bonds are electrostatic in nature,^{13,25} we will use molecular electrostatic potential calculations (MEPs) as a tool to try and explain any observed trends for the system under study.

In this chapter, we are particularly interested in:

- Investigating the capability of the ethynylhalogenated/oxime ligands for simultaneous and/or halogen/hydrogen-bonding.
- Characterizing the co-crystals by IR spectroscopy and establishing the reliability of this technique in characterizing such co-crystalline materials.
- Comparing the relative halogen-bond donor strength of the bromo and iodo substituents.
- Exploring the relative competition between the ethynylhalogenated and oxime moieties.

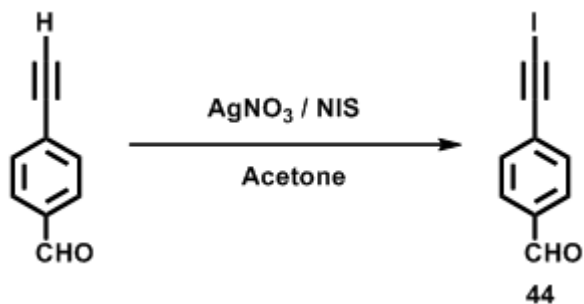
5.2 Experimental

5.2.1 Synthesis

All chemicals were purchased from Aldrich and used without further purification, unless otherwise noted. Melting points were determined on a Fisher-Johns melting point apparatus and

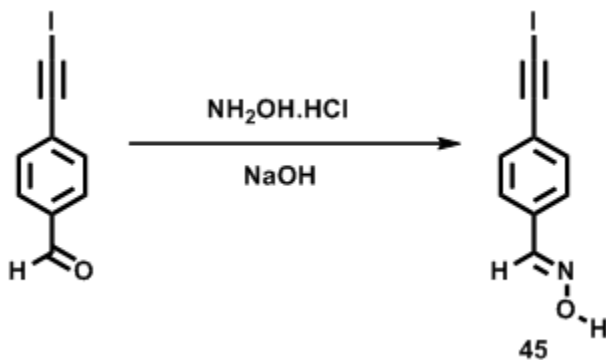
are uncorrected. ^1H and ^{13}C NMR spectra were recorded on a Varian Unity plus 400 MHz spectrometer in CDCl_3 or $\text{d}_6\text{-DMSO}$. Infrared spectroscopy (IR) was done on a Nicolet 380 FT-IR. The synthesis of 4-(bromoethynyl)benzaldehyde oxime (**12**) is described in Chapter 3.

5.2.1.1 Synthesis of 4-(iodoethynyl)benzaldehyde, **44**



To a stirred solution of **7** (0.9 g, 6.92 mmol) in acetone (150 mL) was added 0.12 g of silver(I) nitrate (0.69 mmol). The mixture was stirred for 30 minutes, then N-iodosuccinimide (3.89 g, 17.29 mmol) was added. The mixture was protected from light and stirred for 3 days. Upon completion of the reaction, acetone was evaporated under vacuum and the solid mixture was chromatographed over a short pad of silica gel with hexane as the eluent and the product was isolated as a yellow solid. Yield: 1.27 g (72%); mp 128-132°C; ^1H NMR (δH ; CDCl_3 , 400MHz): $^{\text{26}}$ 7.59 (d, $J=8.06$ Hz, 2 H), 7.84 (d, $J=8.33$ Hz, 2 H), 10.02 (s, 1 H).

5.2.1.2 Synthesis of 4-(iodoethynyl)benzaldehyde oxime, **45**



In a mortar, 0.60 g (2.34 mmoles) of **44** and 0.20 g (2.81 mmoles) of hydroxylamine hydrochloride is ground together with a pestle. Then, 0.12 g (2.81 mmoles) of crushed sodium hydroxide is added and the mixture is ground further with the addition of 0.1-0.2 mL methanol, for 2 minutes at room temperature. The reaction mixture is left for 5 minutes, after which it is ground for another 2 minutes with 0.1-0.2 mL methanol. At this stage the reaction is examined

by TLC. Upon completion of the reaction, a ^1H NMR spectrum of the crude mixture is taken in $\text{d}_6\text{-DMSO}$ to confirm the formation of product. The crude mixture is washed with water to get rid of any inorganic salts and it is air dried, to get a yellow powder of the product. Yield: 0.54 g (85%); mp 145-149°C; ^1H NMR (δH ; DMSO-d_6 , 400MHz): 7.45 (d, $J=8.06$ Hz, 2 H), 7.57 (d, $J=8.33$ Hz, 2 H), 8.14 (s, 1 H), 11.40 (s, 1 H); ^{13}C NMR (δC ; CDCl_3 , 400MHz): 19.66, 92.46, 123.57, 126.41, 132.30, 133.34, 147.49.

5.2.2 Synthesis of co-crystals

5.2.2.1 Synthesis of 4-(bromoethynyl)benzaldehyde oxime:4,4'-bipyridine, 12F

4-(Bromoethynyl)benzaldehyde oxime (15 mg, 0.07 mmol) and 4,4'-bipyridine (10.5 mg, 0.07 mmol) were placed in a vial containing methanol and heated until a clear homogeneous solution was obtained. After two days of slow evaporation, colorless plate-shaped crystals were obtained. M.p. 114-116 °C.

5.2.2.2 Synthesis of 4-(bromoethynyl)benzaldehyde oxime:1,2-bis(4-pyridyl)ethylene, 12K

4-(Bromoethynyl)benzaldehyde oxime (15 mg, 0.07 mmol) and 1,2-bis(4-pyridyl)ethylene (12.2 mg, 0.07 mmol) were placed in a vial containing methanol and heated until a clear homogeneous solution was obtained. After two days of slow evaporation, colorless plate-shaped crystals were obtained. M.p. 138-142 °C.

5.2.2.3 Synthesis of 4-(iodoethynyl)benzaldehyde oxime:4,4'-bipyridine-N-monoxide, 45N

4-(Iodoethynyl)benzaldehyde oxime (15 mg, 0.06 mmol) and 4,4'-bipyridine-N-monoxide (9.5 mg, 0.06 mmol) were placed in a vial containing methanol and heated until a clear homogeneous solution was obtained. After two days of slow evaporation, colorless plate-shaped crystals were obtained. M.p. 159-162 °C.

5.2.3 Molecular electrostatic potential calculations

Charge calculations were performed using Spartan'04 (Wavefunction, Inc. Irvine, CA). All molecules were geometry optimized using DFT B3LYP/6-311++G** *ab initio* calculations, with the maxima and minima in the electrostatic potential surface (0.002 e au $^{-1}$ iso-surface) determined using a positive point charge in vacuum as a probe.

5.3 Results

We have structurally characterized three co-crystals, *i.e.* **12F**, **12K** and **45N**, using single-crystal X-ray diffraction. Table 5.1 (**A-J**) and Table 5.2 (**K-T**) lists the significant IR bands for all the co-crystals of **12** and **45**, obtained from solvent-assisted grind experiments.

Table 5.1 Significant FT-IR bands (**A-J**).

	Original	A	B	C	D	E	F	G	H	I	J
12	2190.23	2193.6	2186.32	2193.13	2195.44	2193.73	2185.37	2194.75	2190.23	2190.23	2193.73
	1626.5	1620.51	1619.19	1625.69	ND	1618.94	1616.4	1610.18	1614.3	ND	ND
	1602.09	ND	1601.85	1605.12	ND	1600.14	ND	1601.72	1600.35	ND	1604.02
	1510.53	1506.33	1511.26	1510.85	1510.88	1511.81	1508.49	1509.53	1512.64	1509.14	1507.12
	1457.29	1463.71	1459.65	1457.19	1447.62	1453	1448.7	1466.16	1447.26	1468.34	1442.78
	1404.08	1407.71	1405.06	1408.48	1407.52	1415.47	1402.29	1400.08	1410.9	1404.84	1400.9
	1301.25	1299.68	1301.76	1300.91	1300.4	1310.82	1294.74	1301.3	1299.58	1297.89	1299.58
	1212.36	1214.52	1210.34	1212.01	1213.13	1212.58	1209.24	1209.27	1207.97	1212.26	1208.77
	971.56	966.81	973.49	971.07	970.43	968.42	958.73	969	973.15	970.18	971.26
	936.9	922.31	931.98	936.56	942.4	922.22	934.93	934.75	928.36	946.25	929.35
	877.25	873.9	873.98	875.91	874.29	883.32	874.36	873.28	869.97	873.93	869.97
	826.78	827.46	825.13	825.92	834.92	820.59	831.54	827.35	826.71	824.54	826.88
	45	2160.43	2154.03	2158.8	2165.78	2166.12	2162.29	2148.32	2169.28	2155.31	2158.24
1683.06		1690.87	1683.78	1683.78	ND	1683.78	1683.78	1687.28	1687.28	1692.03	1684.76
1626.06		1613.84	1621.76	1623.91	1626.33	1614.41	1622.35	1626.13	ND	ND	ND
1593.99		1595.69	1596.46	1592.97	1595.73	1579	1589.59	1596.46	1596.46	1597.39	1596.05
1498.11		1505.74	1484.7	1498.67	1507.64	1501.94	1499.3	1509.14	1509.14	1500.56	1492.14
1462.18		1479.18	1456.75	1459.78	1460.47	1461.04	1456.58	1460.25	ND	1455.32	1456.27
1299.86		1299.52	1299.58	1303.07	1301.13	1307.68	1296.09	1301.22	1298.53	1298.09	1297.82
1209.24		1214.48	1215.75	1208.77	1210.95	1208.85	1212.67	1208.77	1202.26	1208.69	1212.12
966.93		967.47	957.29	967.79	963.98	968.32	958.6	969.18	967.77	962.45	967.02
933.58		923.3	936.33	932.84	939.39	922.36	929.35	932.14	938.76	927.59	934.45
870.11		867.44	873.46	872.47	872.57	871.83	871.94	872.62	870.97	866.59	870.69
824.86		825.97	824.78	824.77	830.97	821.89	830.8	825.82	827.78	835.45	825.8
811.68		807.01	812.76	810.45	813.18	810.6	819.12	811	802.44	815.9	802.28

ND = Not determined

Table 5.2 Significant IR bands (K-T).

	Original	K	L	M	N	O	P	Q	R	S	T
12	2190.23	2183.25	2183.25	2197.22	2182.41	2190.23	2189.09	2186.74	2190.23	2183.25	2193.73
	1626.5	1625.8	1616.7	1624.41	ND	1621.67	1616.3	1616.64	1634.88	ND	ND
	1602.09	1608.31	ND	1612.18	1604.71	ND	ND	1600.67	ND	ND	ND
	1510.53	1505.65	1505.65	1509.14	1502.28	1509.14	1506.92	1508.44	1504.78	1512.64	ND
	1457.29	1459.65	1439.24	1463.74	1467.1	1463.13	1465.79	ND	ND	1453.26	1460.25
	1404.08	1418.33	1414.84	1401.04	1408.47	1404.36	1402.33	1404.36	1393.45	1397.38	1418.33
	1301.25	1292.59	1296.91	1298.28	1302.93	1291.18	1301.18	1299.13	1299.27	1306.56	1299.58
	1212.36	1212.26	1208.77	1212.33	1210.46	1213.34	1212.12	1208.77	1208.56	1219.25	1205.27
	971.56	964.66	969.8	973.07	966.78	ND	966.32	969.21	970.14	965.94	969.81
	936.9	943.74	943.84	935.8	931.6	934.07	931.02	941.71	934.43	927.35	933.64
	877.25	869.97	873.46	869.97	872.96	861.85	872.67	869.97	873.46	873.18	876.96
	826.78	832.1	835.88	829.75	825.56	824.3	830.92	834.74	828.4	830.46	827.9
45	2160.43	2151.81	2155.31	2162.29	2149.2	2165.78	2161.88	2155.31	2165.57	2152.15	2155.31
	1683.06	1687.28	1683.78	ND	1687.1	1688.05	1690.5	1694.26	1686.13	1688.61	1689.36
	1626.06	ND	ND	1621.27	ND	1625.07	ND	1620.51	1635.87	1634.32	ND
	1593.99	1595.26	1599.65	1596.46	1598.1	1589.48	1596.23	1594.66	1599.48	1593.3	1603.45
	1498.11	1502.16	1498.67	ND	1502.25	1508.67	1507.29	1498.67	1482.93	1486.35	1502.16
	1462.18	ND	ND	1464.38	1470.26	1463.74	1466.38	ND	1475.41	1456.58	1458.77
	1299.86	1291.97	1299.58	1302.14	1298.96	1291.18	1300.2	ND	1297.82	1307.9	1289.1
	1209.24	1211.84	1208.85	ND	1213.31	1201.78	1208.69	1213.11	1210.56	1218.97	1201.78
	966.93	965.98	968.11	967.83	966.55	941.9	965.46	ND	974.49	960.97	947.92
	933.58	939.82	938.84	939.41	930.61	933.29	934.93	946.79	934.11	927.59	923.73
	870.11	873.46	873.46	876.63	866.48	861.22	869.32	876.4	872.74	869.32	873.46
	824.86	830.86	838.5	834.85	825.55	828.49	830.93	836.29	832.8	831.29	828.95
	811.68	819.65	818.14	825.44	813.32	822.02	ND	818.1	812.21	824.24	ND

ND = Not determined

5.3.1 Structural characterization of the co-crystals

5.3.1.1 Crystal structure of 12F

The crystal structure analysis of **12F** revealed three interesting features. First, there is an intermolecular hydrogen-bond between one of the 4,4'-bipyridine nitrogen atom and the –O-H group on the oxime moiety ($\text{H}\cdots\text{N}$ 2.705 Å, $\text{O}\cdots\text{N}$ 158.55 °) on adjacent molecules (Figure 5.8). Second, it displays an intermolecular halogen-bond between the bromine atom and the second nitrogen atom of the bipyridyl moiety of an adjacent molecule, which extends the

individual molecules into an infinite 1-D chain ($\text{Br}\cdots\text{N}$ 2.792 Å, $\text{C}-\text{Br}\cdots\text{N}$ 170.72 °). Third, there seems to be a structure-stabilizing $\text{C}-\text{H}\cdots\pi$ interactions between the C-H moiety of 4,4'-bipyridine and the benzene ring of **12** ($\text{C}-\text{H}\cdots\pi$ 2.828 Å) on adjacent molecules.

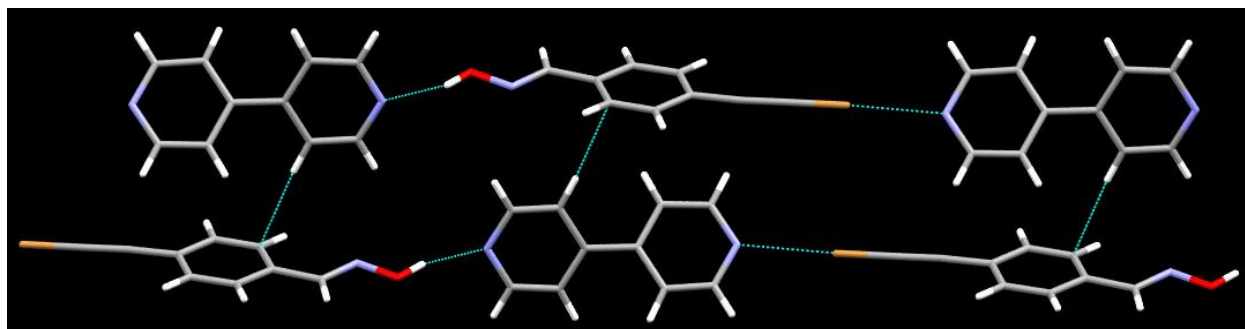


Figure 5.8 Section of the crystal structure of **12F** displaying the infinite 1-D chains formed by a combination of hydrogen-bonds and halogen-bonds.

5.3.1.2 Crystal structure of **12K**

An examination of the crystal structure of **12K** revealed a hydrogen-bond between one of the nitrogen atoms of 1,2-bis(4-pyridyl)ethylene and the $-\text{O}-\text{H}$ group on the oxime moiety ($\text{H}-\text{O}\cdots\text{N}$ 2.684 Å, $\text{O}-\text{H}\cdots\text{N}$ 164.27 °) on adjacent molecules (Figure 5.9). These molecules are assembled into an infinite 1-D chain by a halogen-bond between the bromine atom and the second nitrogen atom of the pyridyl moiety ($\text{Br}\cdots\text{N}$ 2.770 Å, $\text{C}-\text{Br}\cdots\text{N}$ 170.7 °).

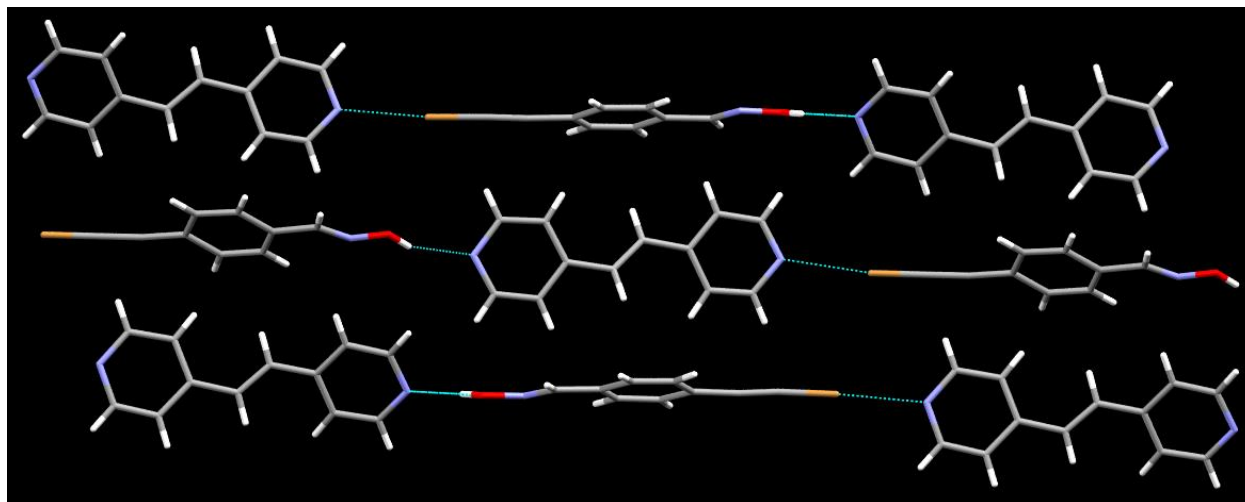


Figure 5.9 Section of the crystal structure of **12K** displaying the infinite 1-D chains formed by a combination of hydrogen-bonds and halogen-bonds.

5.3.1.3 Crystal structure of 45N

The crystal structure analysis of **45N** revealed three interesting features. First, an intermolecular hydrogen-bond between the oxygen atom on the 4,4'-bipyridine-N-monoxide and the –O-H group on the oxime moiety ($\text{H}\cdots\text{O}$ 2.647 Å, $\text{O}\cdots\text{O}$ 173.4 °) (Figure 5.10). Second, an intermolecular halogen-bond between the iodine atom and the nitrogen atom of the bipyridyl moiety, which results in an infinite 1-D chain ($\text{I}\cdots\text{N}$ 2.786 Å, $\text{C}\cdots\text{I}\cdots\text{N}$ 176.95 °). Third, a structure-stabilizing C-H \cdots O interactions between the C-H moiety and the oxygen atom of adjacent 4,4'-bipyridine-N-monoxide molecules, which interconnects adjacent 1-D chains ($\text{HC}\cdots\text{O}$ 3.221 Å, $\text{C}\cdots\text{H}\cdots\text{O}$ 2.342 Å).

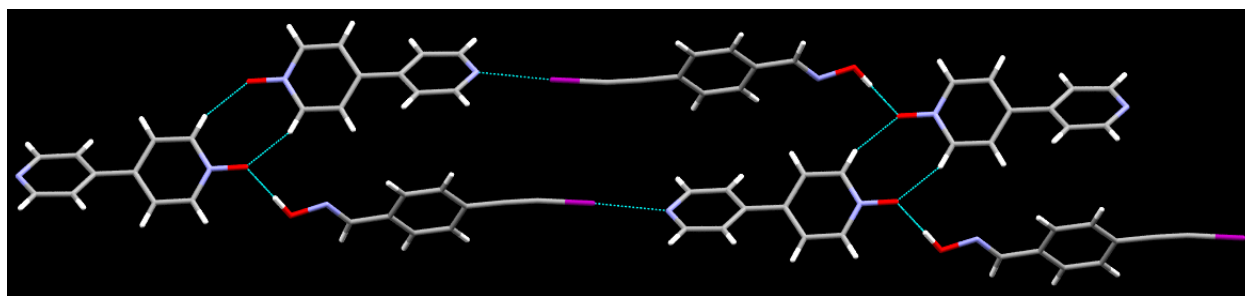


Figure 5.10 Section of the crystal structure of **45N** displaying the infinite 1-D chains formed by a combination of hydrogen-bonds and halogen-bonds.

5.4 Discussion

5.4.1 Characterization of the co-crystals by infra-red spectroscopy (IR)

The two ditopic HB/XB donor molecules were mixed in a 1:1 ratio with a total of 20 HB/XB acceptor molecules (Figures 5.5, 5.6, and 5.7), and were screened for co-crystal formation by solvent-drop grinding method. The resulting solid from each of the 40 reactions was analyzed using IR spectroscopy. The formation of a multi-component co-crystal was determined by a careful examination of the entire IR spectrum for each reaction mixture and comparing it with the IR spectrum of each component, because the fundamental C-I and C-Br stretches, that are likely to be directly affected in the case of any halogen-bonding in the solid-state were outside the detection range of our instrument ($500\text{--}700\text{ cm}^{-1}$). Also, the C=N and the N-O stretches for the aldoxime moiety (directly affected in the case of hydrogen-bonding) sometimes get obscured in the fingerprint region of the IR spectrum ($1000\text{--}1500\text{ cm}^{-1}$).

The characteristic stretches in **12** and **45**, that were utilized for verifying the outcome of the co-crystallization experiments were the C=C stretching bands (1400-1500 cm^{-1} ; 1200-1300 cm^{-1}), the C-H in-plane bending (900-1000 cm^{-1}) and the C-H out-of-plane bends (750-850 cm^{-1}). Apart from this the C \equiv C (2150-2200 cm^{-1}) bond stretch was a very useful indicator of the presence/absence of halogen-bonding in the supramolecular assembly. Also, the C=N stretch (1600-1680 cm^{-1}), and the N-O stretch (900-1000 cm^{-1}) for the oxime moiety helped in deciphering the role of hydrogen-bonding in our system.

A systematic analysis of the tabulated data (Tables 5.3 and 5.4) from the IR spectra of the 40 reactions revealed that co-crystal formation resulted in significant shifts in the modes associated with the C \equiv C, C=N, C=C, N-O and C-H bonds, even though the magnitude of these shifts are relatively small, and they also lack consistency in terms of the direction of the change (blue/red shift). This observation can be rationalized on the basis of the fact that these bonds are not only affected by the primary interactions (HB/XB) in the solid-state, but are also affected by the changes in crystal packing and nearest-neighbors that arise in the co-crystals, when compared to the arrangement in the crystal-lattice of the molecules by themselves.

Table 5.3 FT-IR band shifts (A-J).

	A	B	C	D	E	F	G	H	I	J
12	-3.4	3.9	-2.9	-5.2	-3.5	4.9	-4.5	0.0	0.0	-3.5
	6.0	7.3	0.8	ND	7.6	10.1	16.3	12.2	ND	ND
	ND	0.2	-3.0	ND	2.0	ND	0.4	1.7	ND	-1.9
	4.2	-0.7	-0.3	-0.4	-1.3	2.0	1.0	-2.1	1.4	3.4
	-6.4	-2.4	0.1	9.7	4.3	8.6	-8.9	10.0	-11.1	14.5
	-3.6	-1.0	-4.4	-3.4	-11.4	1.8	4.0	-6.8	-0.8	3.2
	1.6	-0.5	0.3	0.9	-9.6	6.5	-0.1	1.7	3.4	1.7
	-2.2	2.0	0.4	-0.8	-0.2	3.1	3.1	4.4	0.1	3.6
	4.8	-1.9	0.5	1.1	3.1	12.8	2.6	-1.6	1.4	0.3
	14.6	4.9	0.3	-5.5	14.7	2.0	2.2	8.5	-9.4	7.6
	3.4	3.3	1.3	3.0	-6.1	2.9	4.0	7.3	3.3	7.3
	-0.7	1.7	0.9	-8.1	6.2	-4.8	-0.6	0.1	2.2	-0.1
45	6.4	1.6	-5.4	-5.7	-1.9	12.1	-8.9	5.1	2.2	-1.2
	-7.8	-0.7	-0.7	ND	-0.7	-0.7	-4.2	-4.2	-9.0	-1.7
	12.2	4.3	2.2	-0.3	11.7	3.7	-0.1	ND	ND	ND
	-1.7	-2.5	1.0	-1.7	15.0	4.4	-2.5	-2.5	-3.4	-2.1
	-7.6	13.4	-0.6	-9.5	-3.8	-1.2	-11.0	-11.0	-2.5	6.0
	-17.0	5.4	2.4	1.7	1.1	5.6	1.9	ND	6.9	5.9
	0.3	0.3	-3.2	-1.3	-7.8	3.8	-1.4	1.3	1.8	2.0
	-5.2	-6.5	0.5	-1.7	0.4	-3.4	0.5	7.0	0.6	-2.9
	-0.5	9.6	-0.9	3.0	-1.4	8.3	-2.3	-0.8	4.5	-0.1
	10.3	-2.8	0.7	-5.8	11.2	4.2	1.4	-5.2	6.0	-0.9
	2.7	-3.4	-2.4	-2.5	-1.7	-1.8	-2.5	-0.9	3.5	-0.6
	-1.1	0.1	0.1	-6.1	3.0	-5.9	-1.0	-2.9	-10.6	-0.9
	4.7	-1.1	1.2	-1.5	1.1	-7.4	0.7	9.2	-4.2	9.4

ND = Not determined

Table 5.4 FT-IR band shifts (**K-T**).

	K	L	M	N	O	P	Q	R	S	T
12	7.0	7.0	-7.0	7.8	0.0	1.1	3.5	0.0	7.0	-3.5
	0.7	9.8	2.1	ND	4.8	10.2	9.9	-8.4	ND	ND
	-6.2	ND	-10.1	-2.6	ND	ND	1.4	ND	ND	ND
	4.9	4.9	1.4	8.3	1.4	3.6	2.1	5.8	-2.1	ND
	-2.4	18.1	-6.5	-9.8	-5.8	-8.5	ND	ND	4.0	-3.0
	-14.3	-10.8	3.0	-4.4	-0.3	1.8	-0.3	10.6	6.7	-14.3
	8.7	4.3	3.0	-1.7	10.1	0.1	2.1	2.0	-5.3	1.7
	0.1	3.6	0.0	1.9	-1.0	0.2	3.6	3.8	-6.9	7.1
	6.9	1.8	-1.5	4.8	ND	5.2	2.4	1.4	5.6	1.8
	-6.8	-6.9	1.1	5.3	2.8	5.9	-4.8	2.5	9.6	3.3
	7.3	3.8	7.3	4.3	15.4	4.6	7.3	3.8	4.1	0.3
	-5.3	-9.1	-3.0	1.2	2.5	-4.1	-8.0	-1.6	-3.7	-1.1
45	8.6	5.1	-1.9	11.2	-5.4	-1.5	5.1	-5.1	8.3	5.1
	-4.2	-0.7	ND	-4.0	-5.0	-7.4	-11.2	-3.1	-5.6	-6.3
	ND	ND	4.8	ND	1.0	ND	5.6	-9.8	-8.3	ND
	-1.3	-5.7	-2.5	-4.1	4.5	-2.2	-0.7	-5.5	0.7	-9.5
	-4.1	-0.6	ND	-4.1	-10.6	-9.2	-0.6	15.2	11.8	-4.1
	ND	ND	-2.2	-8.1	-1.6	-4.2	ND	-13.2	5.6	3.4
	7.9	0.3	-2.3	0.9	8.7	-0.3	ND	2.0	-8.0	10.8
	-2.6	0.4	ND	-4.1	7.5	0.6	-3.9	-1.3	-9.7	7.5
	1.0	-1.2	-0.9	0.4	25.0	1.5	ND	-7.6	6.0	19.0
	-6.2	-5.3	-5.8	3.0	0.3	-1.4	-13.2	-0.5	6.0	9.9
	-3.4	-3.4	-6.5	3.6	8.9	0.8	-6.3	-2.6	0.8	-3.4
	-6.0	-13.6	-10.0	-0.7	-3.6	-6.1	-11.4	-7.9	-6.4	-4.1
	-8.0	-6.5	-13.8	-1.6	-10.3	ND	-6.4	-0.5	-12.6	ND

ND = Not determined

Only after observing the IR stretches from both components in the IR spectrum of the products, and subsequently examining the magnitude of the shifts in the bond stretches, it was concluded whether a co-crystal had formed or not (Table 5.5).

Table 5.5 Determining the nature of bonding in the co-crystals on the basis of FT-IR shifts (A-T).

Co-former	12		45	
	HB	XB	HB	XB
A	✓	✓	✓	✓
B	✓	✓	✓	✓
C	✗	✗	✓	✓
D	ND	✓	ND	✓
E	✓	✓	✓	✓
F	✓	✓	✓	✓
G	✓	✓	✓	✓
H	✓	✗	✓	✓
I	ND	✗	✓	✓
J	✓	✓	✓	✓
K	✓	✓	✓	✓
L	✓	✓	✓	✓
M	✓	✓	✓	✓
N	✓	✓	✓	✓
O	✓	✗	✓	✓
P	✓	✓	✓	✓
Q	✓	✓	✓	✓
R	✓	✗	✓	✓
S	ND	✓	✓	✓
T	ND	✓	✓	✓

ND = Not determined

In accordance with literature data, coupled with the fact that the C=N and the N-O stretch would shift significantly upon co-crystal formation, as they are directly involved in hydrogen-bonding, we assigned the stretch above 1600 cm^{-1} to the C=N bond of the oxime moiety, whereas

the stretch at 930-940 cm^{-1} was assigned to the N-O bond. These bonds helped us determine whether hydrogen-bonding was involved in the supramolecular assembly in each case (Table 5.5). The $\text{C}\equiv\text{C}$ bond stretch (2150-2200 cm^{-1}) is a good indicator of the presence/absence of halogen-bonding in the crystal lattice.

In the case of **45**, every reaction yielded co-crystals in which both hydrogen and halogen-bonds were participating in the assembly process. This is understandable as the unsaturated iodine atom is a good halogen-bond donor, because the iodine atom has a large σ -hole²⁷ (and higher positive charge) (Table 5.6). Whereas in the case of **12**, there was one experiment (**12C**) which did not produce any significant shifts in the IR stretches, and thus was deemed to be a no-reaction. This can be explained on the basis of molecular electrostatic potentials (MEPs) (Table 5.6 and 5.7). A bromine atom, having the smaller σ -hole, when compared to the iodine atom, coupled with the fact that acceptor **C** has the lowest MEP amongst the different acceptors, leads to a no-reaction in **12C**.

Table 5.6 Molecular electrostatic potentials (MEPs) for **12** and **45**.

Donor	HB (kJ/mol)	XB (kJ/mol)
12	+261	+141
45	+254	+164

Table 5.7 Molecular electrostatic potentials for the HB/XB acceptors, **A-T**.

Co-former	Acceptor 1 (kJ/mol)	Acceptor 2 (kJ/mol)
A	-193	-
B	-214	-
C	-147	-
D	-177	-
E	-172	-
F	-175	-
G	-155	-
H	-162	-
I	-174	-
J	-160	-
K	-182	-
L	-186	-
M	-182	-
N	-184	-170
O	-163	-145
P	-179	-146
Q	-159	-145
R	-172	-166
S	-185	-181
T	-196	-178

5.4.2 Trends and explanations

Although IR spectroscopy was reliably utilized for determining the presence/absence of hydrogen-bonds and halogen-bonds in the co-crystals, it is important to look at the single-crystal structure of the co-crystals, if any information about the selectivity between the two competing intermolecular interactions has to be obtained. We were able to get the solved single-crystal data for three of the 40 reactions, **12F**, **12K** and **45N**, the results of which are discussed in the following sections.

5.4.2.1 Co-crystals with symmetric ditopic acceptors

There are three possible outcomes, when these ditopic HB/XB donors are co-crystallized with symmetric ditopic acceptors (Figure 5.11). Either hydrogen-bonding or halogen-bonding interactions can express themselves in a mutually-exclusive manner in the solid-state, or they can act as complementary interactions to each other (both will be expressed in such a case).

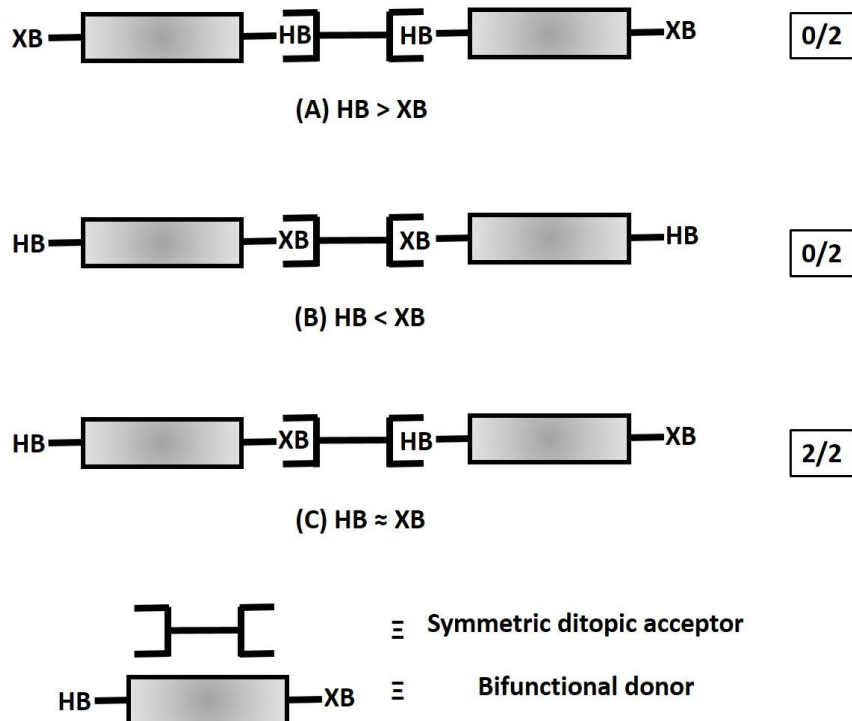


Figure 5.11 Postulated outcomes for co-crystallization with symmetric ditopic acceptors.

In two out of two cases (**12F**, **12K**), both hydrogen-bonds and halogen-bonds were present leading to 1-D infinite chains, which suggests that in a system of “equal opportunities”, both these interactions can be tolerant of each other.

5.4.2.2 Co-crystals with asymmetric ditopic acceptors

When the ditopic HB/XB donors are co-crystallized with asymmetric ditopic acceptors, it gives rise to four possibilities (Figure 5.12); (i) the oxime moiety (HB) will bind to both acceptors, (ii) the ethynylhalogenated moiety (XB) will bind to both acceptors, (iii) oxime moiety (HB) will bind to the best acceptor, whereas the ethynylhalogenated moiety (XB) will bind to the second-best acceptor, and (iv) ethynylhalogenated moiety (XB) will bind to the best acceptor, leaving the second best acceptor for the oxime moiety (HB).

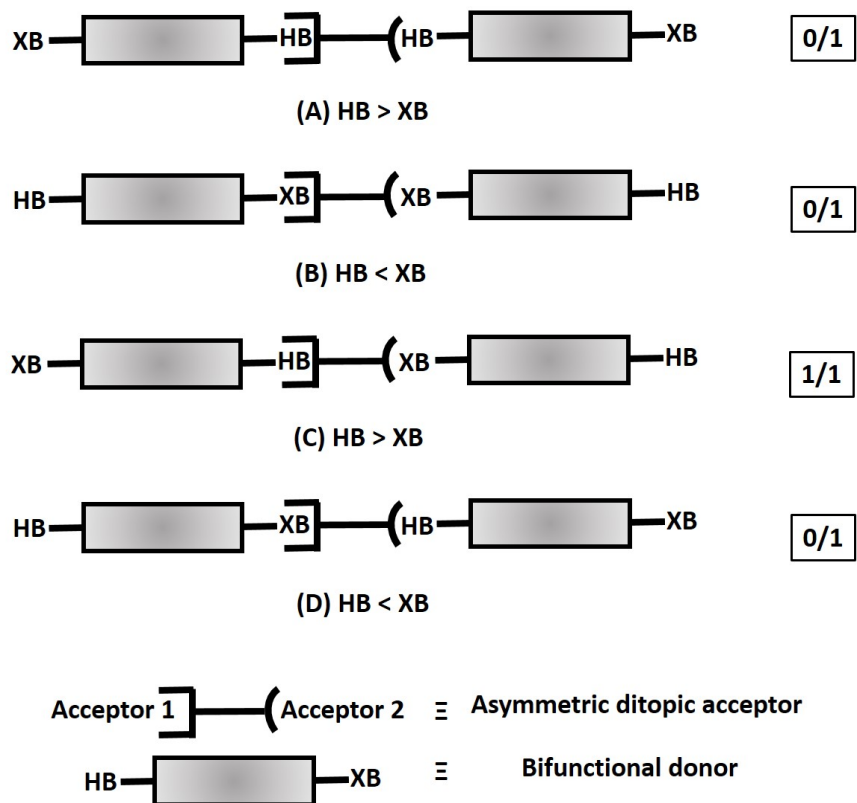


Figure 5.12 Postulated outcomes for co-crystallization with asymmetric ditopic acceptors.

In the only data point for this section (**45N**), the oxime moiety (HB) binds to the best acceptor (N-oxide oxygen atom), whereas the iodine atom binds to the second best acceptor (pyridine nitrogen atom). This can be rationalized on the basis of MEP values of both the HB and the XB donors (Table 5.6), because these intermolecular interactions are electrostatic in nature,^{13,25} and hence molecular electrostatic potentials are a good indicator of their behavior in the solid-state. Oxime O-H moiety has a MEP value of +254 kJ/mol, in comparison to +164 kJ/mol MEP value on the iodine atom, consequently according to the best donor / best acceptor theory,²⁸ it is perfectly reasonable to see the best donor going for the best acceptor in this case.

5.4.2.3 *Br vs I*

The average Br \cdots N bond distance for **12F** and **12K** is 2.792 Å, which corresponds to a Br \cdots N contraction of 17.9% compared to the combined van der Waals radii of Br \cdots N. In comparison, an I \cdots N bond distance of 2.786 Å in **45N** corresponds to a I \cdots N contraction of 21.1% compared to the van der Waals radii of I \cdots N, which demonstrates that the iodine atom is a better halogen-bond donor than the bromine atom (as long as both are ‘activated’ to the same extent).

This is in good agreement with the electrostatic argument which shows that the σ -hole on the iodine atom carries a higher positive charge than that on the bromine atom.²⁷

5.4.3 Comparison with activated perfluorinated systems

A search of the Cambridge Structural Database (CSD)^{29,30} for co-crystals of 2,3,5,6-tetrafluoro-4-bromobenzaldehyde oxime produced two hits, one acceptor was a symmetric ditopic acceptor, whereas the other was a asymmetric ditopic acceptor. In both cases, the bromine atom did not participate in any structure-directing halogen-bonds (Figure 5.13), which is in contrast to our observations with **12** (participated in halogen-bonds). This leads us to believe that unsaturated halogenated compounds are better activators of the halogen atoms when compared to fluorinated compounds, and hence increase the propensity to form halogen-bonds in the solid-state.

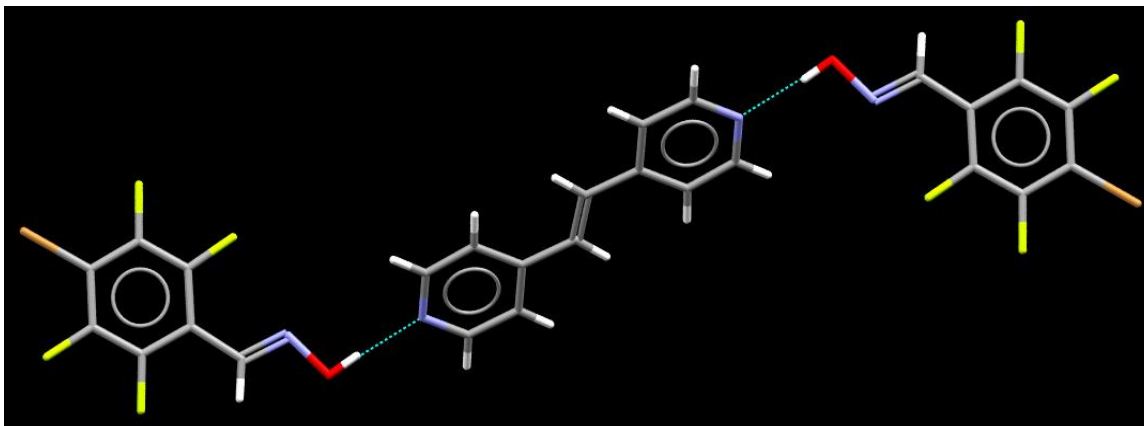


Figure 5.13 Section of the crystal structure of the co-crystal of 2,3,5,6-tetrafluoro-4-bromobenzaldehyde oxime:1,2-bis(4-pyridyl)ethylene.³¹

A search for co-crystals of 2,3,5,6-tetrafluoro-4-iodobenzaldehyde oxime, revealed a total of six hits, of which two acceptors were symmetric ditopic, and four asymmetric ditopic acceptors. In all cases, the activated iodine atom participates in halogen-bonds in the solid-state. For the symmetric acceptors, it acts as a complementary bond to hydrogen-bonds (gives rise to 1-D motifs), whereas for the asymmetric acceptors it binds with the second best acceptor (Figure 5.14), which is in agreement with **45N**.

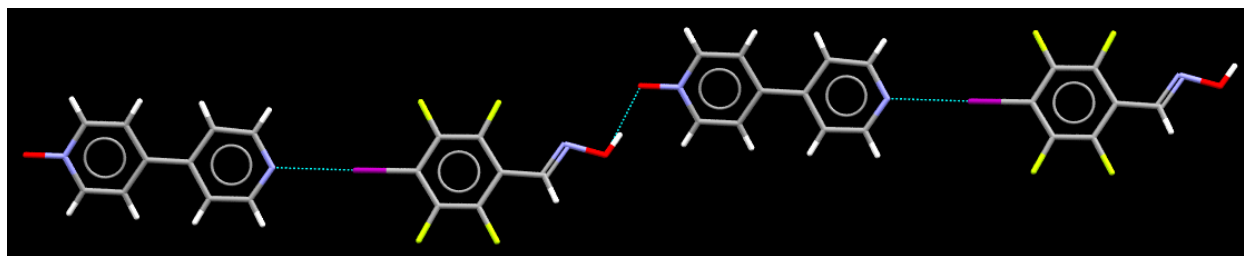


Figure 5.14 Section of the crystal structure of the co-crystal of 2,3,5,6-tetrafluoro-4-iodobenzaldehyde oxime:4,4'-bipyridine-N-monoxide.³²

5.5 Conclusions

We have designed and synthesized two ditopic hydrogen-bond (HB) and halogen-bond (XB) donor ligands and co-crystallized them with a series of 20 different acceptors belonging to three separate categories (monotopic, symmetric ditopic and asymmetric ditopic), for the purpose of investigating the interplay between these two forces of interactions when presented with unbiased and sterically unhindered systems. IR spectroscopy has been used as a preliminary and reliable tool to gather information on the presence/absence of HB/XB in the different cases. Single-crystal data has been used to investigate the selectivity between HB and XB in the solid-state for our system. In two out of two cases with symmetric ditopic acceptors, both HB and XB were present leading to 1-D infinite chains, which suggests that in a system of “equal opportunities”, both these interactions can be tolerant of each other. In the only case with asymmetric ditopic acceptor, the HB donor binds to the best acceptor, whereas XB donor binds to the second best acceptor. This selectivity can be rationalized on the basis of electrostatic considerations, where the HB donor was shown to have a higher molecular electrostatic potential than the XB donor. Also, comparing the relative reduction in the combined $X \cdots N$ van der Waals radii ($X = \text{Br}, \text{I}$), demonstrates that the iodine atom is a better halogen-bond donor than the bromine atom. Finally, we also observed that unsaturated halogenated compounds are better activators of the halogen-bond when compared to fluorinated compounds.

References

- 1 (a) Seto, C. T.; Whitesides, G. M. *J. Am. Chem. Soc.* **1991**, *113*, 712. (b) Aakeröy, C. B.; Seddon, K. R. *Chem. Soc. Rev.* **1993**, *22*, 397. (c) Tiekink, E. R. T.; Vittal, J.; Zaworotko, M. *Organic Crystal Engineering: Frontiers in Crystal Engineering*, 1st ed.; Wiley, John & Sons, Inc.: Chichester, U.K., 2010.
- 2 (a) Lehn, J.-M. *Science* **2002**, *295*, 2400. (b) Wittenberg, J. B.; Isaacs, L. Complementarity and Preorganization. In *Supramolecular Chemistry: From Molecules to Nanomaterials*, 2012; Vol. 1; pp 25-43.
- 3 Metrangolo, P.; Neukirch, H.; Pilati, T.; Resnati, G. *Acc. Chem. Res.* **2005**, *38*, 386.
- 4 Steed, J. W.; Atwood, J. L. *Supramolecular Chemistry*, John Wiley & Sons, Ltd., 2nd ed., 2009.
- 5 Mele, A.; Metrangolo, P.; Neukirch, H.; Pilati, T.; Resnati, G. *J. Am. Chem. Soc.* **2005**, *127*, 14972.
- 6 Bolton, O.; Lee, K.; Kim, H. J.; Lin, K. Y.; Kim, J. *Nat. Chem.* **2011**, *3*, 205.
- 7 Farina, A.; Meille, S. V.; Messina, M. T.; Metrangolo, P.; Resnati, G.; Vecchio, G. *Angew. Chem., Int. Ed.* **1999**, *38*, 2433.
- 8 (a) Aakeröy, C. B.; Desper, J.; Helfrich, B. A.; Metrangolo, P.; Pilati, T.; Resnati, G.; Stevenazzi, A. *Chem. Commun.* **2007**, 4236. (b) Aakeröy, C. B.; Schultheiss, N.; Rajbanshi, A.; Desper, J.; Moore, C. *Cryst. Growth Des.* **2009**, *9*, 432.
- 9 (a) Metrangolo, P.; Meyer, F.; Pilati, T.; Resnati, G.; Terraneo, G. *Angew. Chem. Int. Ed.* **2008**, *47*, 6114. (b) Rissanen, K. *CrystEngComm* **2008**, *9*, 1107.
- 10 Martí-Rujas, J.; Colombo, L.; Lü, J.; Dey, A.; Terraneo, G.; Metrangolo, P.; Pilati, T.; Resnati, G. *Chem. Commun.* **2012**, *48*, 8207.
- 11 Aakeröy, C. B.; Panikkattu, S.; Chopade, P. D.; Desper, J. *CrystEngComm* **2013**, *15*, 3125.
- 12 Priimagi, A.; Cavallo, G.; Forni, A.; Gorynsztejn-Leben, M.; Kaivola, M.; Metrangolo, P.; Milani, R.; Shishido, A.; Pilati, T.; Resnati, G.; Terraneo, G. *Adv. Funct. Mater.* **2012**, *22*, 2572.
- 13 Corradi, E.; Meille, S. V.; Messina, M. T.; Metrangolo, P.; Resnati, G. *Angew. Chem., Int. Ed.* **2000**, *39*, 1782.
- 14 Präsang, C.; Nguyen, H. L.; Horton, P. N.; Whitwood, A. C.; Bruce, D. W. *Chem. Commun.* **2008**, 6164.
- 15 Cho, C. M.; Wang, X.; Li, J. J.; He, C.; Xu, J. *Liq. Cryst.* **2012**, *1*.
- 16 Aakeröy, C. B.; Sinha, A. S.; Epa, K. N.; Chopade, P. D.; Smith, M. M.; Desper, J. *Cryst. Growth Des.* **2013**, *13*, 2687.
- 17 (a) Aakeröy, C. B.; Sinha, A. S.; Epa, K. N.; Spartz, C. L.; Desper, J. *Chem. Commun.* **2012**, *48*, 11289. (b) Aakeröy, C. B.; Sinha, A. S. *RSC Adv.* **2013**, *3*, 8168.
- 18 (a) Aakeröy, C. B.; Salmon, D. J.; Smith, M. M.; Desper, J. *CrystEngComm* **2009**, *11*, 439. (b) Scarso, A.; Pellizzaro, L.; De Lucchi, O.; Linden, A.; Fabris, F. *Angew. Chem., Int. Ed.* **2007**, *46*, 4972. (c) Mazik, M.; Bläser, D.; Boese, R. *Tetrahedron* **1999**, *55*, 7835.
- 19 (a) Burka, L. T. NTP Technical Report on the Toxicity Studies of Methyl Ethyl Ketoxime, 1999. http://ntp.niehs.nih.gov/ntp/htdocs/ST_rpts/tox051.pdf. (b) McGraw-Hill. Oxime, 2007. <http://books.mcgraw-hill.com/EST10/site/supparticles/Oxime-480600.pdf>.

-
- 20 (a) Cavallo, G.; Metrangolo, P.; Pilati, T.; Resnati, G.; Sansotera, M.; Terraneo, G. *Chem. Soc. Rev.* **2010**, *39*, 3772. (b) Metrangolo, P.; Resnati, G. *Science* **2008**, *321*, 918.
- 21 Troff, R. W.; Mäkelä, T.; Topić, F.; Valkonen, A.; Raatikainen, K.; Rissanen, K. *Eur. J. Org. Chem.* **2013**, 1617.
- 22 (a) Padgett, C. W.; Walsh, R. D.; Drake, G. W.; Hanks, T. W.; Pennington, W. T. *Cryst. Growth Des.* **2005**, *5*, 745. (b) Sun, A.; Lauher, J. W.; Goroff, N. S. *Science* **2006**, *312*, 1030. (c) Luo, L.; Wilhelm, C.; Sun, A.; Grey, C. P.; Lauher, J. W.; Goroff, N. S. *J. Am. Chem. Soc.* **2008**, *130*, 7702. (d) Wilhelm, C.; Boyd, S. A.; Chawda, S.; Fowler, F. W.; Goroff, N. S.; Halada, G. P.; Grey, C. P.; Lauher, J. W.; Luo, L.; Martin, C. D.; Parise, J. B.; Tarabrella, C.; Webb, J. A. *J. Am. Chem. Soc.* **2008**, *130*, 4415.
- 23 Yamamoto, H. M.; Kosaka, Y.; Maeda, R.; Yamaura, J.; Nakao, A.; Nakamura, T.; Kato, R. *ACS Nano* **2008**, *2*, 143.
- 24 Liefbrig, J.; Yamamoto, H. M.; Kusamoto, T.; Cui, H.; Jeannin, O.; Fourmigué, M.; Kato, R. *Cryst. Growth Des.* **2011**, *11*, 4267.
- 25 (a) Pedireddi, V. R.; Reddy, D. S.; Gaud, G. S.; Craig, D. C.; Rae, A. D.; Desiraju, G. R. *J. Chem. Soc. Perkin Trans. II* **1994**, *11*, 2353. (b) Metrangolo, P.; Resnati, G. ed. *Halogen Bonding: Fundamentals and Applications, Structure and Bonding*, Springer, Berlin, 2007. (c) Aakeröy, C. B.; Chopade, P. D.; Ganser, C.; Desper, J. *Chem. Commun.* **2011**, *47*, 4688.
- 26 Osowska, K.; Lis, T.; Szafert, S. *Eur. J. Org. Chem.* **2008**, 4598.
- 27 Clark, T.; Hennemann, M.; Murray, J. S.; Politzer, P. *J. Mol. Model.* **2007**, *13*, 291.
- 28 (a) Etter, M. C.; Frankenbach, G. M. *Chem. Mater.* **1989**, *1*, 10. (b) Etter, M. C. *Acc. Chem. Res.* **1990**, *23*, 120. (c) Etter, M. C. *J. Phys. Chem.* **1991**, *95*, 4601.
- 29 Allen, F. H. *Acta. Crystallogr., Sect. B.* **2002**, *B58*, 380.
- 30 *CSD ConQuest 1.15*; Cambridge Crystallographic Data Centre: Cambridge, U.K., 2013.
- 31 Dembowski, S. (Private communication, 2011).
- 32 Schultheiss, N. (Private communication, 2007).

Chapter 6 - Versatile 2,2'-bipyridine-copper(II) based metallo-macrocycles

6.1 Introduction

6.1.1 Macrocyclic compounds

Synthesis and properties of macrocyclic compounds have attracted considerable attention, owing to their immense use in the field of host-guest chemistry and molecular recognition. These frameworks have found multiple applications in ion-transport,¹ chemosensors^{2,3} and imaging,⁴ metallo-enzyme mimics,⁵ drug discovery,⁶ and catalysis.⁷ An example is a calixsalen macrocycle which acts as a fluorescent sensor for the detection of zinc(II) metal ions, and shows high selectivity toward Zn²⁺ over other competitive cations (Figure 6.1).⁸

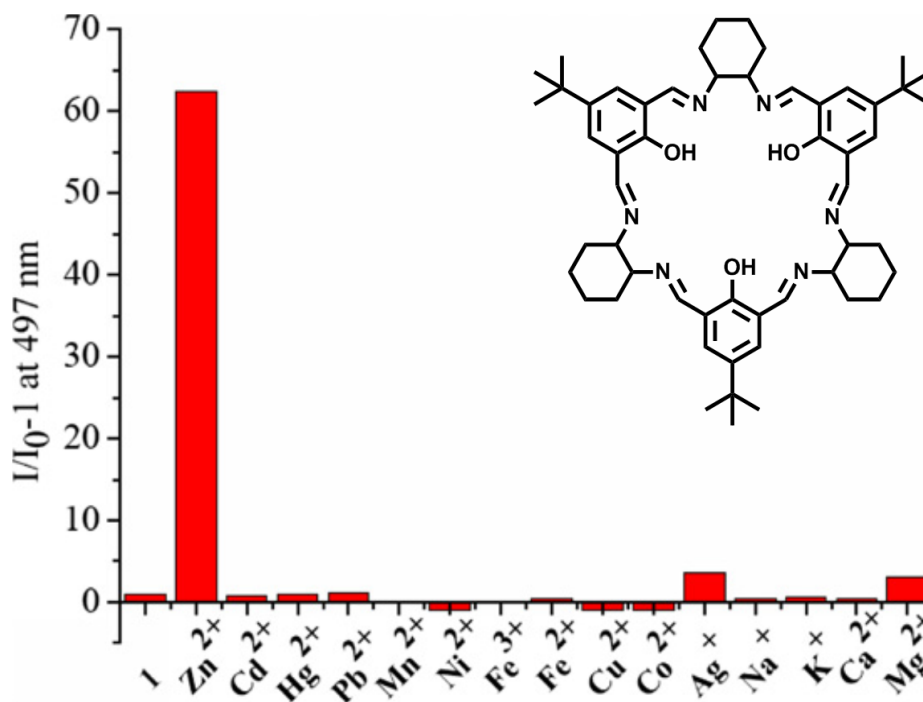


Figure 6.1 A calixsalen macrocycle as a selective fluorescent sensor for zinc(II) ions.⁸

Selectivity of macrocycles and host-guest complex stability is dependent upon two important factors, i.e. cavity size and conformational flexibility.⁹ The binding of the guest to the host is accompanied by a complementary conformational change in the host, and a more flexible and dynamic macrocyclic host may adjust rapidly to the changing conditions, and possibly act as

better sensors due to faster response times and reversible binding.⁹ For example, Shimizu *et. al* synthesized two new 2,2'-bipyridine based macrocycles bridged by either ureas or triazinanone units, in which the metal binding sites could rotate and assume the best possible conformation to accommodate guests of different sizes (Figure 6.2).⁹

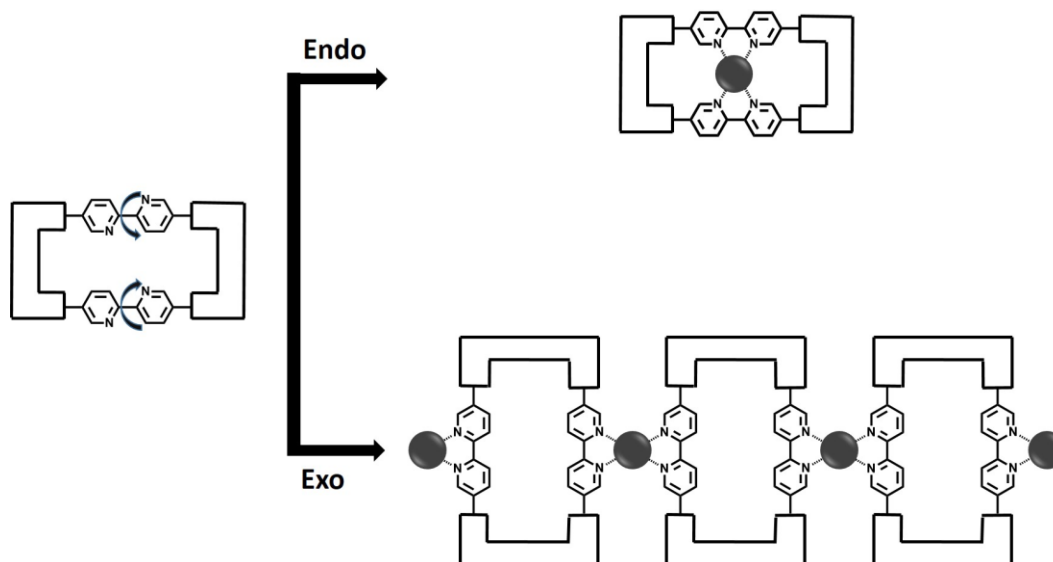


Figure 6.2 Macrocycles with switchable 2,2'-bipyridine based metal binding sites.⁹

6.1.1.1 Anion binding in macrocycles

Anions are ubiquitous in both biological processes and in organic and inorganic chemistry, but inherent problems such as solubility, hydration, large size, and numerous geometries, has made the field of anion binding by synthetic receptors a challenging one.^{10,11} Different synthetic strategies such as recognition by proteins,¹⁰ neutral hosts,¹⁰ Lewis acid receptors,¹¹ organometallic receptors,¹¹ and transition metal complexes¹¹ have been employed over the years, including a hydrogen-bonded strategy to encapsulate anions in macrocyclic receptors, based on the seminal work by Simmons *et. al* (Figure 6.3).¹²

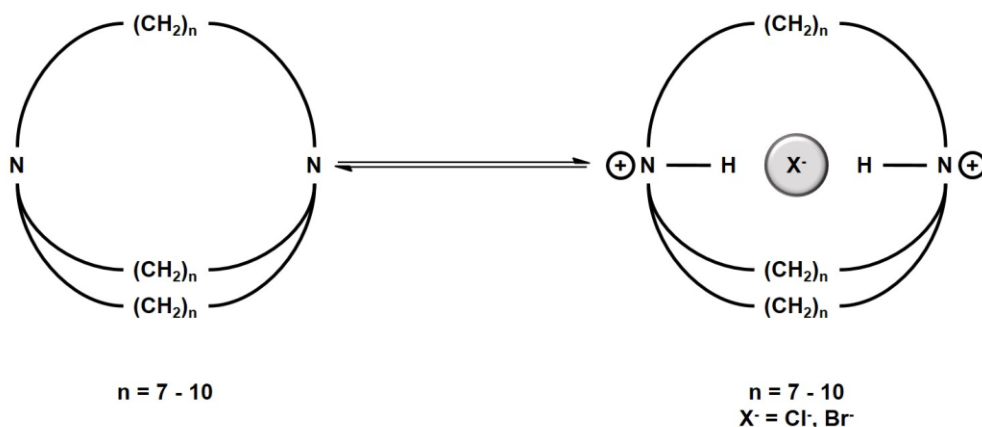


Figure 6.3 Encapsulation of halide ions by diammonium katapinands.¹²

Occasionally, hydrogen-bond based synthetic strategies suffer from problems such as hydration (large energetic penalty for binding to anions) and competing hydrogen-bonding moieties in solution.¹¹ A feasible alternative is the direct bridging of the anion between a positively charged dimetallic center, wherein the assembly of the coordination architecture is controlled by coordinating the metal centers to an organic scaffold.¹⁰ The designed organic scaffold should ideally have chelating sites for the metal atoms, where the metal-metal distance is controlled by the length and rigidity of the organic backbone.¹⁰ A simple example is provided by the Cu(II)-bistren system, wherein the dinuclear copper complex binds chloride ions in water and the anion binding is proven to occur in a μ -bridging fashion (Figure 6.4).¹³

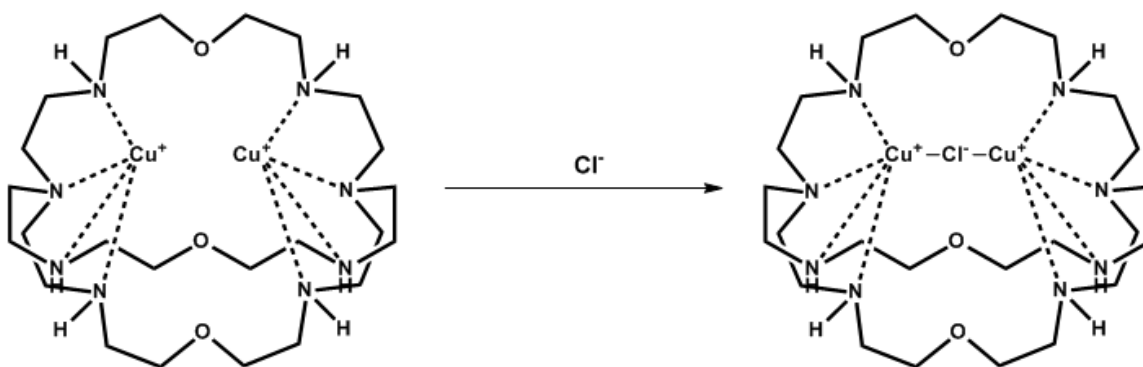


Figure 6.4 A dinuclear Cu(II) complex capable of binding chloride ions.¹³

Although extensive work has been done on dimetallic macrocyclic receptors that can adjust their coordination modes and change their conformation for encapsulating specific anions in solution, there is still a need for versatile and modular receptors in which the organic scaffold is capable of controlling the metal-metal distance (by varying the cavity size), along with encapsulating guests of varying sizes.

6.1.2 Rationale for the design of the metallo-macrocycle

The immense use of dimetallic macrocyclic receptors in the field of anion capture and catalysis, motivated us to design a metallo-macrocycle based on three important factors (Figure 6.5):

- Versatility – develop a model macrocycle based on the 2,2'-bipyridyl backbone that can bind different metal ions and hence can cater to a range of host-guest chemistry.
- Modularity – the flexibility in the arm-length of the macrocycle gives rise to pockets of different sizes.
- Selectivity – the pocket size of the macrocycle can be tailored to the dimensions of the targeted guest.

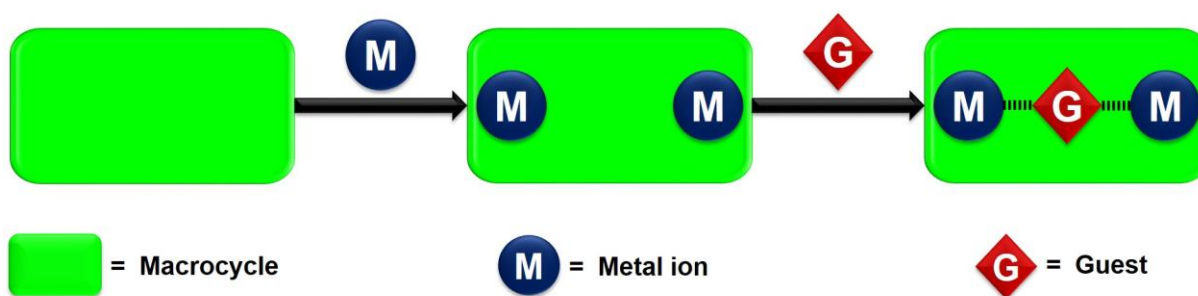


Figure 6.5 Design of a versatile and modular macrocycle capable of guest capture.

6.1.2.1 Molecular modeling of the macrocycle

The validity of the design of the macrocycle was tested by modeling the structure in Spartan'04 (Wave function, Inc. Irvine, CA) using DFT B3LYP/6-31G* *ab initio* calculations, and examining the dimensions of the host cavity (Figure 6.6).

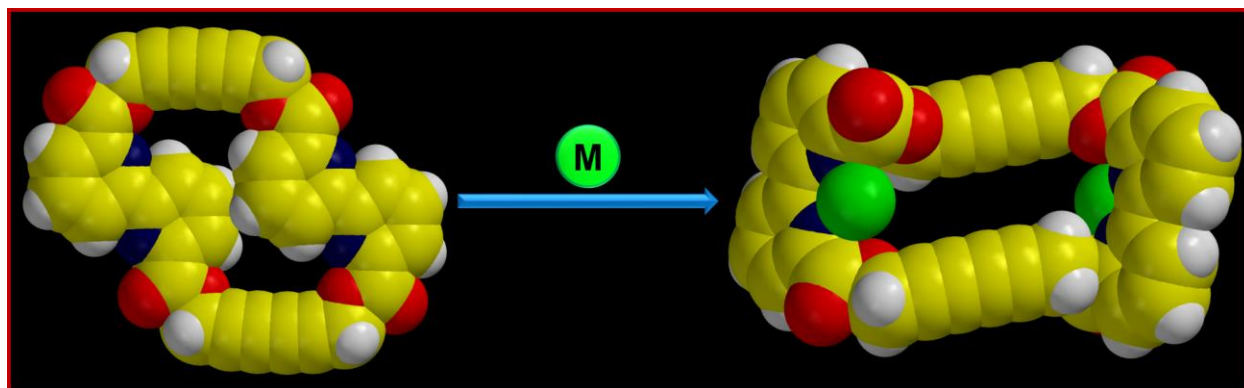


Figure 6.6 Force-field geometry optimization of the macrocycle (left), and the metallo-macrocycle (right).

The geometry optimized structure of the macrocycle shows that the 2,2'-bipyridyl nitrogen atoms exist in the *anti*-conformation, and the overall structure lacks any significant cavities. Upon complexation with copper ions, there is a conformational change in the organic scaffold to accommodate the metal atoms (the bipyridyl nitrogen atoms exist in the *syn*-conformation), which in turn gives rise to a rectangular-shaped pocket (12 Å x 6 Å), where the metal-metal distance is approximately 10 Å. The rectangular pocket can be used for the encapsulation of different guests.

6.1.2.2 Goals

Herein, we have outlined the design of a versatile and modular metallo-macrocycle, which can be used for host-guest chemistry (Figure 6.7).

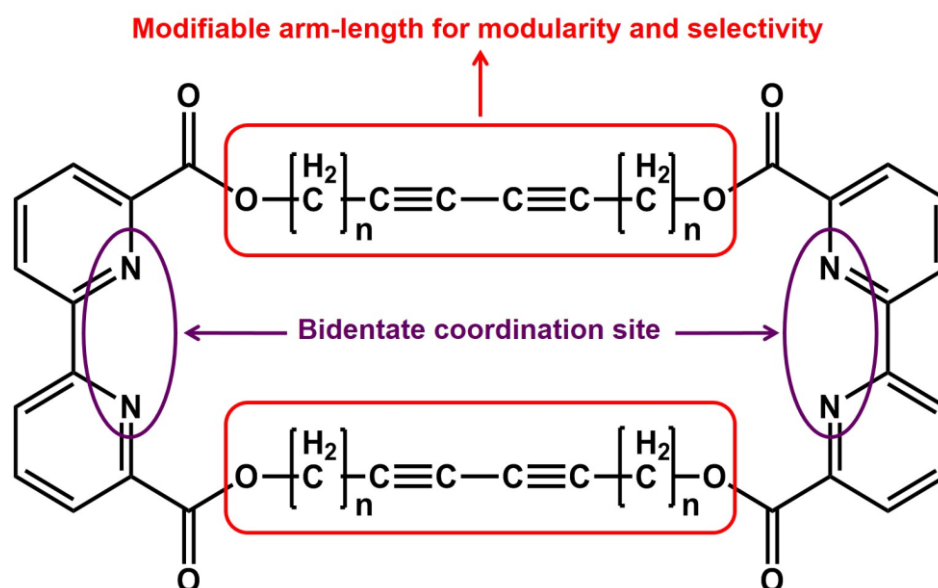


Figure 6.7 Dynamic macrocycle based on the 2,2'-bipyridyl backbone.

In this chapter, we are particularly interested in:

- Synthesizing and successfully characterizing the above macrocycle.
- Determining the macrocycle:metal stoichiometric ratio in solution.

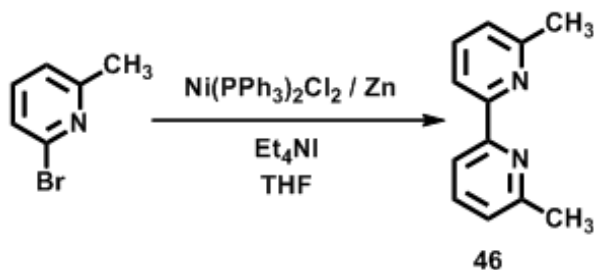
6.2 Experimental

6.2.1 Synthesis

All chemicals were purchased from Aldrich and used without further purification, unless otherwise noted. Melting points were determined on a Fisher-Johns melting point apparatus and

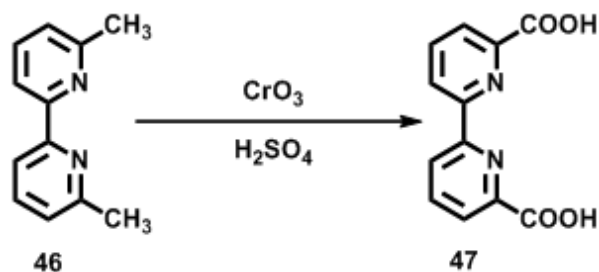
are uncorrected. ^1H and ^{13}C NMR spectra were recorded on a Varian Unity plus 400 MHz spectrometer in CDCl_3 or $\text{d}_6\text{-DMSO}$. Infrared spectroscopy (IR) was done on a Nicolet 380 FT-IR. Electrospray Ionization Mass Spectrometry (ESI-MS) was carried out on a Bruker Daltonics Esquire 3000 Plus.

6.2.1.1 Synthesis of 6,6'-dimethyl-2,2'-bipyridine,¹⁴ 46



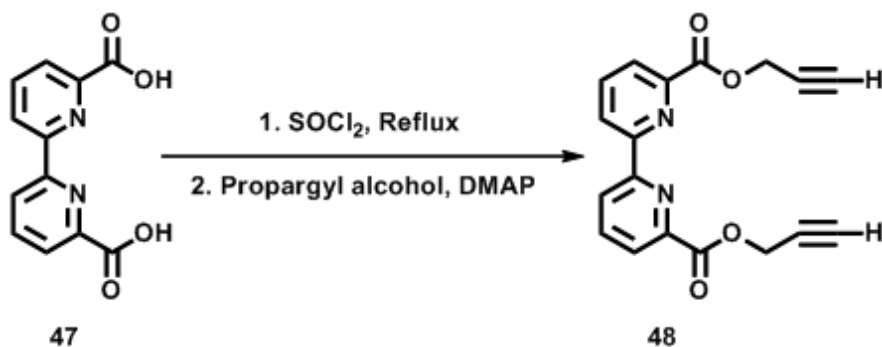
Under a nitrogen atmosphere, dry THF (50.0 mL) was added to a clean and dry round-bottom flask, to which $\text{Ni}(\text{PPh}_3)_2\text{Cl}_2$ (3.42 g, 5.22 mmol) and Et_4NI (4.47 g, 17.4 mmol) was added. Zinc dust (1.71 g, 26.1 mmol) was then added to the resulting slurry, and the mixture was stirred under dinitrogen. After 30 minutes the reaction mixture was heated to 50 °C and 2-bromo-6-methylpyridine (3.0 g, 17.4 mmol) in dry THF (15.0 mL) was added. The resulting mixture was stirred for 16 h at 50 °C, after which it was poured over 2 M aqueous ammonia (80.0 mL), filtered, and washed with diethyl ether (50.0 mL) and hexane (50.0 mL). The organic layer was separated and the aqueous layer was extracted with diethyl ether/hexane (1:1, v/v). The combined organic layer was washed with water and aqueous sodium chloride, dried over anhydrous magnesium sulfate, and evaporated. The residue was purified by silica-gel column chromatography using petroleum ether-ethylacetate (96:4, v/v) as the eluent. The solvent was removed under vacuum, and the resulting white powder was recrystallized from ethylacetate to yield colorless prism-shaped crystals. Yield: 1.18 g (74%); mp 90-93°C (lit., 93-95°C)¹⁴; ^1H NMR (δ_{H} ; CDCl_3 , 400MHz): 2.63 (s, 6 H), 7.15 (d, $J=7.81$ Hz, 2 H), 7.68 (t, $J=7.81$ Hz, 2 H), 8.17 (d, $J=7.81$ Hz, 2 H).

6.2.1.2 Synthesis of 2,2'-bipyridine-6,6'-dicarboxylic acid,¹⁵ 47



To a solution of **46** (1.0 g, 5.43 mmol) in 15.0 mL of concentrated sulfuric acid, 3.26 g (32.58 mmol) of CrO_3 was added in small portions at 70 °C. The reaction mixture was stirred for 1 h at 70 °C, after which the resulting green slurry was allowed to reach room temperature, and then poured over 30 g of crushed ice. The white precipitate was filtered, washed several times with water, and air dried. Yield: 1.15 g (87%); mp 287 °C d (lit., 286 °C)¹⁶; ^1H NMR (δ_{H} ; DMSO-d_6 , 400MHz): 8.10 - 8.23 (m, 4 H), 8.75 (d, $J=7.91$ Hz, 2 H), 13.29 (br. s, 2 H).

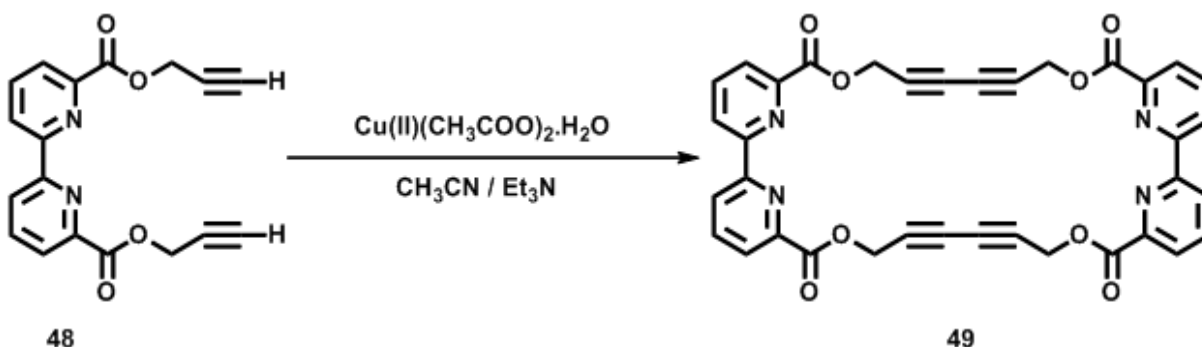
6.2.1.3 Synthesis of di(prop-2-yn-1-yl)[2,2'-bipyridine]-6,6'-dicarboxylate, 48



In a round-bottom flask, 0.90 g (3.69 mmol) of **47** was mixed with 8.0 mL of thionyl chloride. The reaction mixture was refluxed overnight, and the solvent from the resulting clear solution was removed under vacuum to obtain a white residue, which was washed twice with petroleum ether, and dissolved in dry THF. The resulting solution was slowly added dropwise into a mixture of 20.0 mL of dry THF containing 0.65 mL (0.62 g, 11.07 mmol) propargyl alcohol and 1.35 g (11.07 mmol) DMAP (4-(dimethylamino)pyridine) at the temperature of an ice-bath. The resulting slurry was then stirred for 24 hr at room temperature, after which the solvent was removed under vacuum, and the white residue was extracted in ethylacetate, and washed with water (50.0 mL x 2), and brine (50.0 mL). The organic layer was removed under vacuum and the product was obtained as a white powder. Yield: 0.98 g (83%); mp 156-158 °C;

^1H NMR (δ_{H} ; DMSO- d_6 , 400MHz): 3.66 (t, $J=2.15$ Hz, 2 H), 5.05 (d, $J=2.15$ Hz, 4 H), 8.14 - 8.30 (m, 4 H), 8.64 (d, $J=7.78$ Hz, 2 H); ^{13}C NMR (δ_{C} ; DMSO- d_6 , 400MHz): 53.05, 78.23, 124.44, 125.82, 139.29, 146.80, 154.60, 163.72; IR (neat, ν/cm^{-1}): 3257, 2135 ($\text{C}\equiv\text{C}$), 1718 ($\text{C}=\text{O}$), 1578, 1439, 1372, 1300, 1254, 1143, 1072, 990, 949, 830.

6.2.1.4 Synthesis of bis(di(prop-2-yn-1-yl)[2,2'-bipyridine]-6,6'-dicarboxylate), **49**



In a 5.0 L round-bottom flask, 0.78 g (3.88 mmol) of $\text{Cu(II)(CH}_3\text{COO)}_2\cdot\text{H}_2\text{O}$ was dissolved in an acetonitrile (600 mL) and triethylamine (1000 mL) mixture (solution A). In another round-bottom flask, 0.62 g (1.94 mmol) of **48** was dissolved in acetonitrile (400 mL) (solution B). Solution B was added dropwise to solution A with rapid stirring, over a period of eight hours (for experimental set-up, see Figure 6.8). Upon completion of the addition, the resulting green solution was stirred at room temperature for 15 h, after which a light blue precipitate could be seen floating in the solution. The precipitate was filtered, washed with water (20 mL x 4), and air dried. The light blue powder was then suspended in 2 M aqueous ammonia, and the resulting slurry was stirred at room temperature for 30 minutes, after which the light brown precipitate was filtered, washed with water (20 mL x 3), and air dried to obtain pure product. Yield: 0.17 g (28%); mp 218°C d; ^1H NMR (δ_{H} ; DMSO- d_6 , 400MHz): 5.19 (s, 8 H), 8.15 - 8.16 (m, 8 H), 8.43 - 8.46 (m, 4 H); IR (neat, ν/cm^{-1}): 3085, 2975, 2268 ($\text{C}\equiv\text{C}$), 2155 ($\text{C}\equiv\text{C}$), 1748 ($\text{C}=\text{O}$), 1726 ($\text{C}=\text{O}$), 1584, 1560, 1433, 1373, 1305, 1255, 1243, 1220, 1142, 1130, 1094, 1075, 980, 950, 823; ESI-MS m/z 637 ($[\mathbf{49} + \text{H}]^+$).

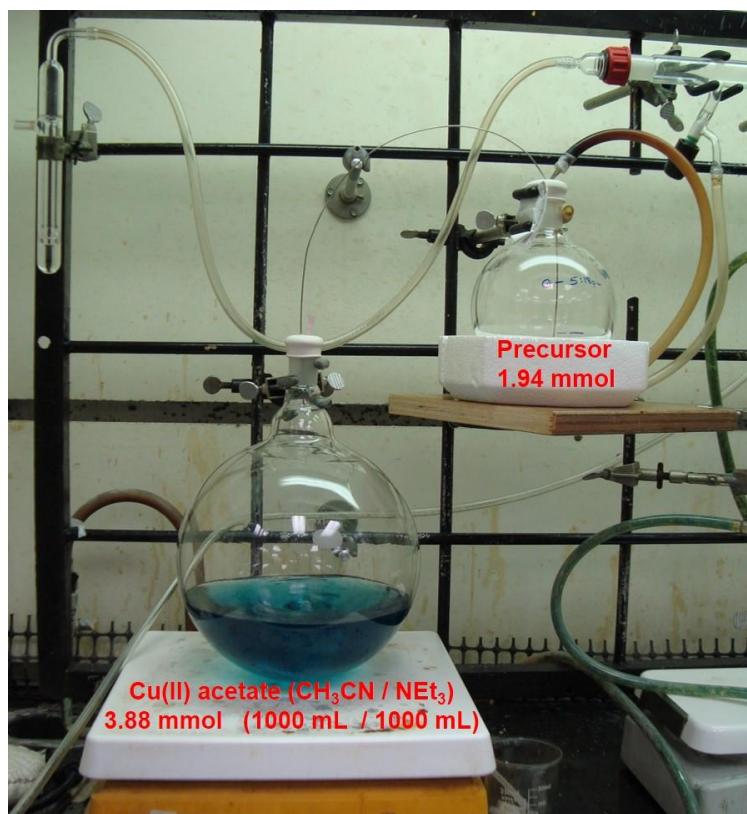


Figure 6.8 High dilution synthesis of **49**.

6.2.2 UV-visible spectroscopy titrations

The UV-visible spectrum of the macrocycle (**49**) was recorded on a Shimadzu UV-Vis-1650PC spectrophotometer in spectrophotometric grade dimethyl sulfoxide (DMSO) as solvent. The macrocycle : copper(II) stoichiometry was determined by Job's continuous variation method involving UV-visible titrations.¹⁷ A series of solutions containing **49** and $\text{Cu(II)(ClO}_4)_2 \cdot 6\text{H}_2\text{O}$ were prepared such that the sum of the total metal ion and **49** concentration remained constant ($50 \mu\text{M}$). The mole fraction (X) of **49** was varied from 0.0 to 1.0. The corrected absorbance ($A_{\text{observed}} - A_{\text{macrocycle}} - A_{\text{copper(II)}}$) at 330 nm (Table 6.1) and 338 nm (Table 6.2) was plotted against the molar fraction of the macrocycle solution to obtain the Job's plot.

Table 6.1 UV-visible data for the Job's plot at $\lambda_{\max} = 330 \text{ nm}$.

<u>Host</u> <u>Conc.</u>									
2.5mg	10mL DMSO	0.00039 mol/L							
M.W. - 636.0									
	Diluted to								
3.18mL stock	25mL DMSO	0.00005 mol/L	$\lambda_{\max} =$ 330.0 nm	A = 0.004	$\epsilon = 80$				
<u>Guest</u> <u>Conc.</u>									
8.2mg	10mL DMSO	0.00221 mol/L							
M.W. - 370.53									
	Diluted to								
0.565mL stock	25mL DMSO	0.00005 mol/L	$\lambda_{\max} =$ 330.0 nm	A = 0.054	$\epsilon = 1080$				
					$\lambda_{\max} = 330.0$ nm				
S. No.	Vol. Host (mL)	Vol. Guest (mL)	A(obs.)	Conc. Host (mol/L)	A(host)	Conc. Guest (mol/L)	A(guest)	A(obs.) - A(host) - A(guest)	(Conc. Host) / Total Conc.
1	4.00	0.00	0.0040	0.00005000	0.0040	0.00000000	0.0000	0.000000	1.0000
2	3.50	0.50	0.0110	0.00004375	0.0035	0.00000625	0.0068	0.000750	0.8750
3	3.00	1.00	0.0180	0.00003750	0.0030	0.00001250	0.0135	0.001500	0.7500
4	2.00	2.00	0.0340	0.00002500	0.0020	0.00002500	0.0270	0.005000	0.5000
5	1.50	2.50	0.0420	0.00001875	0.0015	0.00003125	0.0338	0.006750	0.3750
6	1.25	2.75	0.0440	0.00001563	0.0013	0.00003438	0.0371	0.005625	0.3125
7	1.00	3.00	0.0470	0.00001250	0.0010	0.00003750	0.0405	0.005500	0.2500
8	0.00	4.00	0.0540	0.00000000	0.0000	0.00005000	0.0540	0.000000	0.0000

Table 6.2 UV-visible data for the Job's plot at $\lambda_{\max} = 338 \text{ nm}$.

Host Conc.									
2.5mg	10mL DMSO	0.00039 mol/L							
M.W. - 636.0									
	Diluted to								
3.18mL stock	25mL DMSO	0.00005 mol/L	$\lambda_{\max} =$ 338.0 nm	A = 0.012	$\epsilon = 240$				
Guest Conc.									
8.2mg	10mL DMSO	0.00221 mol/L							
M.W. - 370.5									
	Diluted to								
0.565mL stock	25mL DMSO	0.00005 mol/L	$\lambda_{\max} =$ 338.0 nm	A = 0.041	$\epsilon = 820$				
					$\lambda_{\max} = 338.0$ nm				
S. No.	Vol. Host (mL)	Vol. Guest (mL)	A(obs.)	Conc. Host (mol/L)	A(host)	Conc. Guest (mol/L)	A(guest)	A(obs.) - A(host) - A(guest)	(Conc. Host) / Total Conc.
1	4.00	0.00	0.0120	0.00005000	0.0120	0.00000000	0.0000	0.000000	1.0000
2	3.50	0.50	0.0160	0.00004375	0.0105	0.00000625	0.0051	0.000375	0.8750
3	3.00	1.00	0.0210	0.00003750	0.0090	0.00001250	0.0103	0.001750	0.7500
4	2.00	2.00	0.0310	0.00002500	0.0060	0.00002500	0.0205	0.004500	0.5000
5	1.50	2.50	0.0360	0.00001875	0.0045	0.00003125	0.0256	0.005875	0.3750
6	1.25	2.75	0.0370	0.00001563	0.0038	0.00003438	0.0282	0.005063	0.3125
7	1.00	3.00	0.0390	0.00001250	0.0030	0.00003750	0.0308	0.005250	0.2500
8	0.00	4.00	0.0410	0.00000000	0.0000	0.00005000	0.0410	0.000000	0.0000

6.2.3 Molecular modeling

Molecular modeling was performed on the macrocycle (**49**) using Spartan'04 (Wavefunction, Inc. Irvine, CA). The molecular geometry was optimized using DFT B3LYP/6-

31G* *ab initio* calculations, with the maxima and minima in the electrostatic potential surface (0.002 e au⁻¹ iso-surface) determined using a positive point charge in the vacuum as a probe. Also force-field geometry optimization was performed on the macrocycle-copper(II) complex.

6.3 Results and discussion

6.3.1 Characterization of 49

6.3.1.1 Infra-red spectroscopy

IR spectroscopy is a reliable tool for the characterization of the products in the synthesis of **49**. A salient feature in the IR spectra of **47-49** is the presence of the carbonyl stretch around 1700 cm⁻¹, which varies with the substituent. **47** being a carboxylic acid shows a carbonyl stretch at 1697 cm⁻¹, which shifts to 1718 cm⁻¹ upon conversion to the corresponding ester in **48**. Furthermore, the C≡C stretch in **48** at 2135 cm⁻¹, also serves as a distinctive marker. Finally, there is a clear change in the IR spectrum of **48** upon conversion to the macrocycle (**49**), where the carbonyl stretch at 1718 cm⁻¹ shifts to 1726 cm⁻¹ (Figure 6.9), along with the appearance of a new carbonyl stretch at 1748 cm⁻¹, which is possibly due to the existence of the carbonyl moieties in different environments in the strained macrocycle.

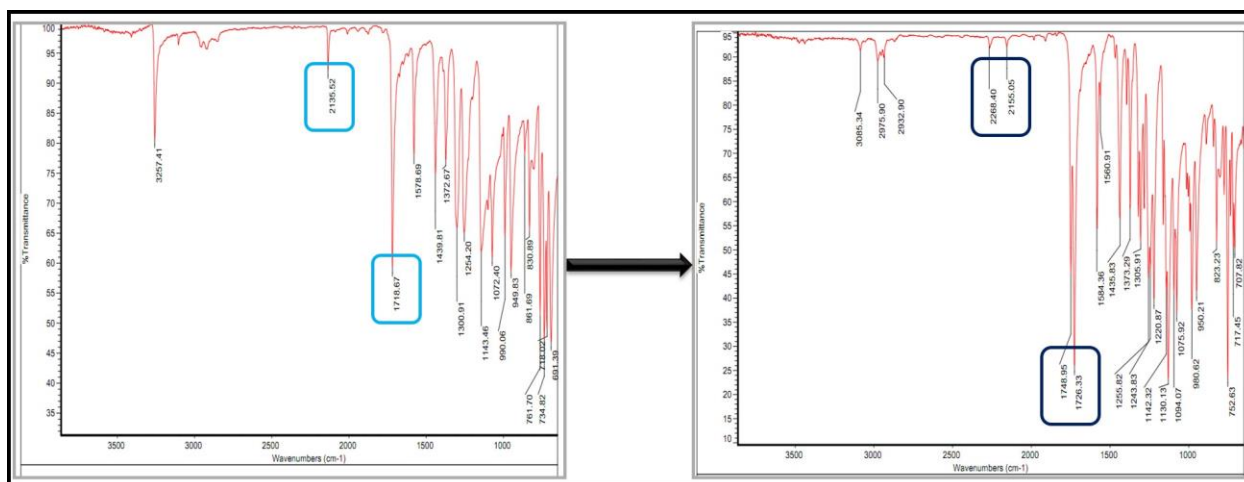


Figure 6.9 IR spectra illustrating the conversion of the alkyne pre-cursor (**48**) to the macrocycle (**49**).

6.3.1.2 ¹H NMR spectroscopy

¹H NMR spectroscopy has been successfully employed for the characterization of the products (**46-49**). The ¹H NMR spectrum of **48** has two important features (apart from the

aromatic region), the doublet at 5.05 ppm for the methylene protons, and the triplet at 3.68 ppm for the terminal alkyne proton (Figure 6.10). The conversion of **48** to the corresponding macrocycle (**49**) results in distinctive changes in the NMR spectrum. As expected, the terminal alkyne protons are completely absent in **49** (because of bridging of the terminal alkynes), whereas the methylene protons shift by 0.13 ppm, and appear as a singlet in the absence of long-range coupling with the terminal alkyne proton.

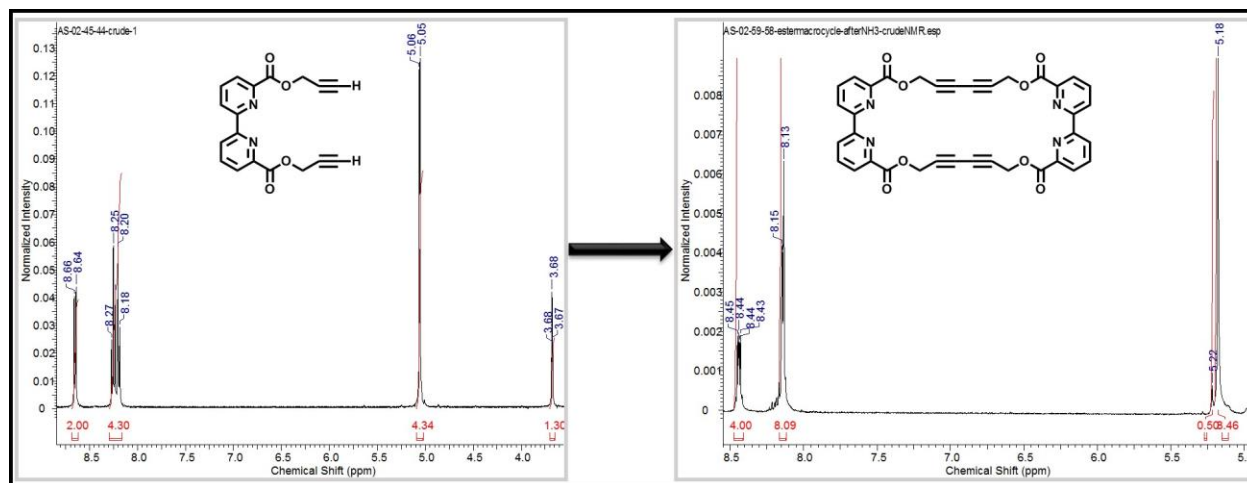


Figure 6.10 ¹H NMR spectra illustrating the conversion of the alkyne pre-cursor (**48**) to the macrocycle (**49**).

6.3.1.3 Mass spectroscopy

ESI-MS analysis confirms the successful synthesis and characterization of the macrocycle, as evidenced by the presence of m/z 637 [**49** + H]⁺ and 659 [**49** + Na]⁺ (Figure 6.11). Also, the observed isotopic pattern matches the expected isotopic pattern (Figure 6.11 - Inset).

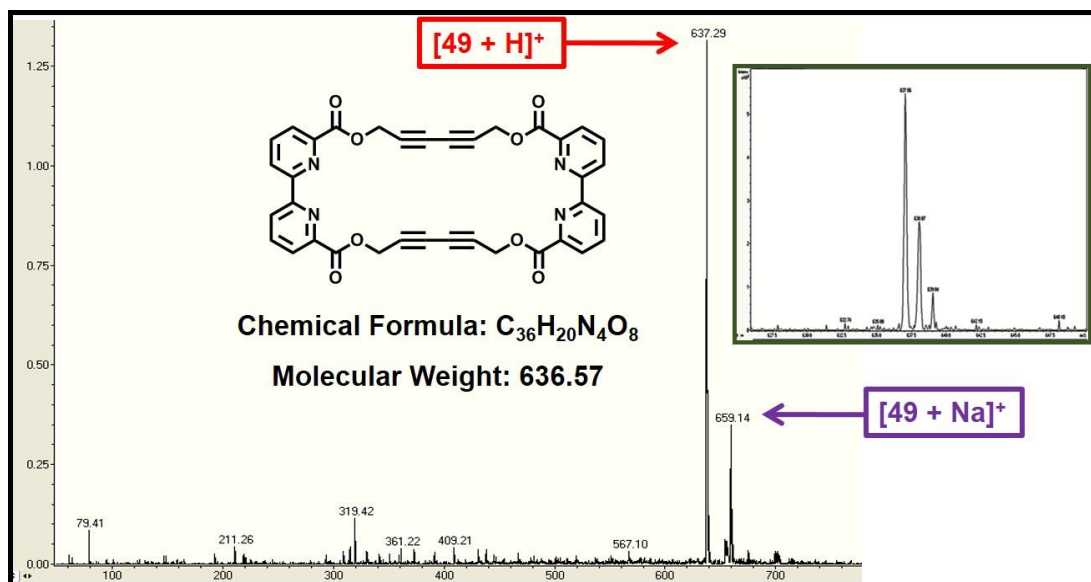


Figure 6.11 ESI-MS spectrum of **49** (Inset - isotopic pattern).

6.3.1.4 UV-visible spectroscopy

The UV-visible spectrum of the macrocycle (**49**) shows two absorption bands, centered at $\lambda_{\max} = 258.5$ and 283.0 nm (Figure 6.12).

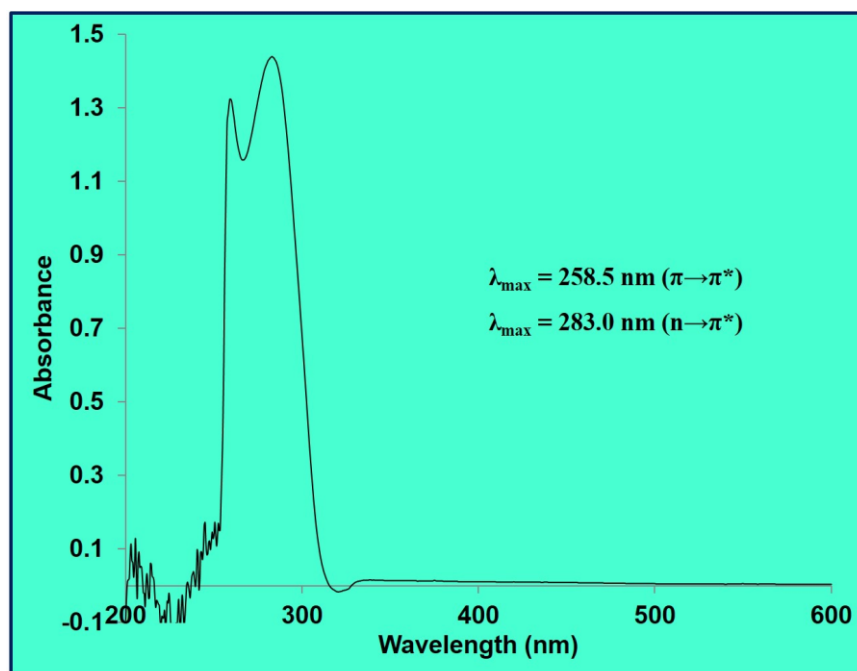
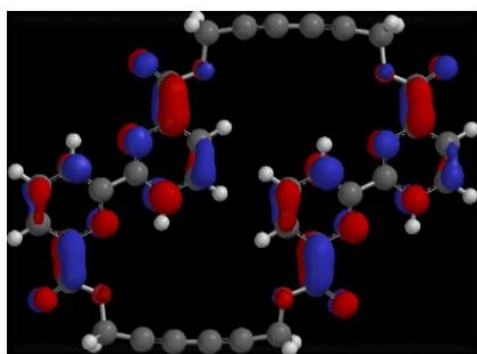


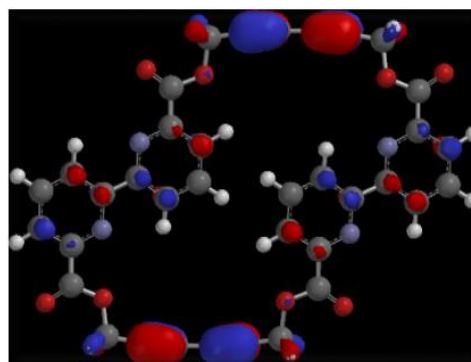
Figure 6.12 UV-visible spectrum of **49**.

The highest occupied molecular orbital surfaces (HOMO) and the lowest unoccupied molecular orbital surfaces (LUMO) have been determined by DFT B3LYP/6-31G* *ab initio*

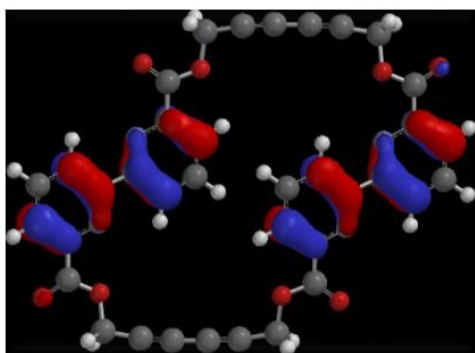
methods (Figure 6.13), which shows that the LUMO is located on the bipyridyl ring, whereas the HOMO and HOMO{-1} are spread out over the conjugated alkyne bridge. Finally, HOMO{-2} and HOMO{-3} are located on the aromatic rings and the lone pairs on the nitrogen atoms, which gives rise to the possibility of $\pi \rightarrow \pi^*$ and $n \rightarrow \pi^*$ transitions between HOMO{-2} / HOMO{-3} and the LUMO.¹⁸ As a result, the absorption bands at 258.5 nm and 283.0 nm in the UV-visible spectrum of **49**, can be assigned to $\pi \rightarrow \pi^*$ and $n \rightarrow \pi^*$ transitions, respectively.



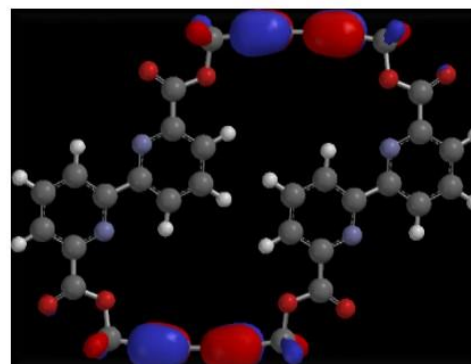
LUMO (E = - 183.08 kJ/mol)



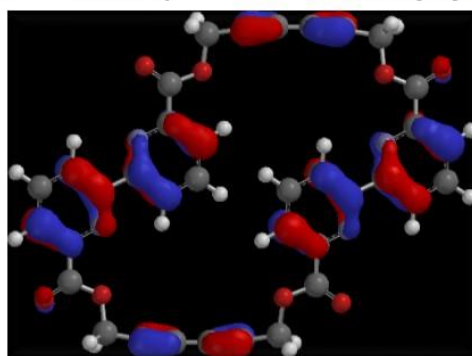
HOMO (E = - 658.13 kJ/mol)



HOMO{-2} (E = - 665.75 kJ/mol)



HOMO{-1} (E = - 656.09 kJ/mol)

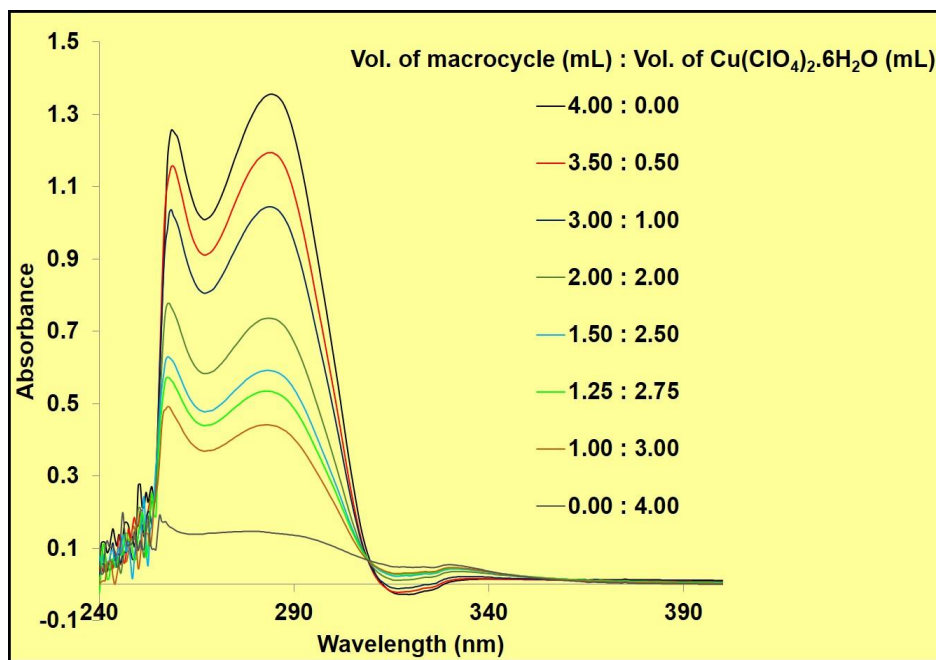


HOMO{-3} (E = - 665.75 kJ/mol)

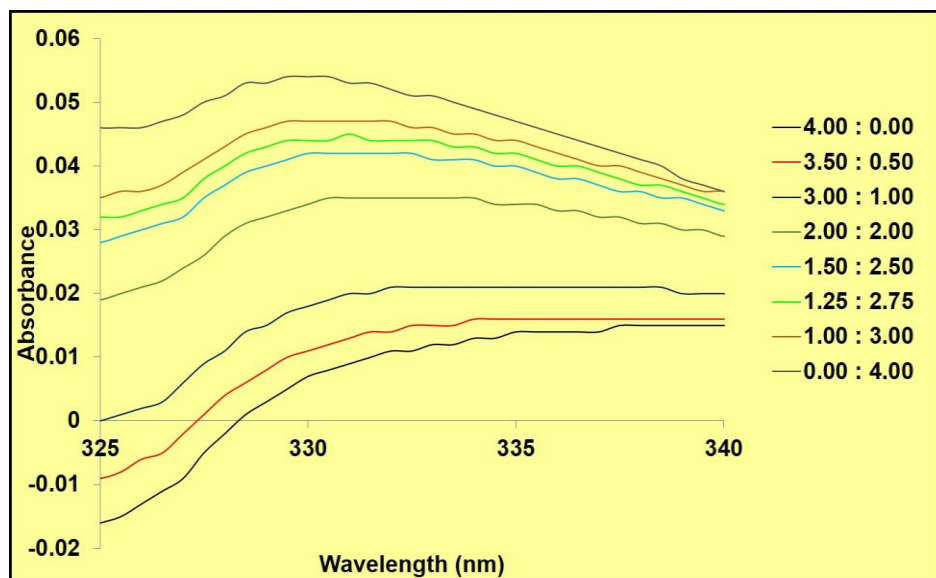
Figure 6.13 Calculated molecular orbitals (HOMO and LUMO) for **49**.

6.3.2 Coordination of 49 with copper(II) ions and determination of stoichiometry

The macrocycle:Cu(II) stoichiometry has been determined in solution by Job's continuous variation method utilizing UV-visible spectroscopy.¹⁷ The UV-visible spectra of the prepared solutions were recorded and plotted as a single graph (Figure 6.14).



(a)

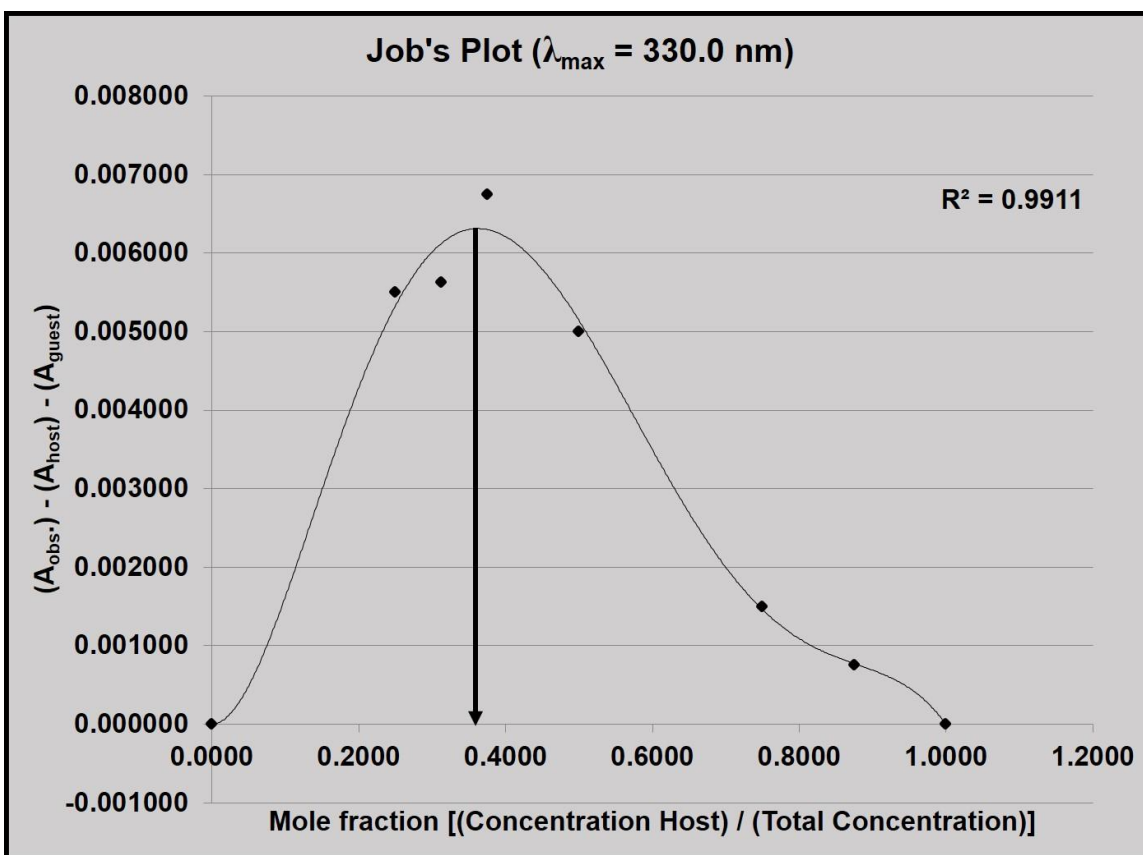


(b)

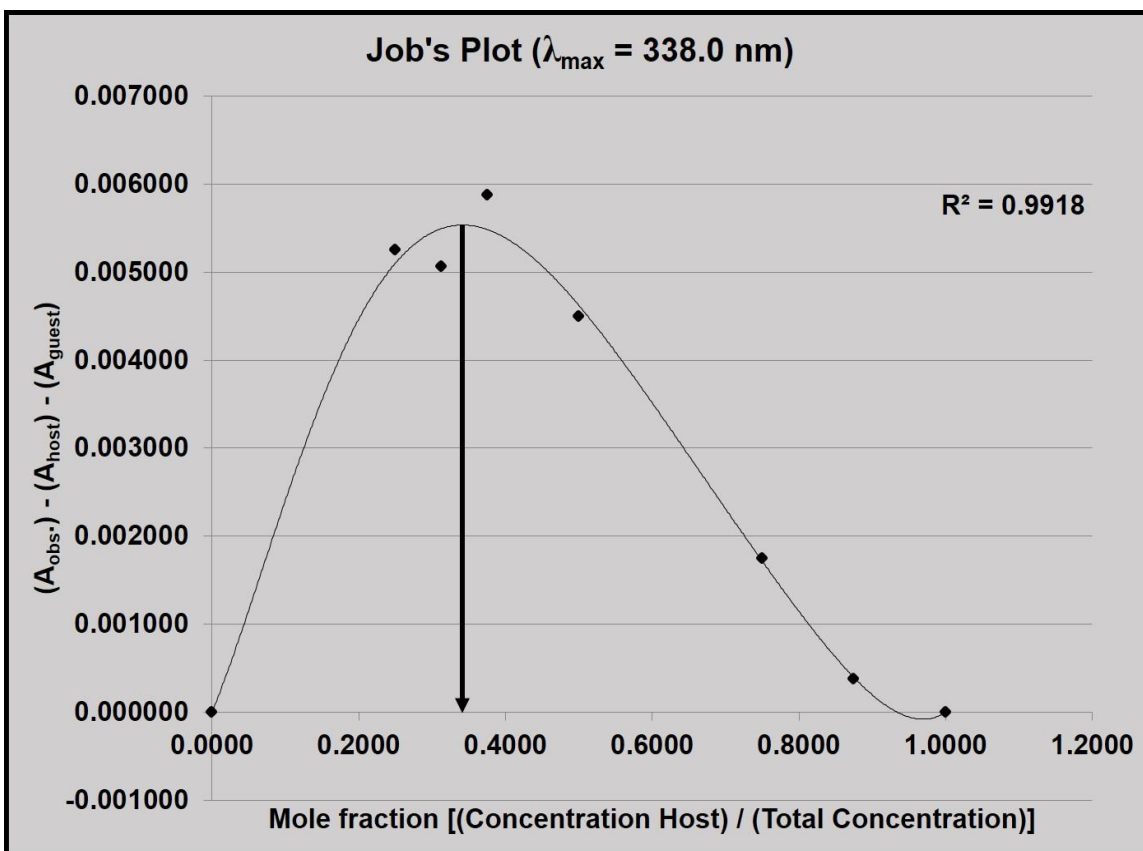
Figure 6.14 Determination of 49 : Cu²⁺ stoichiometry by continuous variation method using UV-visible spectroscopy (a); new absorption band (b).

There are three notable observations from the UV-visible titrations of the **49** with copper(II); (i) First, the appearance of a new absorption band at 330 nm, possibly due to conformational changes in **49** upon complexation with Cu(II), (ii) second, the decrease in the intensity and subsequent broadening of the band at 283 nm, due to loss of $n \rightarrow \pi^*$ transitions in **49** (because of the coordination of the nitrogen atoms on the bipyridyl rings to the metal atoms), and (iii) third, the decrease in the intensity of the band at 258.5 nm resembling a dilution event (this band is unaffected by the metal complexation, as it is probably arising from $\pi \rightarrow \pi^*$ transitions).

The corrected absorbance ($A_{\text{observed}} - A_{\text{macrocycle}} - A_{\text{copper(II)}}$) at 330 nm (Figure 6.15 a) and 338 nm (Figure 6.15 b) was plotted against the molar fraction of the macrocycle solution to obtain the Job's plot.



(a)



(b)

Figure 6.15 Job's plot for determining the macrocycle : metal stoichiometry at $\lambda_{\max} = 330.0 \text{ nm}$ (a), and at $\lambda_{\max} = 338.0 \text{ nm}$ (b).

The maximum corrected absorbance in the Job's plot corresponds to a macrocycle mole fraction of 0.36 - 0.38, which proves that the correct macrocycle:copper(II) stoichiometry is 1:2. This is expected, as the two 2,2'-bipyridyl sites in **49** are capable of binding a metal atom each.

6.3.3 Future work

6.3.3.1 Modularity in the macrocyclic system

The pocket size of the macrocycle can be easily varied by changing the number of bridging methylene carbons in the arms of the macrocycle (Figure 6.16), which in turn will enable in tuning the metal-metal distance within the metallo-macrocyclic cavity. This versatility in the synthesis can help in designing macrocycles with greater selectivity for different guests, and thus can be applied in various fields, such as anion-binding and hydrolysis of organophosphorus compounds.^{19,20}

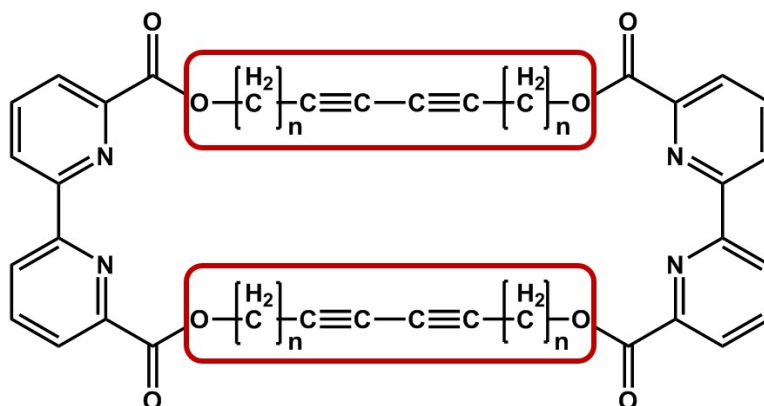


Figure 6.16 Easily modifiable arms for tuning the selectivity and the pocket size.

6.3.3.2 Modifying the solubility

Often, solubility is a challenging factor in the host-guest studies involving macrocyclic compounds. This can be overcome in our system by adding R groups, which tend to improve solubility (such as acids and oximes) in the 5,5' position on the aromatic rings.

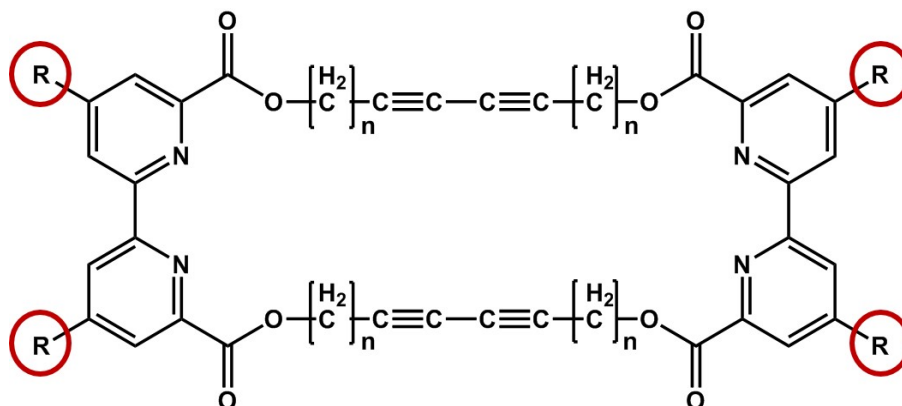


Figure 6.17 Improving the solubility by functionalizing the macrocycle with solubilizing groups.

6.4 Conclusions

Macrocyclic compounds having dimetallic centers are very useful in the field of host-guest chemistry (anion capture, catalysis, and sensing), and hence there is a need to synthesize dynamic and versatile metallo-macrocycles. We have synthesized and successfully characterized a modular and versatile 2,2'-bipyridyl based metallo-macrocyclic system, wherein it is easy to control the size of the cavity, and hence the selectivity of the system. The macrocycle:metal stoichiometry has been determined by Job's continuous variation method, and is found to be in the expected 1:2 ratio.

References

- 1 (a) Cazacu, A.; Tong, C.; Lee, A. V.; Fyles, T. M.; Barboiu, M. *J. Am. Chem. Soc.* **2006**, *128*, 9541. (b) Seo, J.; Park, S.; Lee, S. S.; Fainerman-Melnikova, M.; Lindoy, L. F. *Inorg. Chem.*, **2009**, *48*, 2770.
- 2 (a) Lindoy, L. F. *Dalton Trans.* **2006**, *43*, 5115. (b) Kim, J. S.; Quang, D. T. *Chem. Rev.* **2007**, *107*, 3780.
- 3 Bazzicalpi, C.; Bencini, A.; Biagini, S.; Bianchi, A.; Faggi, E.; Giorgi, C.; Machetta, M.; Totti, F.; Valtancoli, B. *Chem. Eur. J.* **2009**, *15*, 8049.
- 4 (a) Deetz, M. J.; Shang, M.; Smith, B. D. *J. Am. Chem. Soc.* **2000**, *122*, 6201. (b) Beer, P. D.; Gale, P. A. *Angew. Chem., Int. Ed.* **2001**, *40*, 486.
- 5 (a) Izzet, G.; Douziech, E.; Prange, T.; Tomas, A.; Jabin, I.; Le Mest, Y.; Reinaud, O. *Proc. Natl. Acad. Sci. U.S.A.* **2005**, *102*, 6831. (b) Bakirci, H.; Koner, A. L.; Dickman, M. H.; Kortz, U.; Naw, W. M. *Angew. Chem., Int. Ed.*, **2006**, *45*, 7400.
- 6 Mallinson, J.; Collins, I. *Future Med. Chem.* **2012**, *4*, 1409.
- 7 Gao, J.; Martell, A. E. *Org. Biomol. Chem.* **2003**, *1*, 2801.
- 8 Fu, Y.; Xing, Z.; Zhu, C.; Yang, H.; He, W.; Zhu, C.; Cheng, Y. *Tet. Lett.* **2012**, *53*, 804.
- 9 Tian, L.-L.; Wang, C.; Dawn, S.; Smith, M. D.; Krause, J. A.; Shimizu, L. S. *J. Am. Chem. Soc.* **2009**, *131*, 17620.
- 10 Dietrich, B.; Hosseini, M. W. Historical View on the Development of Anion Coordination Chemistry. In *Supramolecular Chemistry of Anions*; Bianchi, A.; Bowman-James, K.; Garcia-Espana, E., Ed.; Wiley-VCH: New York, 1997; pp. 45-62.
- 11 O'Neil, E. J.; Smith, B. D. *Cood. Chem. Rev.* **2006**, *250*, 3068.
- 12 Park, C. H.; Simmons, H. E. *J. Am. Chem. Soc.* **1968**, *90*, 2431.
- 13 Motekaitis, R. J.; Martell, A. E.; Dietrich, B.; Lehn, J.-M. *Inorg. Chem.* **1984**, *23*, 1588.
- 14 Rajalakshmanan, E.; Alexander, V. *Syn. Commun.* **2005**, *35*, 891.
- 15 Alyapyshev, M. Y.; Babain, V. A.; Borisova, N. E.; Kiseleva, R. N.; Safronov, D. V.; Reshetova, M. D. *Mendeleev Commun.* **2008**, *18*, 336.
- 16 Burstall, F. H. *J. Chem. Soc.* **1938**, 1662.
- 17 Hirose, K. *J. Inclusion Phenomena Macrocyclic Chem.* **2001**, *39*, 193.
- 18 Balachandran, V.; Laxmi, A.; Janaki, A. *J. Mol. Struct.* **2012**, *1013*, 75.
- 19 Burstyn, J. N.; Deal, K. A. *Inorg. Chem.* **1993**, *32*, 3585.
- 20 Gellman, S. H.; Petter, R.; Breslow, R. *J. Am. Chem. Soc.* **1986**, *108*, 2388.

Chapter 7 - Summary

Supramolecular chemistry relies on a variety of non-covalent intermolecular interactions such as coordinate bonds, hydrogen bonds, halogen bonds, and π - π interactions, for assembling supramolecular architectures. Although the use of non-covalent interactions brings reversibility to supramolecular synthesis, the formation and isolation of pure products become more challenging in comparison to organic synthesis, where the use of stronger covalent bonds allows for multi-step synthesis and the isolation and purification of intermediates. Hence, for the purpose of a predictable and reliable assembly, it is all the more important to identify and establish robust supramolecular synthons for building supermolecules.

We identified oximes as reliable supramolecular synthons as they are ubiquitous in both research laboratories (self-complementary hydrogen-bond donors and effective metal-coordinating ligands), and in industries (antidote for organophosphate poisoning). A series of aldoximes and ketoximes were synthesized via a “green” and versatile mechanochemical route, and in order to test the limits and limitations (if any) of this synthetic pathway, we decorated them with a range of electron-withdrawing, electron-donating, structurally active, multifunctionalized, and aliphatic functional groups. Our synthetic route was found to be robust, and tolerant of a range of aldehyde/ketone-oxime conversions. The relative reactivity of aldehydes vs ketones, and any electronic effects involved in these transformations were also investigated, and it was found that aldehydes showed a greater reactivity, and also that electron-withdrawing substituents enhanced the reactivity.

Thereafter, we investigated and established the nature of oxime...oxime homomeric intermolecular interactions present in the solid-state for four major categories of oximes (aldoxime, ketoxime, amidoxime, and cyano-oxime) by systematically examining the existing single-crystal data on oximes in the Cambridge Structural Database (CSD), complemented by three of our own crystal structures. We found that the oximes could be divided into four categories based on the distinct supramolecular synthons that they presented in the solid-state: (i) O-H...N dimers ($R_2^2(6)$), (ii) O-H...N catemers (C(3)), (iii) O-H...O catemers (C(2)), and (iv) oximes in which the R' group accepts a hydrogen bond from the oxime moiety catemers (C(6)).

This study will add to the existing knowledge of crystal engineers who are seeking supramolecular assembly based on the oxime motif.

The competitive or complementary nature of hydrogen bonds and halogen bonds in a system has been an area of research for the past decade, as the possibility of utilizing both these tools of communication simultaneously to build complicated supramolecular architectures can lead to exciting possibilities with applications in ion-pair recognition and chemical separations. As a result, we designed and synthesized two supramolecular reactants containing distinct hydrogen-bond donor (oxime motif) and halogen-bond donor sites (ethynyl-halogenated species) on the same organic backbone, so as to avoid any kind of geometric or steric bias. These donors were co-crystallized with a series of twenty different acceptors, and the resulting co-crystals have been analyzed by infra-red spectroscopy (IR) for the presence/absence of hydrogen/halogen bonds in the solid-state. Also, the nature of selectivity and competition between the two intermolecular forces has been revealed by an examination of the three new single-crystal structures, wherein it is observed that the two forces of interaction act in a complementary manner and are tolerant of each other in systems with 'equal' opportunities.

Finally, we designed and successfully carried out a multi-step synthesis (via high dilution methods) of a versatile and robust metallo-macrocycle based on the 2,2'-bipyridine backbone that is capable of controlling the metal-metal distance within the macrocyclic cavity. The macrocycle:copper(II) stoichiometric ratio has been determined to be 1:2 by Job's continuous variation method utilizing UV-visible spectroscopy. This research directly benefits chemists working in the field of anion-recognition, host-guest chemistry, catalysis, and sensing.

Appendix A - ^1H and ^{13}C NMR data

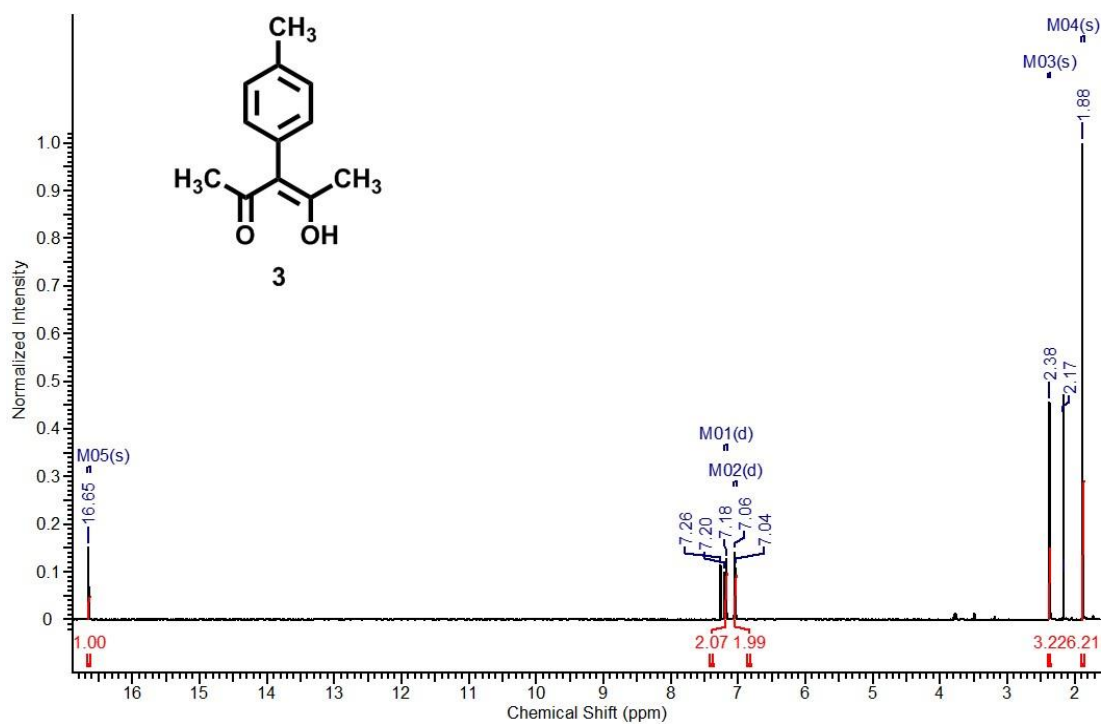


Figure A.1 ^1H NMR spectrum of **3**.

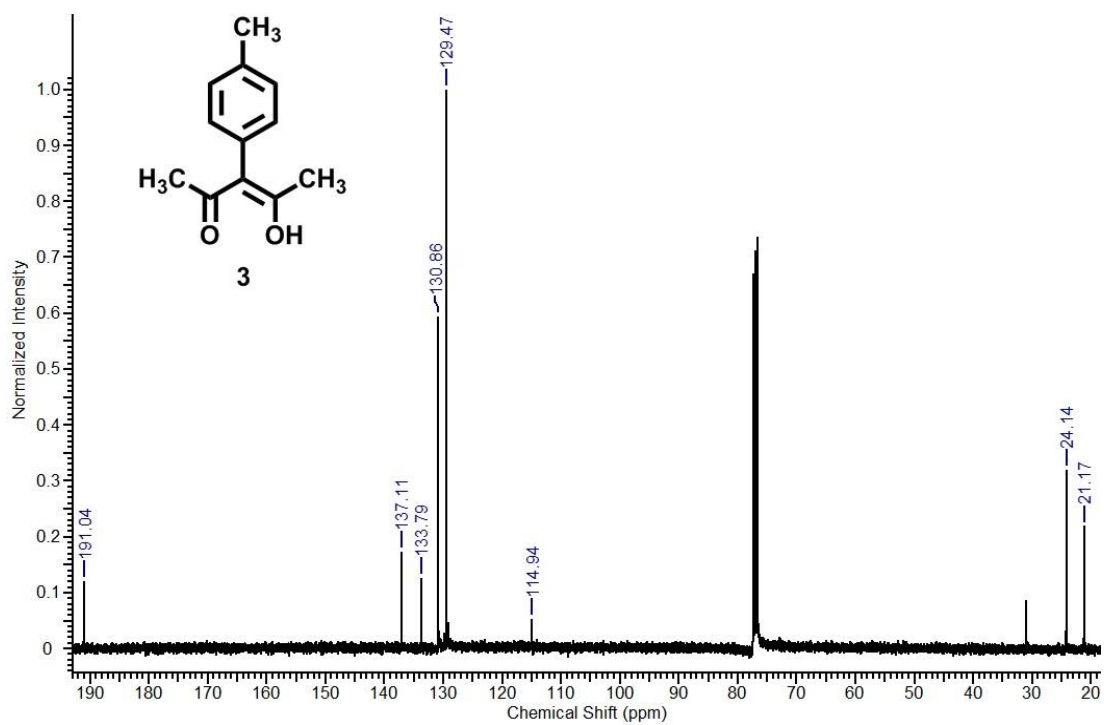


Figure A.2 ^{13}C NMR spectrum of **3**.

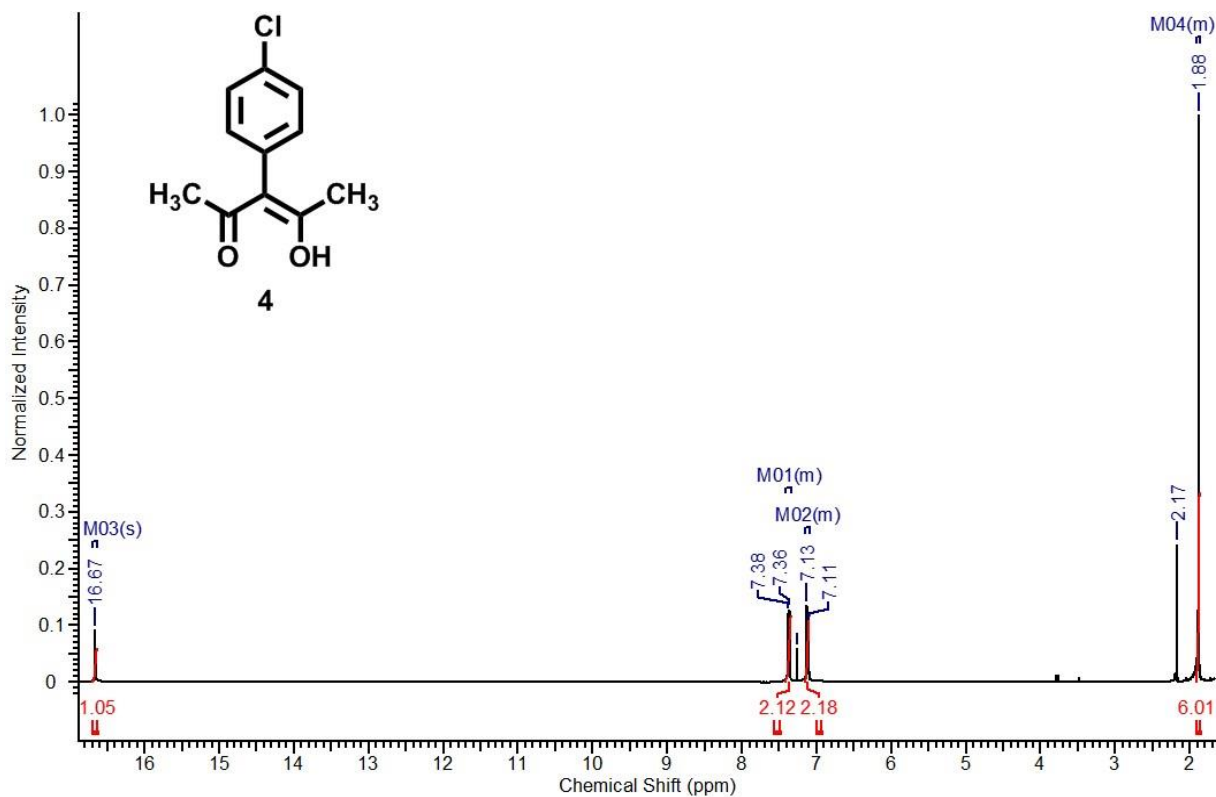


Figure A.3 ^1H NMR spectrum of **4**.

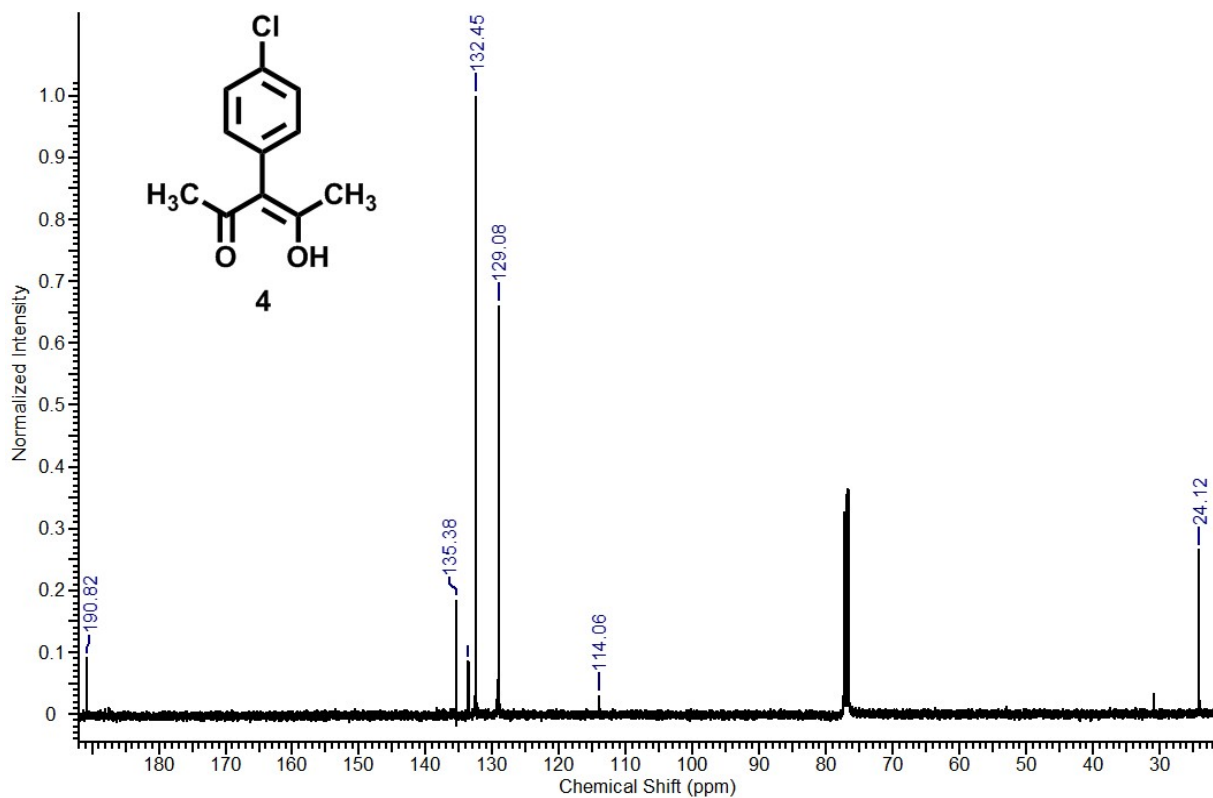


Figure A.4 ^{13}C NMR spectrum of **4**.

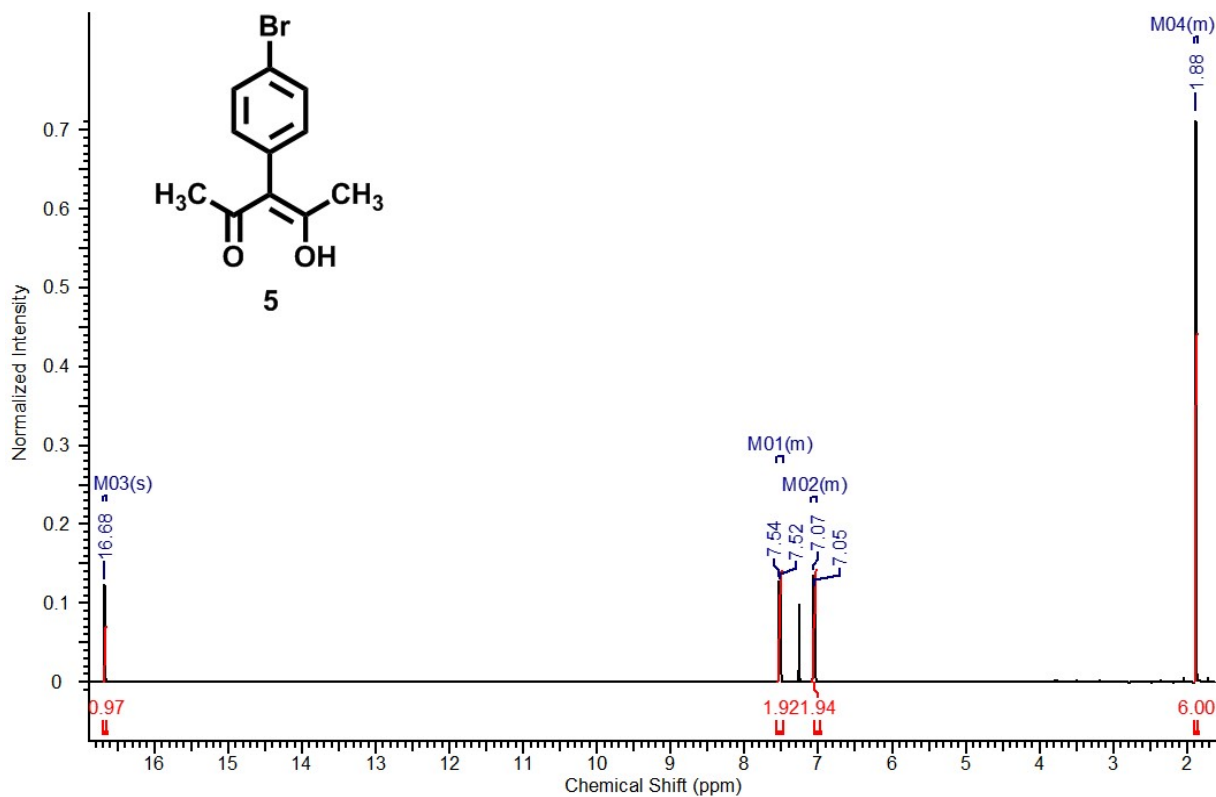


Figure A.5 ^1H NMR spectrum of 5.

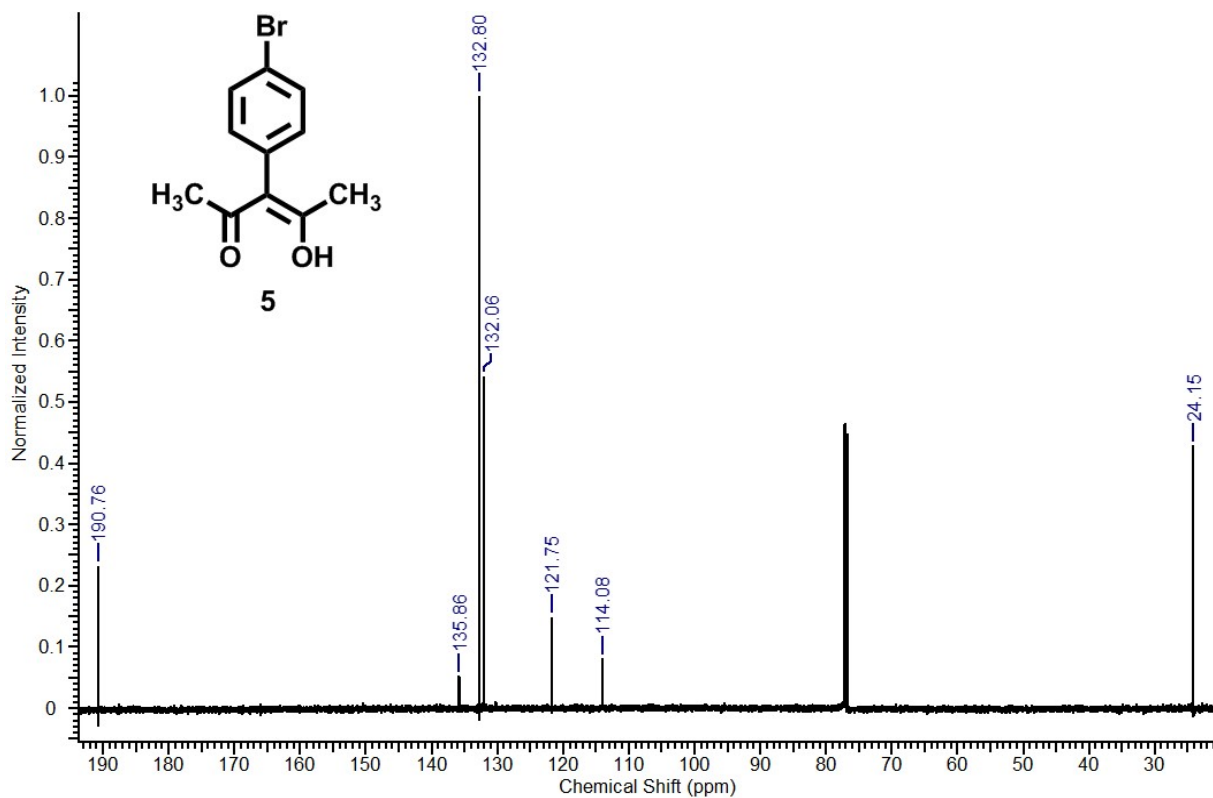


Figure A.6 ^{13}C NMR spectrum of 5.

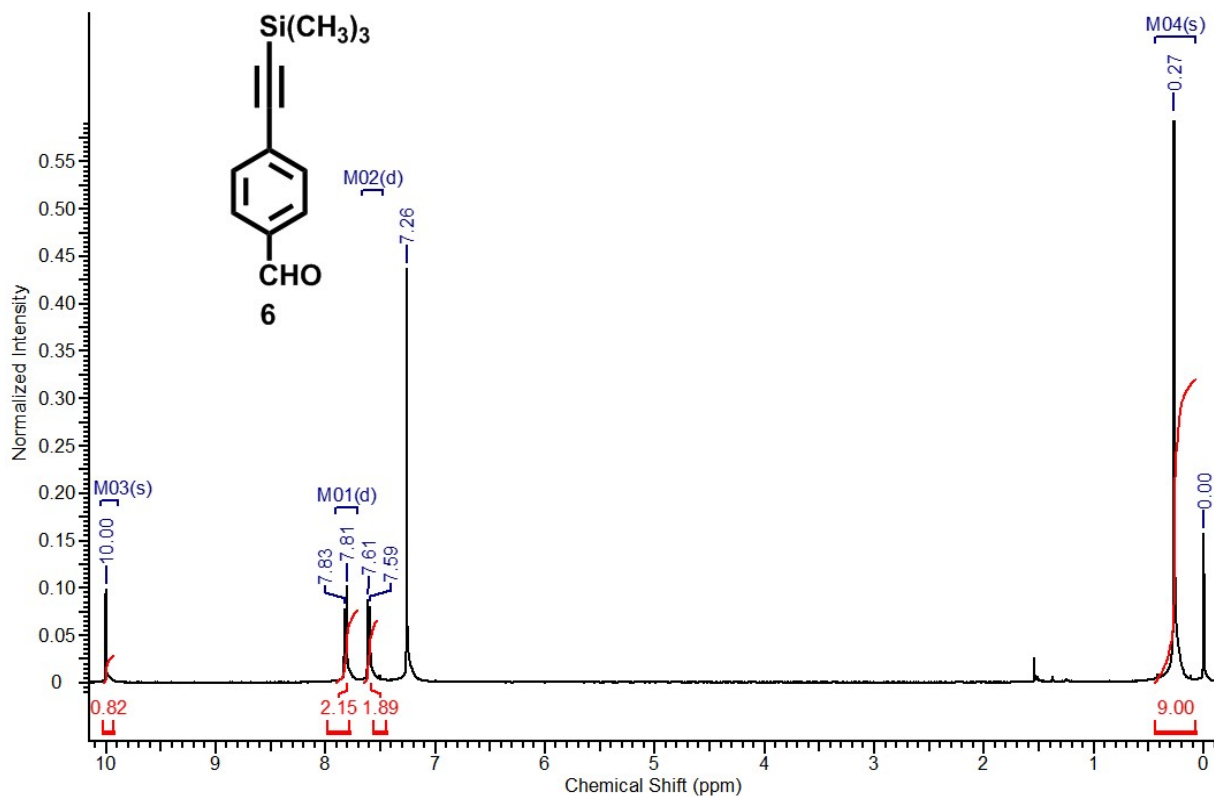


Figure A.7 ^1H NMR spectrum of **6**.

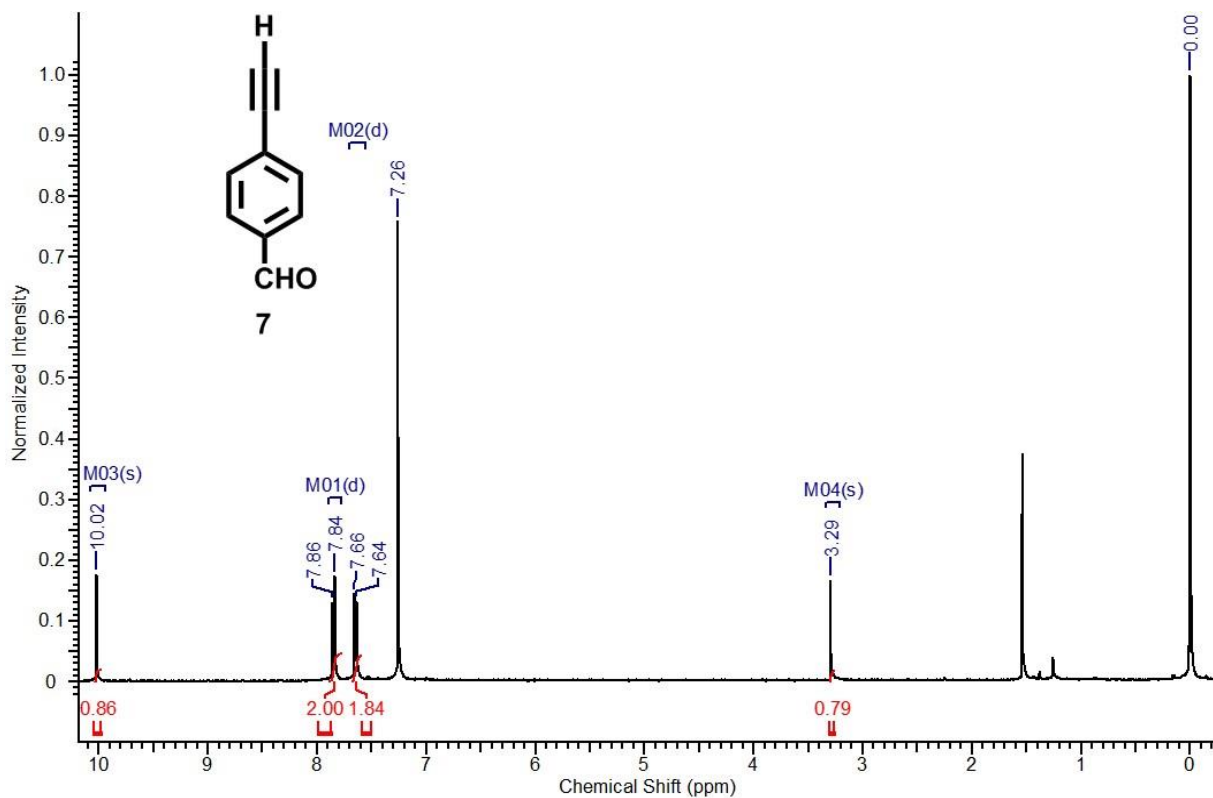


Figure A.8 ^1H NMR spectrum of **7**.

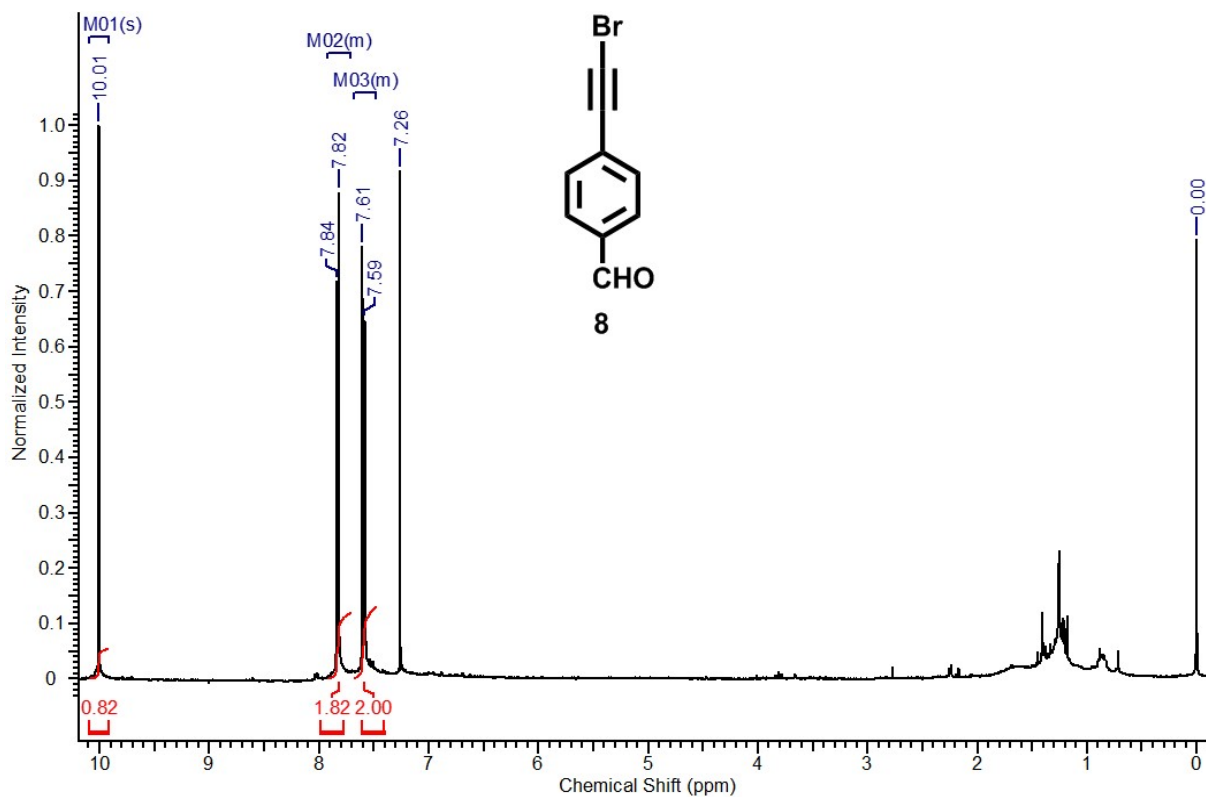


Figure A.9 ^1H NMR spectrum of **8**.

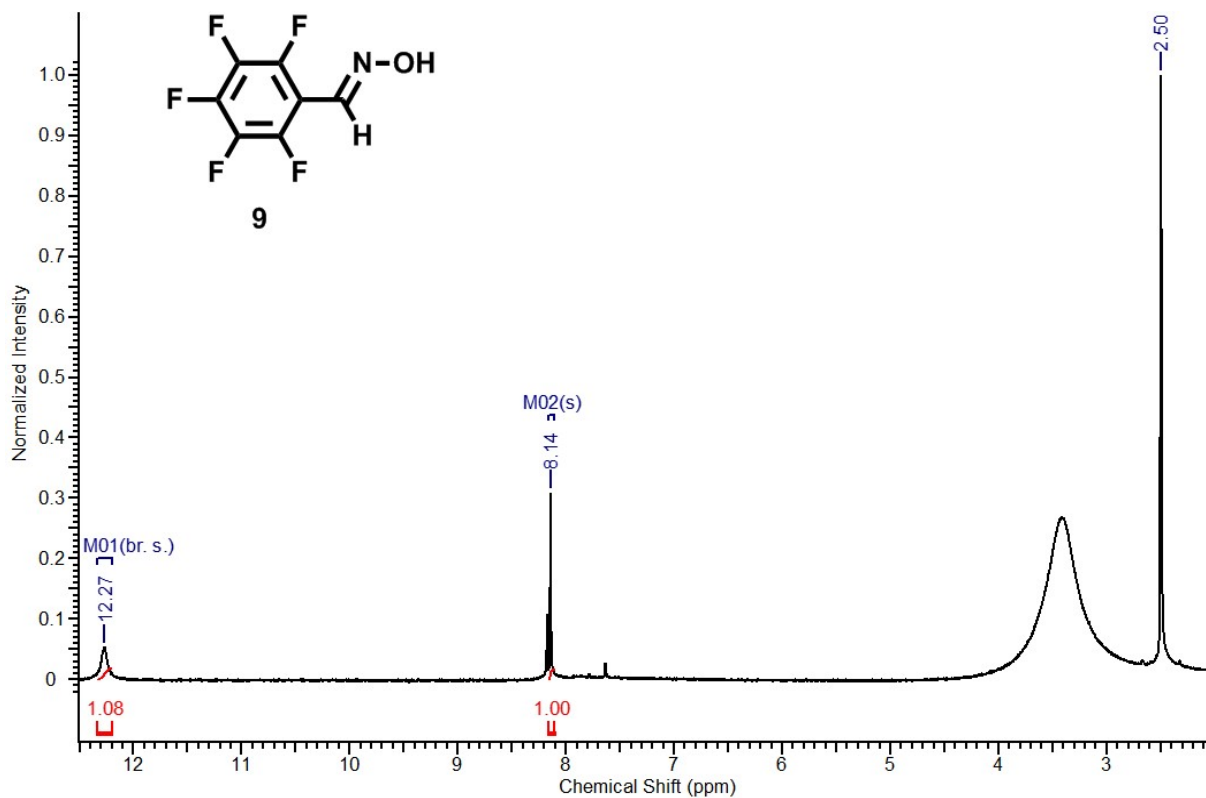


Figure A.10 ^1H NMR spectrum of **9**.

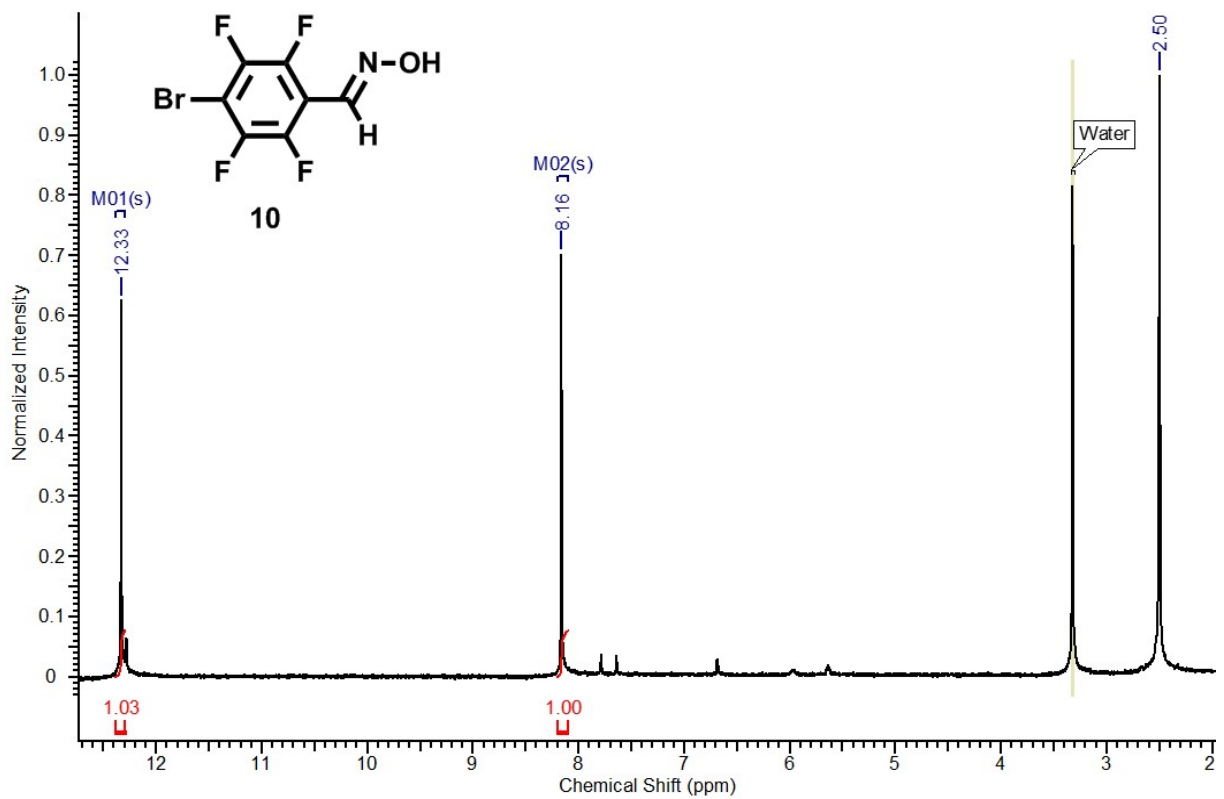


Figure A.11 ^1H NMR spectrum of **10**.

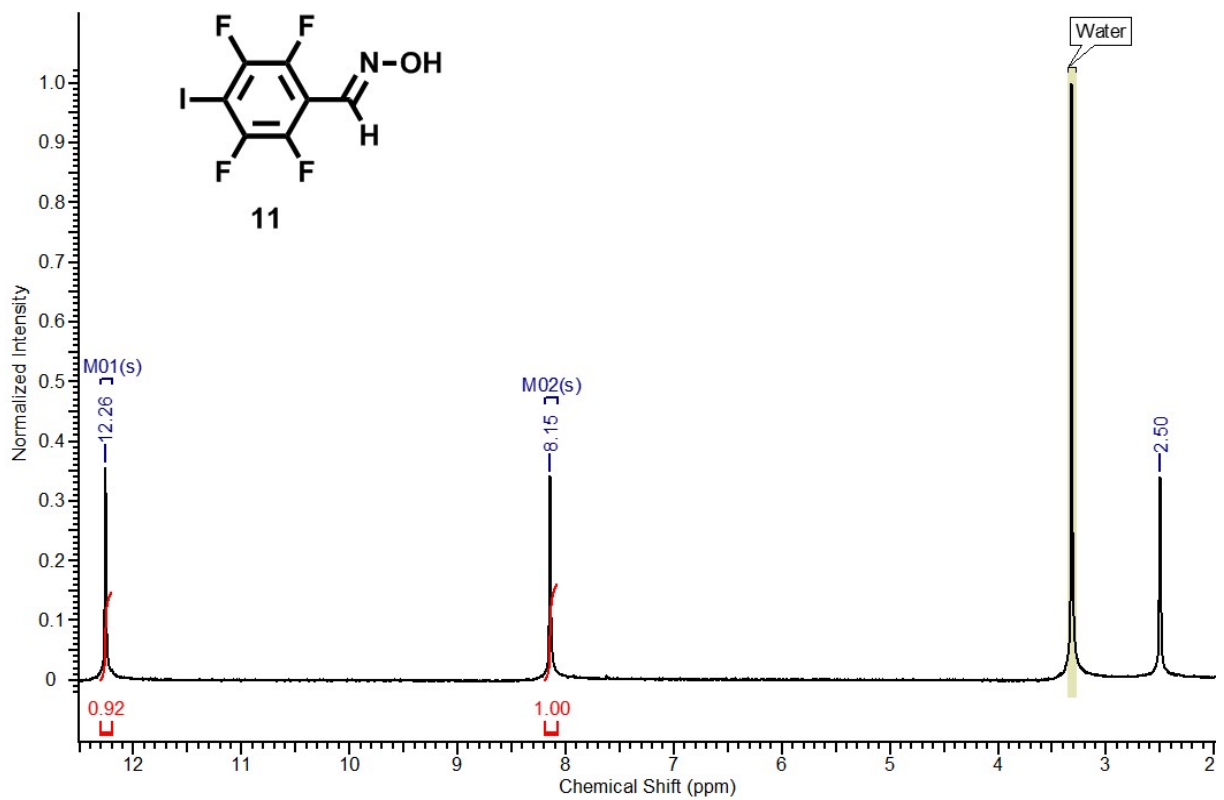


Figure A.12 ^1H NMR spectrum of **11**.

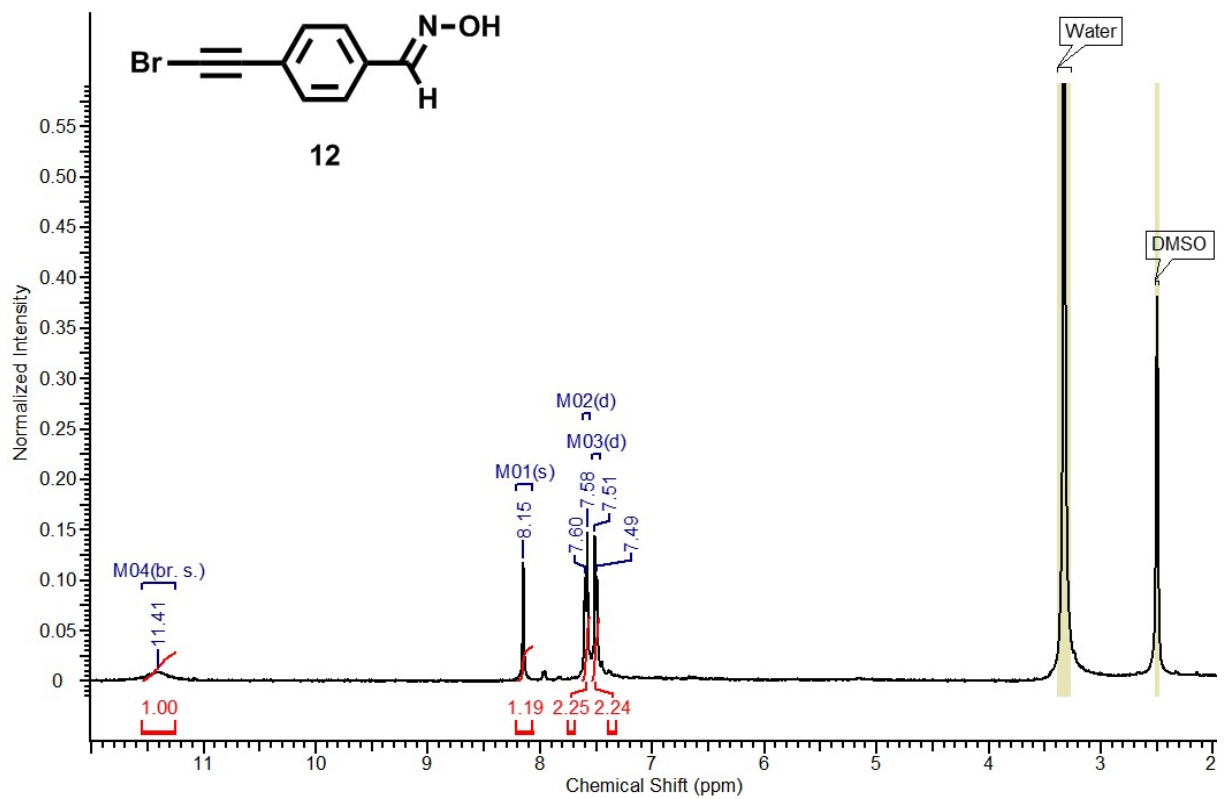


Figure A.13 ^1H NMR spectrum of **12**.

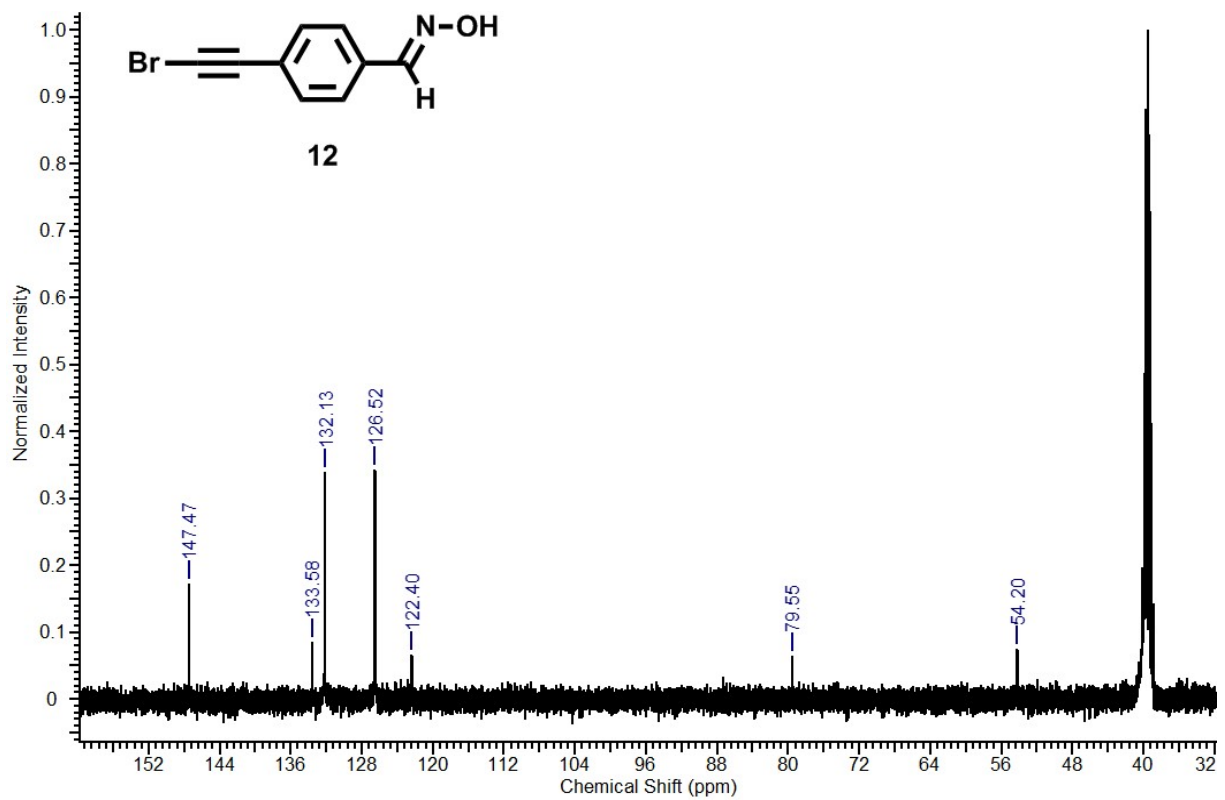


Figure A.14 ^{13}C NMR spectrum of **12**.

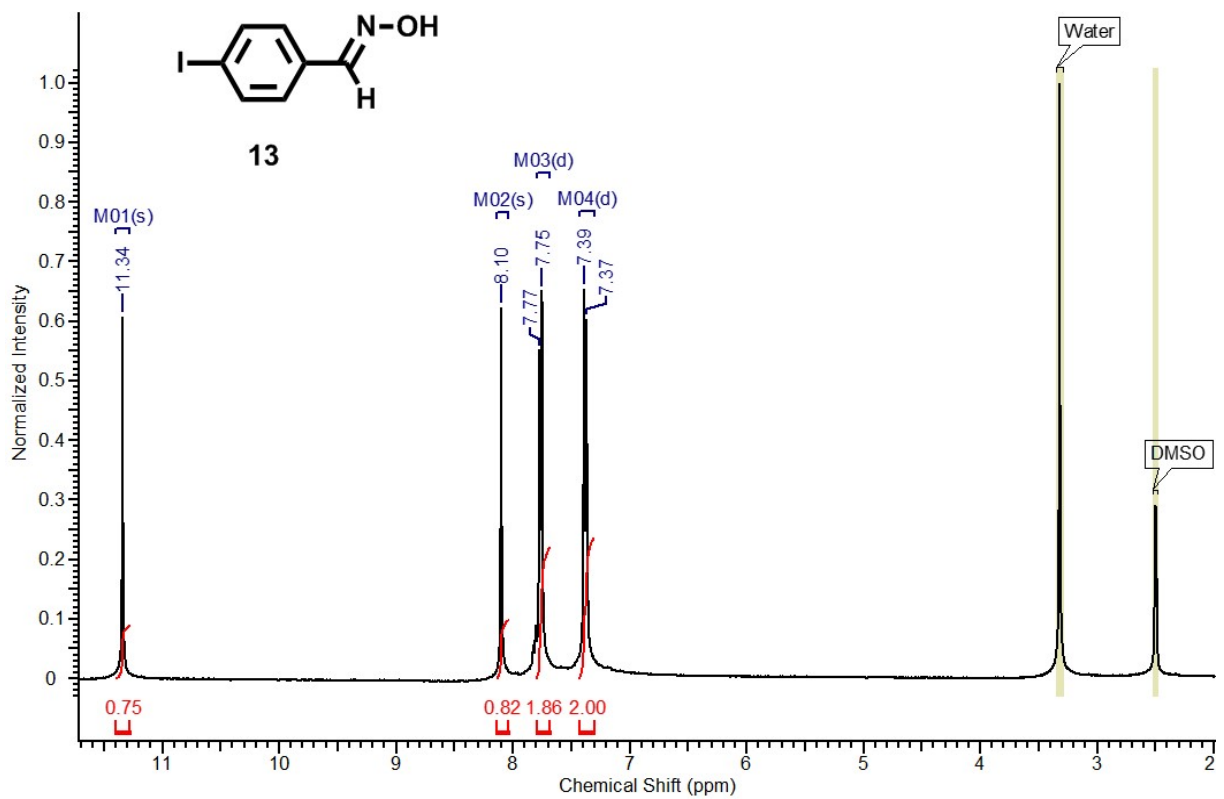


Figure A.15 ^1H NMR spectrum of **13**.

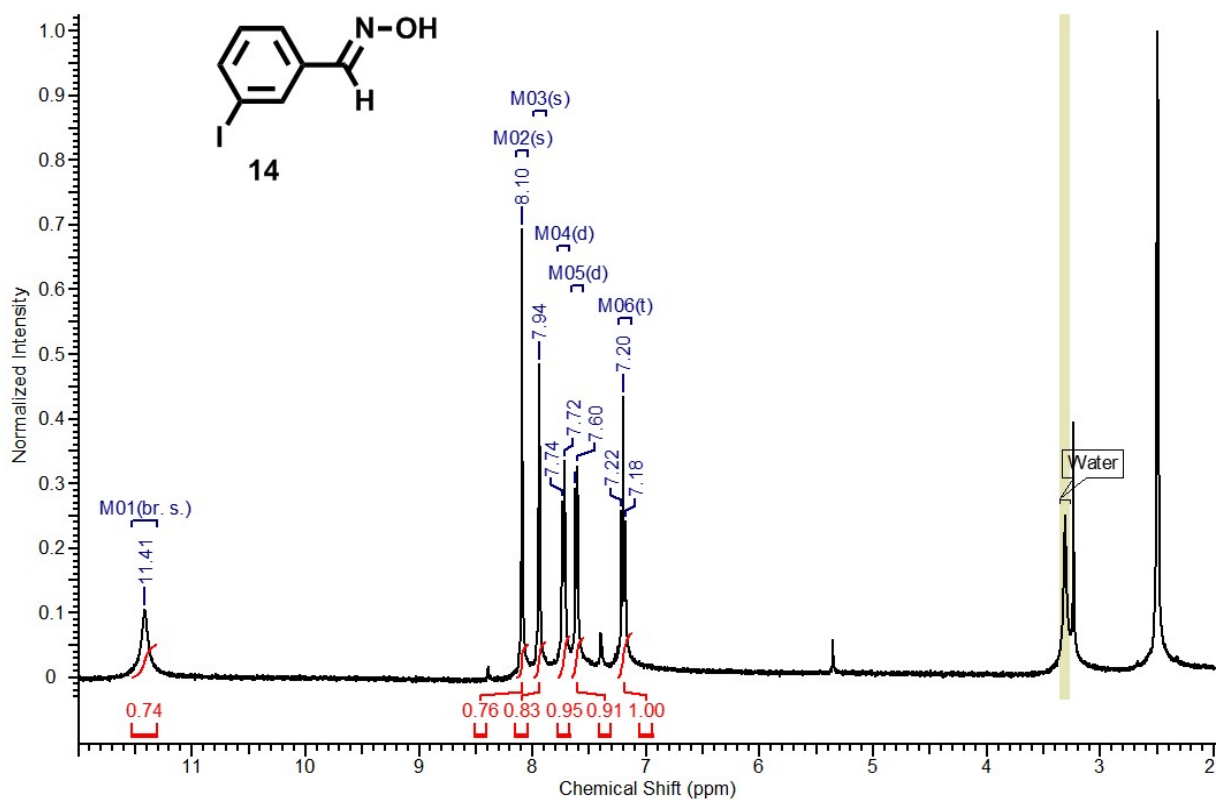


Figure A.16 ^1H NMR spectrum of **14**.

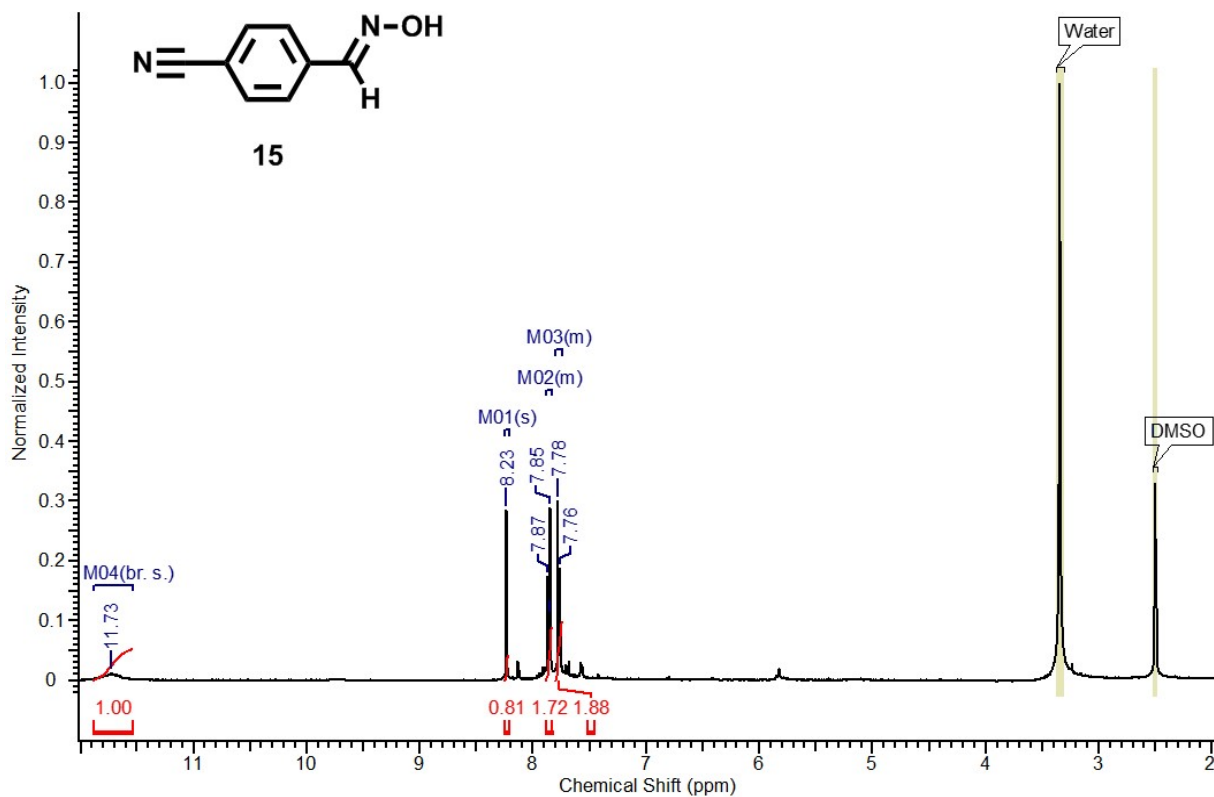


Figure A.17 ¹H NMR spectrum of **15**.

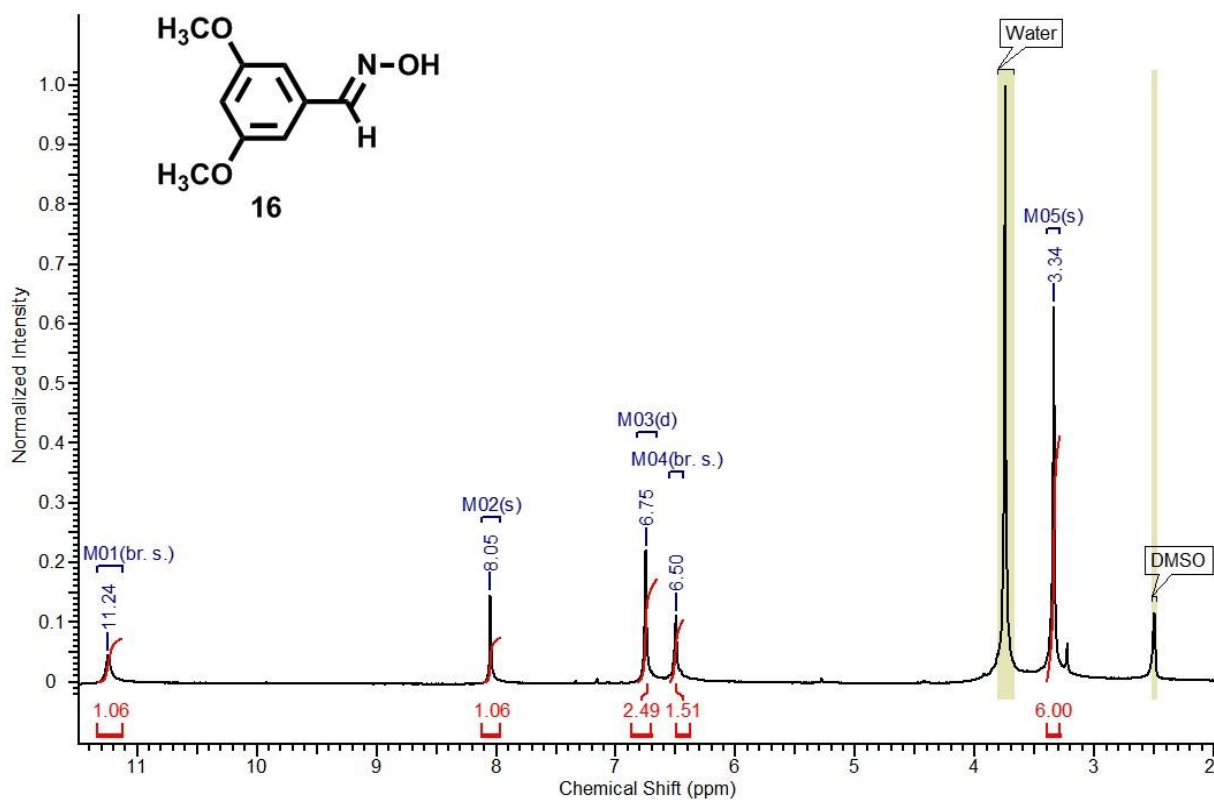


Figure A.18 ¹H NMR spectrum of **16**.

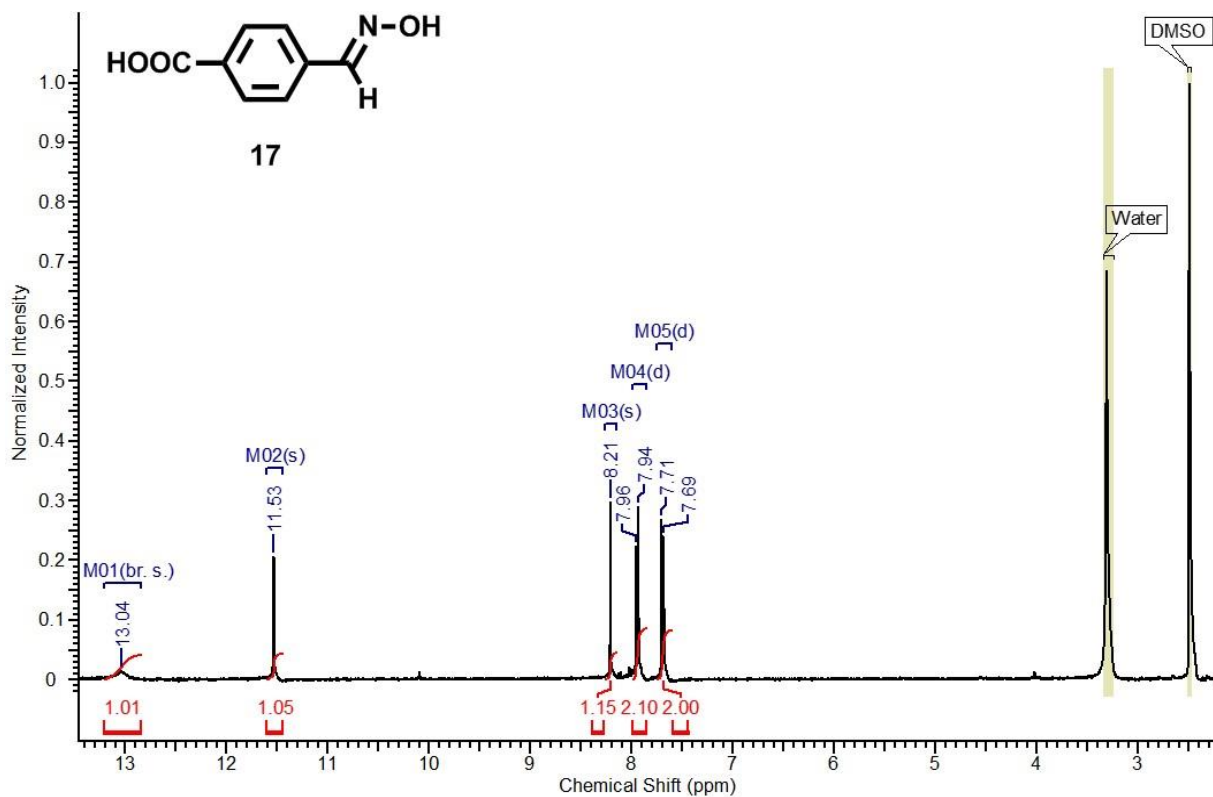


Figure A.19 ^1H NMR spectrum of 17.

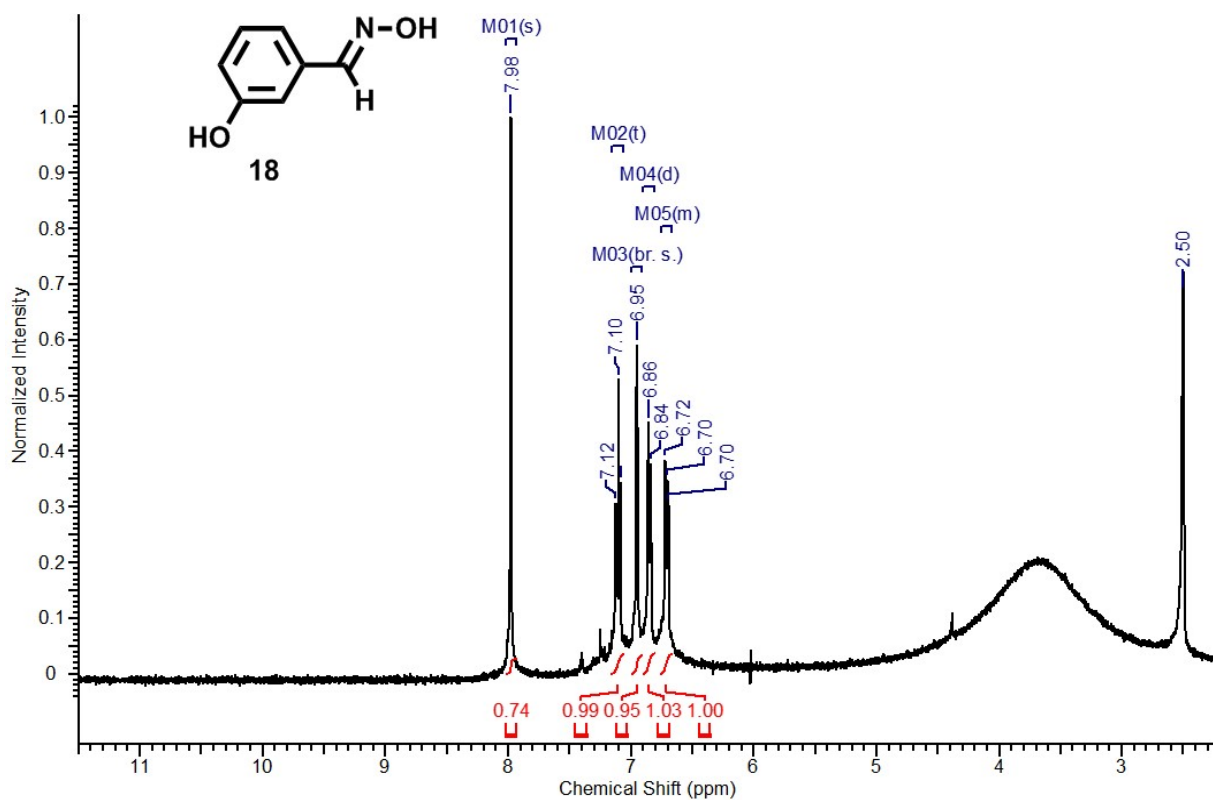


Figure A.20 ^1H NMR spectrum of 18.

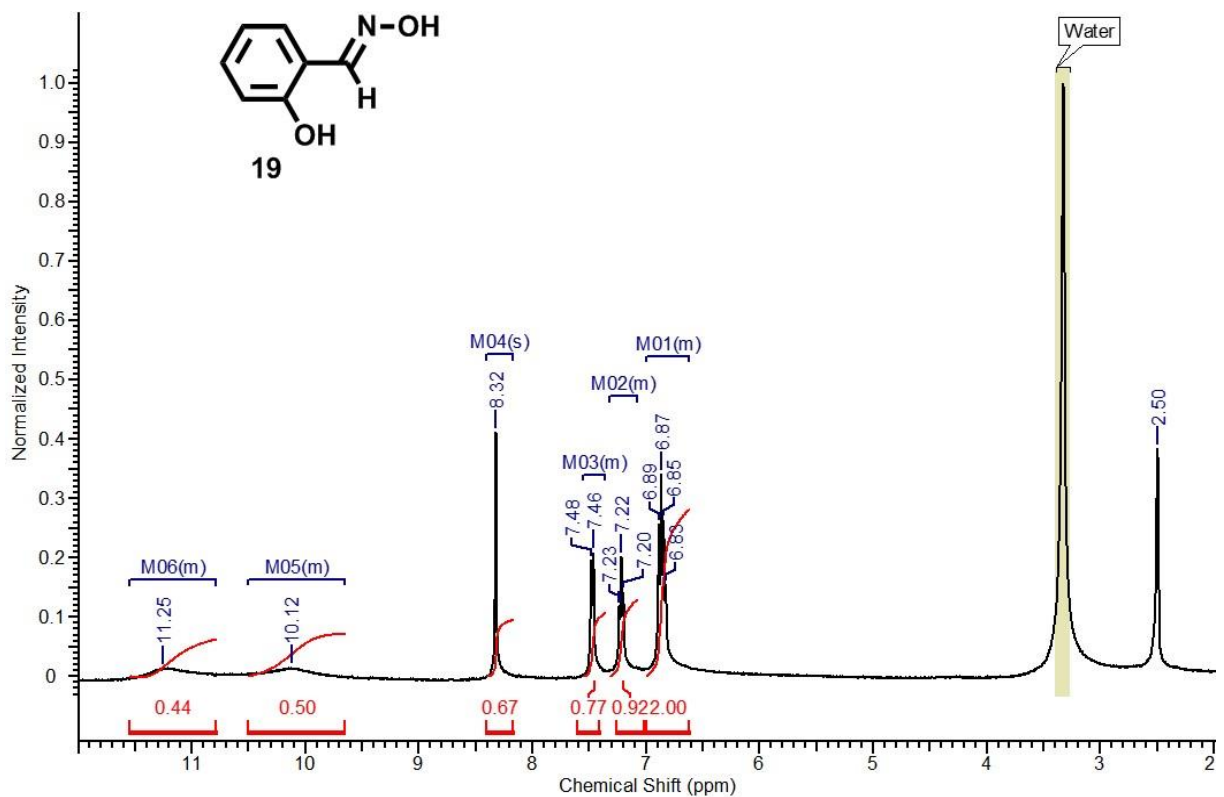


Figure A.21 ¹H NMR spectrum of **19**.

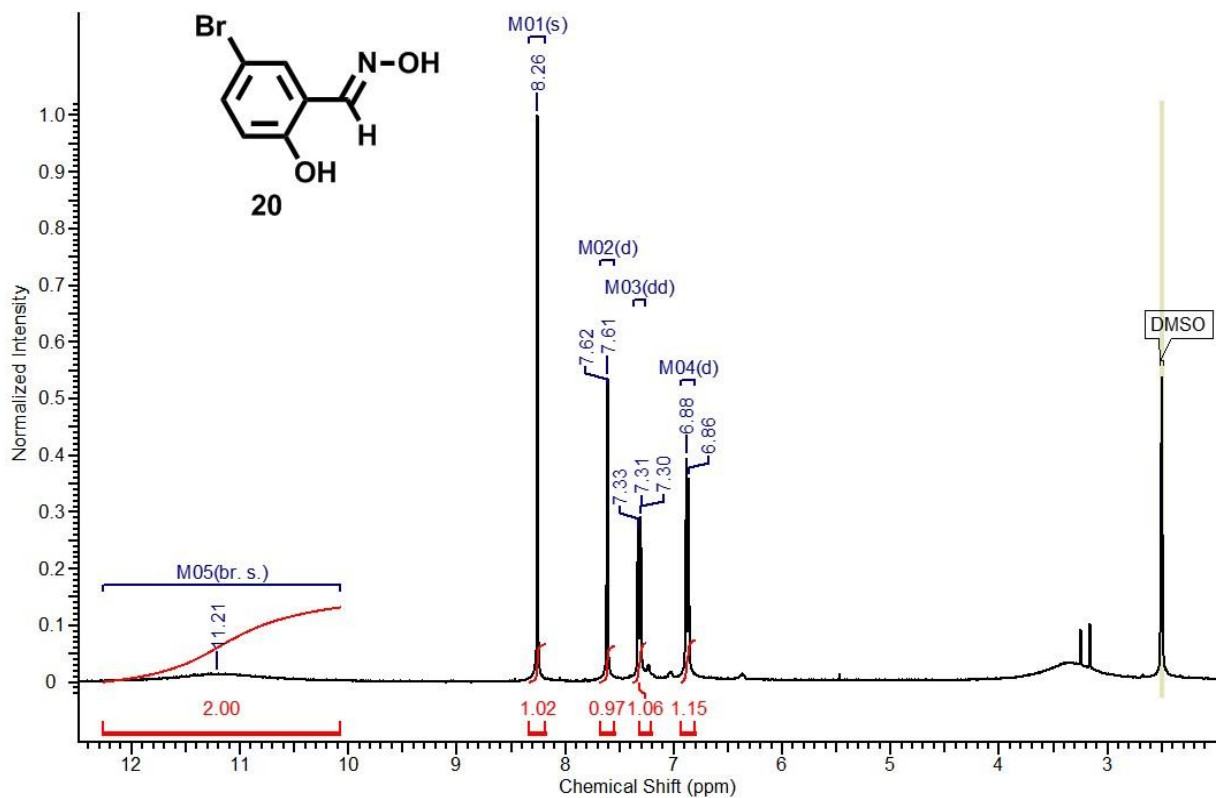


Figure A.22 ¹H NMR spectrum of **20**.

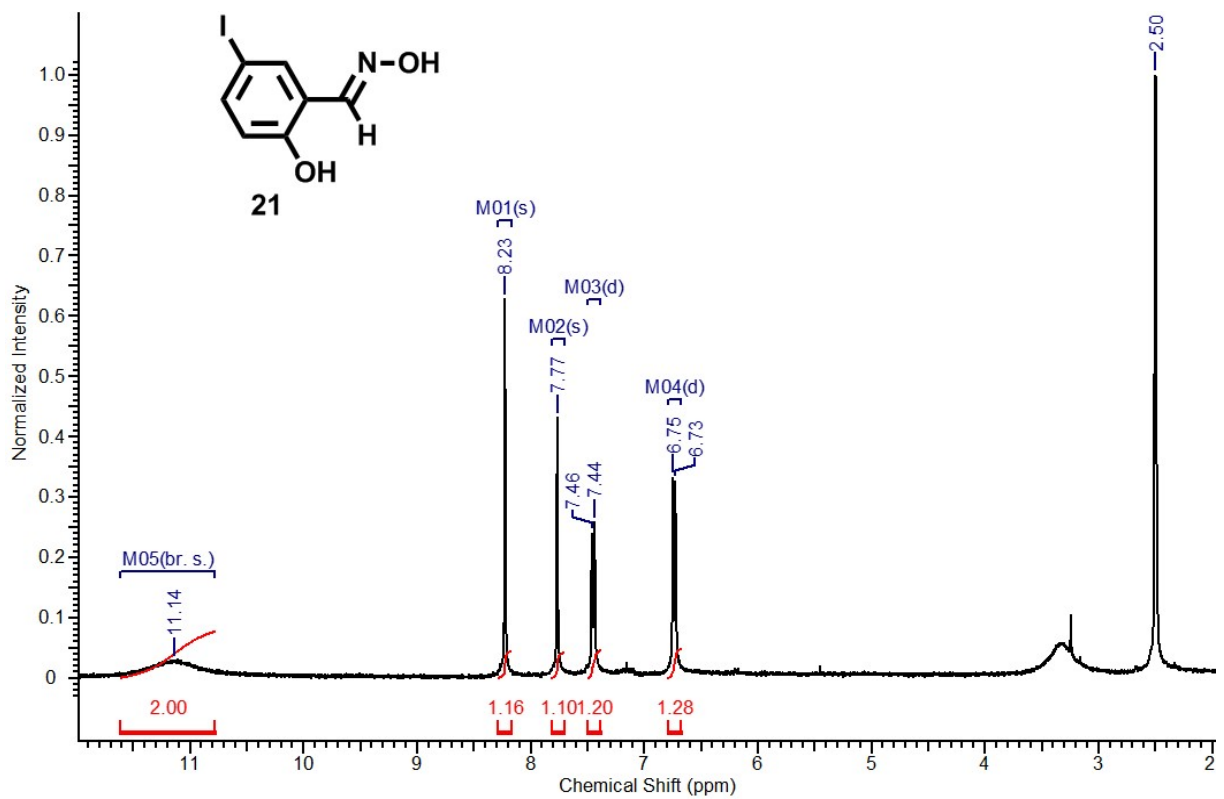


Figure A.23 ^1H NMR spectrum of 21.

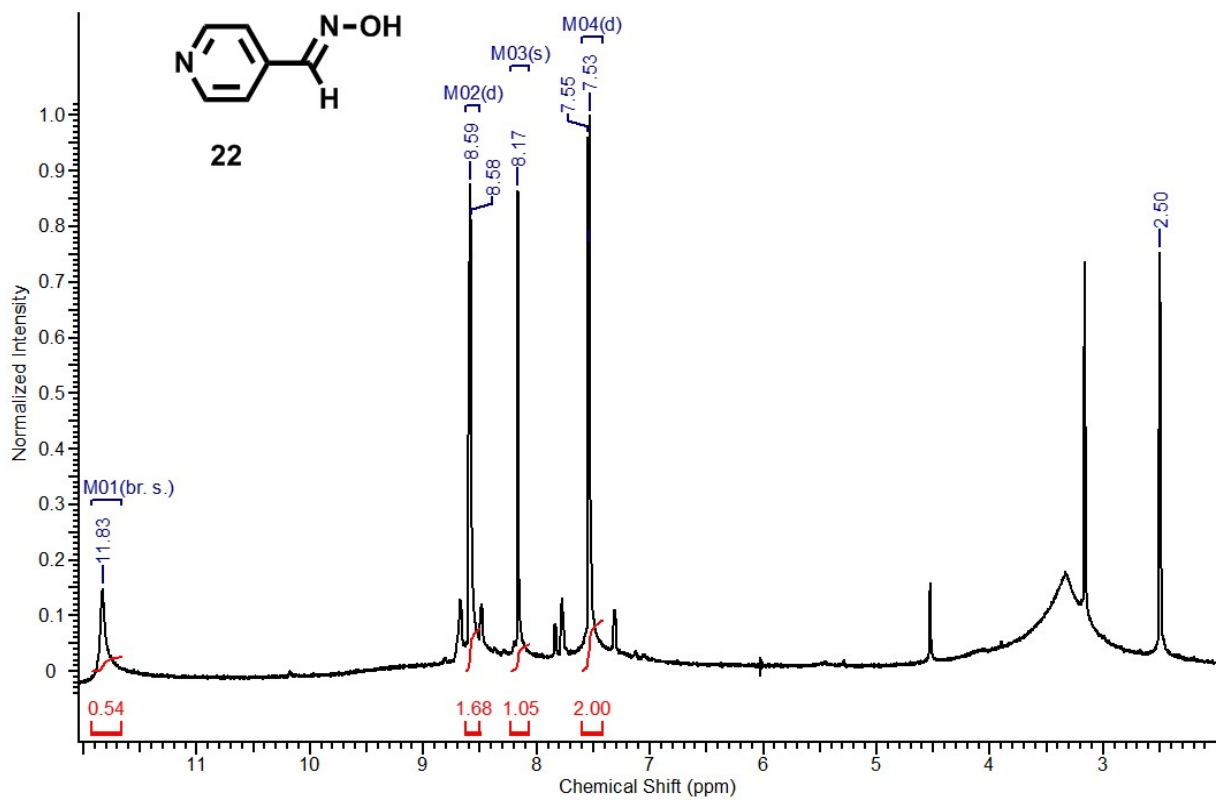


Figure A.24 ^1H NMR spectrum of 22.

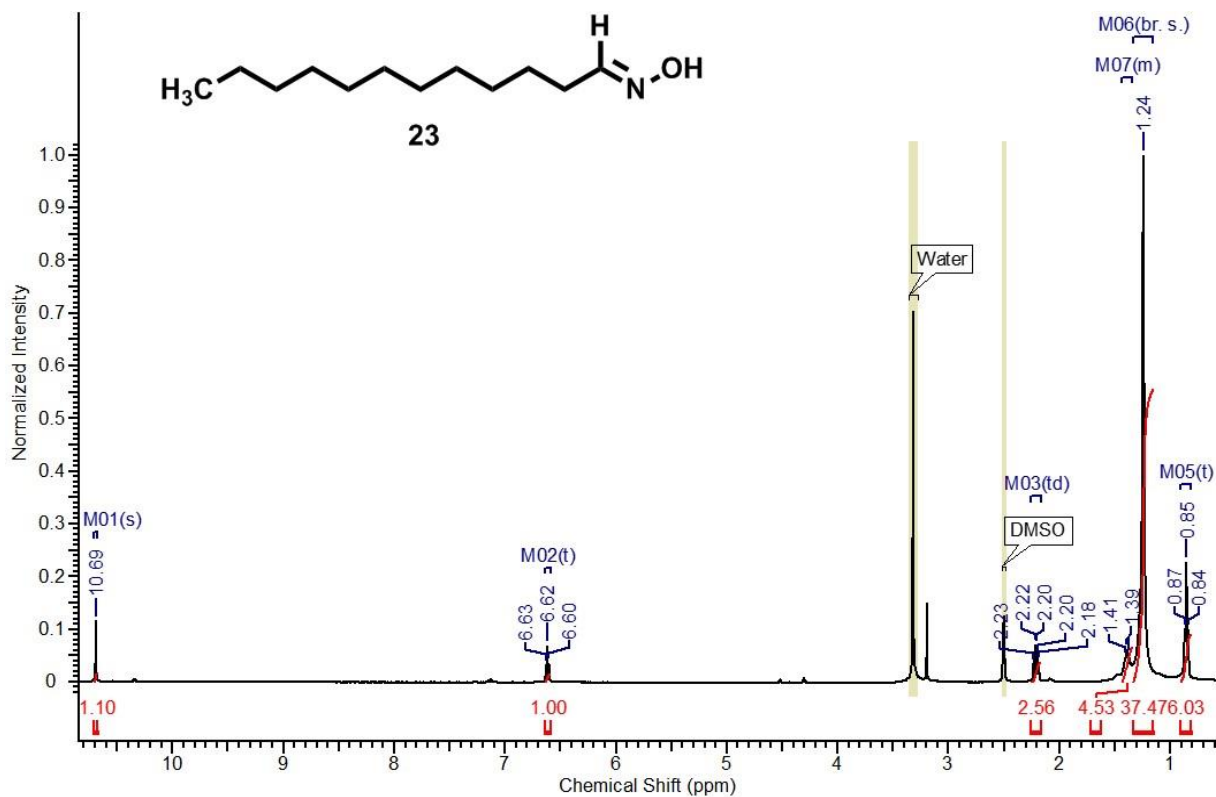


Figure A.25 ¹H NMR spectrum of **23**.

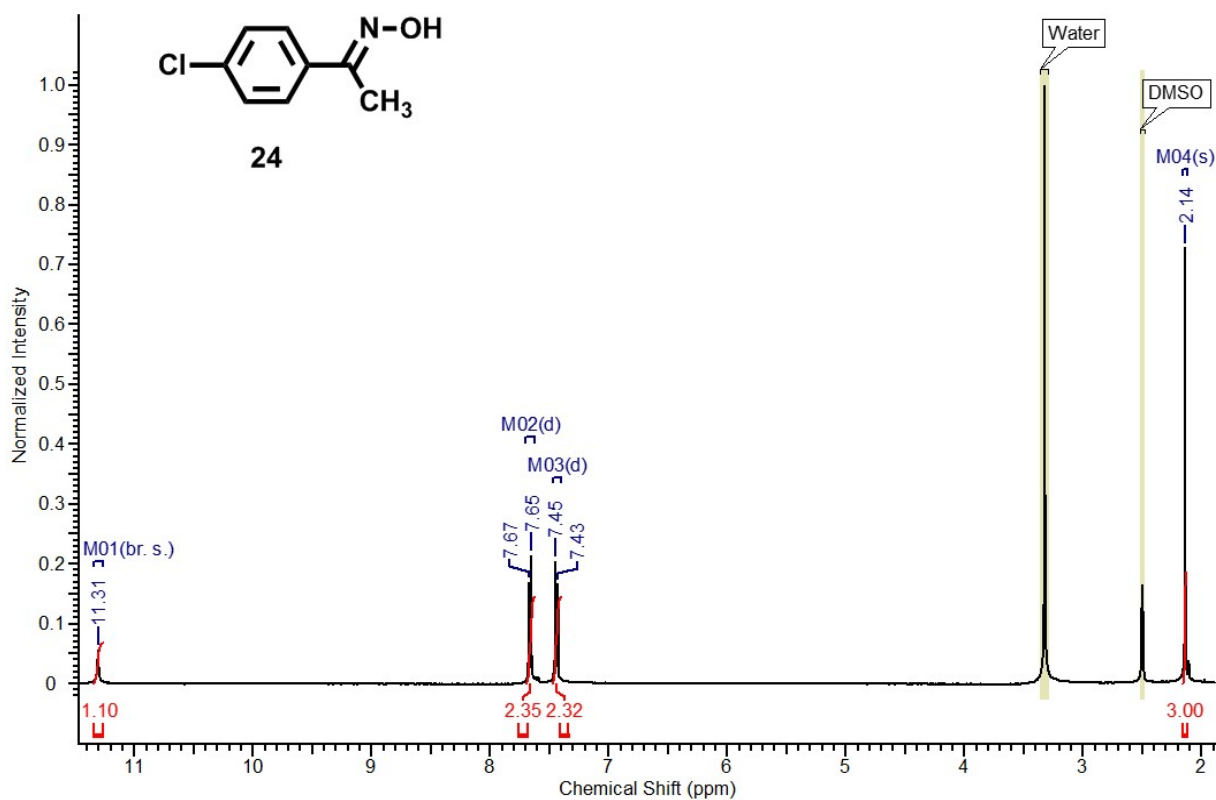


Figure A.26 ¹H NMR spectrum of **24**.

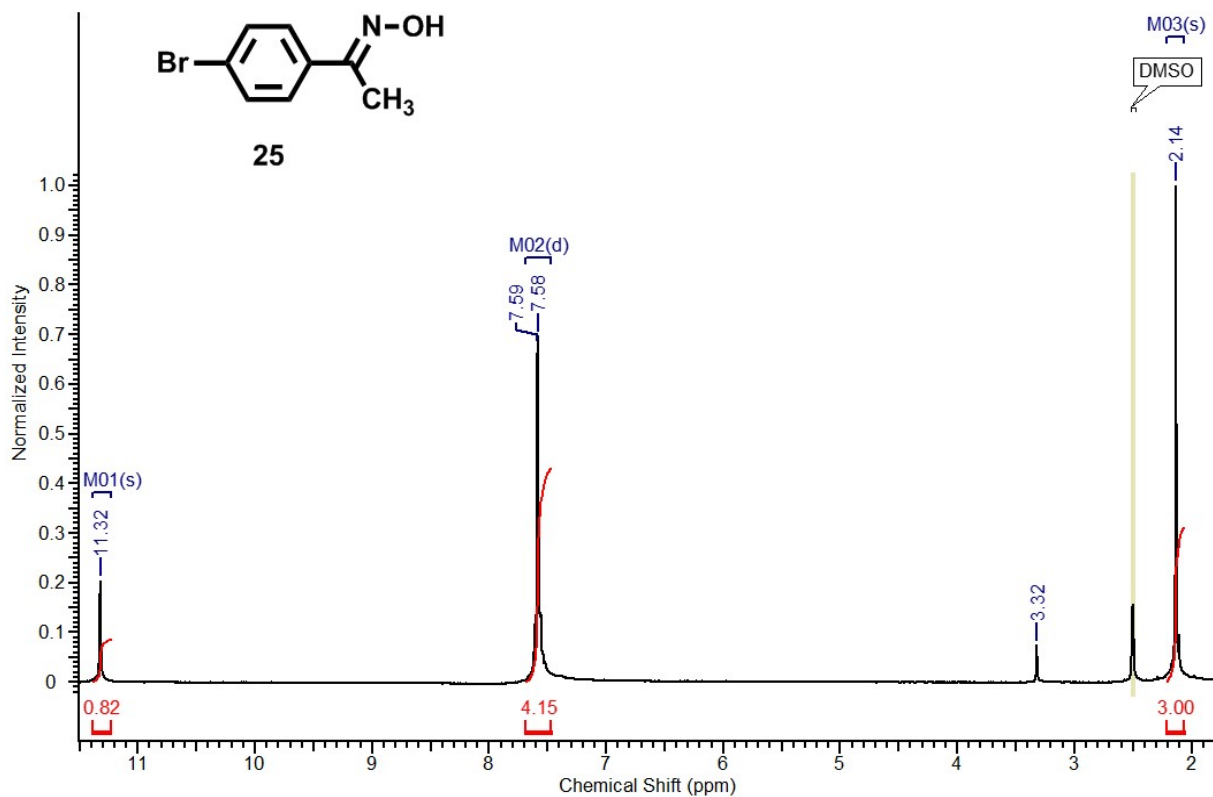


Figure A.27 ¹H NMR spectrum of **25**.

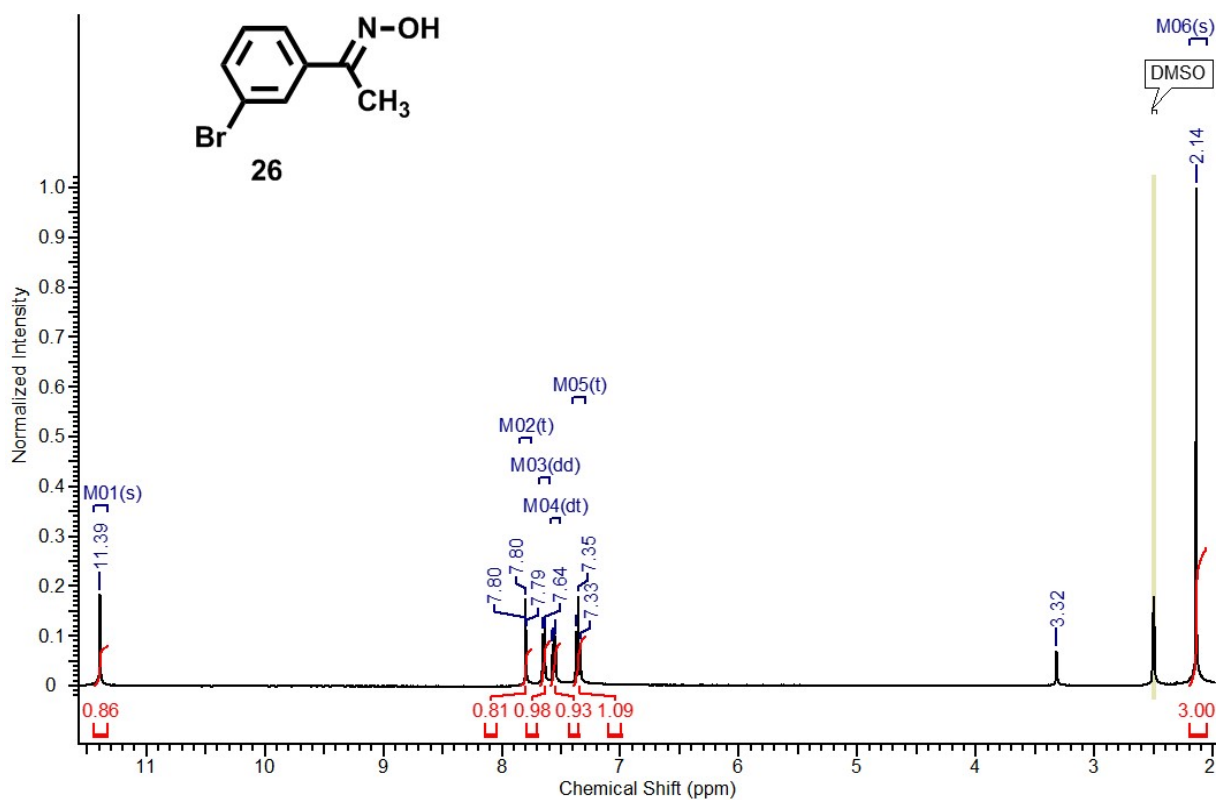


Figure A.28 ¹H NMR spectrum of **26**.

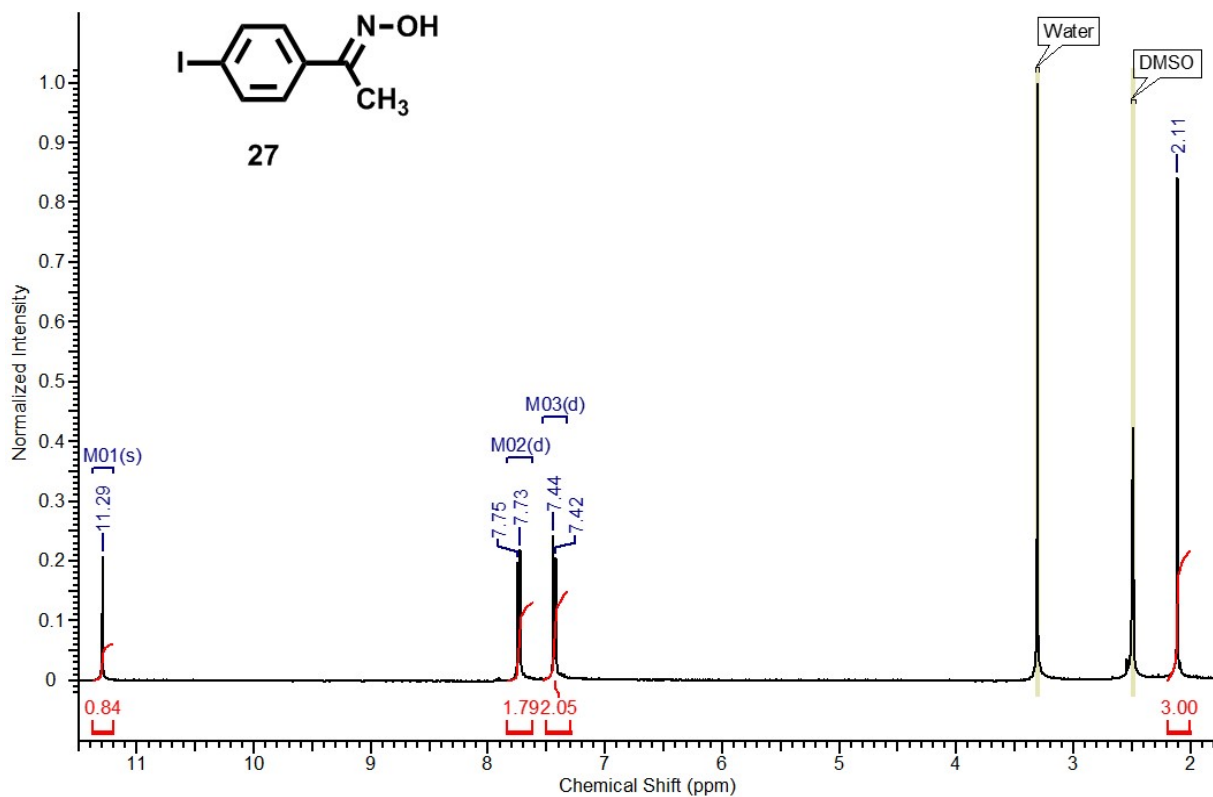


Figure A.29 ¹H NMR spectrum of **27**.

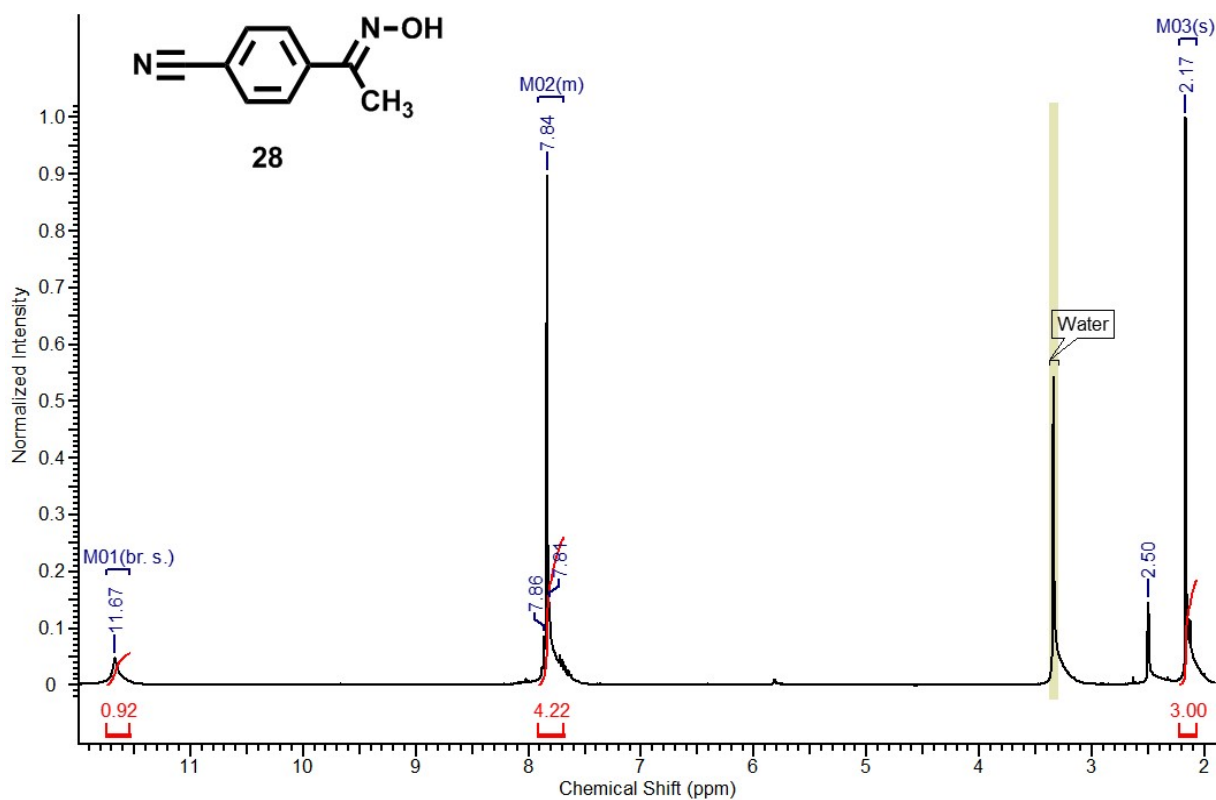


Figure A.30 ¹H NMR spectrum of **28**.

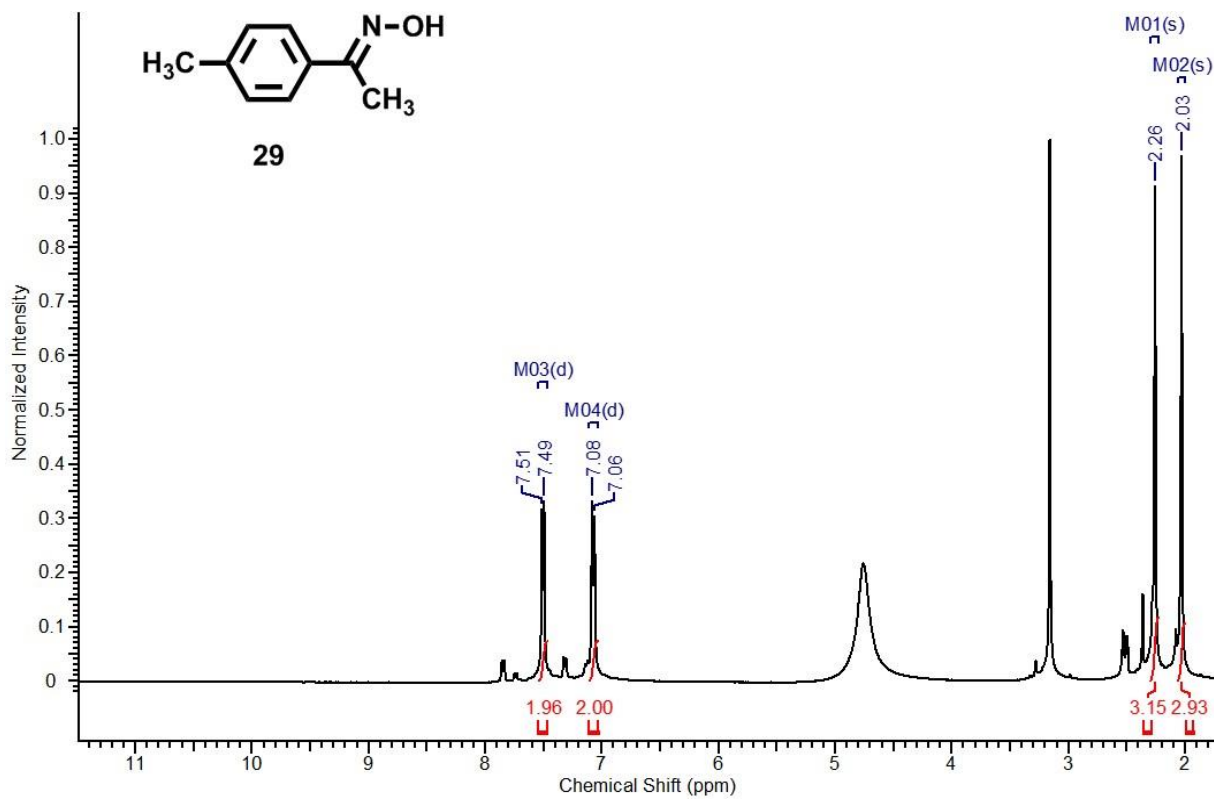


Figure A.31 ¹H NMR spectrum of **29**.

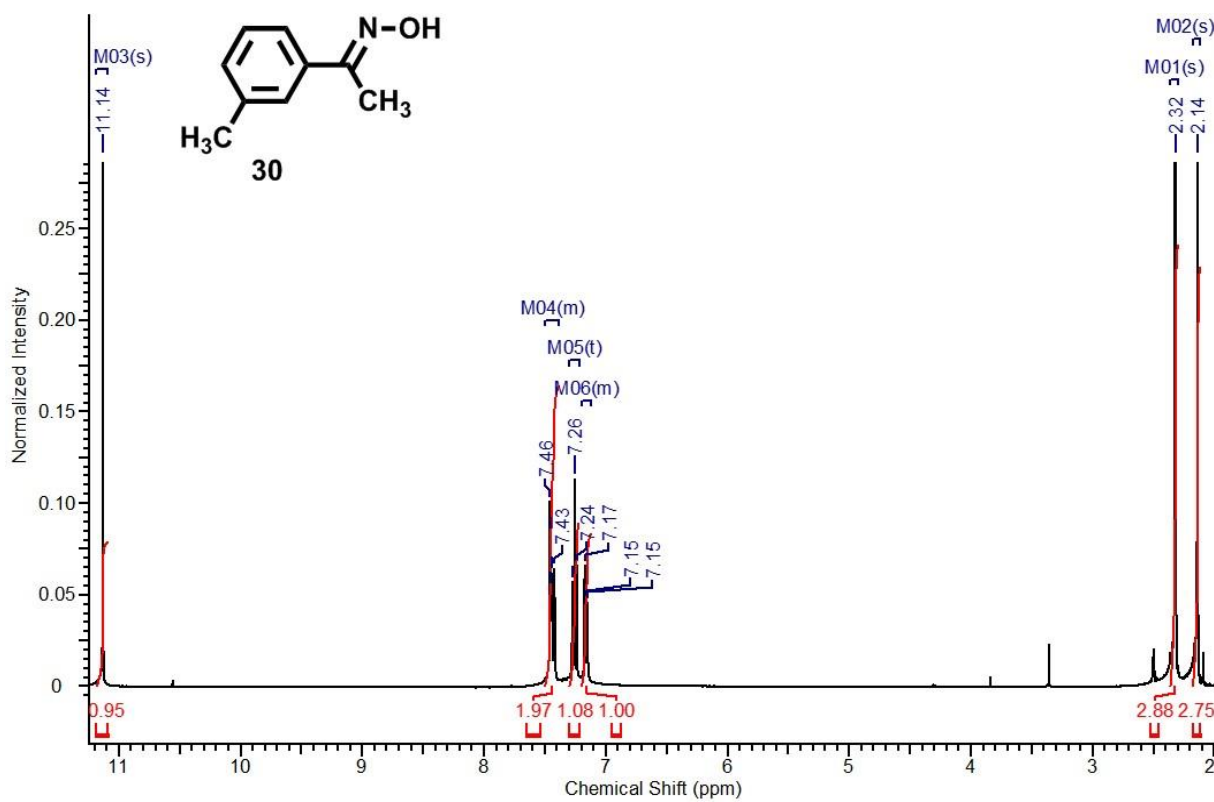


Figure A.32 ¹H NMR spectrum of **30**.

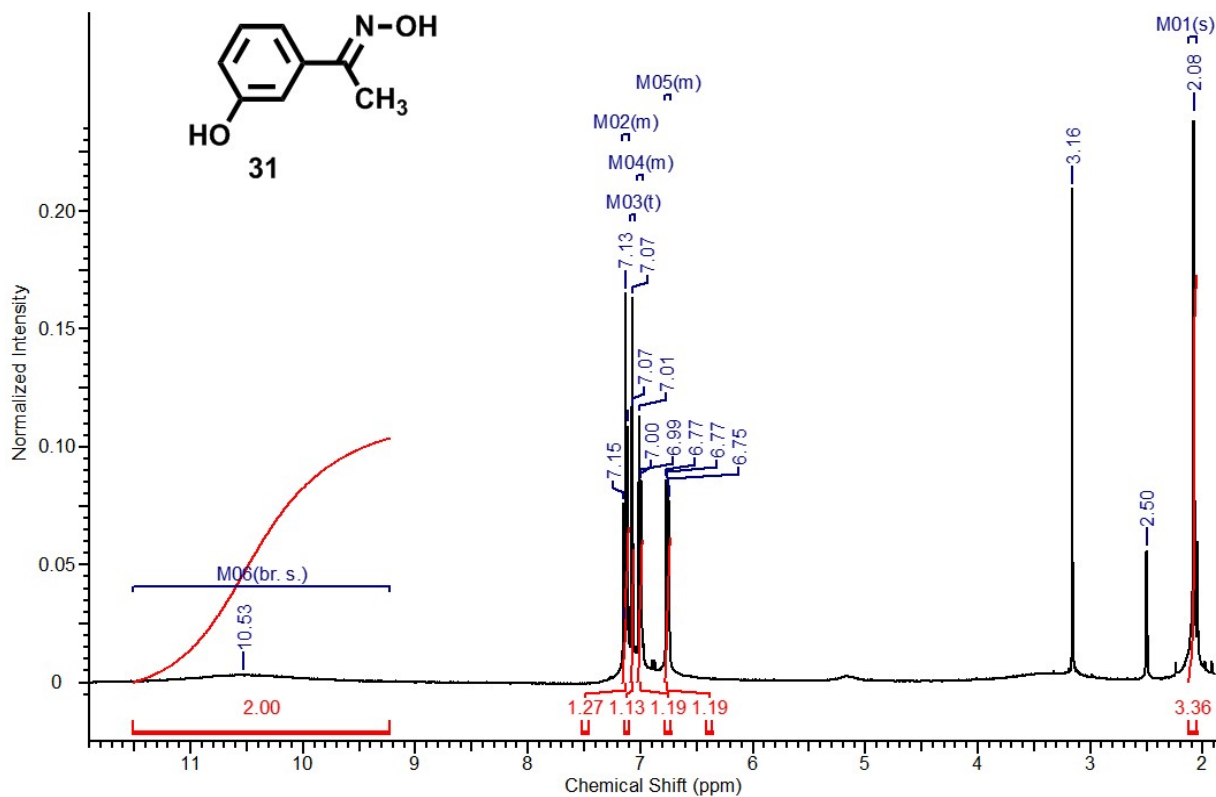


Figure A.33 ^1H NMR spectrum of **31**.

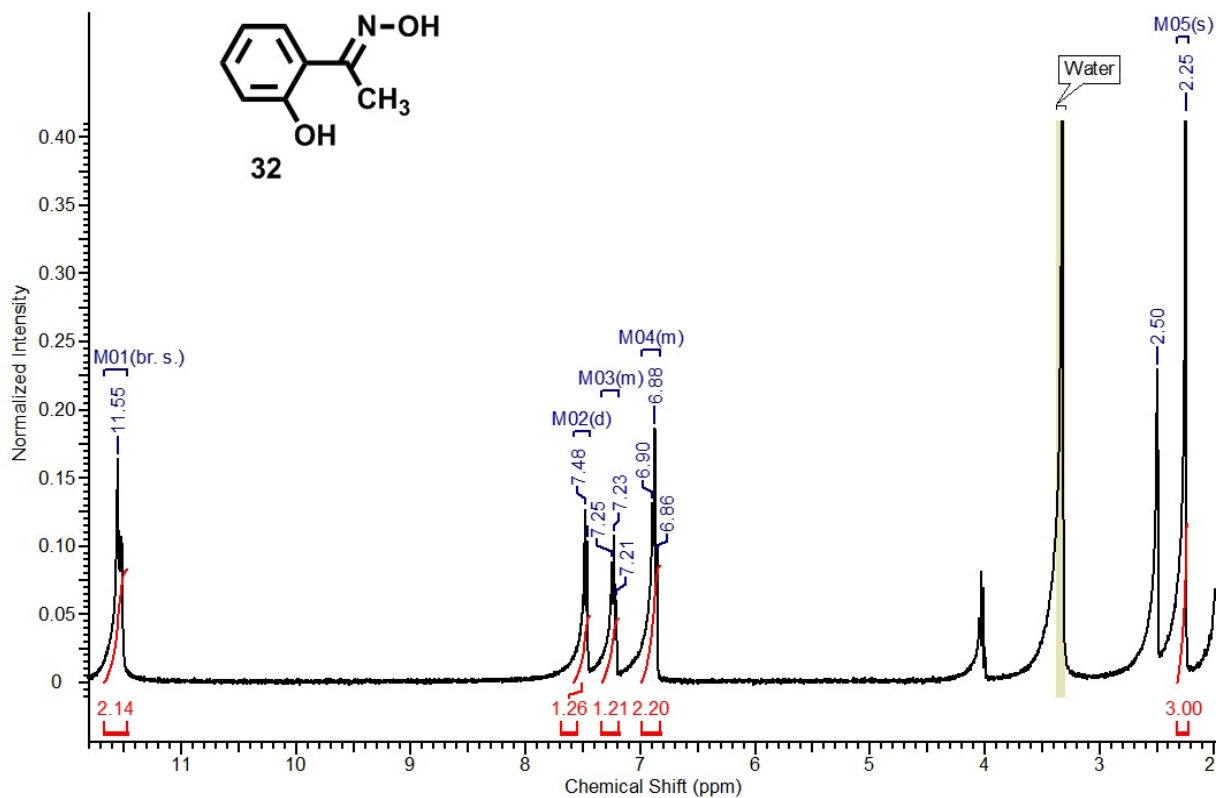


Figure A.34 ^1H NMR spectrum of **32**.

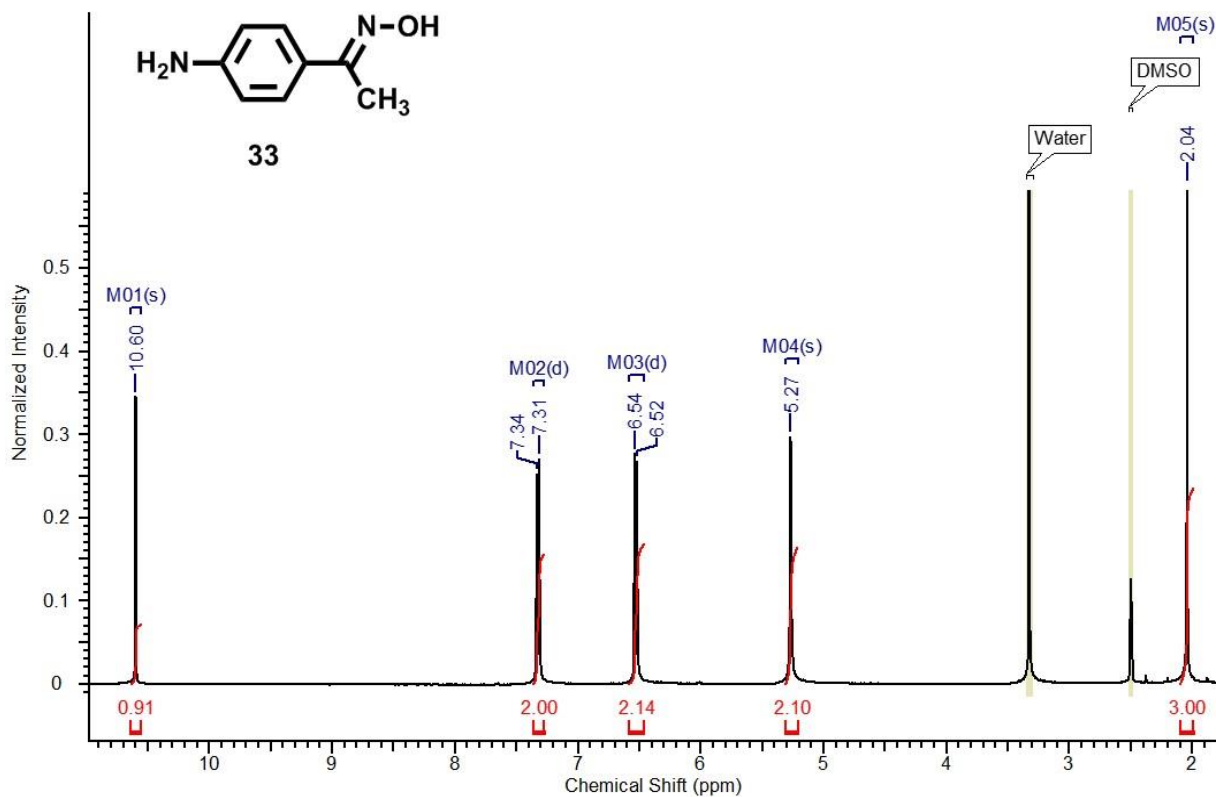


Figure A.35 ¹H NMR spectrum of **33**.

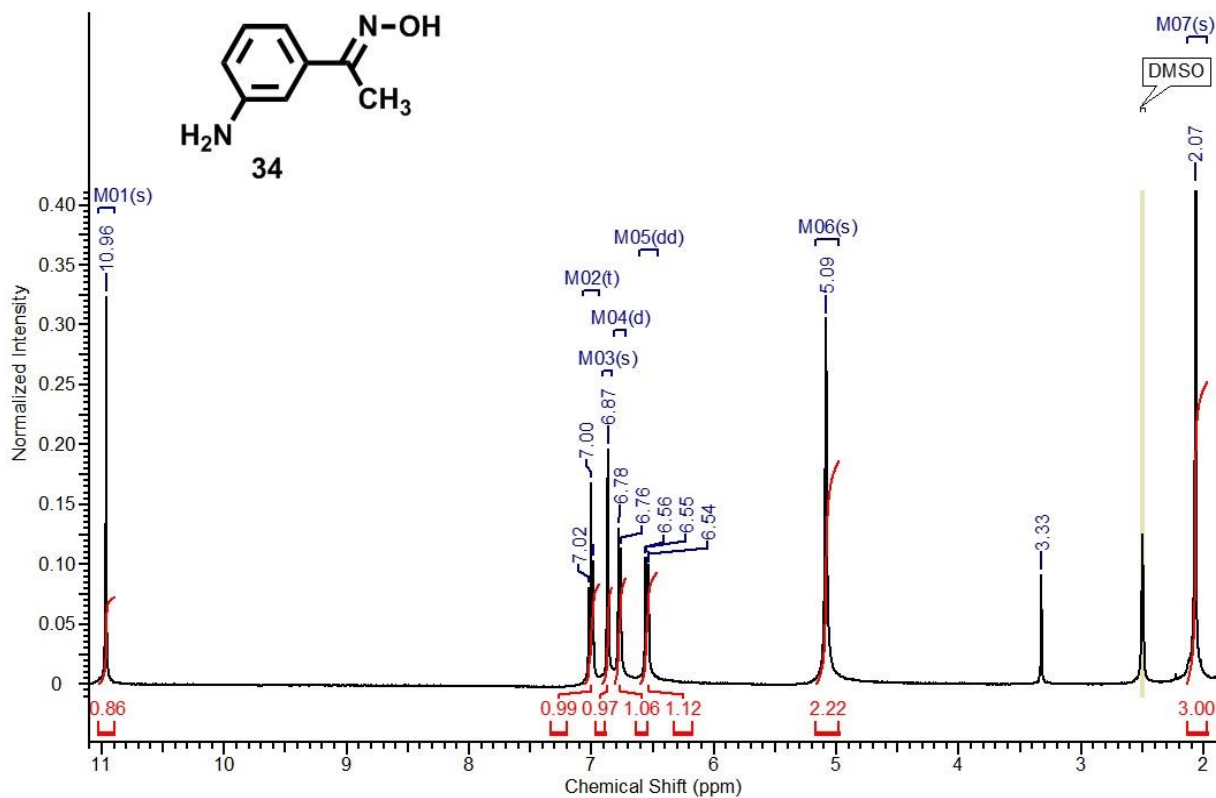


Figure A.36 ¹H NMR spectrum of **34**.

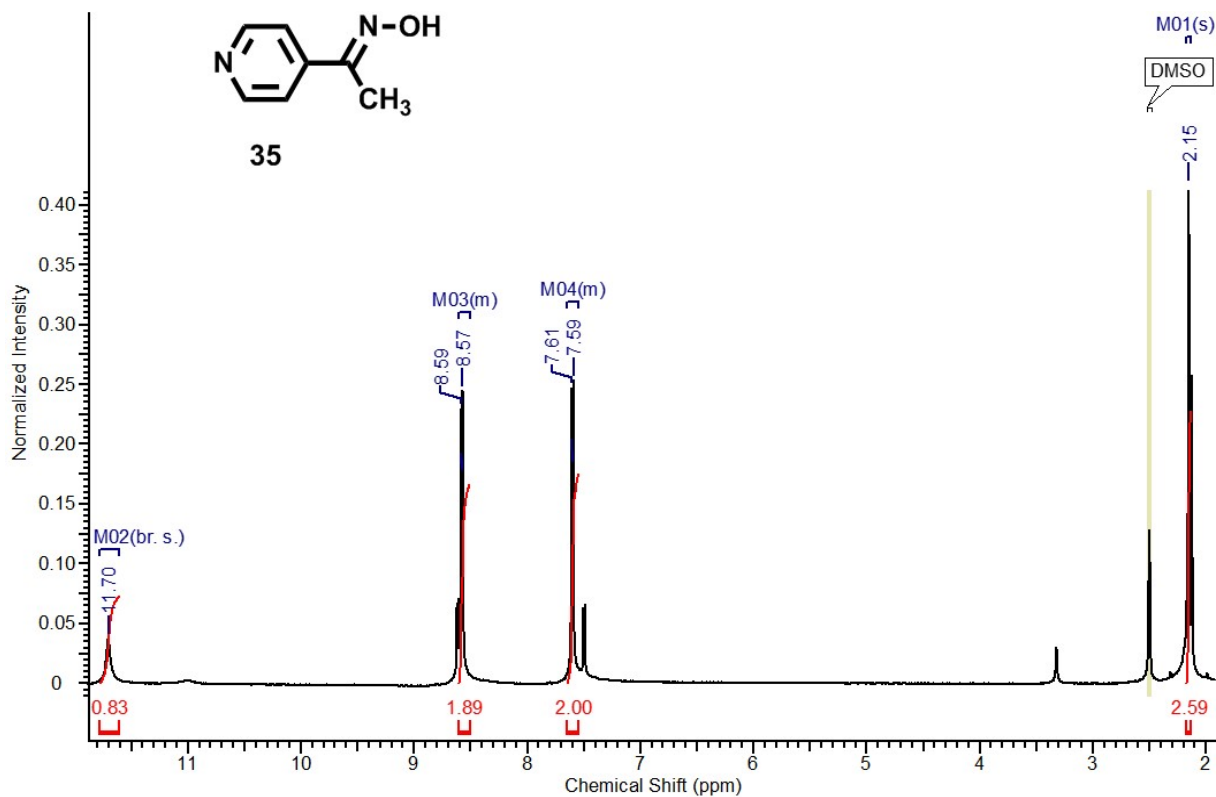


Figure A.37 ^1H NMR spectrum of **35**.

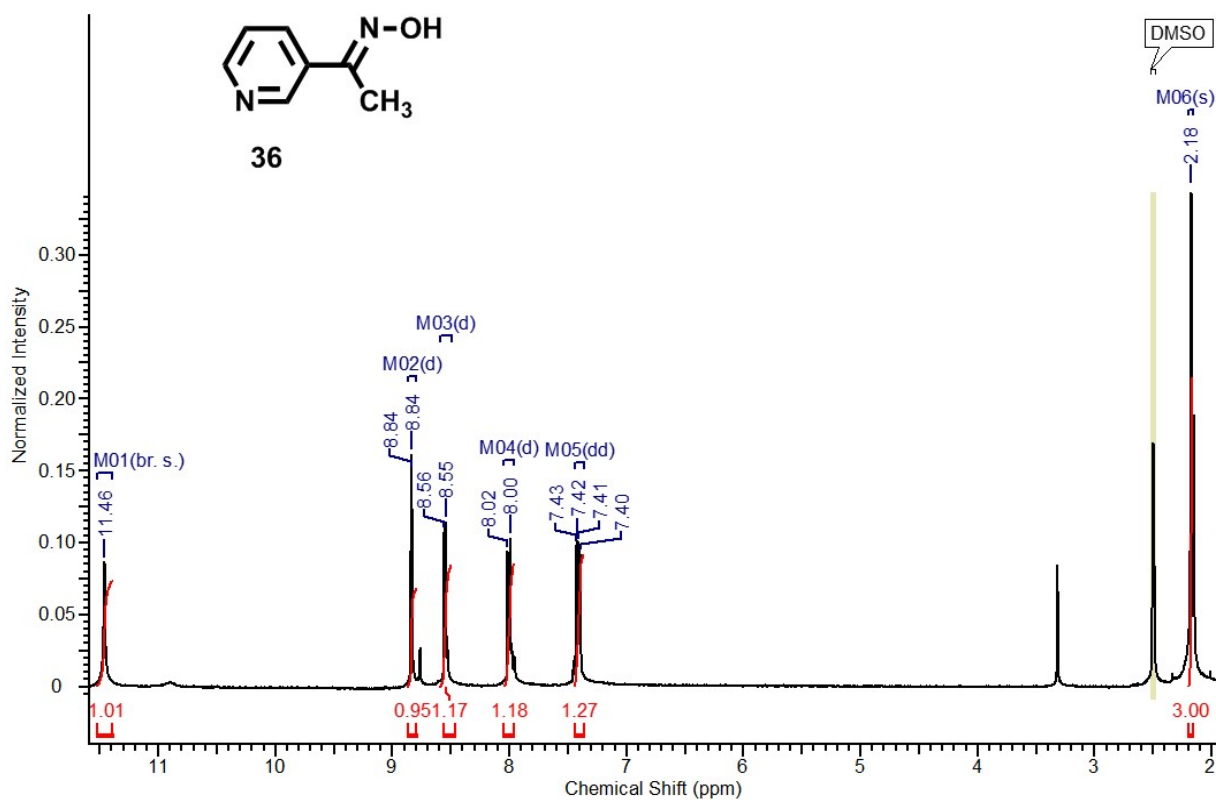


Figure A.38 ^1H NMR spectrum of **36**.

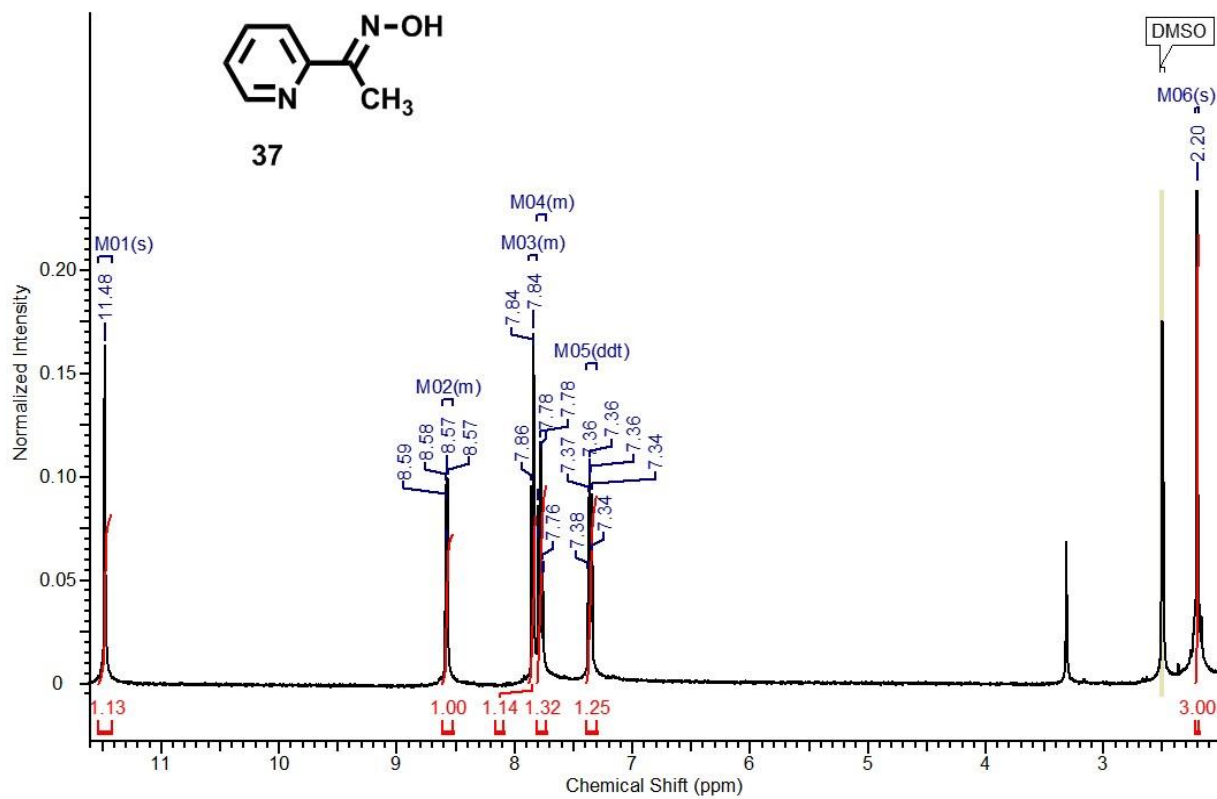


Figure A.39 ^1H NMR spectrum of **37**.

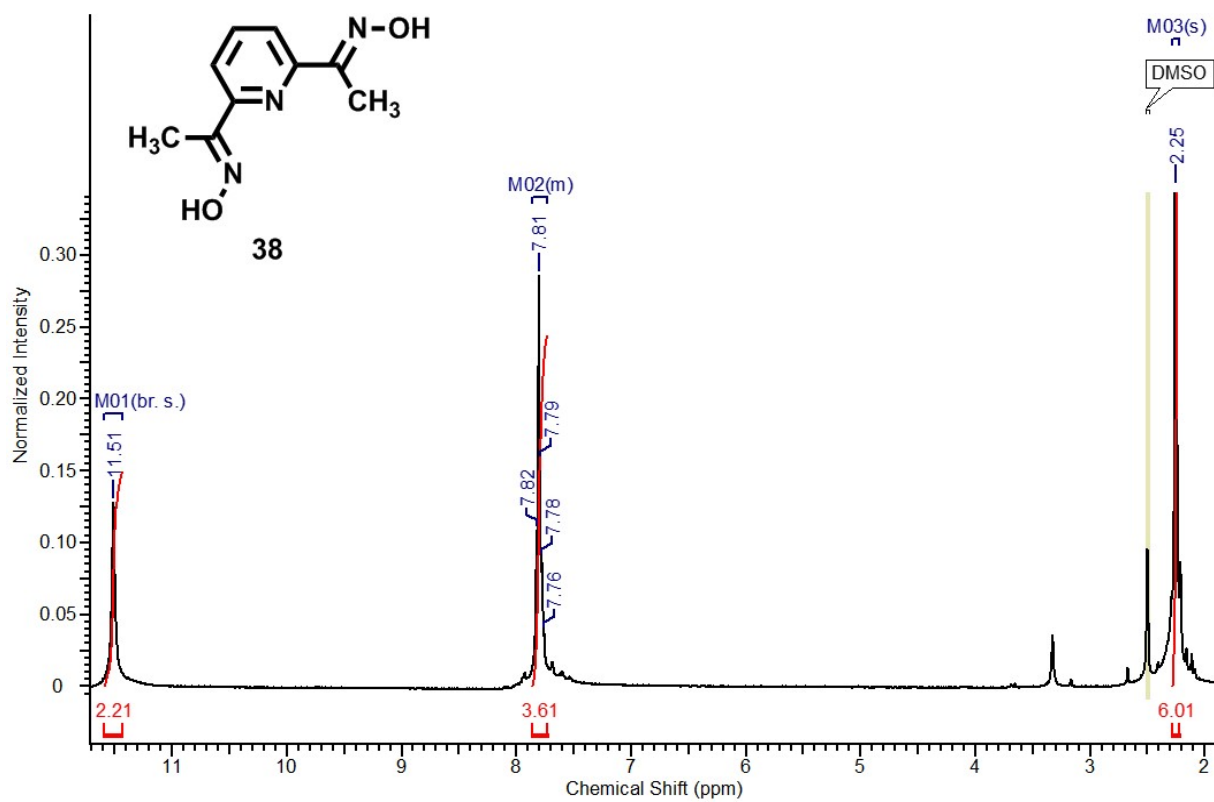


Figure A.40 ^1H NMR spectrum of **38**.

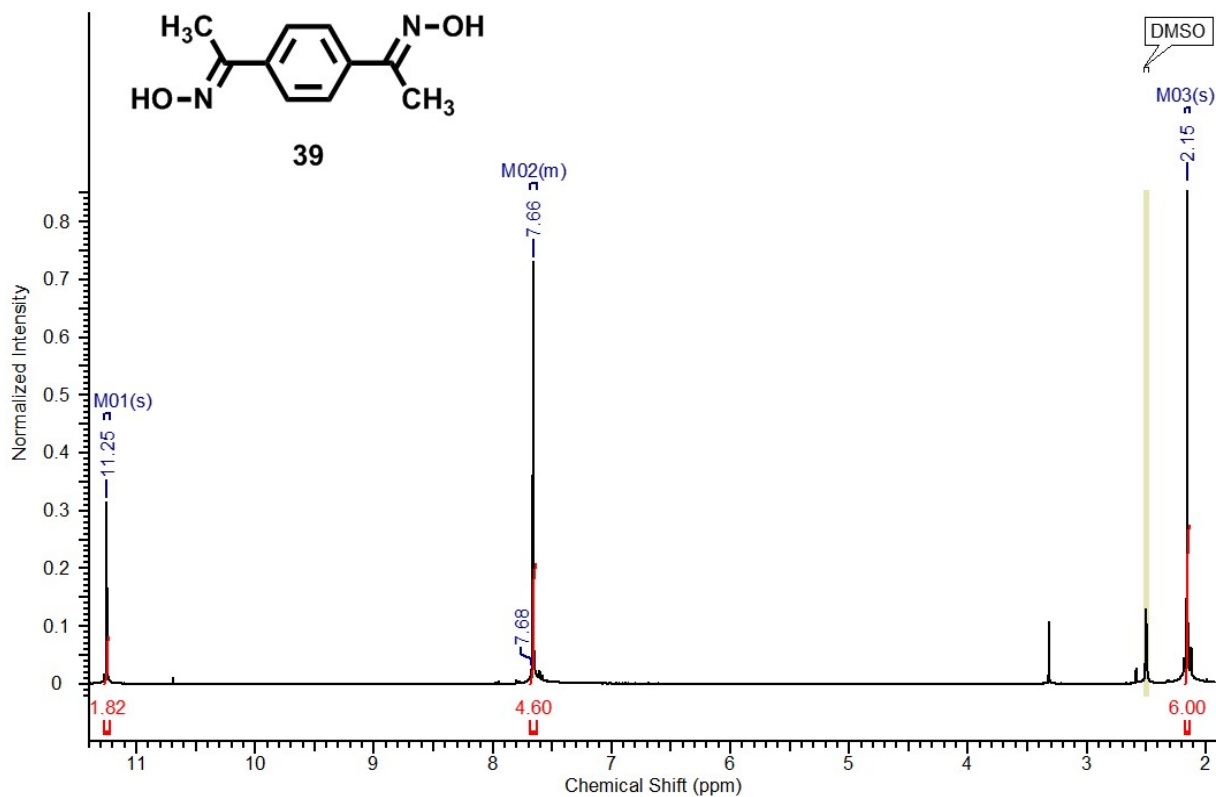


Figure A.41 ^1H NMR spectrum of **39**.

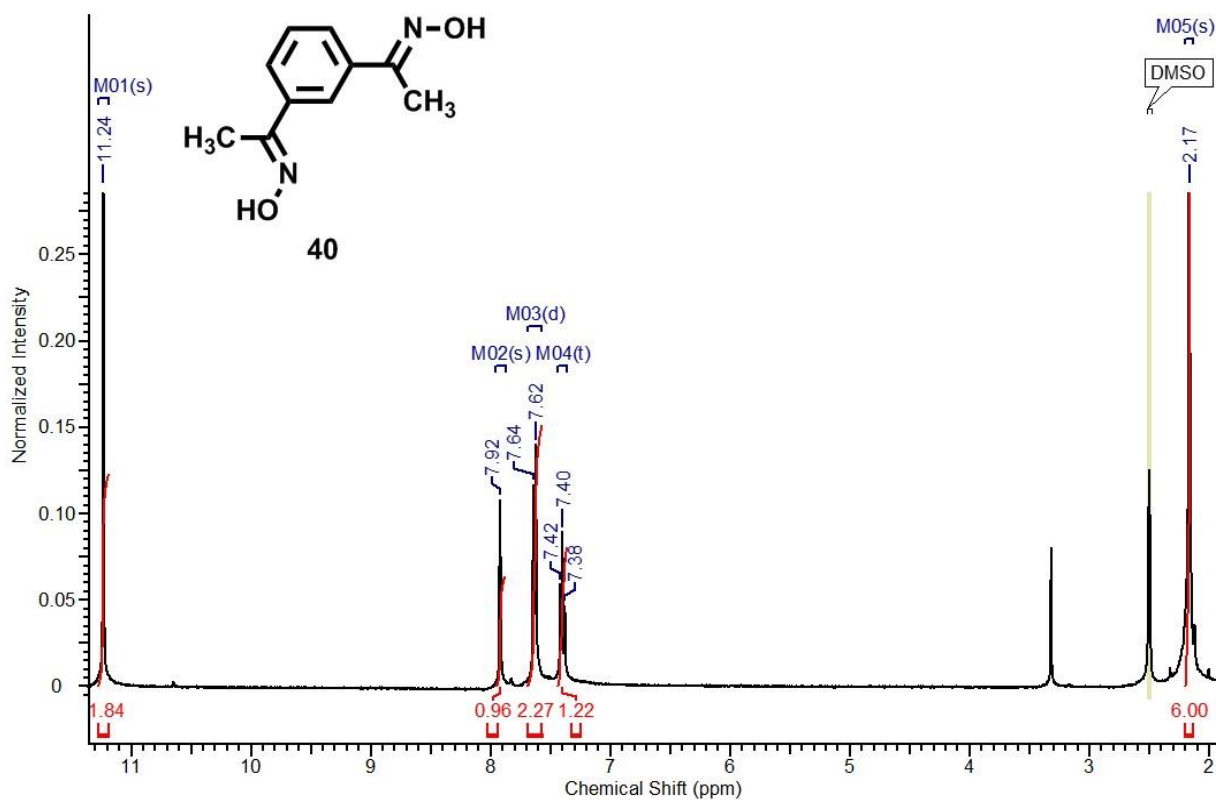


Figure A.42 ^1H NMR spectrum of **40**.

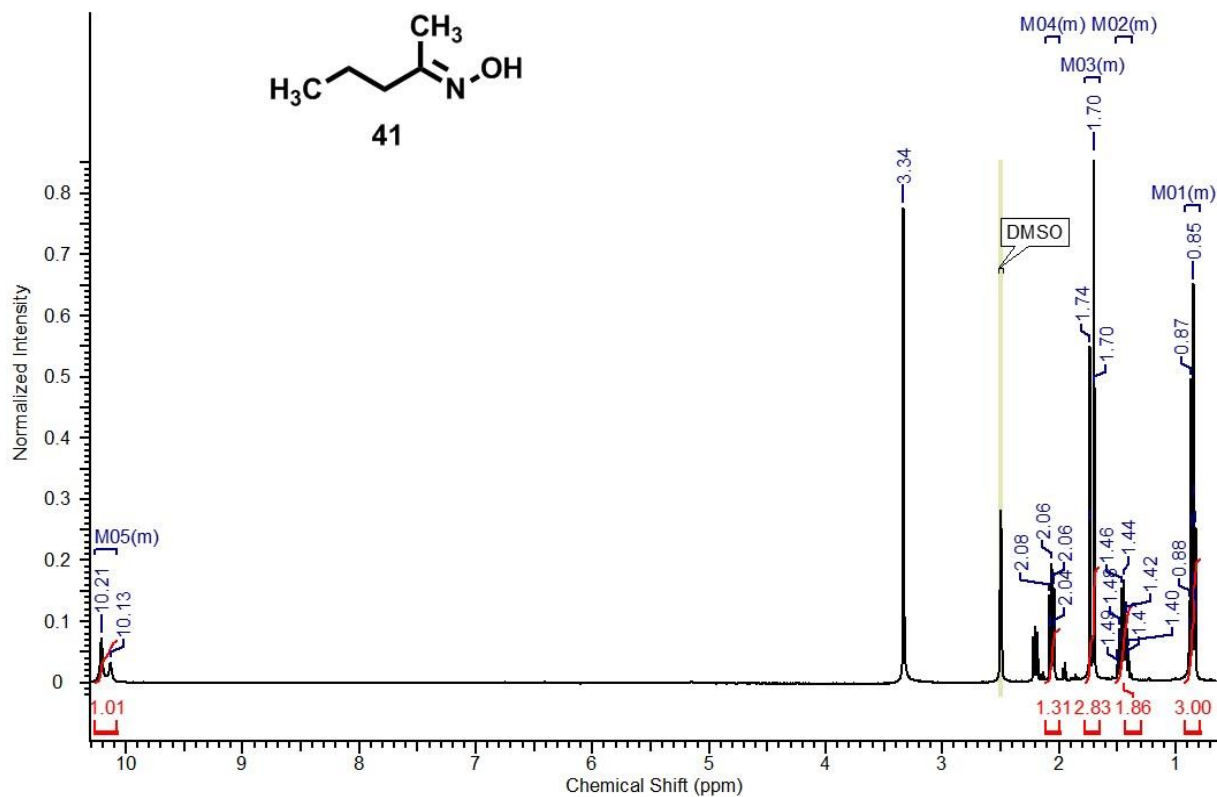


Figure A.43 ¹H NMR spectrum of 41.

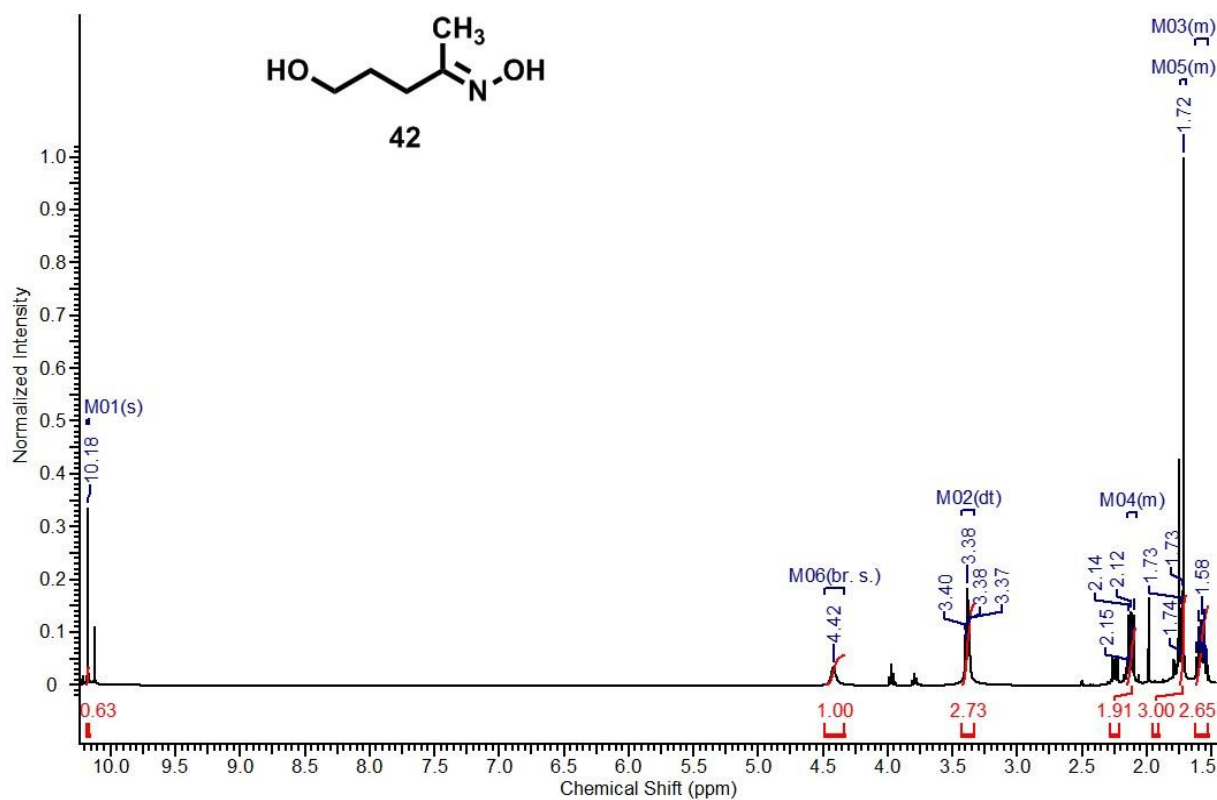
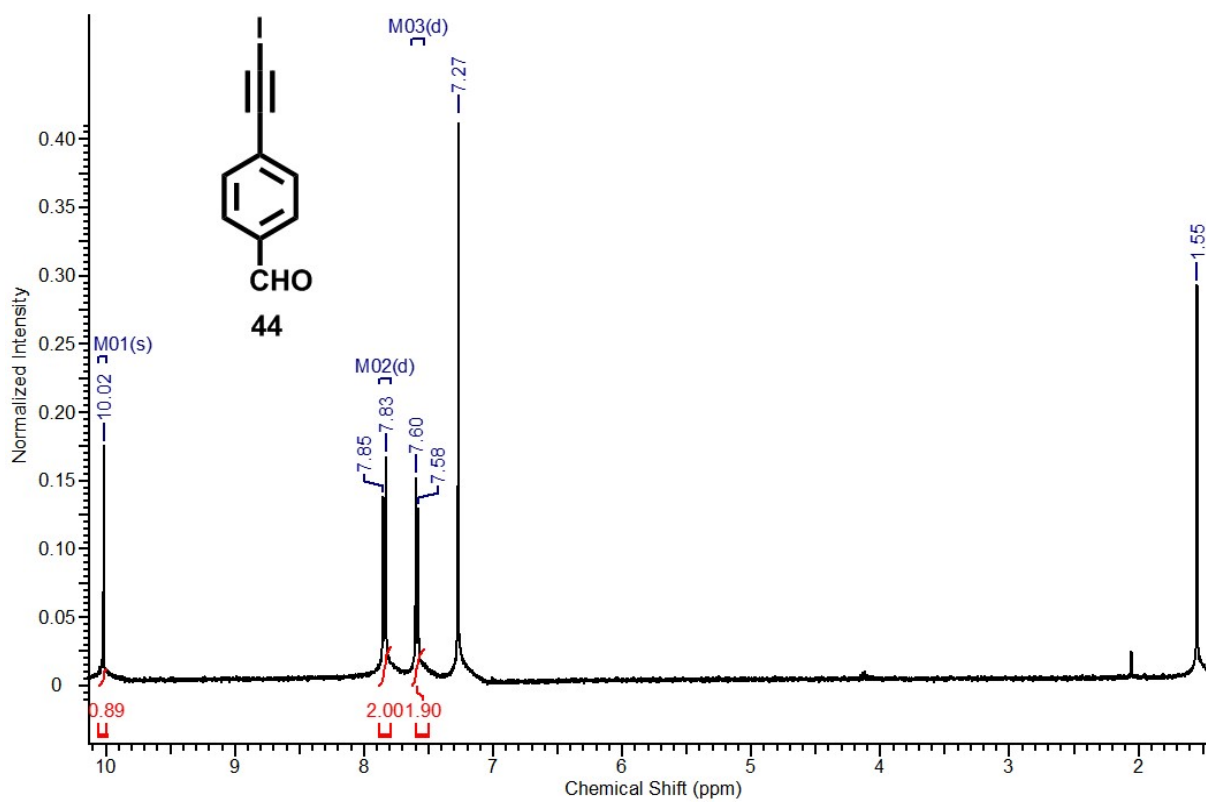
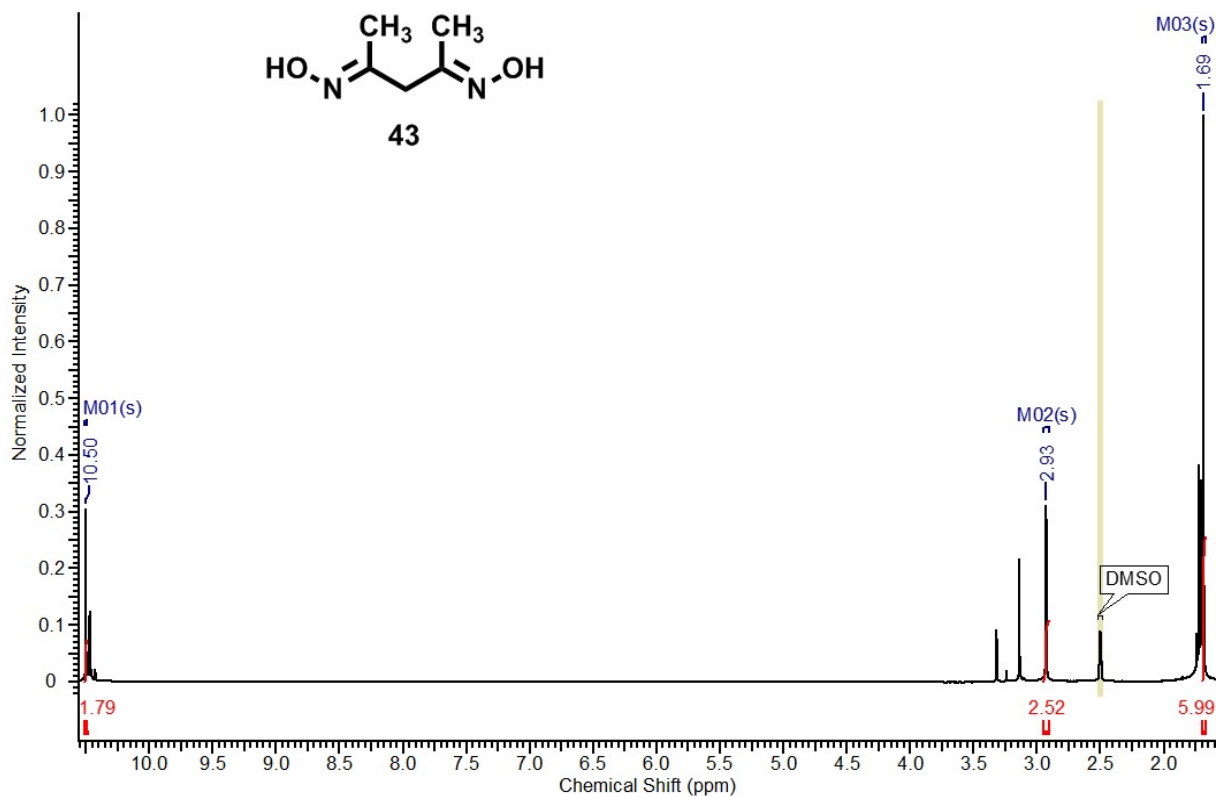


Figure A.44 ¹H NMR spectrum of 42.



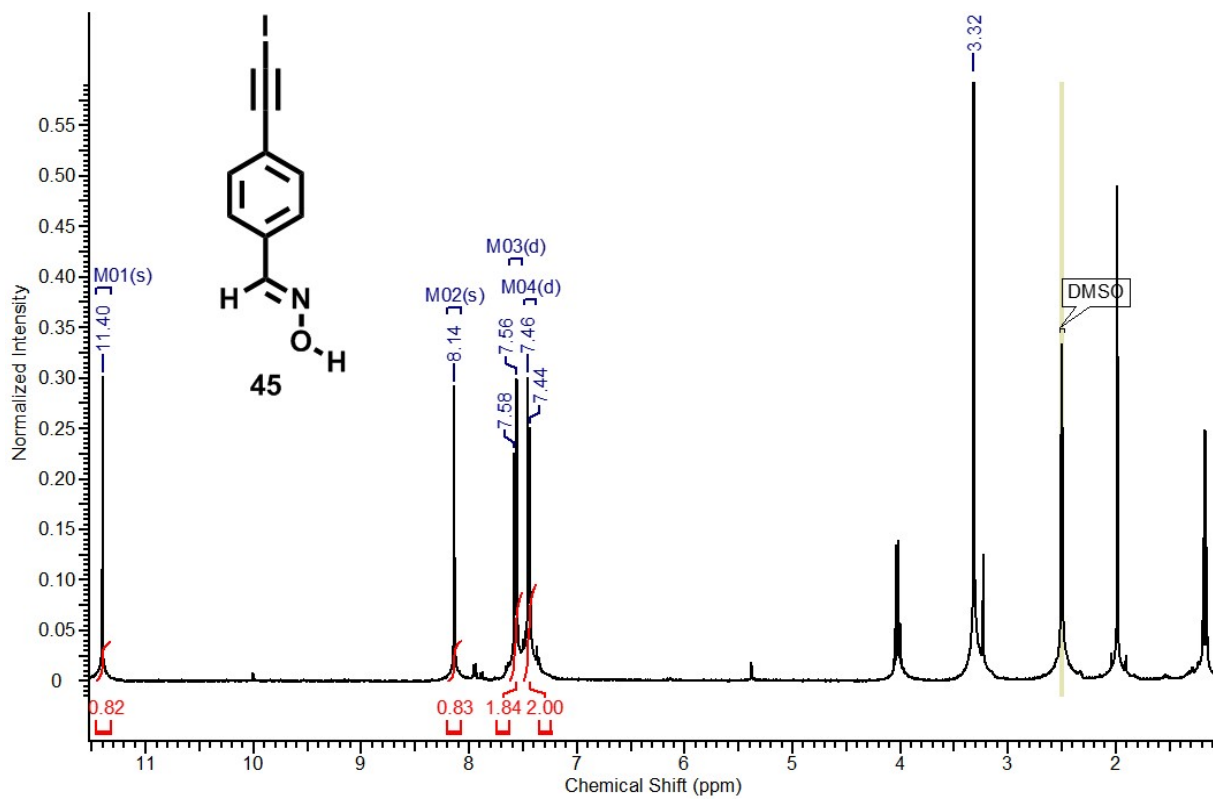


Figure A.47 ^1H NMR spectrum of **45**.

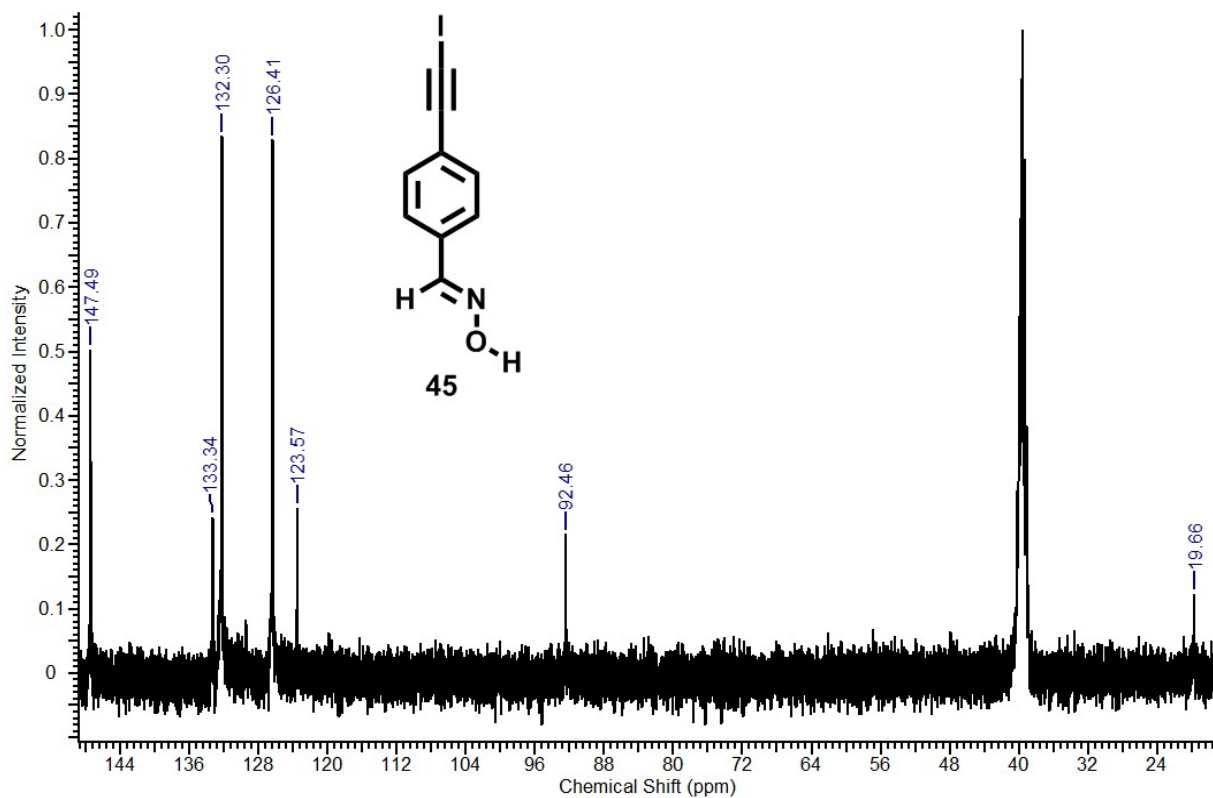


Figure A.48 ^{13}C NMR spectrum of **45**.

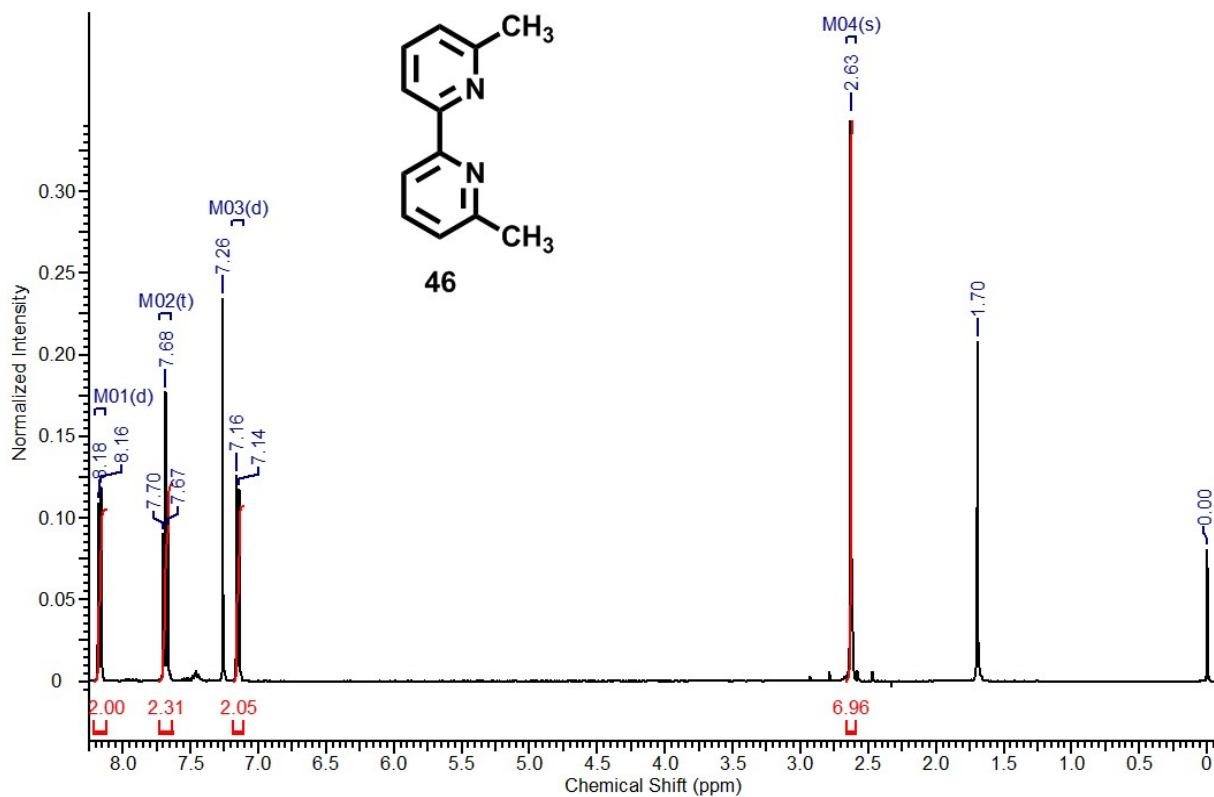


Figure A.49 ¹H NMR spectrum of 46.

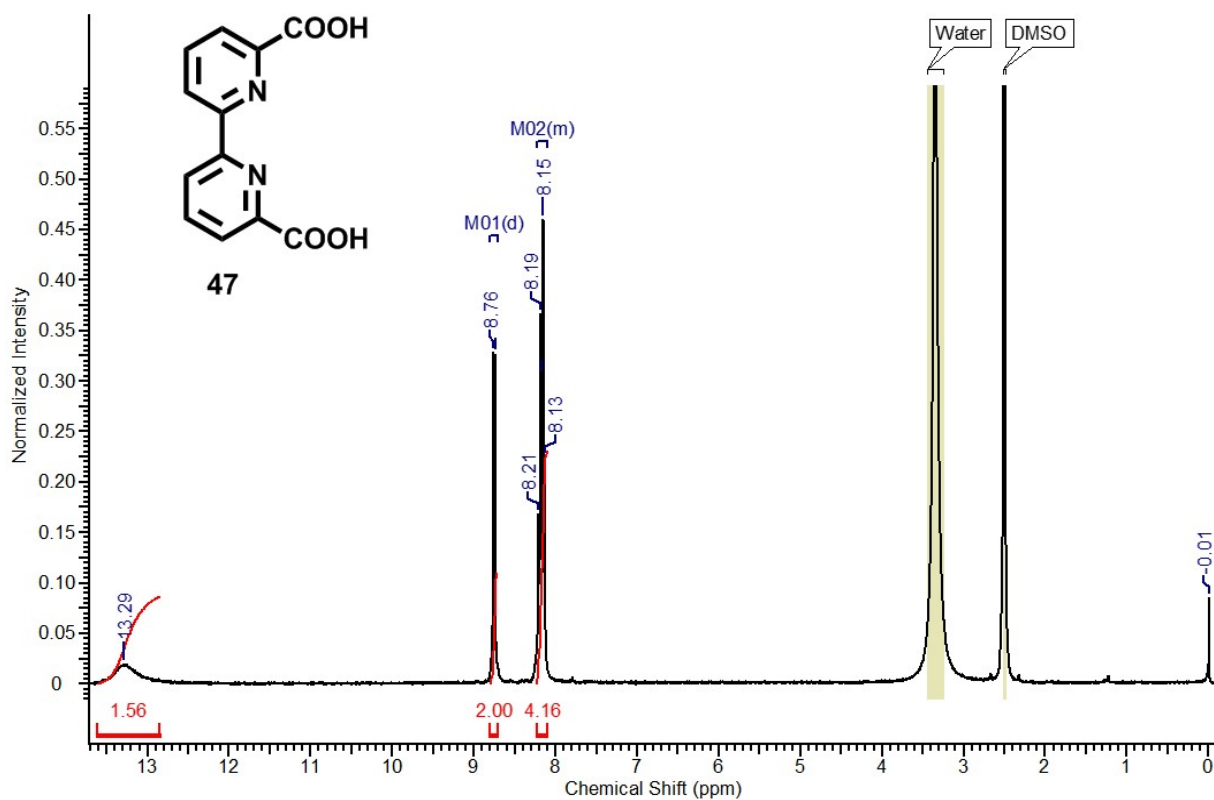


Figure A.50 ¹H NMR spectrum of 47.

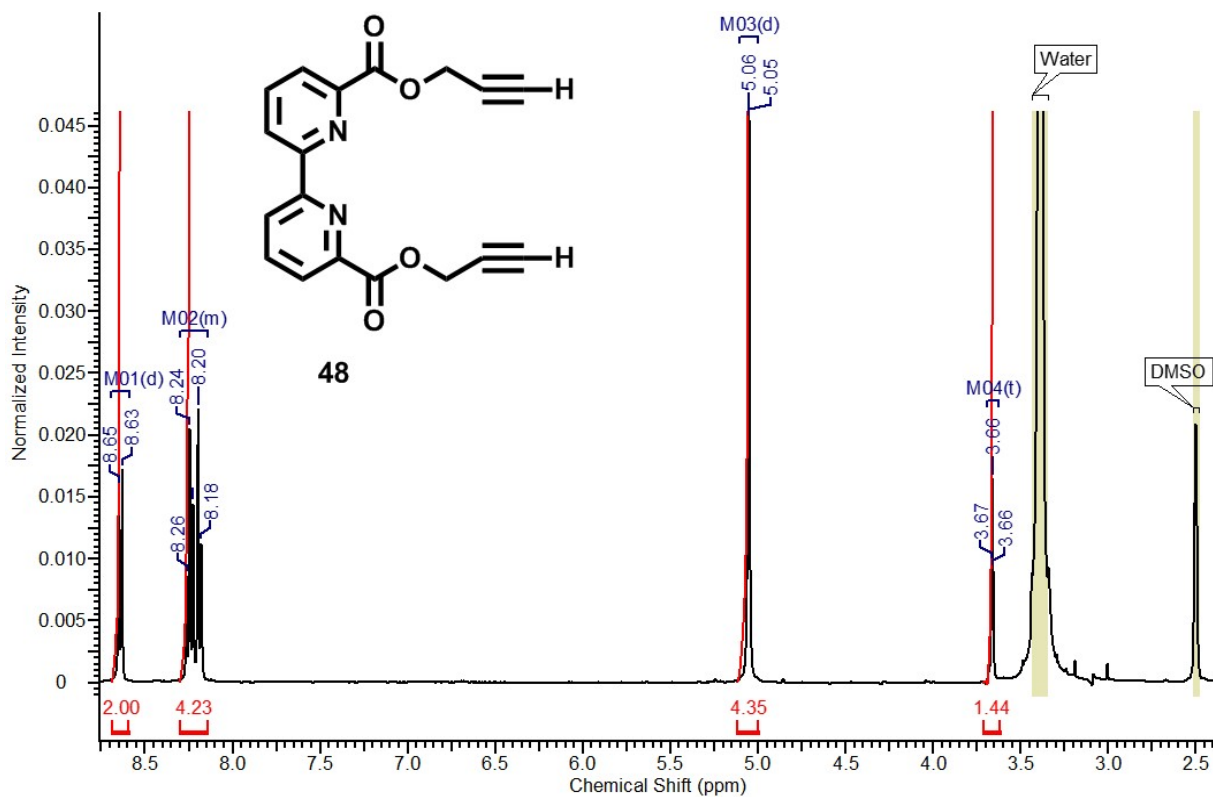


Figure A.51 ^1H NMR spectrum of **48**.

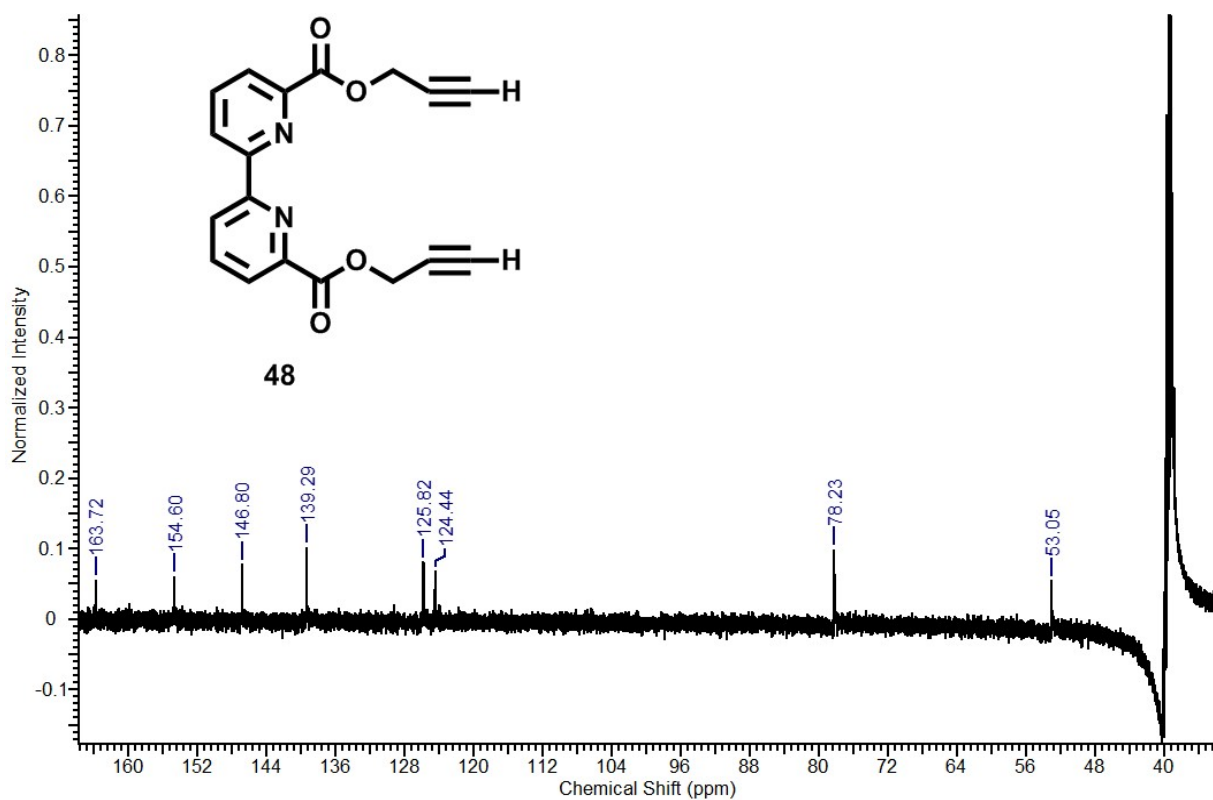


Figure A.52 ^{13}C NMR spectrum of **48**.

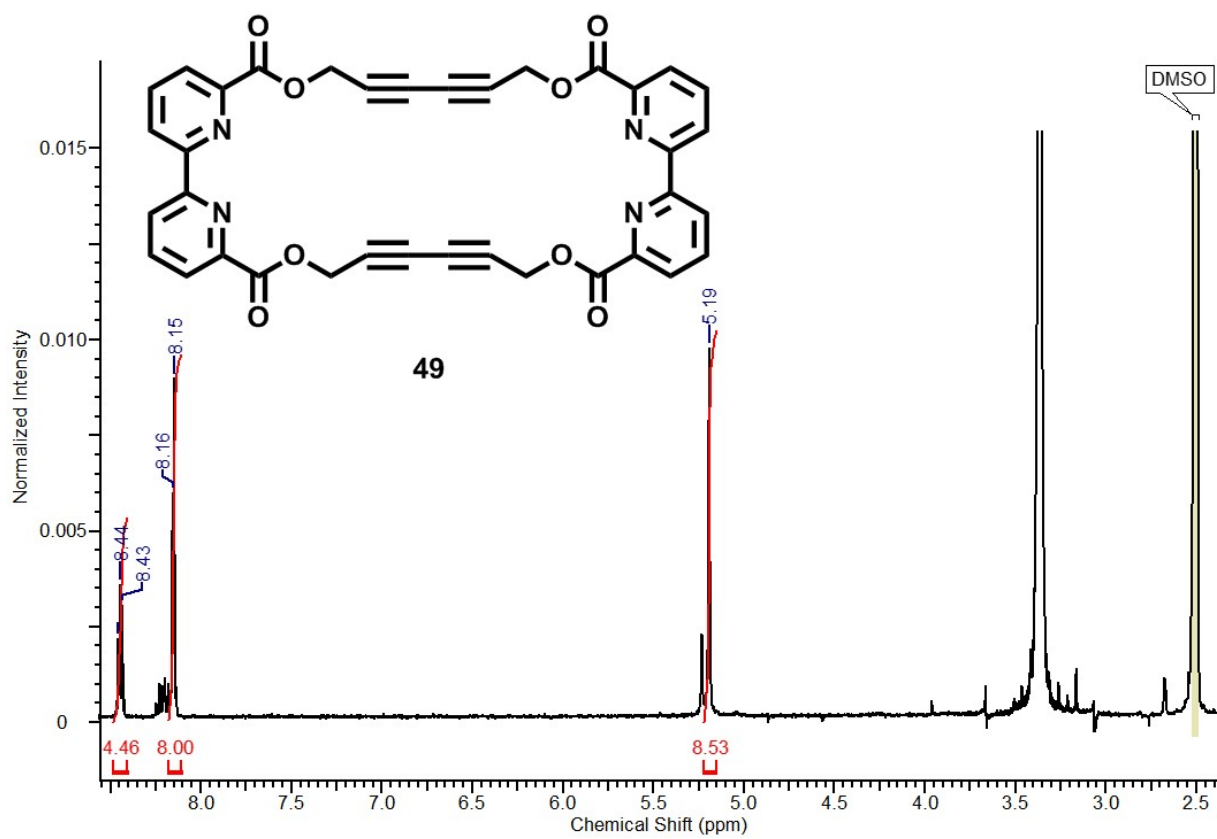


Figure A.53 ^1H NMR spectrum of **49**.